CONTRACT REPORT S-71-4

MEASUREMENT OF STRESS AND STRAIN DURING ONE-DIMENSIONAL COMPRESSION OF LARGE COMPACTED SOIL AND ROCKFILL SPECIMENS

by

M. W. C. Emerson, A. J. Hendron, Jr.

September 1971

Sponsored by Defense Nuclear Agency

Conducted for U. S. Army Engineer Waterways Experiment Station, Vicksburg, Mississippi

Under Contract No. DACA 39-67-C-0023

By Department of Civil Engineering, University of Illinois, Urbana, Illinois

ARMY-MRC VICKSBURG, MISS.

Unclassified
Security Classification

DOCUMENT CONTROL DATA - R & D

(Security classification of title, body of abstract and indexing annotation must be entered when the overall report is classified)

1. ORIGINATING ACTIVITY (Corporate author)	2a. REPORT SECURITY CLASSIFICATION
University of Illinois Department of Civil Engineering Urbana, Illinois	Unclassified 2b. GROUP

3. REPORT TITLE

MEASUREMENT OF STRESS AND STRAIN DURING ONE-DIMENSIONAL COMPRESSION OF LARGE COMPACTED SOIL AND ROCKFILL SPECIMENS

4. DESCRIPTIVE NOTES (Type of report and inclusive dates)

Final report

5. AUTHOR(S) (First name, middle initial, last name)

M. W. C. Enerson
A. J. Hendron, Jr.

6. REPORT DATE	7a. TOTAL NO. OF PAGES	7b. NO. OF REFS
September 1971	251	26

8a. CONTRACT OR GRANT NO.	9a. ORIGINATOR'S REPORT NUMBER(S)
DACA 39-67-C-0023 b. PROJECT NO. c. d.	9b. OTHER REPORT NO(S) (Any other numbers that may be assigned this report) U. S. Army Engineer Waterways Experiment Station Contract Report S-71-4

10. DISTRIBUTION STATEMENT

Approved for public release; distribution unlimited.

11. SUPPLEMENTARY NOTES	12. SPONSORING MILITARY ACTIVITY
Prepared under contract for U. S. Army Engineer Waterways Experiment Station, Vicksburg, Mississippi	Defense Nuclear Agency Washington, D. C.

13. ABSTRACT A testing device which is capable of testing one-dimensional compression specimens 48 inches in diameter and up to 14 inches in height was developed as a part of this study. The device is capable of developing static axial pressures of 1600 psi and dynamic axial pressures of at least 800 psi with pressure-rise times as fast as 3 msec with cold gas used as the loading medium. The load is applied to the test specimen by means of a flexible diaphragm, and deflections are measured by monitoring the movement of the top surface of the test specimen relative to the bottom surface with a slide wire gage which is mounted below the test specimen. The pore water pressures may be measured and the water content of the test specimen may be altered during a test if desired. The testing device was proof-tested following construction by a series of calibration tests and a series of static and dynamic tests employing Ottawa sand as a standard. Subsequent to the proof-testing of the testing device, an experimental study was conducted to investigate the effects of the variation of certain parameters on the one-dimensional compression characteristics of granular materials and included tests on Ottawa sand, crushed limestone, Wabash River gravel, and North Dakota River gravel. The study was, in general, limited to a stress range of from 0 to 500 psi, although some tests were carried to 1000 psi. The variation of parameter study included investigation into: (1) the effect of variation of particle shape and composition; (2) the effect of variation of particle size; (3) the effect of variation of gradation; (4) the effect of saturation prior to and subsequent to load application; and (5) the effect of rate of loading. Soil samples were also collected from three missile sites in the United States. Specimens which simulated in situ conditions were prepared from the samples collected and subjected to both static and dynamic loading.

DD FORM 1 NOV 68 1473 REPLACES DD FORM 1473, 1 JAN 64, WHICH IS OBSOLETE FOR ARMY USE.

Unclassified
Security Classification

Unclassified
Security Classification

14. KEY WORDS	LINK A		LINK B		LINK C	
	ROLE	WT	ROLE	WT	ROLE	WT
Dynamic tests						
Laboratory equipment						
One-dimensional compression tests						
Rock test specimens						
Soil test specimens						
Static tests						
Strain measurement						
Stress measurement						
Test equipment						

Unclassified
Security Classification

FOREWORD

The research presented herein was for the purpose of developing equipment for investigating the static and dynamic stress-strain properties of large-sized granular materials. In addition a limited number of static and dynamic test results are presented on various general backfill materials from three missile sites in the United States. The purpose of this research was to define the stress-strain properties of large-sized granular materials which are frequently used to backfill around protective structures such as missile silos or launch control centers. This work is in conjunction with research on propagation of ground shock through soils being conducted by the Soils Division, U. S. Army Engineer Waterways Experiment Station, for the Defense Nuclear Agency.

This report was prepared under Contract No. DACA 39-67-C-0023 with the Department of Civil Engineering, University of Illinois. Project monitors were Mr. J. G. Jackson, Chief, Impulse Loads Section and Mr. E. B. Perry.

Directors of the Waterways Experiment Station were COL John R. Oswalt, Jr., CE, COL Levi A. Brown, CE, and COL E. D. Peixotto, CE. Technical Directors were Mr. J. B. Tiffany and Mr. F. R. Brown.

ABSTRACT

A testing device which is capable of testing one-dimensional compression specimens 48 inches in diameter and up to 14 inches in height was developed as a part of this study. The device is capable of developing static axial pressures of 1600 psi and dynamic axial pressures of at least 800 psi with pressure-rise times as fast as 3 msec with cold gas used as the loading medium. The load is applied to the test specimen by means of a flexible diaphragm, and deflections are measured by monitoring the movement of the top surface of the test specimen relative to the bottom surface with a slide wire gage which is mounted below the test specimen. The pore water pressures may be measured and the water content of the test specimen may be altered during a test if desired.

The testing device was proof-tested following construction by a series of calibration tests and a series of static and dynamic tests employing Ottawa sand as a standard.

Subsequent to the proof-testing of the testing device, an experimental study was conducted to investigate the effects of the variation of certain parameters on the one-dimensional compression characteristics of granular materials and included tests on Ottawa sand, crushed limestone, Wabash River gravel, and North Dakota river gravel. The study was, in general, limited to a stress range of from 0 to 500 psi, although some tests were carried to 1000 psi. The variation of parameter study

included investigation into: 1) the effect of variation of particle shape and composition; 2) the effect of variation of particle size; 3) the effect of variation of gradation; 4) the effect of saturation prior to and subsequent to load application; and 5) the effect of rate of loading.

Soil samples were also collected from three missile sites in the United States. Specimens which simulated in situ conditions were prepared from the samples collected and subjected to both static and dynamic loading.

CONTENTS

CHAPTER 1

INTRODUCTION

1.1 STATEMENT OF PROBLEM

Granular materials are used for backfill in the construction of the vast majority of structures which extend below the ground surface more than a few feet. In particular, granular materials have been used as backfill for many of the buried missile structures and will most surely be used for any future system of shallow cut-and-cover structures built for the protection of personnel during a nuclear attack.

The design of such underground structures as mentioned above necessitates an evaluation of the possible ground motion of the surrounding granular material, which, in turn, necessitates a systematic study of the stress-strain behavior of large-sized granular material such as is commonly utilized for backfill. Ground motions resulting from blast loading are generally separated for the purpose of investigation of the effects into two separate categories, viz., air-blast-induced motions and direct-induced motions. This separation is utilized for the simplification of computation of ground motions; however, for pressure levels lower than 1000 psi, the direct-induced motions do not generally govern the design and usually only the air-blast-induced motions are significant. Under such conditions, the direction of propagation of the disturbance is nearly vertical, and if the soil strata may be assumed to be laterally confined, the problem may be approximated by a one-dimensional model. Therefore, the soil property of

interest for predicting ground motions is the stress-strain relation observed in a one-dimensional compression or uniaxial strain test.

Presently in the United States, there are a number of devices which have been developed for testing specimens which are composed of granular materials in one-dimensional compression. These devices include those developed by Zaccor, et al. (1965), Schindler (1967), Taylor (1954), Durbin (1964), Hendron (1963), and others. In all of these devices, the specimen size is limited to a diameter of 10 inches or less and a thickness of 3 inches or less. Several devices have been developed for the testing of specimens composed of gravel-sized particles in one-dimensional compression. These include those developed by Bjerrum (unpublished), Marsal (1965) and Fumagalli (1969). A review of existing laboratory devices is given by Feese (1970). However, these testing devices are limited in that they are only capable of static testing, and therefore, to date, there has been no device developed which can measure the one-dimensional dynamic stress-strain properties of gravel-sized materials.

1.2 OBJECTIVES OF STUDY

The objectives of this study were 1) to develop a device capable of testing granular materials with particle sizes up to 3 inches in diameter in one-dimensional compression under static and dynamic loading conditions; 2) to test backfill materials from certain selected missile sites; and 3) to conduct a variation of parameter study on granular materials commonly used as structural fill throughout the midwestern United States.

The variation of parameter study was conducted using samples of four materials. These materials were: Ottawa sand, crushed limestone, Wabash River gravel and North Dakota river gravel. The samples were used to investigate the effects on the one-dimensional compression characteristics of the variation of particle shape, mineralogical composition, particle size, particle gradation, rate of loading, and specimen saturation prior to and subsequent to load application.

The testing device was developed as a modification to the University of Illinois Dynamic Load Generator (DLG) which is capable of developing static overpressures of up to 1600 psi and dynamic overpressures of at least 800 psi with pressure-rise times as fast as 3 msec. The specimen size for which the DLG was designed was 8 feet in height and 4 feet in diameter. The modification for these tests included the design and construction of a pedestal to allow the testing of a specimen 1 foot high and 4 feet in diameter and the design of a deformation monitoring system to measure the compression of the top surface of a specimen with respect to the bottom surface during testing.

After the testing device was designed and constructed, the deformation measuring system was proof-tested for accuracy and the entire device was proof-tested by a series of static and dynamic tests. Subsequent to proof-testing, specimens of the backfill obtained from three missile sites were tested at densities and water contents simulating as nearly as possible in situ conditions.

1.3 SCOPE

In the following chapter the design and construction of the equipment used to modify the DLG for determining the one-dimensional stress-strain behavior is presented. The pressure and deformation measuring systems utilized for static and dynamic tests are described. Also, the factors considered in the design of the equipment are discussed in detail.

Chapter 3 describes the proof-testing of the deformation measuring system and of the device with a test specimen. The procedure followed for specimen placement is described and the results of the proof-testing program are presented. The results of the proof-testing with Ottawa sand are compared with the results on Ottawa sand obtained with other devices. Incidental problems which were discovered are reported in detail. The effect of seating error and an analysis of the pressure distribution over the top surfaces of the test specimen are also discussed.

Chapter 4 describes the variation of parameter study conducted on samples of the two river gravels and the crushed limestone in addition to the standard Ottawa sand. The granular materials tested are described in detail and the effects of particle shape, mineralogical composition, particle size, particle gradation, rate of loading, and the effects of specimen saturation prior to and subsequent to load application are discussed in detail utilizing the test results obtained.

Chapter 5 presents a summary of this study and conclusions regarding the performance of the one-dimensional compression device and the variation of parameter study. Suggestions are made for future research which appears justifiable in view of the test results obtained in this study.

Appendix A presents the results of the dynamic tests on the samples from the missile sites. Appendix B presents a brief description of the DLG and describes the operation of the loader.

CHAPTER 2

DESIGN AND DEVELOPMENT OF EQUIPMENT

2.1 INTRODUCTION AND SUMMARY

The Dynamic Load Generator (DLG) was constructed primarily for the study of static and dynamic responses of structural models embedded in soil specimens, arching in soil, soil-structure interaction, and stress-wave propagation. To facilitate such investigations, the soil container was constructed to accommodate a test specimen 4 feet in diameter and 8 feet deep. The utilization of the DLG for investigation of the stress-strain behavior of compacted soils and rockfill materials in one-dimensional compression required the design and construction of a deformation measuring system capable of monitoring the deformation of a test specimen during dynamic or static loading and the modification of the specimen container to permit testing of a specimen with a ratio of diameter to height of greater than one.

The modification of the specimen container to test a specimen of thickness less than 8 feet necessitated the consideration of four primary factors: viz., sidewall friction acting on the specimen, sufficient gage length to reduce boundary and nonuniformity of specimen effects, dynamic response, and electrical access to and housing of instrumentation. The instrumentation systems were designed in accordance with criteria established by the anticipated behavior of soil and rockfill specimens during testing. These criteria were as follows: 1) the deformation measuring

system must accurately measure the deformation of the top surface of the test specimen relative to the bottom surface; 2) the pressure measuring system must accurately measure the pressure acting over the surface of the test specimen; 3) the deformation and pressure measuring systems must be electronic to enable recording during dynamic testing; 4) the deformation and pressure measuring systems must be protected from moisture in the test specimen; 5) the deformation measuring system must be capable of measuring deformations as large as 2 inches with a threshold of approximately 0.001 inches; and 6) the instrumentation systems must not significantly affect the stress-strain behavior of the test specimen.

The modification of the specimen container was accomplished by the design and construction of a reinforced concrete pedestal with a top plate of 2-inch-thick steel and a bottom plate of 1-inch-thick steel. The overall pedestal height was 82.25 inches, thus permitting a test specimen thickness of approximately 12 inches, and, consequently, a specimen aspect ratio (ratio of specimen diameter to height) of approximately four. The large aspect ratio served to minimize sidewall friction effects and permitted testing of specimens with particle sizes of the order of 3 inches. The dynamic response of the pedestal was such that the pressure-rise times employed in this study could be considered as static. The pedestal is shown in place in the DLC specimen container in Figure 2.1.

The pressure measuring system utilized for this study was the same as that originally developed for the DLC. The pressure acting over the top surface of the test specimen during rapid testing was sensed by Kistler quartz pressure transducers which were located in the seal ring of

the DLG. During static testing the pressure acting on a test specimen was monitored by a Bourdon-type gage connected to the expansion chamber.

The deformation measuring system employed consisted of a slide wire gage mounted in the top plate of the pedestal and actuated by the movement of a steel deformation plate which rode on the top surface of the test specimen. The movement of the deformation plate was transmitted to the slide wire gage by an actuating rod which served as a mechanical link between the deformation plate and the electrical pickup of the slide wire gage. The slide wire gage had a threshold of 0.0003 inches and was capable of measuring deformations of up to 4.5 inches. The repeatability of the gage was shown to be better than 99%. The deformation plate, which was constructed of 1/8-inch steel, was very flexible compared to the stiffness of the test specimens so that the stress distribution acting on the top surface of the test specimens was nearly unaffected by the presence of the deformation plate.

The actuating rod was protected from frictional forces, which could be imposed upon it by the soil specimen by a 1-inch-diameter bellows which was flexible in the axial direction and stiff in the radial direction. The bellows is shown installed in Figure 2.2 and a working drawing of a segment of the bellows is presented in Figure 2.3. The bellows completely encased the actuating rod from the top plate of the pedestal to the bottom side of the deformation plate. The actuating rod was protected from contact with the bellows by a rigid stainless-steel tube which was enclosed by the bellows. The stainless-steel tube was rigidly mounted in the top plate of the pedestal and enclosed the actuating rod to a height such that the anticipated deformation of the soil specimen could occur without contact

between the deformation plate and the tube. The deformation measuring system is shown in place in the soil container in Figure 2.2.

2.2 Pedestal Design and Construction

2.2.1 Design Consideration

2.2.1.1 Introduction

In order to obtain a more favorable aspect ratio for one-dimensional compression tests, a pedestal was designed and constructed to reduce the effective height of the soil container. In the design of the pedestal, four considerations were of primary importance. These design considerations were as follows: 1) the test specimen must be thick enough that boundary effects at the top and bottom of the test specimen are minimized, even when testing materials with particle sizes approaching 3 inches, and to ensure that vertical deformation of the surface of the specimen may be accurately measured to the nearest 0.001 inch, and thin enough so that the aspect ratio (D/H) of the test specimen will be as large as possible in order to minimize sidewall friction effects; 2) the pedestal must be constructed such that the dynamic response of the pedestal does not significantly influence the behavior of the test specimen during loading; and 3) the pedestal must provide a means for housing deformation measuring instrumentation as well as access ports to allow hydraulic communication to the specimen and outlets for wires connected to transducers within the specimen.

2.2.1.2 Height of Pedestal

The height of the pedestal was determined by the height of the test specimen required and the height of the DLG soil container. The diameter of a soil test specimen was fixed by the diameter of the soil container (48 inches); therefore, the height of the test specimen was determined by consideration of sidewall friction and the accuracy required for deformation measurements of the top of the specimen.

The larger the test specimen thickness, the larger the axial deformation under a given axial pressure and the greater the possible accuracy in measuring the deformation with a given deformation measuring device. However, the greater the specimen height, the less favorable the aspect ratio of the test specimen with respect to sidewall friction. The effect of aspect ratio on the transmission of static stress through sand in cylindrical tanks has been investigated by Abbott (1967). Abbott's research showed that with an aspect ratio of four, one could expect at least a transmission of 85%, and that if a greased liner is used between the specimen and the tank wall, the minimum transmission increases to approximately 90% for a steel tank. Further, analysis of work done by Rohmaller (1968) and Paul and Goel (1968) indicated that the transmission of static stress with an aspect ratio of one should be greater than 90% if a neoprene tank liner is used with Lubriplate grease between the steel wall and the neoprene liner. Lubriplate grease used in conjunction with a neoprene liner were determined to be the most efficient tank liner and lubricant in a study conducted by Prendergast (1968). Thus from the standpoint of sidewall friction with a steel container, an aspect ratio

of approximately four used in conjunction with a tank liner and Lubriplate grease resulted in static stress transmission of at least 90% and probably greater than 95%.

Assuming a soil specimen aspect ratio of four and a constrained modulus of 50,000 psi, the deformations which would result from an axial stress of as low as 100 psi can be demonstrated to be of sufficient magnitude to be accurately measured by a deformation measuring device with a resolution of 0.001 inches. If an instrumentation resolution of 0.001 inches is assumed, the deformation resulting from an overpressure of 100 psi can be measured to within 4%. This is a conservative estimate of the accuracy attainable in the study conducted, since typical constrained moduli of interest were on the order of 10,000 to 30,000 psi.

Based on the considerations of sidewall friction and magnitude of axial deformation as discussed above, a specimen height of 12 inches was selected. A test specimen of 12 inches provided sufficient thickness to virtually eliminate boundary effects which might have been induced by too thin a specimen and to preclude any significant nonuniformity in test specimens.

An additional consideration affected the design height of the pedestal. The successful completion of a static or dynamic test on a given specimen is dependent on the integrity of the loading diaphragm. If the loading diaphragm were to bear directly on test specimens such as crushed limestone, the diaphragm would certainly be ruptured by the sharp particles or would exceed its tensile strength in being extruded into the voids near the surface of the specimen. In order to preclude

such a failure of the loading diaphragm, the height of the pedestal required for a test specimen was reduced by 2 inches. The additional 2 inches was filled with Ottawa sand which functioned as a cushion for the loading diaphragm. Invasion of the Ottawa sand into the test specimen was prevented by a cushion-specimen interface membrane. The interface membrane was retained against the soil specimen container liner by a clamping ring. The placement procedure is described in Section 3.3.2. The general features of the soil specimen container are illustrated in Figure 2.2.

2.2.1.3 Dynamic Response of Pedestal

The testing program performed under this study included tests which were to determine the one-dimensional behavior of soils under dynamic conditions as discussed in Section 1.2. Thus, the loading rates varied from static to pressure-rise times of 25 msec. The dynamic tests usually employed a pressure-rise time of approximately 25 msec, a dwell time of 25 msec, and a decay time of 300 msec.

Because of the dynamic character of the imposed load on the soil specimen and pedestal, the dynamic response of the pedestal was a factor which influenced the pedestal design. The incident pressure pulse on the top of the pedestal is probably best treated as a step pulse having a versed sine or cycloidal pressure-rise shape. Examination of the response of a system with respect to maximax displacement reveals that if the ratio of the pressure-rise time to the fundamental period (τ/T) is greater than two, the system will behave as if the pressure were applied statically, Figure 2.4; thus, dynamic considerations dictated that the pedestal be constructed such that the fundamental period would be less than about 10 msec.

Assuming the pedestal to be composed of reinforced concrete, the natural period of the pedestal was computed assuming the pedestal to be a spring-mass system and assuming the pedestal to be a solid cylinder, Timoshenko (1955). The computations of the natural frequency of the pedestal by both methods are presented in Figures 2.5 and 2.6.

2.2.1.4 Housing of Instrumentation and Access to Test Specimen

The position of the test specimen relative to the loader of the DLG and the decision to use a slide wire type gage to monitor the deformation of the test specimen required that for dynamic tests, the slide wire gage be located within the pedestal. This location was particularly favorable because if a deformation gage were to be mounted to any part of the system other than the pedestal, such as the forging, then the movement of the top plate of the pedestal relative to the gage mount would have to be monitored during a test. The deformation of the test specimen would then be computed as the difference between the apparent deformation as indicated by the slide wire gage and the movement of the top plate of the pedestal. Thus, the top plate of the pedestal was designed with a central port to accept a plug which served as a mount for the slide wire gage. Also, the central portion of the pedestal, immediately below the top plate, was designed with a cavity to house the slide wire gage.

The existence of the void beneath the center of the top plate of the pedestal and the discontinuity in the top plate led to deflection of the center of the top plate, i.e., the central instrumentation port. The deflection of the instrumentation plug under static loads can be computed by making certain simplifying assumptions. The lip of the top plate of

the pedestal, which the instrumentation plug rests upon, was supported by the pedestal at a diameter of 7.650 inches. A conservative assumption regarding support conditions is that the plug is simply supported at its edge. The deflection of the plug is computed in Figure 2.7, employing expressions for the deflection of a simply supported circular plate as presented by Timoshenko (1959).

Assuming that a test specimen has a secant modulus of 100,000 psi, an axial pressure of 1000 psi yields an axial strain of 1%, and, with an initial specimen thickness of 12 inches, an axial deformation of 0.12 inches. The resulting error caused by deflection of the instrumentation plug amounts to less than 0.5%, and is insignificant. Further, the deflection of this central plug during testing was reduced by arching.

Electrical access ports were provided in the bottom of the DLG soil container. A 3-inch-diameter pipe leading from the slide wire gage housing through the pedestal and matching the position of one of the ports in the soil container served as passage for the electrical leads from the slide wire gage.

In order to permit other instrumentation within the soil specimen, four additional small-diameter instrumentation ports were included in the design of the top plate of the pedestal. The ports were located to match the access ports in the bottom of the soil container. All ports and plugs were designed for O-rings so that, if desired, airtight integrity of the specimen could be maintained. Special purpose plugs and blank plugs were designed and constructed to be fitted into the instrumentation ports.

Two plugs were designed and constructed to allow saturation of specimens. A working drawing of these plugs is presented in Figure 2.8. When these plugs were employed, copper tubing was passed from a water source, through the concrete pedestal, and connected to the plugs. When Hydrocal was used on the top plate of the pedestal to prevent seating errors with coarse-grained samples, the water inlet holes were covered with tape prior to the pouring of the Hydrocal and the placement of the first lift of the specimen. After the Hydrocal hardened, the material immediately over the inlet holes was removed and the Hydrocal and tape over the water inlet holes removed. The placement of the additional lifts of the specimen was then completed.

One plug was designed and constructed to provide a means to relieve the air pressure built up during saturation of test specimens. A working drawing of this plug is presented in Figure 2.9. As the water invaded the test specimen being saturated, the pore air pressure increased since the top of the specimen was sealed by the loading diaphragm. The de-airing line, which was a copper tube passing through the test specimen and open at the top was connected to the bottom of the de-airing plug and passed through the concrete pedestal and was vented to the atmosphere with the open end at the same elevation as the top of the test specimen within approximately 1 inch. This line also served to maintain the level of the water at the top of the specimen.

Finally, a third special purpose plug was designed to monitor the pore air pressure inside the test specimens which were tested in an air-dry state. This special purpose plug was designed with a porous stone

exposed to the test specimen and connected to a Bourdon-type gage external to the test specimen chamber. A working drawing of this plug is presented in Figure 2.10.

2.2.2 Construction Details

Based on the design considerations presented in Section 2.2.1, the pedestal was constructed of reinforced concrete with top and bottom steel bearing plates. The pedestal is shown in place in the DLG soil container in Figure 2.1 and a detailed working drawing of the pedestal is presented in Figure 2.11.

The top plate of the pedestal was constructed of 2-inch-thick 212 Grade B firebox steel. The plate was machined to a diameter of 47.955 inches with an O-ring groove cut to facilitate a watertight seal between the top plate and the soil container wall. Instrumentation access holes and lift holes were cut in the top plate. Three-inch-diameter electrically welded pipes centered on the instrumentation access holes and continuous between the top and bottom plates were provided as conduits for electrical and hyraulic leads to the specimen. Lifting nuts (1-8, C12B, 74-kip-proof load) were welded to 4-x 4-inch mild steel plates which were welded to the bottom side of the top plate centered over the lift holes. The lifting nuts were encased in capped 16-gauge, 3-inch-diameter, electrically welded pipes.

Intermediate grade No. 4 reinforcing rods were welded to the bottom side of the top plate and to the bottom plate 3.1/4 inches to either side of the center lines of the lifting points for the pedestal. Thirty intermediate grade No. 3 reinforcing rods at a spacing of 12° and on a radius of 20.5

inches were welded to the bottom of the top plate and to the top of the bottom plate with intermediate grade No. 2 reinforcing rods used as tie bars at the third points of the longitudinal steel. Finally, eight 12-inch lengths of intermediate grade No. 3 reinforcing rods were welded to the top plate on a radius of 14 inches to serve as anchor studs for the top plate.

A form for the pouring of the concrete pedestal was constructed of 10-gauge steel. The form was forced into a groove cut into the bottom side of the top plate and welded into place. The top plate was utilized as a temporary base; the instrumentation conduits and reinforcing rods were positioned with a template;and the pedestal form was filled with concrete. After the concrete was poured, the bottom plate was placed and welded to the reinforcing rods leaving a 3/4-inch void between the concrete and the bottom plate. The void was filled with non-shrink Embeco grout after the initial shrinkage of the concrete. The bottom plate was constructed of 1-inch-thick firebox steel.

Two concrete test cylinders (6 x 12 inches) were poured during the placing of the concrete for the pedestal. The 28-day strengths of the cylinders were 4280 and 5022 psi. The stress-strain curves for these cylinders are presented in Figures 2.12 and 2.13.

In order to eliminate the necessity of providing a grout bed for the pedestal each time it was placed in the soil container to level the top plate, the bottom plate was machined parallel to the top plate. The center lines of the top and bottom plates did not and need not have the same center line since the bottom plate and the pedestal form are 45 inches in diameter and the soil container inside diameter is 48 inches. Before

pouring concrete for the pedestal, the form was fixed such that the cylindrical wall did not deviate more than 0.25 inches from the vertical over the entire height. Thus, when the pedestal was in the soil container, the top plate was exactly centered in the soil container and the bottom plate was not; however, the top and bottom plates were parallel.

2.3 INSTRUMENTATION DESIGN AND CONSTRUCTION

2.3.1 Pressure Measuring System

The pressure measuring system employed in this study was identical to that originally developed for the DLG. During dynamic testing, the pressure acting over the top surface of the test specimen was sensed by Kistler quartz pressure transducers, Model Nos. 601-A and 606-A. The transducers were installed in their respective mounts and placed in the seal ring ports of the DLG. The pressure transducers produce an electrical charge proportional to the change in pressure to which they are subjected; therefore, by grounding the transducers immediately prior to the application of the dynamic overpressure and subsequent to the application of the static preload, the measured pressures corresponded to the dynamic increment only. The electrical charges produced by the pressure transducers were converted to voltages by Kistler electrostatic charge amplifiers, Model No. 504MSA. The outputs of the charge amplifiers were recorded on tape. Immediately prior to the test, a calibration step corresponding to the anticipated dynamic overpressure was recorded on tape utilizing the Kistler charge amplifiers and Kistler Model 5384 charge calibrators.

The seal ring was tapped at twelve locations to provide ports for the installation of pressure measuring devices. These twelve locations were such that the pressure measuring devices could be located directly beneath or in between loading machines Nos. 1, 2, 3, 5, 6, and 7. The loading machines are described in Appendix B. The location of the pressure measuring devices as described above provided a means for evaluation of the time of firing of the machines relative to one another with the exception of machine No. 4, and provided a means for an evaluation of the uniformity of pressure at least along the periphery of the expansion chamber. A study of the uniformity of pressure over the surface of a test specimen by the evaluation of accelerometer records and pressure-time traces has been made and reported by Prendergast (1968). The results of this study indicated that for very fast rise times on the order of 3 msec, the maximum pressure variations are less than 20% of the peak surface pressures. An analysis of the pressure variation over the surface of a test specimen is presented in Section 3.3.4.4.

During static testing, the Kistler transducers were removed and the ports plugged. The pressure acting on the specimen was monitored by a Bourdon-type gage which was connected to the expansion chamber.

2.3.2 Deformation Measuring System

2.3.2.1 Design Considerations

2.3.2.1.1 Introduction

The design of the DLC did not leave much latitude for the design of the deformation measuring system. The expansion chamber was designed to be as small as possible to reduce the expansion of the loading medium and

thereby maintain a large ratio of final pressure to charging chamber pressure without making the expansion chamber so small as to result in large pressure gradients over the surface of the test specimen. Because of the small expansion chamber volume, the location of a deformation measuring system in the expansion chamber was impractical, if not impossible, for dynamic tests. Also, because of the relative movement between the DLG forging and the soil container, a deformation measuring device mounted anywhere except to the top plate or the pedestal would require a correction for the movement of the gage mount relative to the top plate of the pedestal. Therefore, the design of the DLG required that the deformation measuring device, at least for dynamic tests, be mounted to the top plate of the pedestal. The movement of the top surface of the test specimen relative to the top plate of the pedestal was transmitted to the gage by a mechanical link between a deformation plate resting on the top surface of the specimen and the gage.

2.3.2.1.2 Selection of Gage Type

The selection of the type of gage to be built to monitor deformations was based primarily upon consideration of the magnitude of the deformations to be measured. Based on the results obtained by other researchers, strains of the order of 10 to 15%, or deformations of the order of 2 inches, were anticipated. Moreover, because of the S-shaped stress-strain behavior typical of soil materials in one-dimensional compression, a threshold of the order of 0.001 inches was required to enable the stiffer portions of the stress-strain curves to be defined.

Two types of gages are commonly used which are sensitive to small displacements over fairly large total distances, viz., linear variable differential transformers (LVDT'S) and slide wire gages. LVDT'S are rela-

tively delicate and expensive and slide wire gages are frequently quite sensitive to dynamic effects. In an effort to prevent unnecessary expenditures of time and money, the decision was made to construct a slide wire gage as the primary deformation measuring device with a detachable LVDT mounted on the frame of the gage. Then, if the slide wire gage did not function satisfactorily, the LVDT could be utilized, and if the slide wire gage did function satisfactorily, the LVDT could be detached from the mount. Because of the expense of a long-travel LVDT, a surplus short-travel LVDT was mounted on the slide wire gage frame for proof-testing and subsequently detached when the slide wire gage proved satisfactory.

2.3.2.1.3 Threshold and Repeatability of Measurements

The repeatability of measurements made with slide wire gages is primarily dependent upon the precision of construction of the various component parts of the gage. Particular attention must be focused on the travel of the pickup over the slide wires. The pickup must be constrained to inhibit movement in any direction other than that in which measurements are to be made. In addition, all slack must be eliminated in the mechanical link which transmits the deformation to be measured to the slide wire gage.

Another factor affecting the repeatability is the pickup-slide wire point-of-contact. This contact must be firm to prevent loss of contact during dynamic tests and yet must not be so firm as to cause significant straining of the wire during movement of the pickup. Also, the contact should be as nearly a point-contact as possible. A prime requisite of high repeatability is a highly finished slide wire and pickup. Periodic refinishing of the slide wire and pickup are essential for maintaining repeatability.

As a means of reducing the wear as much as possible and, therefore, prolonging the life of the slide wire, the slide wire should be hard relative to the slide wire pickup. For this reason, the slide wires were composed of 24-gauge Nickel-Chromium wire and the pickups were composed of brass.

A slide wire gage is basically a potentiometer which can be directly excited by a voltage source; displacements of the pickup are measured by reading the changes in voltage drop between the pickup and either end of the slide wire. Although such a system will function, the attainment of a reasonable threshold requires a high-voltage DC power source and a precision voltmeter. To attain a reasonable threshold without the use of a high-voltage source, the slide wire was incorporated in a Wheatstone bridge circuit as shown in Figure 2.14. The function of the null slide wire, which is shown in Figure 2.14, was to null any inbalance in the bridge immediately prior to a dynamic test to simplify the reduction of test data. The null slide wire served no function and required no adjustment during a static test.

2.3.2.1.4 Connection Between Deformation Plate and Slide Wire Gage

Because of the location of the slide wire gage below the test specimen in the pedestal, a mechanical connection between the deformation plate which rests on the top surface of the test specimen and the slide wire gage was required. In the design of such a mechanical connection, four considerations were of primary importance, viz., the connecting rod must be sufficiently free from frictional effects so that the behavior of the test specimen is accurately measured; the dynamic response of the link must

be such that inertial effects are minimal; the connections to the deformation plate must be such that the actuating rod need not be normal to the deformation plate; and, finally, it must be possible for the soil specimen container to remain watertight.

Frictional effects can arise from two different sources. In the passage of the actuating rod through the test specimen, the actuating rod must be protected from contact with the specimen. In protecting the actuating rod from the test specimen, the rod must be enclosed in a sleeve which will deform axially with the test specimen and yet be of the same order of radial stiffness as the soil specimen. Several researchers have utilized segmented rings to contain test specimens. These rings are slightly separated when the test specimen is unloaded and can move together as the specimen is loaded and deformed axially. This method has proved satisfactory and is reported by Zaccor et al. (1965), Fumagalli (1969), and others. This segmented ring idea was considered to provide protection for the actuating rod from the soil specimen; however, this concept was found to be impractical because of the small diameter and the difficulty of holding the rings in place during placement of a specimen.

The second possible solution is a bellows which is soft in the axial direction and stiff in the radial direction. Such a system is less difficult to set up and invasion of soil into the void around the actuating rod is prevented unless the bellows ruptures. Further, bellows are commercially available while segmented rings would have to be machined to order and, therefore, would be considerably more expensive than the bellows. Thus, a bellows device was selected as the protective method to be employed. Since the bellows is flexible, the actuating rod could still

suffer from frictional effects if, during specimen placement, the bellows came into contact with the actuating rod. Enclosure of the actuating rod with a stainless steel tube which in turn was enclosed by the bellows provided an adequate solution to this problem.

Another source of frictional forces resulted from the passage of the rod through the top plate of the pedestal. Since the slide wire gage was mounted inside the pedestal, at some point along the actuating rod, there was the opportunity for frictional forces to develop. Several methods for reducing these forces to a minimum were considered such as teflon coating or machining to a high finish. The latter method was selected and a testing program was employed to determine the magnitude of the resulting frictional forces. These forces were shown to be negligible as described in Section 3.2.1.

The dynamic characteristics of the actuating rod-pickup system are probably best examined by the method suggested by Jacobsen and Ayre (1958). By this method the natural frequency f_n of the system is computed as shown below:

$$f_n = \left[\frac{k}{m_1 + \frac{m_2}{3}}\right]^{1/2}$$

where $k = AE/L$

A = cross-sectional area of rod

E = Young's modulus for rod

L = length of rod

m_1 = mass of pickup

m_2 = mass of rod

The use of either stainless steel or aluminum for the actuating rod and a relatively lightweight material for the pickup body results in a fundamental period of the order of less than 1 msec, and is, therefore, not subject to inertial forces during loading of test specimens when rise times of the order of 20 to 30 msec are employed. During proof-testing, accelerometers were attached to the slide wire pickup and the deformation plate. An SR-4 wire strain gage was mounted on the actuating rod just above the slide wire pickup to measure any inertial effects. The analysis showed the actuating rod-pickup system to be virtually free from inertial effects. This analysis is presented in Section 3.3.4.2.

The top surface of any given test specimen could not be placed so as to be perfectly flat. Therefore, the connection between the actuating rod and the deformation plate was required to swivel in order that the actuating rod could pass axially through the test specimen along the specimen center line and the deformation plate could be rigidly fixed to the actuating rod and yet not be perfectly normal to the rod. Several possible methods involving ball joints were considered but the easiest and most economical proved to be the use of spherical washers in the connection.

Finally, a means to achieve watertight integrity was required. The passage of the actuating rod through the top plate to the slide wire gage gave rise to a breach in the watertight integrity of the specimen container. An O-ring seal system was designed to provide a seal between the top plate and the actuating rod without inducing large frictional forces on the actuating rod. In addition, this seal system was designed

such that the close tolerance pieces, which could induce large frictional forces, could be completely removed when watertight integrity was not required.

2.3.2.1.5 Deformation Plate

The deformation plate was required to move with the top surface of the test specimen and yet not influence significantly the stress-strain behavior of the test specimen. The size of the plate had to be sufficient to portray the deformation of the test specimen, flexible enough to not significantly alter the uniform stress distribution over the surface of the test specimen imposed by the gas pressure acting on the loading diaphragm, and sufficiently light so as to not impose significant stresses on the test specimen because of inertial effects. In addition, the deformation plate had to be small enough in diameter so that it did not extend over that portion of the surface of the test specimen most affected by sidewall friction and was sufficiently stiff over the central portion to reduce the overstress originating from the passage of the bellows through the specimen.

The influence of the stiffness of the deformation plate on the stress distribution over the surface of the test specimen may be approximated by assuming that the test specimen is a half-space and that linear elastic conditions prevail. A solution to the distribution of pressure between a plate and a linear elastic half-space has been presented by Borowicka (1936). Using Borowicka's method and assuming a plate diameter of 24 inches and a thickness of 1/8 inch, the relative stiffness K of the deformation plate-soil specimen system may be approximated as illustrated in Figure 2.15. A K-value of infinity indicates an infinitely stiff plate

relative to the soil specimen, while a K-value of zero indicates a completely flexible plate. Stress distributions corresponding to various K-values are presented by Scott (1963). The relative stiffness computed for the deformation plate corresponded to an almost completely flexible plate. Therefore, the stress distribution over the top of the soil specimen may be assumed to be unaffected by the presence of the deformation plate.

The inertial forces which would be imposed on the top surface of a test specimen during a dynamic test were estimated employing the static stress-strain behavior of Ottawa sand as determined using the device designed by Hendron (1963). Ottawa sand was placed at densities of approximately 100 and 110 pcf and loaded to 1000 psi. The resulting stress-strain behavior was assumed to be identical to the dynamic stress-strain behavior and pressure-time curve was assumed to be linear with a rise time of 25 msec. Utilizing these assumptions, the maximum accelerations and decelerations were estimated to be on the order of 100 g's.

Assuming that accelerations of the order of 100 g's were reasonable and that the deformation plate was composed of 1/8-inch-thick steel, the inertial stresses which could be induced on the top surface of a test specimen by the deformation plate were computed to be less than 5 psi. Thus, even if the maximum accelerations were to range up to 200 g's, the imposed inertial stress would still not exceed 10 psi. Measured accelerations are presented in Section 3.3.4.2.

The presence of the void through the center of the test specimen to accommodate the passage of the mechanical link between the deformation

plate and the slide wire pickup produced an overstress of the soil in the immediate vicinity of the void. If no provisions were made to stiffen the plate in the vicinity of this void, excessive deflection of the slide wire pickup would have resulted as a consequence of the overstress acting on the specimen in the immediate vicinity of the void and deflections of the deformation plate over the void. An aluminum stiffener 6 inches in diameter was designed and mounted on the center of the deformation plate. The stiffener served to distribute the overstress over a larger area. If the overstress is assumed to be limited to the area of the stiffener, then the overstress amounts to less than 3%.

The relative stiffness of the deformation plate to a test specimen was such that the plate is flexible and the pressure distribution was very nearly uniform as demonstrated above. However, this computation assumes intimate contact between the test specimen and the soil specimen. In most instances, the placement of a test specimen did not result in a perfectly flat top surface; rather, there were slight undulations over the surface. If no seating measures were taken, the deformation plate rode on the tops of these undulations and tended to flatten the surface and to bend to conform to the surface. This bending and flattening constituted seating error which resulted in an apparent stress-strain behavior which was not as stiff as the true stress-strain behavior. Also, when testing large granular materials, the point contacts between the particles and the steel plate resulted in excessive strain due to crushing of point contacts on the steel deformation plate. With large granular materials, an identical seating error resulted at the bottom of the test specimen. In an effort to overcome

this seating error without modifying the design of the deformation plate, a seating compound was placed on the deformation plate prior to placing the plate on the surface of the test specimen. When testing large granular materials, the seating compound was also placed on the top plate of the pedestal prior to the placement of the first lift. This method, which is discussed in greater detail in Section 3.3.4.3, proved to be quite satisfactory in eliminating point crushing at the boundaries of test specimens.

2.3.2.2 Construction Details

The slide wire gage itself was constructed of aluminum. A photograph of the gage with the auxillary LVDT mount is presented in Figure 2.16 and detailed working drawings of the individual components comprising the gage are presented in Figures 2.17 through 2.21. The frame of the gage was first constructed and assembled and then the pickup body was constructed such that a close tolerance fit existed between the pickup and the gage frame. This close tolerance was required to eliminate error resulting from play of the pickup in the gage frame.

The pickup itself was threaded on both the top and the bottom such that connection could be made to the actuating rod and also to a rod extending from the bottom of the slide wire gage to which an LVDT core could be fixed. The LVDT body was mounted in the micarta mount which could be attached to the bottom of the slide wire gage. The LVDT is shown mounted in the photograph presented in Figure 2.16, and a detailed working drawing of the micarta LVDT mount is presented in Figure 2.22.

Movement of the pickup contact relative to the slide wire was prevented by boring the mounting hole for the contact slightly under size

and then polishing the contact with emery cloth until the contact could barely be forced into the pickup body. Opposite the face of the contact, a spring-loaded bumper was mounted to ensure intimate contact between the slide wire and the pickup contact.

Two slide wires and two pickups were incorporated into the gage. The two slide wires were mechanically linked and electrically independent. This system precluded any variation between measured deformation by the two slide wire gages unless, because of wear, the pickup body could move in any direction other than axially in its track. To inhibit wear, the aluminum guides and the micarta pickup body were heavily impregnated with powdered graphite. After six months of use, the pickup body showed little sign of wear, and any wear that had occurred was not sufficient to present a detectable error in the readout of the gage.

The slide wires were composed of 24-gauge Nickel-Chromium wire. Prior to affixing the slide wires on the gage, the wires were stressed nearly to yield and then polished, first with emery cloth and then crocus cloth. This preparation was necessary in order to provide a smooth surface for the pickup to ride on. The pickup contact was also finished to a high degree with emery cloth and crocus cloth. Upon assembly of the slide wire gage, a complete calibration of the gage was required to ascertain that nonlinearity of the gage did not exist because of local yielding of the slide wires or other problems. To prevent frequent changing of the slide wires because of wear, the pickups were composed of brass. The excessive wearing of the brass necessitated frequent refacing of the pickups but greatly lengthened the satisfactory life of the slide wires.

The pickup actuating rod employed was a 3/16-inch-diameter steel rod threaded on either end. The connection to the pickup body was made by threading the rod into the body and fixing it in place by a lock nut. The connection to the deformation plate is shown in Figure 2.23. The spherical washers used in the deformation plate mount allowed a deviation from the normal of the actuating rod to the plate of approximately 4°. In order to prevent the actuating rod from being acted upon by frictional forces in case the protective bellows should be displaced laterally, the actuating rod was enclosed in a stainless steel tube with an inside diameter of 5/16-inch. The tube was mounted in a recess in the central instrumentation plug and could be easily removed and replaced. The length of tube used for a given test was determined based on the initial height of the test specimen and the anticipated axial deformation. The stainless steel tube also acted to prevent any significant bowing of the actuating rod during loading. The stainless steel tube is shown in place in Figure 2.2.

Protection of the actuating rod and stainless steel tube was provided by the bellows which completely enclosed the rod and tube and extended from the top plate of the pedestal to the deformation plate. The bellows assembly was composed of five Fulton Sylphon, 2-ply, 5/16-inch-diameter, hydraulic bellows. The individual bellows were silver soldered together to form the assembly. The connection of the assembly to the top plate of the pedestal was accomplished by a threaded section which was silver soldered to the bottom-most bellows of the assembly, and the top-most bellows was fixed in place by the taper on the bottom side of the deformation plate.

The deformation plate was constructed of 10-gauge mild steel (thickness of 0.1345 inches). The diameter of the deformation plate was 24 inches. An aluminum stiffener 6 inches in diameter was mounted on the center of the deformation plate. The stiffener served to distribute the overstress initiated by the void for the actuating rod through the center of the test specimen over a larger area. A working drawing of the deformation plate is presented in Figure 2.24.

The watertight seal around the actuating rod was achieved by a special insert which could be removed when testing dry materials. The details of the seal are presented in Figure 2.25. The seal increased the friction acting on the actuating rod by a factor of approximately two but this still amounted to only approximately 0.2 lb and was insignificant.

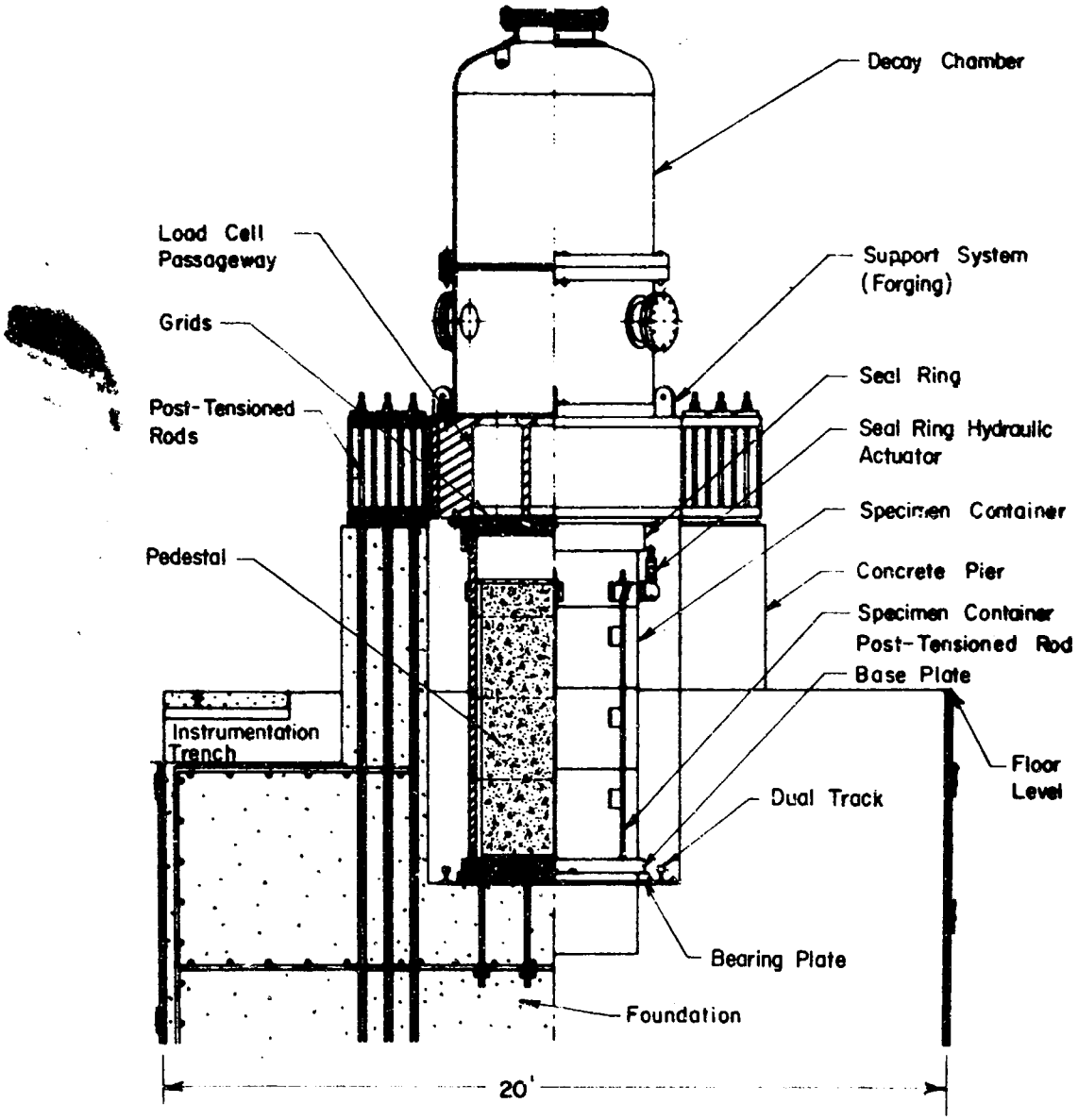

FIGURE 2.1 CROSS SECTION OF DYNAMIC LOAD GENERATOR WITH SPECIMEN CONTAINER AND PEDESTAL IN PLACE

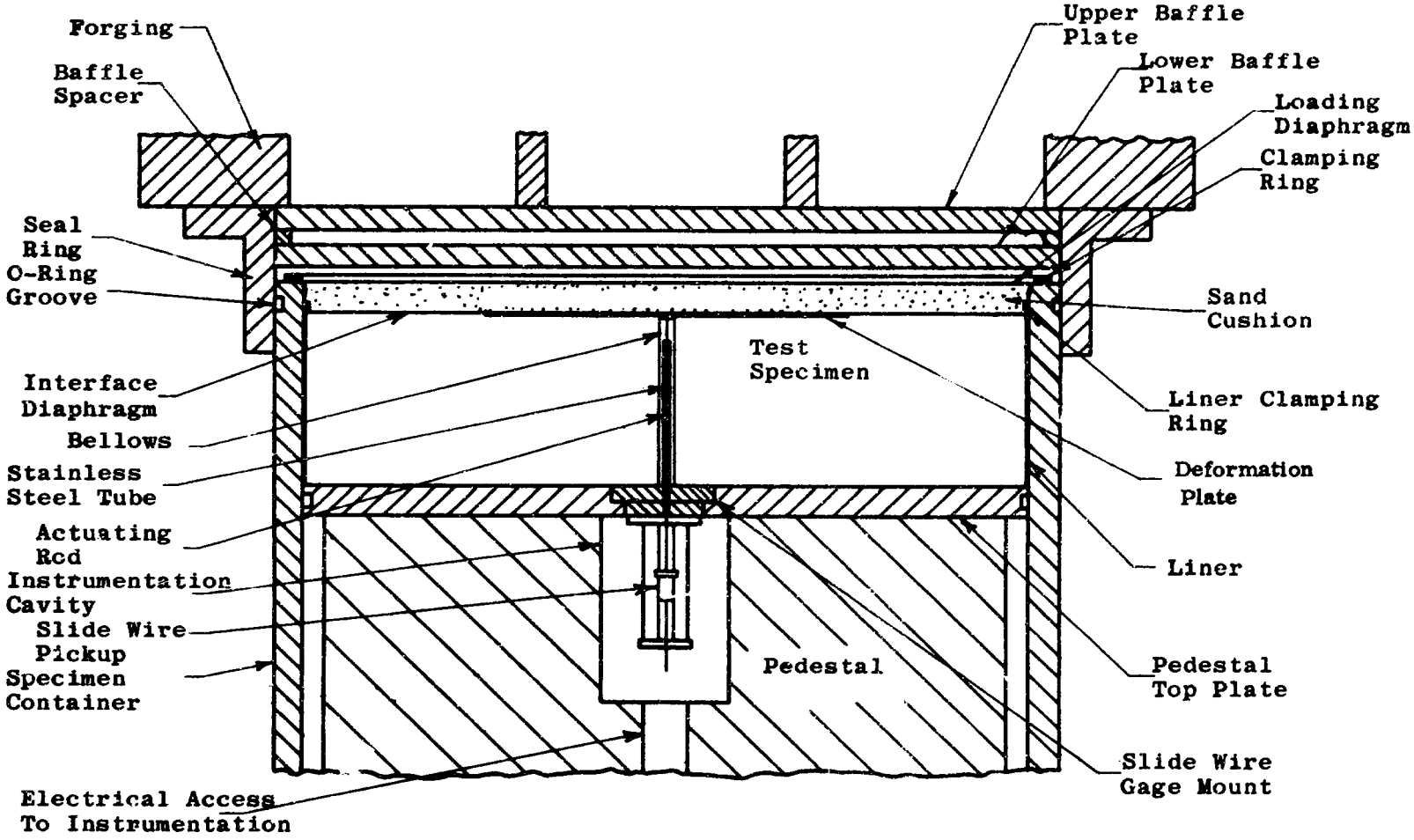

FIGURE 2.2 CROSS SECTION OF SPECIMEN CONTAINER

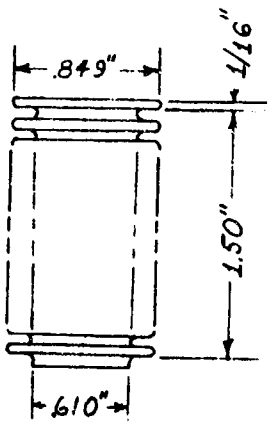

Material: Phosphorus-bronze

Wall thickness: 0.023 in.

FIGURE 2.3 WORKING DRAWING OF INDIVIDUAL BELLOWS

X_m Maximum absolute displacement

X_s Characteristic displacement of forcing function

τ Pressure rise time

T Characteristic period of forcing function

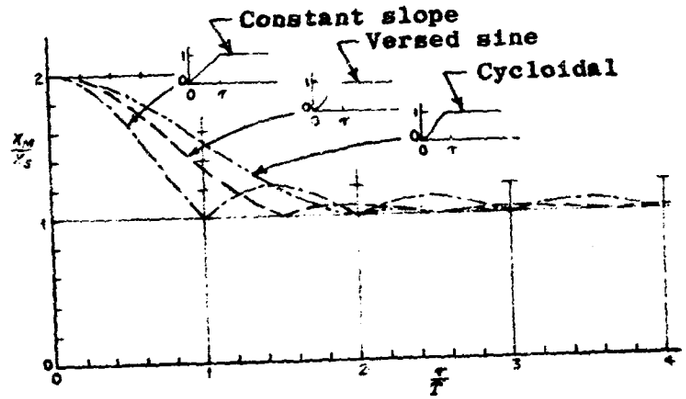

From Engineering Vibrations, by L. S. Jacobsen and R. S. Ayre.
Copyright 1958. Used with permission of McGraw-Hill Book Company.

FIGURE 2.4 SPECTRA OF MAXIMUM DISPLACEMENT RESULTING FROM STEP FUNCTIONS HAVING EQUAL RISE TIME (after Jacobsen and Ayre)

Basic relation $T = 2\pi\sqrt{m/k}$

where $k = p/d$

Definitions:

- T = fundamental period of pedestal
- m = mass of pedestal
- p = imposed load on pedestal
- d = deflection induced by imposed load p
- E_c = Young's modulus for concrete
- E_s = Young's modulus for steel
- A_c = area of concrete
- A_s = area of steel
- W = weight of pedestal
- g = acceleration due to gravity
- L = height of pedestal

$$k = p/d = \frac{A_s E_s + A_c E_c}{L}$$

$$= \frac{(40\,in^2.)(30\times10^6\,lb/in^2.) + (1.55\times10^3\,in^2.)(4\times10\,lb/in^2.)}{82\,in.}$$

$$\doteq 1\times10^8\,lb/in.$$

$$m = W/g = \frac{12{,}400\,lb}{32.2\,ft./sec^2.}$$

$$\doteq \frac{32\,lb\text{-}sec^2.}{in.}$$

$$T = 2\pi\sqrt{m/k} = 2\pi\sqrt{\frac{32\,lb\text{-}sec^2./in.}{10\,lb/in.}}$$

$$\doteq 4\,msec.$$

FIGURE 2.5 FUNDAMENTAL PERIOD OF PEDESTAL ASSUMING SPRING-MASS SYSTEM

Basic relations $c = \sqrt{E/p}$ and $T = 2L/c$

Definitions:

- T = fundamental period of pedestal
- c = velocity of stress-wave propagation through pedestal
- E = Young's modulus of pedestal
- L = height of pedestal
- p = mass density of pedestal
- W = weight of pedestal
- V = volume of pedestal
- g = acceleration due to gravity
- E_c = Young's modulus for concrete
- E_s = Young's modulus for steel
- A_c = area of concrete
- A_s = area of steel
- A = total area of pedestal

$$p = W/Vg = \frac{12{,}400 \text{ lb}}{(86\text{ft}^3)(32.2\text{ft./sec}^2)}$$
$$\doteq 450 \text{ lb-sec}^2/\text{ft}^4$$

$$E = \frac{E_s A_s + E_c A_c}{A} =$$
$$= \frac{(401\text{in}^2)(30\text{x}10^6 \text{ lb/in}^2)+(1.55\text{x}10^3 \text{in}^2)(4\text{x}10^6 \text{ lb/in}^2)}{1.59\text{x}10^3 \text{in}^2}$$
$$\doteq 46.5\text{x}10^5 \text{ psi}$$

$$c = \sqrt{E/p} = \sqrt{\frac{46.5\text{x}10^5 \text{ lb/in}^2}{450 \text{ lb-sec}^2/\text{ft}^4}}$$
$$= 1.2\text{x}10^3 \text{ ft/sec.}$$

$$T = 2L/c = \frac{(2)(82\text{in.})}{1.2\text{x}10^3 \text{ft./sec.}}$$
$$\doteq 1.1 \text{ msec.}$$

FIGURE 2.6 FUNDAMENTAL PERIOD OF PEDESTAL ASSUMING STRESS-WAVE PROPAGATION VELOCITY GIVEN BY $c = \sqrt{E/p}$

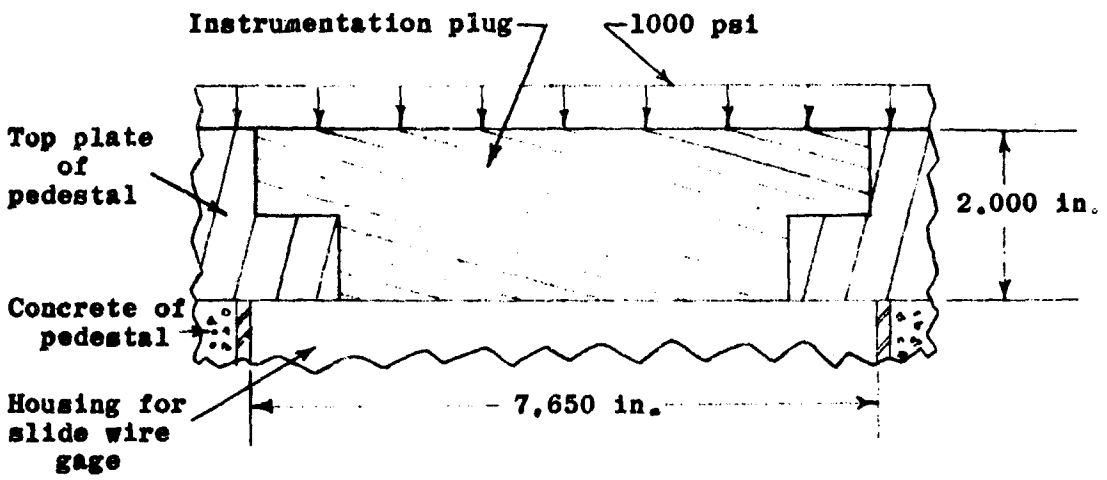

Basic relation $$w = \frac{(5+\nu)\,qa^4}{64(1+\nu)\,D}$$

where $D = Eh^3/12(1-\nu^2)$

Definitions

E = Young's modulus of steel
a = radius of plate
h = thickness of plate
q = applied load
ν = Poisson's ratio

$$w = \frac{(5 + 0.28)\,(1000\ \text{lb/in.}^2)\,(3.825\ \text{in.})^4\,(12)\,[1-(0.28)^2]}{(64)\,(1+0.28)\,(30\times10^6\ \text{lb/in.}^2)\,(2.0\ \text{in.})^3}$$

$$w = 0.00064\ \text{in.}$$

FIGURE 2.7 COMPUTATION OF DEFLECTION OF INSTRUMENTATION PLUG

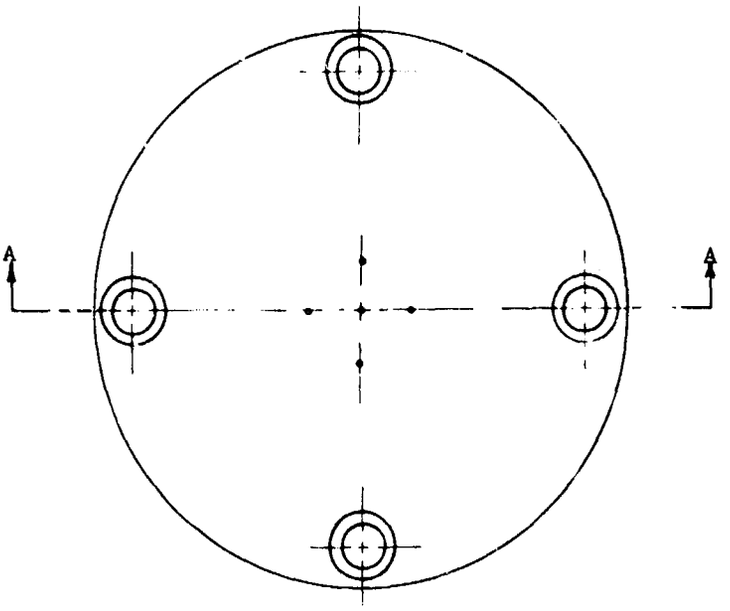

PLAN VIEW

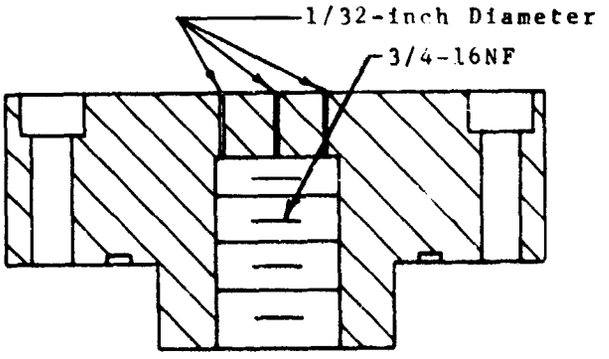

SECTION A-A

Full Scale

FIGURE 2.8 WORKING DRAWING OF SATURATING PLUGS

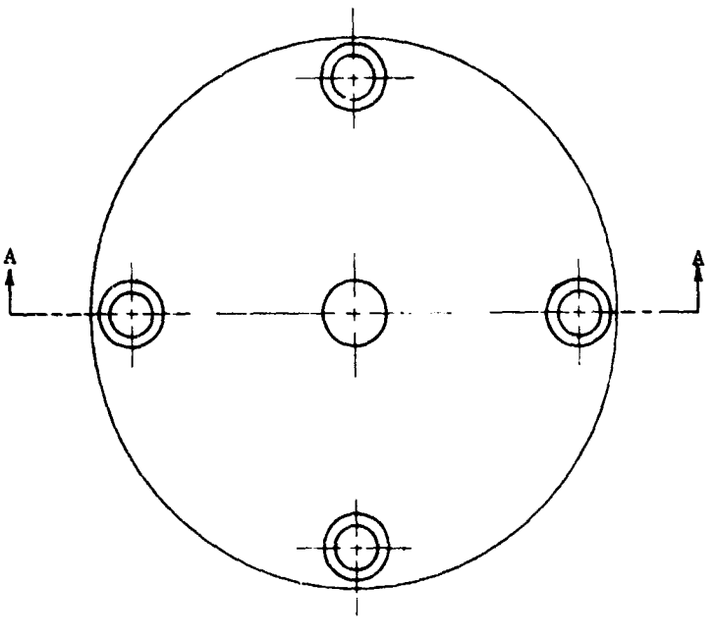

PLAN VIEW

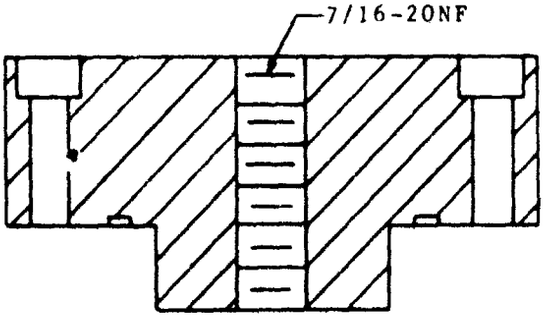

SECTION A-A

Full Scale

FIGURE 2.9 WORKING DRAWING OF DE-AIRING PLUG

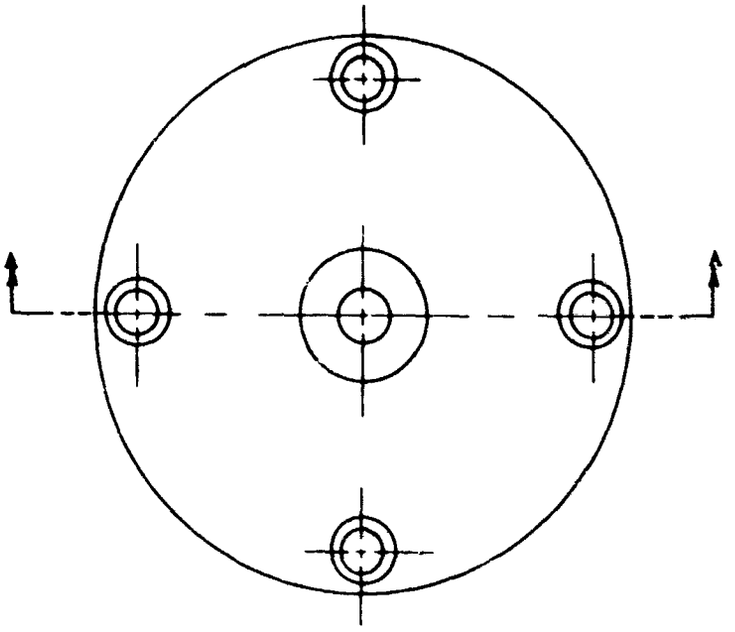

PLAN VIEW

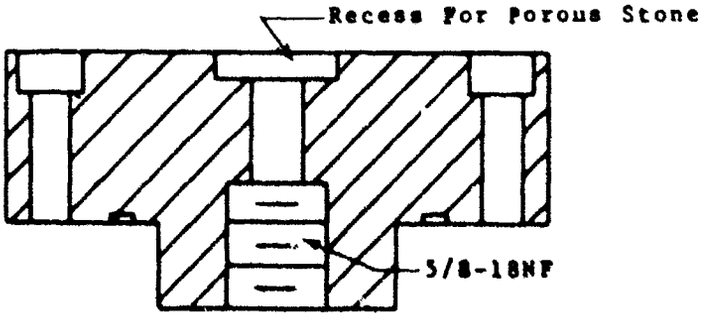

SECTION A-A

Full Scale

FIGURE 2.10 WORKING DRAWING OF PLUG WITH POROUS STONE

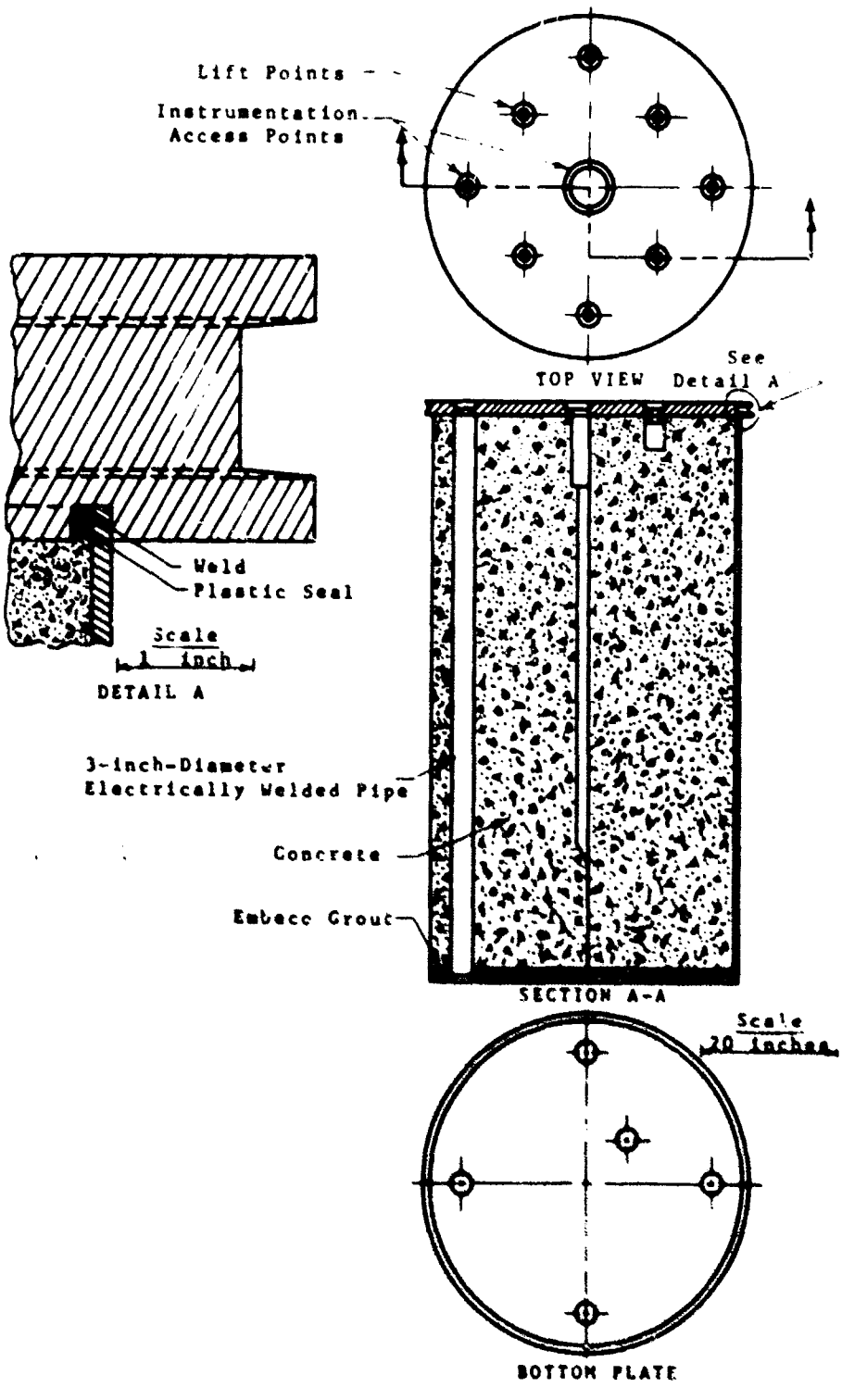

FIGURE 2.11 WORKING DRAWING OF CONCRETE PEDESTAL

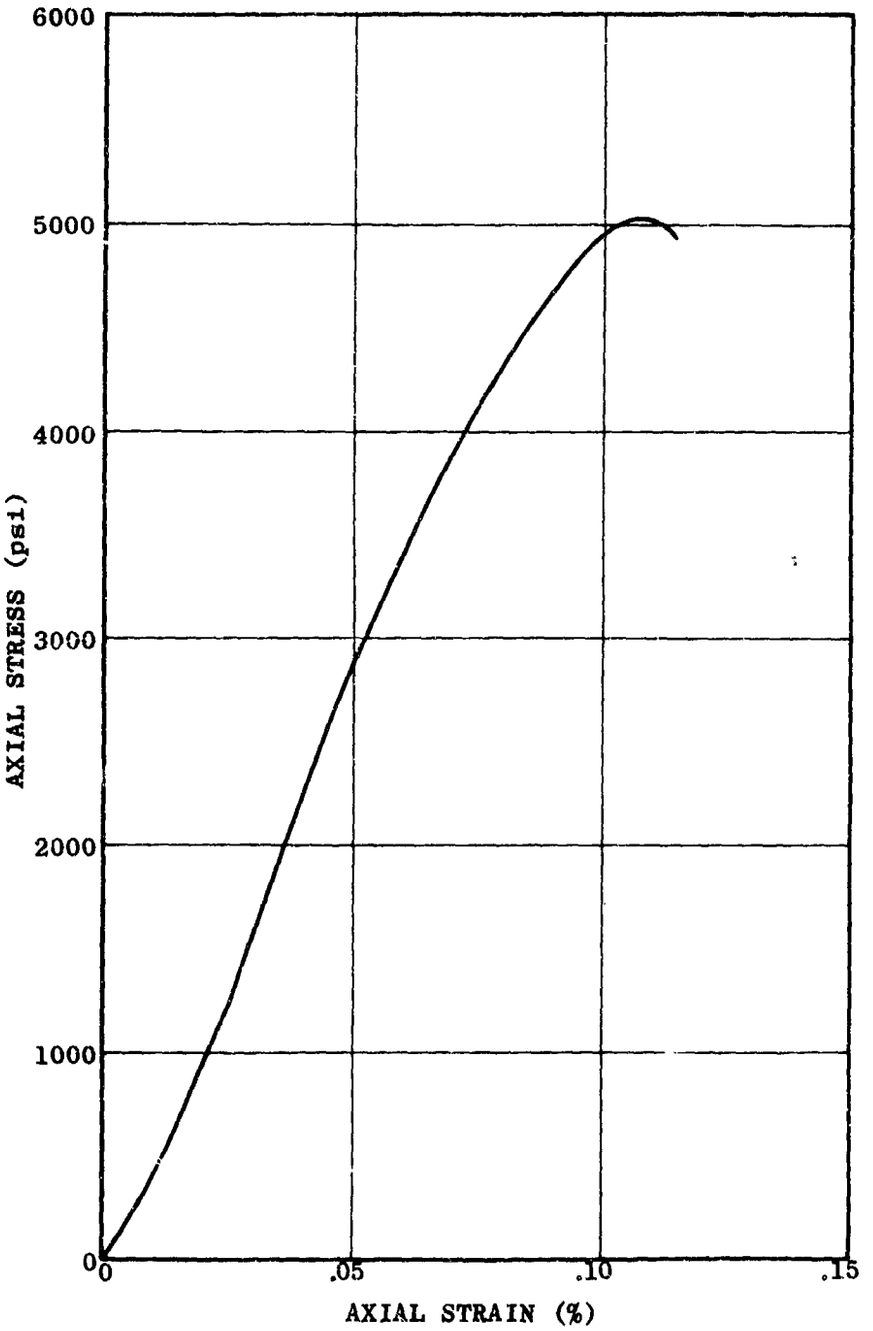

FIGURE 2.12 STRESS-STRAIN CURVE FOR TEST CYLINDER A

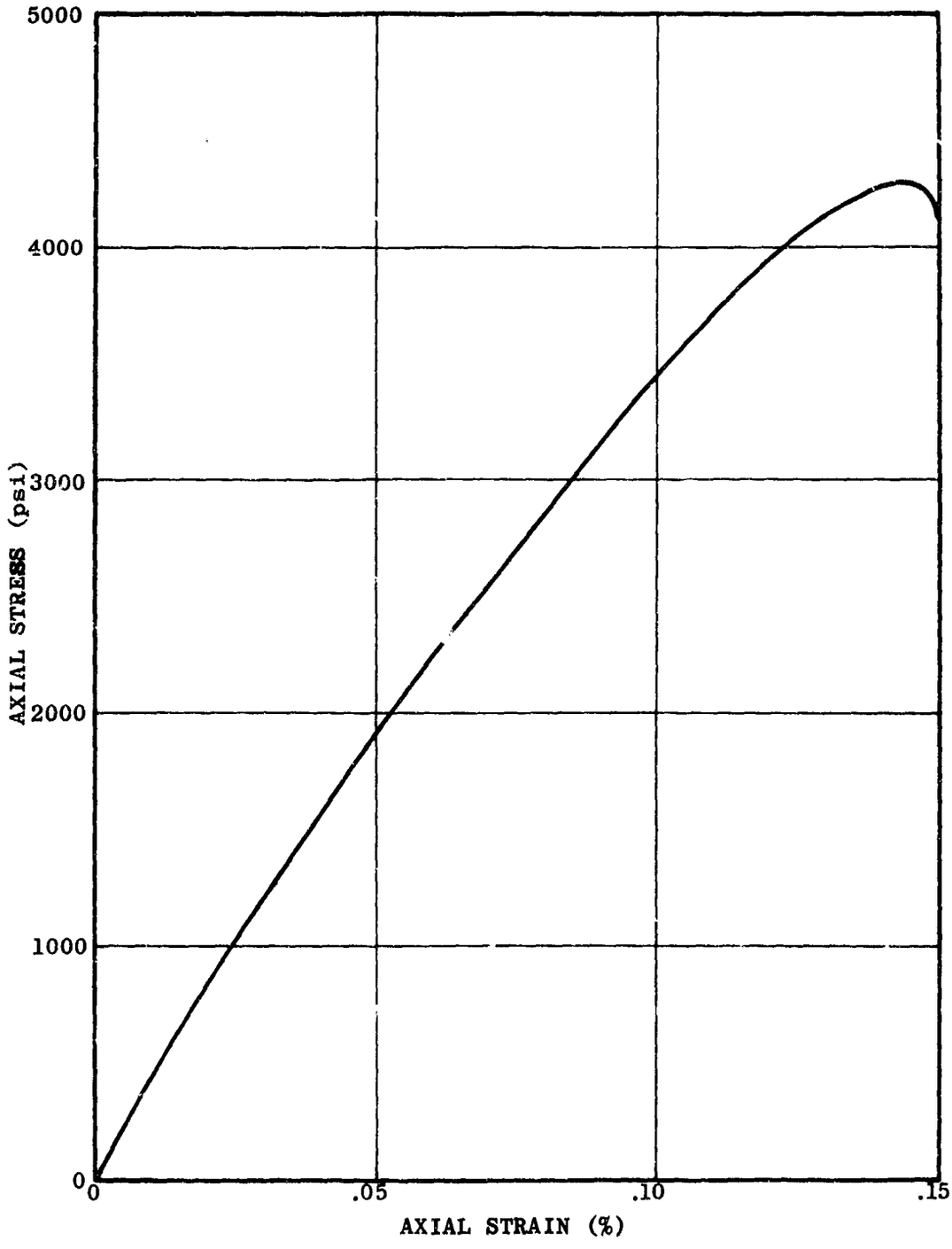

FIGURE 2.13 STRESS-STRAIN CURVE FOR TEST CYLINDER B

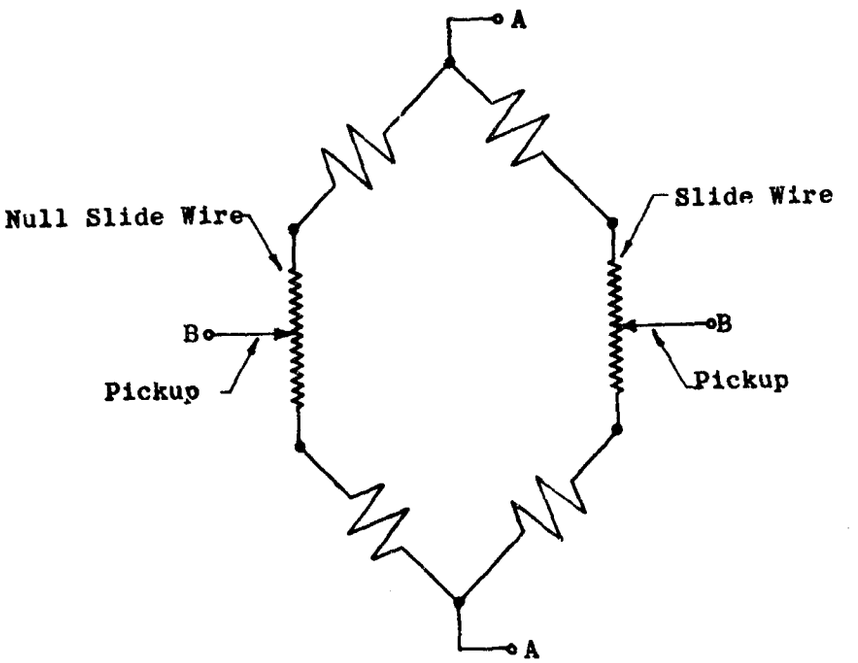

FIGURE 2.14 ELECTRICAL SCHEMATIC OF SLIDE WIRE GAGE

Basic relation

$$K = (1/6)(1-\nu_s^2)/(1-\nu_p^2)\ (E_p/E_s)(h/a)^3$$

where

K = relative rigidity of deformation plate to test specimen
ν_s = Poisson's ratio for test specimen
ν_p = Poisson's ratio for deformation plate
E_s = Young's modulus for test specimen
E_p = Young's modulus for deformation plate
h = thickness of deformation plate
a = radius of deformation plate

assume

$\nu_s = \nu_p$
E = 30,000,000 psi
E = 10,000 psi

then

$$K = (1/6)(1/1)(30,000,000/10,000)(1/8)^3(1/12)^3$$
$$= 0.0005$$

FIGURE 2.15 COMPUTATION OF RELATIVE RIGIDITY OF DEFORMATION PLATE

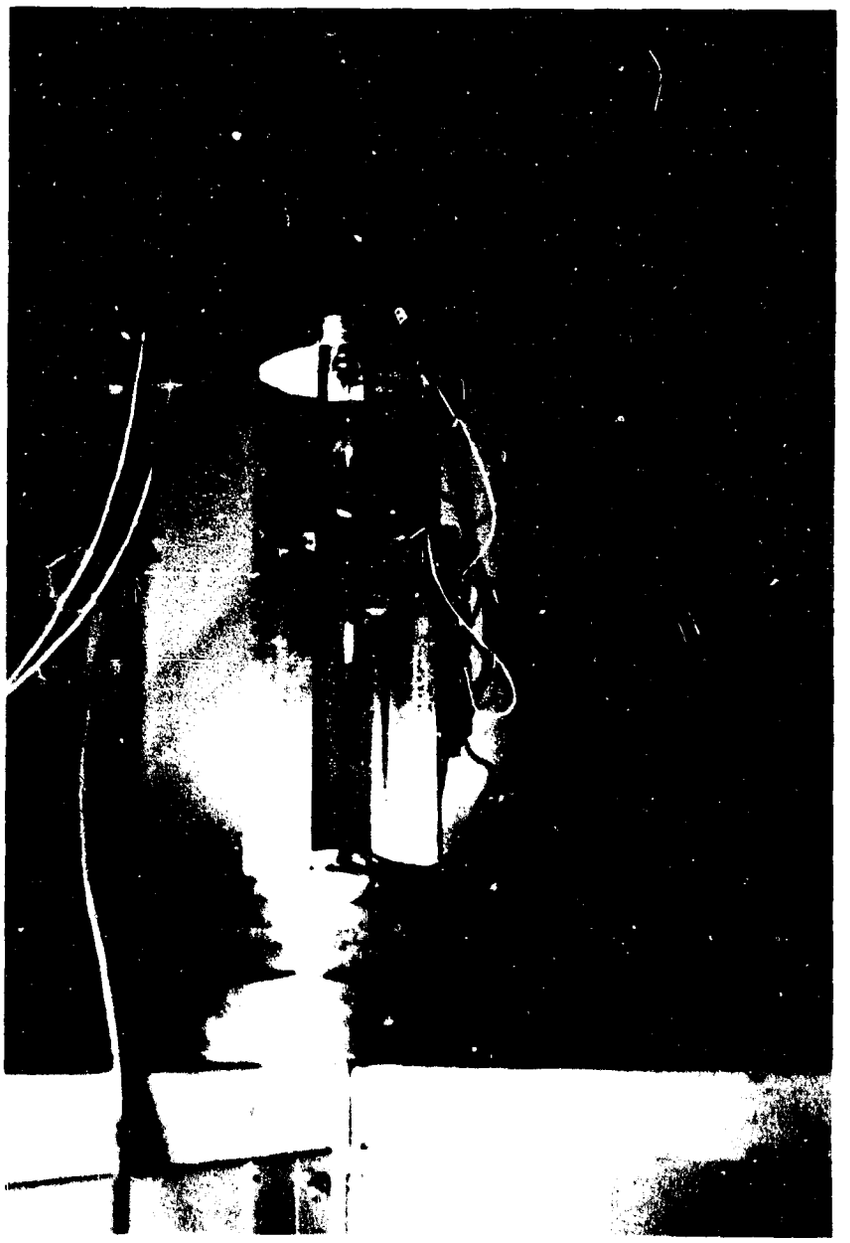

FIGURE 2.16 PHOTO OF SLIDE WIRE DEVICE

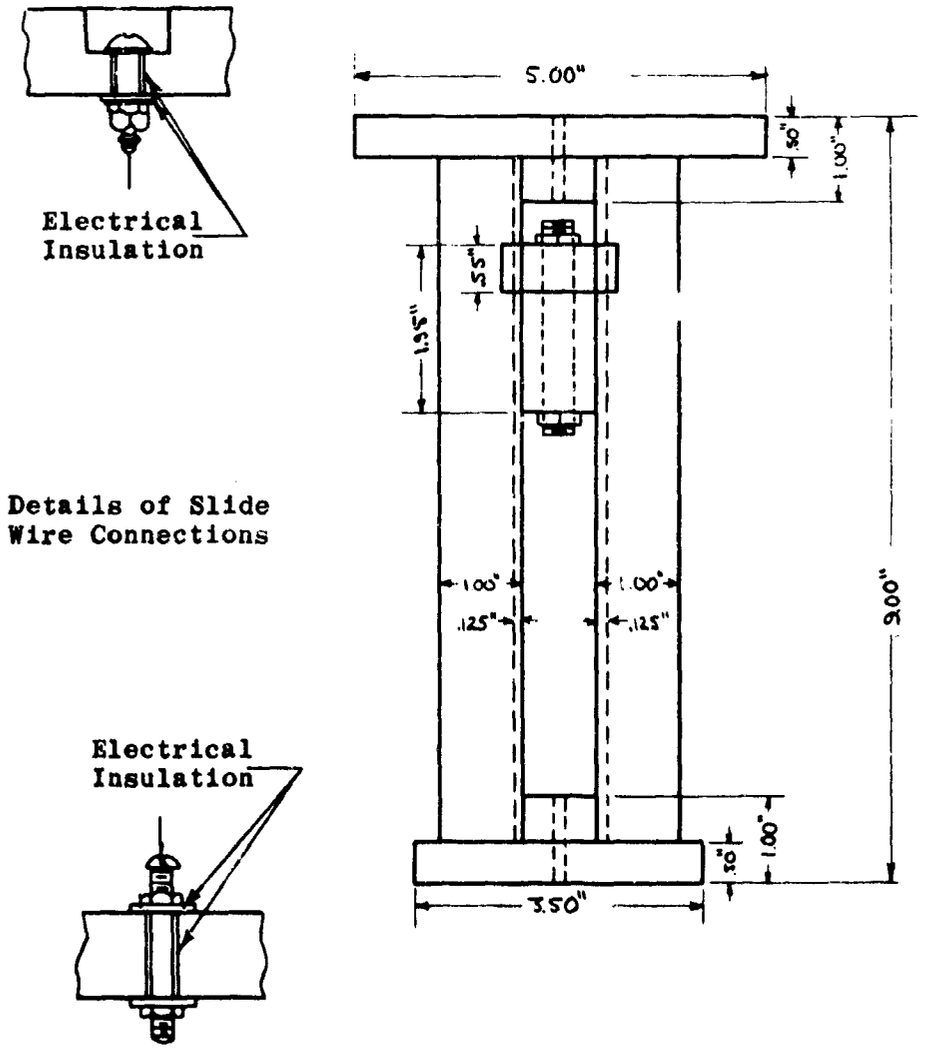

FIGURE 2.17 DETAILED DRAWING OF SLIDE WIRE GAGE

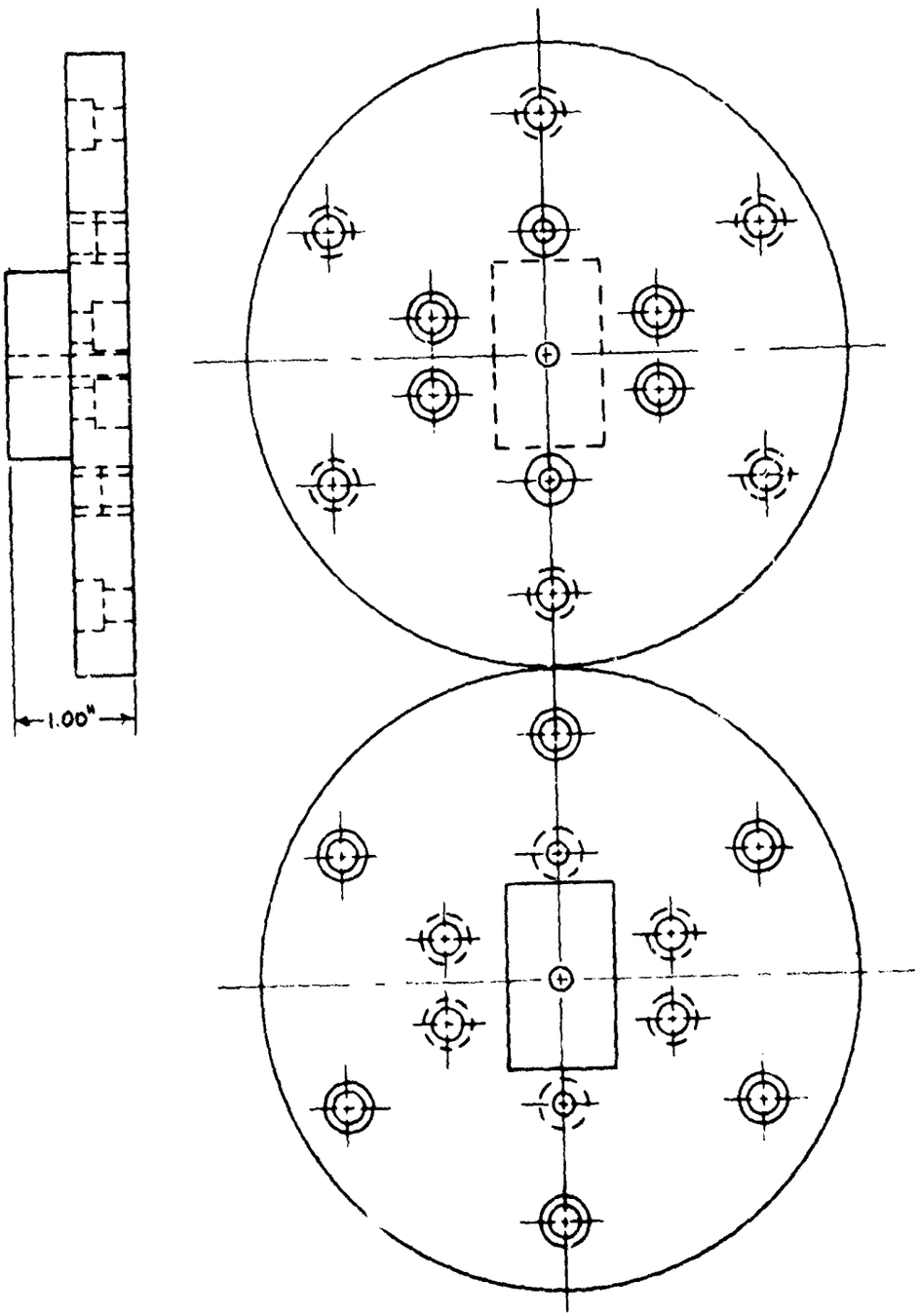

FIGURE 2.18 WORKING DRAWING OF TOP OF SLIDE WIRE GAGE

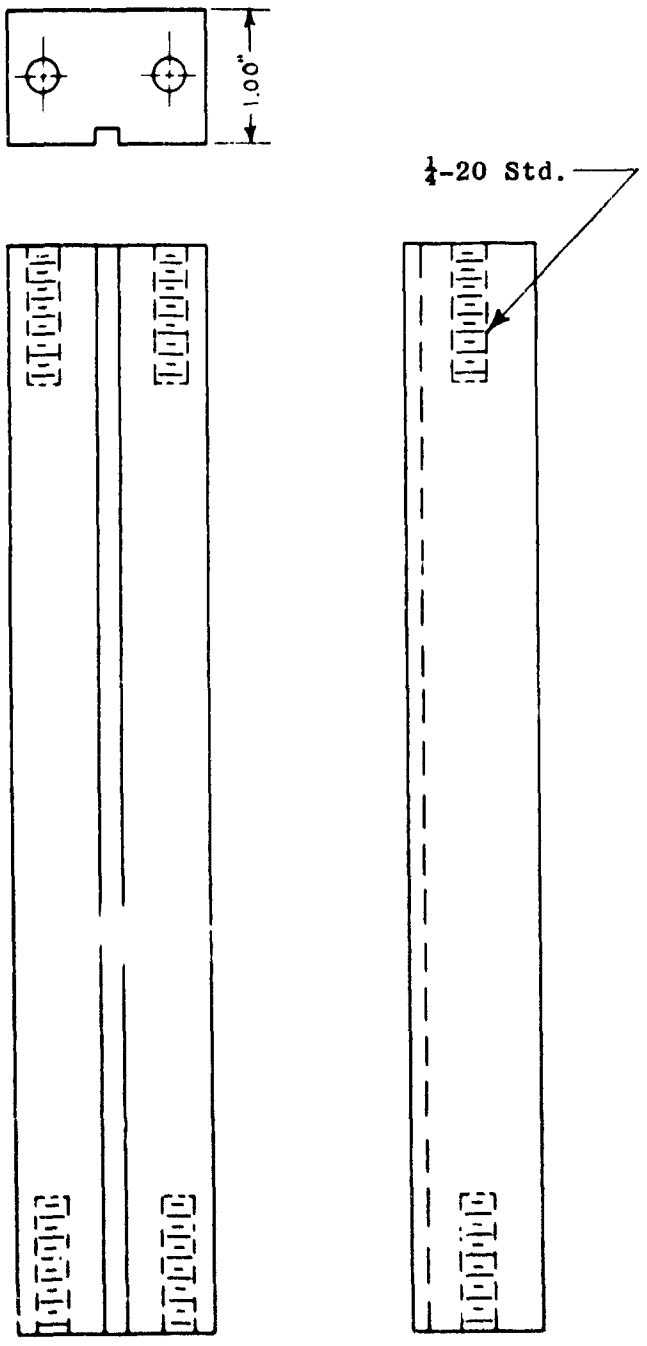

FIGURE 2.19 WORKING DRAWING OF RIB OF SLIDE WIRE GAGE

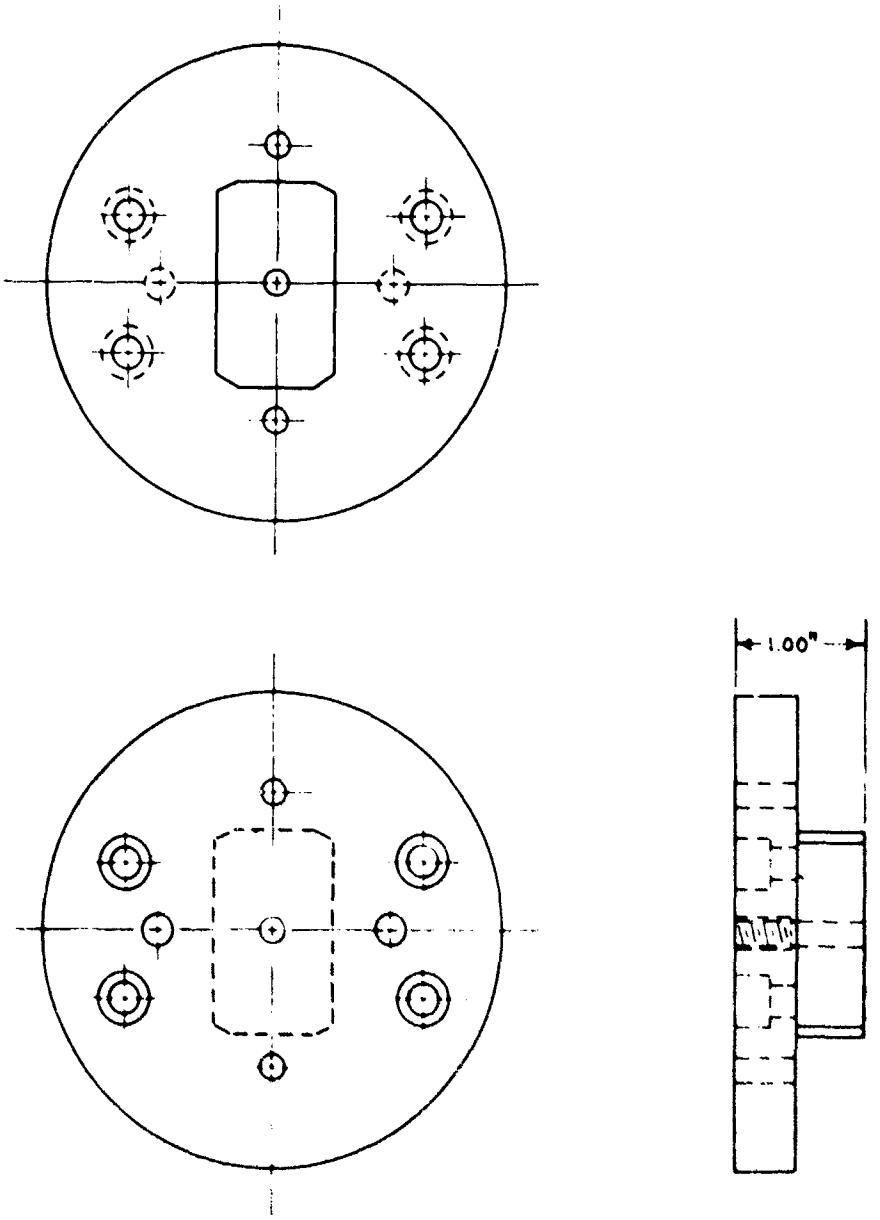

FIGURE 2.20 WORKING DRAWING OF BOTTOM OF SLIDE WIRE GAGE

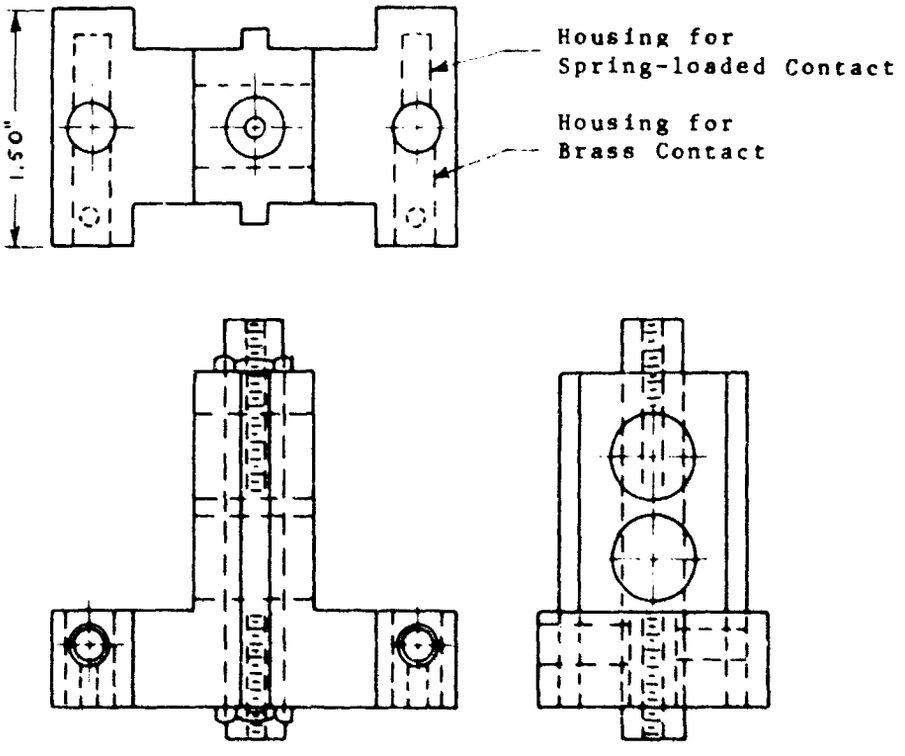

FIGURE 2.21 WORKING DRAWING OF SLIDE WIRE PICKUP

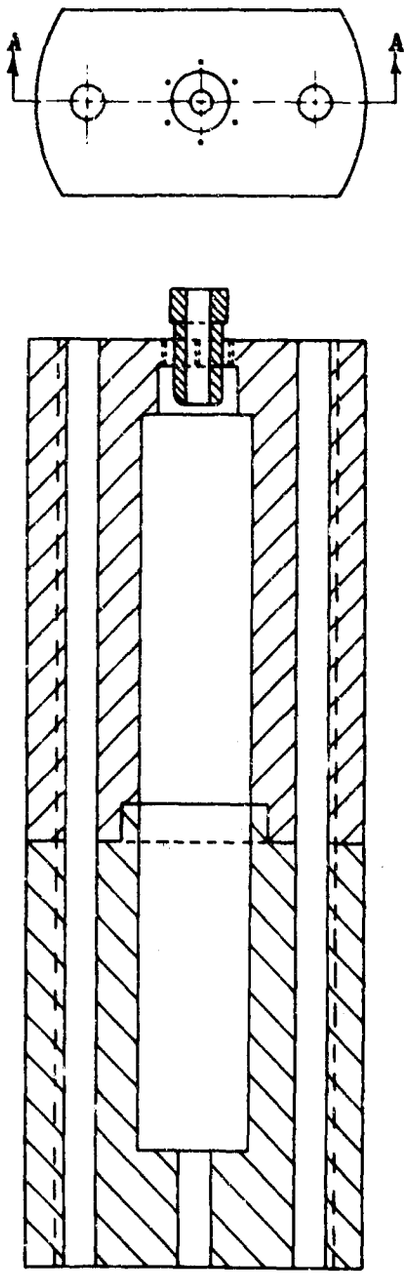

SECTION A-A

FIGURE 2.22 WORKING DRAWING OF LVDT MOUNT FOR SLIDE WIRE GAGE

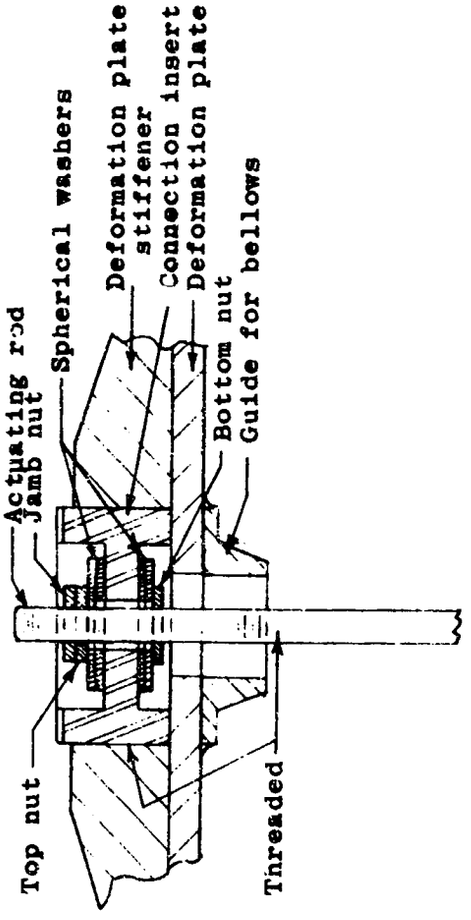

FIGURE 2.23 SKETCH OF CONNECTION BETWEEN DEFORMATION PLATE AND ACTUATING ROD

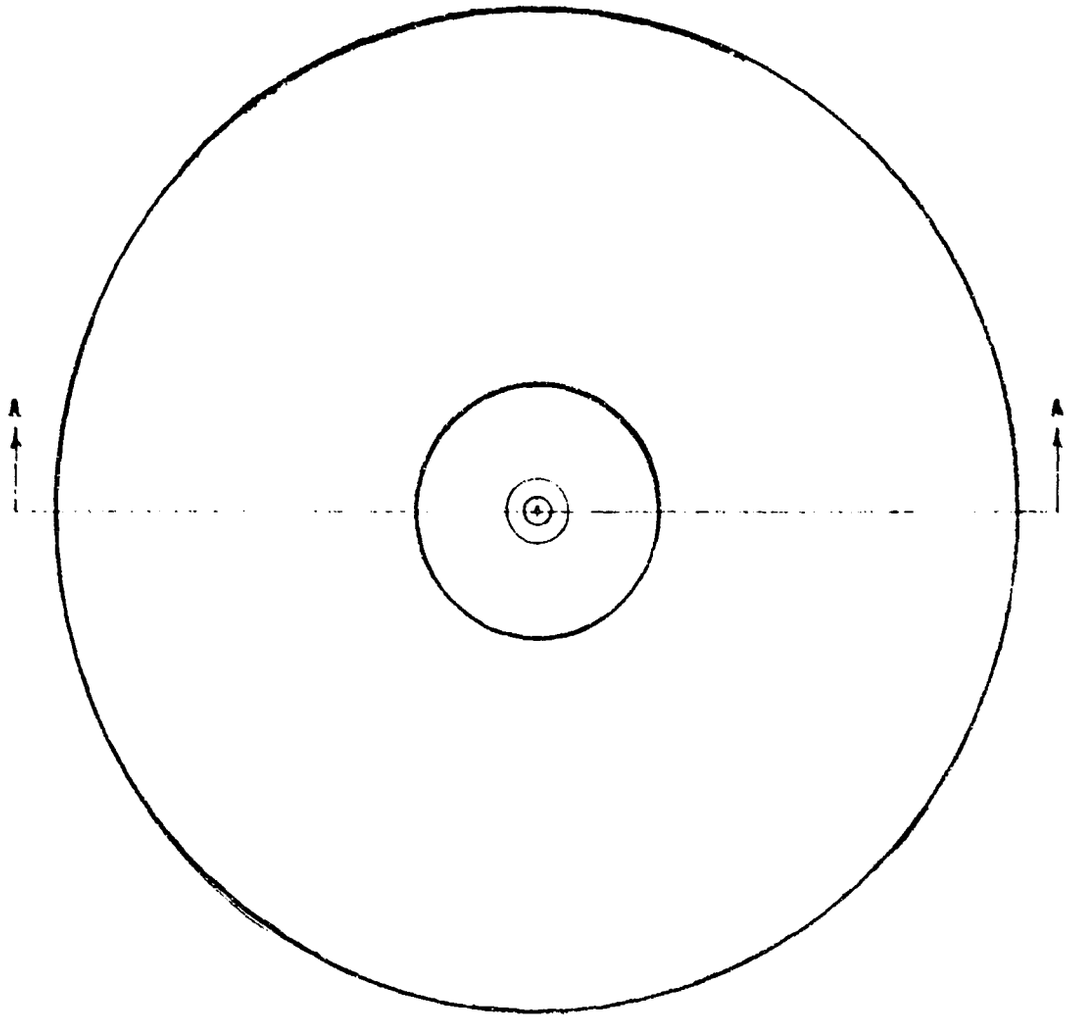

FIGURE 2.24 WORKING DRAWING OF DEFORMATION PLATE

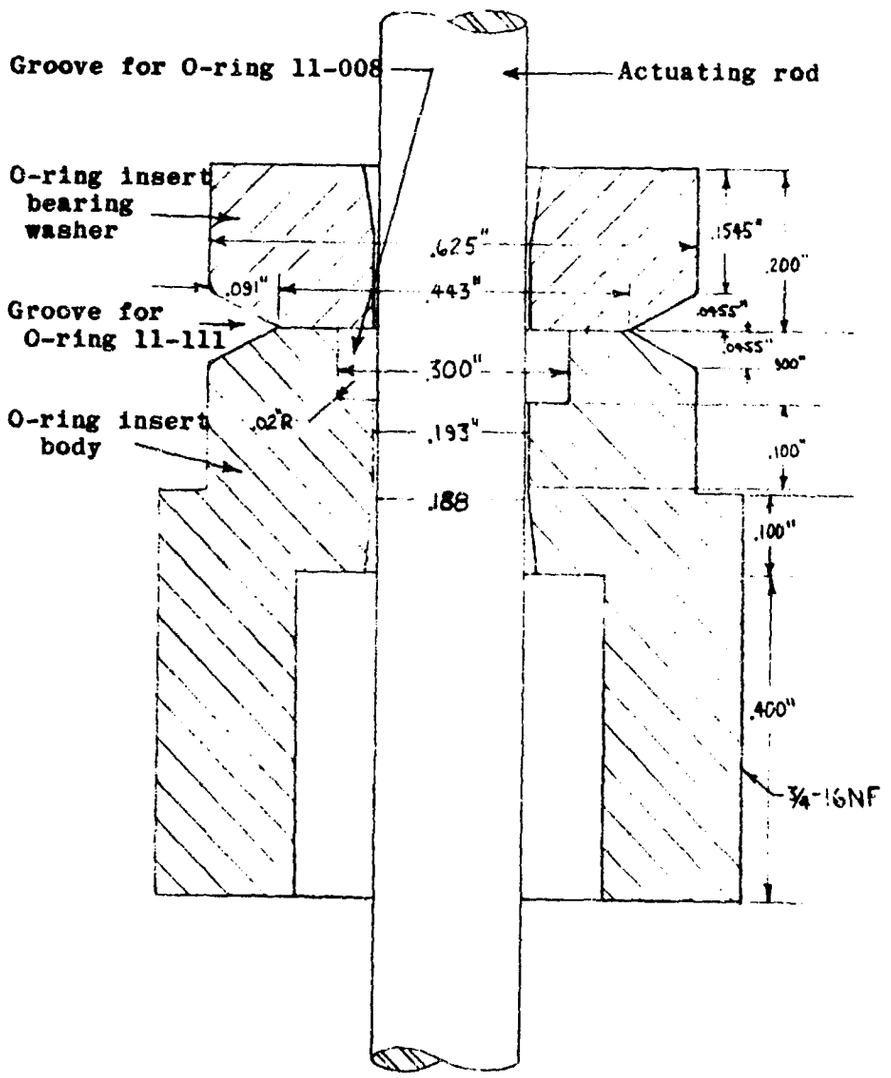

FIGURE 2.25 WORKING DRAWING OF SEAL FOR ACTUATING ROD

CHAPTER 3

PROOF-TESTING OF EQUIPMENT

3.1 INTRODUCTION AND SUMMARY

In order to determine the accuracy with which granular materials could be tested in one-dimensional compression in the DLG and to define and resolve problems associated with such testing, a proof-testing program was conducted on the slide wire gage without a soil specimen and on samples of Ottawa sand and crushed limestone.

The results of the testing program on the slide wire gage indicate that the slide wire gage has a threshold of 0.0003 inches and a repeatability of better than 99% as indicated by a percent deviation from the mean of less than 1%. The results of the testing program on Ottawa sand and crushed limestone indicated the following: 1) static test results obtained on Ottawa sand are nearly identical to those of other experimenters using the most sophisticated one-dimensional compression devices; 2) because of the variation in stresses along the axis of a specimen at early times during a dynamic test, only that portion of the record after 12 msec should be considered as representing an average dynamic stress and an average dynamic strain in the specimen; 3) the dynamic stress-strain behavior of a sample can be determined as accurately as the static stress-strain behavior with the device developed; and 4) special seating precautions must be exercised to prevent point crushing on the top plate of the pedestal and the deformation plate when testing large granular

materials, and when testing fine-grained soils, special seating precautions must be exercised to provide intimate contact between the deformation plate and the top of the soil specimen.

3.2 TESTING OF SLIDE WIRE GAGE

3.2.1 Static Testing

Prior to the utilization of the slide wire gage to measure deformation of a soil test specimen, the gage was tested statically to determine the threshold and repeatability of the instrument as defined by Cerni and Foster (1962).

The gage was first tested statically on the test stand shown in Figure 3.1. The slide wires constituted arms of 4-arm bridges as described in Section 2.3.2.1.3. The unbalance in the bridge induced by movement of the slide wire pickup was read on a BLH model 120-C portable strain indicator (PSI), and the movement of the pickup was measured by a 4-inch-travel Ames dial indicator which could be read to the nearest 0.0005 inches. Typical test results from a static proof test on the test stand are presented in Figure 3.2.

Based on the test results shown in Figure 3.2 and assuming that the BLH strain indicator can be read to the nearest division, i.e., to the nearest 1 μin/in, then the slide wire gage threshold was shown to be 0.0003 inches. This threshold corresponded to a strain of 0.0025% if the specimen being tested had a gage length of 12 inches. This threshold was demonstrated to be more than adequate for the testing of granular materials at stresses not exceeding 1000 psi since on the first cycle of

loading, the tangent modulus of the stiffest soils should not exceed 250,000 psi and should only approach this value at stresses near 1000 psi. Assuming a tangent modulus of 250,000 psi and a gage threshold of 0.0003 inches, the smallest pressure increment which could be manifested in a change in reading on a BLH strain indicator is 7.5 psi, which corresponded to a pressure sensitivity of more than 99%.

The repeatability of the slide wire gage was determined using a different testing arrangement in order to preclude, as nearly as possible, the effects of ambient temperature variation. The gage was mounted in the pedestal and the movement of the slide wire pickup was induced and measured by a 1-inch-travel micrometer mounted on an aluminum channel with nominal size of 5 x 2 inches and a weight of 4 lb/ft, as shown in Figure 3.3. The channel spanned 49 inches and some deflection and rotation of the channel occurred as the actuating rod was forced down by the micrometer; however, this factor was eliminated as nearly as possible by approaching the micrometer readings of interest in an identical fashion for each reading. Further, prior to testing, the force required to displace the slide wire pickup was measured and determined to be less than 0.1 lb, which corresponds to a deflection of the channel of less than 0.0001 inches assuming no rotation of the channel. The repeatability thus determined was greater than 99% as denoted by the percent deviation from the mean value.

3.2.2 Dynamic Testing

The slide wire gage was tested dynamically to ascertain that wiper lift would not occur and that the gage system could withstand dynamic forces

without deleterious effects such as yielding of the actuating rod or slide wires.

The test stand shown in Figure 3.1 was also used to proof-test the slide wire gage dynamically. For the dynamic proof-test, the slide wire gage was actuated by a gas-propelled piston which was electrically actuated. The pickup was subjected to a displacement of approximately 2 inches with a travel time of 13 msec. The slide wires constituted the arms of a 4-arm bridge as in the static tests, and the output was fed to B&F conditioning modules, then to Dana DC data amplifiers, and finally recorded on tape. Acquisition and reduction of dynamic data are discussed in Section 3.3.3.

A typical displacement-time curve for a dynamic test is presented in Figure 3.4. The trace is seen to be exceptionally clean with no wiper lift. The travel of the piston which displaced the pickup was halted by a rigid stop; therefore, to prevent damage to the pickup, the actuating rod and the piston were not connected in line but rather by an eccentric. This eccentric served as a source for some vibration at the end of the piston movement as may be noted at times greater than 7 msec.

No attempt was made to investigate the accuracy of the slide wire gage under dynamic conditions on the test stand because the inertial forces were so much higher than those to which the gage would be subjected to under actual testing conditions with a soil specimen. In addition, since the slide wire gage had been tested for threshold and reliability statically, and the slide wires were not strained any appreciable amount as would have been indicated by a change in tone of the slide wire when

plucked prior to and subsequent to the rapid displacement or by a different calibration factor upon recalibration, the dynamic characteristics of the gage exclusive of the deformation plate and actuating rod were assumed equivalent to the static characteristics already described. Theoretical considerations, as discussed in Sections 2.3.2.1.4 and 2.3.2.1.5 indicate that inertial effects with respect to the deformation plate and actuating rod-pickup system are not significant.

3.3 PROOF-TESTING OF SYSTEM WITH SOIL SPECIMEN

3.3.1 Proof-Testing Program

The proof-testing program as completed is delineated in Table 3.1. The program was designed to accomplish the following objectives: 1) provide stress-strain characteristics of a well-documented material such that a comparison between the results obtainable with the DLG and the results obtained by other experimenters was possible; 2) determine the accuracy obtainable with a soil as stiff as that which might be reasonably assumed to be of usual interest; 3) define any problems which might arise during the testing program; and 4) investigate the effect of seating error.

Static Tests S-1 and S-2 were conducted on 20-30 Ottawa sand in order to compare the test results with those of other experimenters. Dynamic Test D-1 was likewise run on 20-30 Ottawa sand to investigate the accuracy possible with a very stiff soil by comparing the results obtained with those of other experimenters. Static Test S-3 and Dynamic Test D-3 provided data on a very soft granular material. Static Test S-2, C-6 (cycle 6) provided test data on a very stiff material. Tests

S-3 and D-3 on crushed limestone employed no seating medium to prevent particle crushing against the deformation plate and the top of the pedestal and Tests S-4 and D-4 on crushed limestone were run with Hydrocal as a seating medium.

3.3.2 Specimen Placement

The specimen placement technique was essentially constant throughout the proof-testing program; therefore, unless otherwise noted, all test specimens may be assumed to be placed in accordance with the following described technique.

Prior to the specimen placement procedure, the slide wire gage was checked electrically for proper operation, and the actuating rod was checked for proper height so that it would not bottom out before the specimen experienced the estimated maximum deflection. If the specimen to be tested had been estimated to deform axially one inch, then the initial slide wire pickup position was set such that the pickup could move vertically downward at least one inch prior to coming to rest at the bottom stop. The proper length of 5/16-inch-diameter stainless-steel tube was selected, based on the specimen height and the predicted deformation, and installed. The stainless-steel tube was selected such that the clearance between the top of the tube and the bottom of the deformation plate was equal to approximately 1.5 times the predicted deformation for a given test. The protective bellows together with the steel support tube was then installed as shown in Figure 2.2.

The inner surface of the specimen container was washed with solvent and wiped dry. A thin coat of Lubriplate 630-AA grease, approximately 0.006-inches thick, was applied by hand to the inner surface of the speci-

men container. A clean 1/16-inch-thick, fiber-reinforced, neoprene-rubber liner was placed against the wall of the soil container and taped at the lap; the liner was held in place by the grease. The container liner was 13.125-inches high while the container was 14.000-inches high. Thus the container was unlined over the top 0.875 inches; this unlined portion of the container was required to prevent rupture of the loading diaphragm as will be explained below.

Placement of the soil specimen was started after installation of the container liner. Two different techniques were utilized in the placement of the soil. The first technique was utilized only with the Ottawa sand specimens and employed a sprinkling device, more commonly referred to as a rainer. A detailed working drawing of the rainer is presented in Figure 3.5. The rainer was connected, by a 2-inch-diameter hose, to an eight cubic foot mobile storage bucket which was suspended over the specimen container by a travelling crane. The rate of flow of the sand was controlled by the vertical position of the 2-inch-diameter disk on the threaded rod. The height of fall from the last screen to the surface of the soil specimen was maintained at 22 inches for Test S-1 and 24 inches for Test S-2.

The second placement technique was utilized with all specimens other than those composed of dry Ottawa sand. This technique employed a pneumatic tamper with a steel foot 8-1/2 inches in diameter. A photo of the tamper with the foot in place is presented in Figure 3.6. The soil was placed in the container in 4- to 5-inch uncompacted lifts and then compacted with the tamper, the tamper moving continuously over the entire surface of the specimen.

As the height of the specimen was increased by additional lifts of material being placed, the height of the bellows was adjusted such that after placement, the top of the bellows was flush with the top surface of the soil specimen. With the specimens of Ottawa sand, upon attaining a specimen height of approximately 12 inches, the surface of the specimen was struck off to 12 inches to the nearest 1/32 inch, and the deformation plate was placed on the surface of the specimen and attached to the actuating rod. The remainder of the soil specimen container was then filled with Ottawa sand and struck off even with the top of the soil container. The unit weight of the specimen was determined by weighing the amount of soil required for the 12-inch-high specimen and knowing the volume of the container occupied by the specimen.

With materials other than dry Ottawa sand, when the desired height of the specimen had been obtained, the height from the top of the specimen to the top of the container was determined by taking the average of at least eight measurements made over the surface of the specimen to the bottom of the aluminum beam, which was also employed in slide wire gage calibration, spanning the container. The straightness of the aluminum beam was checked against the bearing plate for the DLC soil container and the measurements to the specimen surface were made to the nearest 1/32 inch, resulting in an accuracy in the measurement of the initial specimen height of about 99.7% assuming a 12-inch-thick specimen.

The deformation plate was placed on the surface of the soil specimen and attached to the slide wire gage actuating rod. An interface membrane 48 inches in diameter was placed over the soil specimen and deformation plate, and then a second interface membrane 50 inches in diameter was placed over the first with the full inch of overlap carefully turned up against

the container wall. Ottawa sand was employed to fill the remaining height of the soil container. The Ottawa sand used to top off the container was utilized as cushion for the loading diaphragm since, if the loading diaphragm were to bear directly on such materials as crushed limestone, the diaphragm would be ruptured by the sharp particles or would exceed its tensile strength in being extruded into the voids near the surface of the specimen.

When the container was filled and the sand cushion struck off even with the top of the soil container, the sand was vacuumed away from the 1/2 inch round at the inside top edge of the soil container. The round edge and the clamping ring O-ring groove were greased with Lubriplate 630-AA grease, and the clamping ring O-ring and loading diaphragm were placed and clamped by the clamping ring. Following placement of the seal ring O-ring, the preparation of the soil specimen and container was complete, and the container was moved into place beneath the machine as described in Appendix B.

3.3.3 Test Procedure and Data Reduction

3.3.3.1 Static Tests

Following placement of a test specimen as described in Section 3.3.2, the specimen container was moved into place beneath the loading machine; the seal ring was bolted to the support system; and the necessary gas and electric lines were connected. All ports in the seal ring except Nos. 4 and 8 were blocked off. Gas was fed into the expansion chamber through port No. 8 and Bourdon-type pressure gages were attached to a line running from port No. 4. Axial pressure was applied to the top of a test specimen by manually opening a valve and allowing gas to pass into the expansion chamber with the main valves in the closed position so that pressurizing of the

charging chamber as well as the expansion chamber was not necessary. A detailed description of the mechanics of the DLG is presented in Appendix B. When a given pressure was attained, the deformation of the soil specimen was measured by noting the change in the slide wire gage reading on a BLH Portable Strain Indicator. The final strain reading at a given pressure level was recorded when the rate of deformation criterion for the particular test was satisfied. After the final strain reading at a particular stress level had been taken, the pressure was increased to the next stress level of interest and the corresponding deformation noted as already described. This procedure was continued to the highest stress level of interest. The unloading of a test specimen was accomplished in a similar manner. The pressure acting on a test specimen was decreased by bleeding off the gas until the pressure level of interest was reached. When the rate of rebound criterion for the particular test was satisfied, the final strain reading was recorded and the unloading process continued.

The specimen pore pressure was noted during testing by a Bourdon-type pressure gage which was connected to the porous stone instrumentation plug described in Section 2.2.1.4. The pore pressure did not become large enough to measure in the unsaturated tests unless the loading diaphragm leaked, in which case the test was stopped and the diaphragm was replaced.

In some instances test specimens were saturated prior to loading. The specimen was saturated following placement beneath the loading machine by addition of water through the perforated instrumentation plugs described in Section 2.2.1.4. Water was added until the specimen was saturated to the level of the sand cushion which was approximately the same level as the de-airing line. The de-airing line was composed of a 1/8-inch-diameter

copper tube passing from the de-airing instrumentation plug, which is described in Section 2.2.1.4, up through the test specimen to the level of the deformation plate. The open end of the tube was covered with a lead plate to prevent punching through the interface membrane as shown in Figure 3.7. A copper tube was connected to the bottom of the de-airing instrumentation plug and extended outboard of the soil container to the approximate level of the deformation plate in order that the hydrostatic pressure level at the surface of the test specimen was approximately zero. Prior to taking deformation readings on saturated test specimens, the de-airing line was checked to ascertain that the flow of water from the test specimen initiated by the deformation of the specimen had stopped. In tests in which the specimen was saturated after loading but prior to unloading, the procedure was similar, the only difference being the maintaining of pressure on the specimen during saturation.

The raw data from a static test consisted of pressure readings and deformation readings. The pressure readings required no correction as the Bourdon-type gage was periodically calibrated and adjusted as necessary. The deformation readings were converted to actual deformations by multiplication by the gage calibration factor which was determined prior to and subsequent to each test using the beam and micrometer as described in Section 3.2.1. The deformations were then converted to strains by dividing by the initial height of the specimen. The test results were then portrayed by plots of axial pressure versus axial strain. The computations for a static test and the axial pressure-axial strain plot are presented in Figures 3.8 and 3.9.

3.3.3.2 Dynamic Tests

The test procedure for a dynamic test with respect to placement of the specimen under the loading machine was identical to that for static tests except that the hookup of the electrical leads and gas leads was modified such that the application of the gas pressure and the data recording were electrical rather than manual. The deformation and pressure measuring systems are described in Section 2.3. During dynamic testing, a minimum of four ports were utilized in order to obtain a measure of the average pressure over the top of the specimen, and to preclude the loss of data for a test in case a pressure transducer malfunctioned. The ports usually utilized were 1, 3, 6, and 12, thus providing measurements directly beneath machines 3 and 5 and in-between machines 1 and 2, and 6 and 7. The axial pressure on the test specimen was taken as the average of the pressures measured at the four ports. The connections to ports 4 and 8 as described for static testing were maintained. These static connections were utilized for the application of static preload when simulating a field specimen at some depth below ground surface. The static connections were also used for the determination of the axial pressure on the test specimen after the electrical measuring system had been shut off some time after the axial pressure had been decayed to a value less than one-half of the maximum peak axial pressure. In the former case, the decay was accomplished as in a static test, and in the latter case, usually only that deformation corresponding to zero dynamic overpressure was noted.

During dynamic testing, monitoring of the specimen deformation was completely automated. The unbalance in the Wheatstone bridge circuit,

of which the slide wire gage was a component part, was first nulled by the null slide wire described in Section 2.3.2.1.3. Then, during the test, the unbalance in the bridge brought about by movement of the slide wire pickup was input to a B and F transducer conditioning module, Model 1-211A8-1. The conditioning module was used to apply a well-regulated excitation voltage to the bridge by means of an isolated power supply and to apply a calibration step to the tape recorder immediately prior to a test. The output from the transducer conditioning module was input to a Dana DC Data Amplifier, Model 3500. The amplification factor was adjusted such that the anticipated output from the slide wire gage would be sufficiently large to drive the recorder yet not so large as to overdrive the system. The output from the data amplifier was input to a Sangamo Model 4712 tape recorder.

As was described in Section 2.3.2.1.2, the deformation measuring system was designed such that if the slide wire gage did not prove satisfactory, the deformations could be monitored by a LVDT. The LVDT was employed during proof-testing of the slide wire gage, but because of the satisfactory performance of the slide wire gage, the LVDT was not employed during the testing of soil specimens.

The LVDT was connected electrically so that it opposed an identical LVDT mounted external to the soil container. Thus, prior to dynamic testing, the output of the inbosrd LVDT could be nulled to facilitate recording of the output during a test. The LVDT's employed were Schaevitz Engineering, Type 500S-L, with a 1-inch linear travel when excited by 6 volts (rms), at a frequency of 3,000 cps; however, for this study, the LVDT was excited by a 3-volt (rms), 20,000-cps source. The deviation from the design

specifications, with respect to excitation, resulted in a reduction of the linear travel to 0.4 inches. The excitation and signal amplification were supplied by a Consolidated Electrodynamics Corporation (CEC) Carrier Amplifier Type 1-127. The operation of the LVDT was identical for the static and dynamic tests with the exception of read-out. During static testing, the voltage differences brought about by movement of the core were measured on a Vidar 500 integrating digital voltmeter. During dynamic testing, the voltage differences were recorded on tape.

The raw data from a dynamic test consisted of axial pressure-time data and axial deformation-time data recorded on tape. The data was taken from tape and electrically plotted to scale. The axial pressure-time plots for the different pressure transducers were averaged and then axial pressure-strain curves were constructed by noting the pressure and deformation of the test specimen at common times. The deformation was converted to strain by dividing by the initial specimen height or the height of the specimen immediately prior to application of the dynamic pressure increment if a static preload had been applied.

Raw data from a dynamic test is presented in Figures 3.10 through 3.13. The reduction of this data is presented in Figure 3.14, and the resulting axial pressure-axial strain curve is presented in Figure 3.15.

3.3.4 Proof-Test Results

3.3.4.1 Comparison of Test Results with Those of Other Experimenters

To provide a comparison of the test results obtainable with the DLG with those of other experimenters employing other devices, static and

dynamic tests were performed on 20-30 Ottawa sand. This sand was selected as a test sample primarily because a number of experimenters have published the results of one-dimensional compression tests on the sand. Ottawa sand is a well-rounded, even-textured, quartz sand and is readily available from a quarry of St. Peter sandstone near Ottawa, Illinois.

A summary of the static and dynamic tests performed on Ottawa sand in the DLG is presented in Table 3.1. The specimens for Tests S-1 and S-2 were placed with the rainer as described in Section 3.3.2. The initial relative densities of the test specimens were 67.0 and 80.6% for test specimens 1 and 2, respectively. The computed relative densities are based on an assumed specific gravity of solids G_s of 2.65, and maximum and minimum relative densities of 0.739 and 0.445, respectively, as reported by Prendergast (1968). The relative densities were determined in accordance with methods recommended by Bauer and Thornburn (1962). The resulting stress-strain curves for Tests S-1 and S-2 are presented in Figures 3.16 and 3.17, respectively.

As standards for comparison, test results utilizing four different devices were selected. The first results considered were those published by Whitman (1964).

The results presented by Whitman are derived from a variety of sources and the data suffers from sidewall friction, as pointed out by Whitman, and probably seating error and compressibility of the loading assembly. The initial density of the Ottawa sand was 103.5 pcf. The test results are presented in Figure 3.18.

United Research Services (URS) developed two different devices for the testing of materials in one-dimensional compression. The first

device to be considered employed a fluid boundary and is reported on by Durbin (1964). The results of three tests on Ottawa sand by Durbin are presented in Figure 3.19.

A second device which utilized a segmented ring specimen container employed by URS is reported on by Zaccor, et al. (1965). The results of two tests on Ottawa sand by Zaccor, et al., are presented in Figure 3.20. This device suffered rigid cap loading; however, the gage length of 14.3 inches was sufficiently large that with reasonable care in specimen preparation, any error was insignificant.

The last device used for comparison of test results is that developed by Hendron (1963). Tests on Ottawa sand were performed by Prendergast and Emerson and reported in part by Prendergast (1968). The results of these tests are presented in Figure 3.21. This device suffers from solid cap loading and sidewall friction; however, it is the one device which employs controlled lateral strain and for the purpose of this investigation no lateral strain was allowed to occur.

The stress-strain characteristics as determined by all devices cited above are presented in Figure 3.22. The results obtained using Durbin's fluid boundary device are obviously in error, probably primarily because the criterion of zero radial strain was violated. Whitman's results are seen to approximate those obtained by taking the stiffest results obtained using Hendron's device, thus implying that the criterion of zero radial strain is approximated These test results obtained using Zaccor's segmented ring device are in excellent agreement with those obtained utilizing the DLG as illustrated in Figure 3.23. In Fig. 3.23, the origin for the stress-strain curve obtained using the DLG was shifted to that

strain corresponding to an axial pressure of 5 psi as Zaccor, et al. (1965), reported utilizing a seat load of from 5 to 10 psi to stabilize the soil column with the rings in place prior to the removal of the ring holder.

Thus comparison of the one-dimensional behavior of Ottawa sand as measured by the various devices indicates good agreement between Zaccor, Hendron, and the DLG with the best agreement between Zaccor and the DLG. The conclusion that the test results obtained with the DLG are valid can also be reached by examination of the most probable sources for error. The axial pressure was applied to the top of the test specimen by a gas acting on a flexible neoprene diaphragm and was, therefore, uniform over the top surface of the test specimen. Deformations were monitored by means of a deformation plate riding on the top surface of the test specimen, see Section 2.3.2.2. The top surface of the specimen was carefully smoothed prior to placement of the deformation plate, and the deformation plate was extremely flexible relative to the test specimen so that seating error with respect to the deformation plate was not of consequence. Further, the large gage length (12 inches) minimized such errors. Radial deformation of the test specimen because of deformation of the soil container in the radial direction was negligible because of the large specimen diameter and the very stiff container. Sidewall friction was not a significant problem with the DLG as discussed in Section 2.2. Finally, stiffness of the device was of no concern because the deformation measuring instrumentation is independent of the specimen container and loading device.

Test S-2 on Ottawa sand consisted of six cycles. Subsequent to the last cycle, C-6, the DLG was rigged for dynamic testing and Test D-1

was conducted. The purpose of Test D-1 was to demonstrate the ability of the DLG to measure small total deformations and to provide dynamic test data for a material of known stress-strain behavior in order to allow a comparison of results of dynamic behavior as measured by the DLG with the known behavior.

Test D-1 consisted of two cycles. Cycle C-1 consisted of a dynamic pressure increment of approximately 50 psi and an initial static preload of 50 psi. Cycle C-2 consisted of a dynamic pressure increment of approximately 200 psi and an initial static preload of 50 psi. The pressure-time plots for Test D-1, C-1, and D-1, C-2, are presented in Figures 3.24 and 3.25, and the stress-strain curves for these two tests are presented in Figures 3.26 and 3.27. These stress-strain curves are presented together with the results from Test S-2, C-6, in Figure 3.28. The origins for the two dynamic tests correspond to a pressure of 50 psi, which was the preload, and an initial axial strain which was estimated from the cyclic data presented in Figure 3.17. The specimen utilized in Test D-1, C-1, and D-1, C-2, was the same specimen used in Test S-2; i.e., following the completion of cycle six of Test S-2, the DLG was hooked up for dynamic testing and Test D-1 was run.

The agreement seen between the dynamic tests and the static test is good, and since there should not be any variation between the static and dynamic behavior of Ottawa sand, it may be concluded that the dynamic results obtained with the DLG are of the same order of accuracy as the static results.

3.3.4.2 Investigation to Define Incidental Problems

In order to define any incidental problems which might occur with the DLG and related equipment during the testing of typical materials, static and dynamic tests were performed on Ottawa sand and crushed limestone which represented the stiffest and the softest materials that were likely to be encountered in our testing program. Tests S-2, C-6, (Figure 3.17) D-1, C-1, (Figure 3.26) and D-1, C-2 (Figure 3.27) demonstrate the static and dynamic behavior of Ottawa sand. Tests S-3 (Figure 3.29) and D-3 (Figure 3.30) demonstrate the static and dynamic behavior of crushed limestone.

The results of the static tests on the soft specimens indicated the existence of one major problem in that the softer specimens deformed axially to such an extent that the loading diaphragm, which rested on the top surface of the test specimen, was ruptured. The rupturing of the loading diaphragm also occurred in the dynamic tests on the softer specimens. The results of the dynamic tests on the soft and stiff materials demonstrated the existence of nonuniformity of stress conditions due to wave propagation effects throughout the test specimen during early times in the tests.

The rupturing of the diaphragms when testing softer specimens was determined to have basically two origins. The first resulted from the large particle size of the soft specimens rather than the stiffness of the specimens. The large voids between the individual particles allowed the interface membrane to be extruded into the voids and in some instances to be torn. After the membrane was torn, the cushion sand trickled down into the test specimen until the loading diaphragm was itself extruded

into the test specimen and ruptured. The second resulted from the discontinuity at the loading diaphragm-sand cushion-soil container interface. This interface is illustrated in Figure 3.31. One problem at this interface was the existance of sand grains between the one-half-inch round and the loading diaphragm. These sand grains would not perforate the diaphragm but would give rise to stress concentrations and cause excessive wear of the membrane. The second problem at this interface resulted from the limited area over which the loading diaphragm could distribute the deformation required to allow it to follow the top surface of the test specimen. As the test specimen deformed axially, the deformation of the loading diaphragm was restricted primarily to that small area where the diaphragm was in direct contact with the steel container because the diaphragm would not slip on the surface of the sand cushion when under pressure. As a consequence of the small area over which to distribute the deformation of the loading diaphragm, the diaphragm was often ripped in spite of its allowable elongation of more than 500%.

The problems arising because of the discontinuity at the loading diaphragm-sand cushion-soil container interface could have been easily solved by the use of a collar underneath the loading diaphragm, as shown in Figure 3.32, the collar being made from very strong, flexible, tough, and impermeable material. The collar would require strength so that it could slide over the sand cushion rather than tear, flexibility so that the pressure distribution over the test specimen would be uniform, toughness so that it could withstand punching by sand grains, and impermeability so that the gas pressure would not leak into the specimen container. Such a material was the object of an unsuccessful search. As a temporary

measure, which proved sufficient for the materials tested in this study, the area over which the loading diaphragm could distribute the deformation was increased by removal of the cushion sand immediately adjacent to the container wall down to the top of the container liner which was cut to a height of 13.125 inches, thus allowing 0.875 inches for the diaphragm to distribute the deformation it experienced during axial deformation of the test specimen. The exposed portion of the container was wiped clean of any sand grains and coated with Lubriplate grease. In addition, two loading diaphragms were used with the interface between the diaphragms greased. Thus, even if the lower diaphragm ruptured, the upper diaphragm functioned long enough to allow the test to be completed. Some sand-grain damage still was evident after each test; therefore, to preclude the loss of test data, a given loading diaphragm was used only once as an upper diaphragm, and once as a lower diaphragm, and then used for other purposes such as a sand cushion-specimen interface membrane. This system is illustrated in Figure 3.33.

The difficulties experienced with the loss of cushion sand resulting from damage to the cushion sand-specimen interface membrane were overcome by the use of two or more interface membranes and replacement of the bottom-most membrane when the wear became excessive.

The nonuniformity of stress conditions throughout the test specimens during early times in a test resulted from using a fast rise time. A typical axial pressure-rise time curve is presented in Figure 3.25. The rise time employed for this test was 24 msec. This rise time was approximately in accordance with recommendation of Whitman (1963) that the rise time t be greater than 25 times the height of the test specimen divided by the

wave-propagation velocity through the specimen as demonstrated in Figure 3.34. Employing a rise time of this general magnitude allowed a sufficient number of passages of the stress wave through the specimen to result in a relatively uniform state of stress throughout the test specimen. The selection of a fast pressure-rise time was necessary to determine the dynamic stress-strain characteristics of the test specimens; however, as a consequence of the fast pressure-rise time, the stress-strain curves resulting from the dynamic tests are not valid at early times during the tests because the stress levels throughout the specimens were not uniform. This phenomenon was borne out by the simplified computation of the transient stress levels at the top and bottom of the test specimen as presented in Figure 3.35.

The computation of the stress levels presented in Figure 3.35 was facilitated by three simplifying assumptions as follows: 1) the test specimen was assumed to be perfectly elastic; 2) the ratios of reflected stresses to incident stresses at the top and bottom of the specimen were assumed to be -1 and 1, respectively; and 3) the entire 14 inches from the loading diaphragm to the top of the concrete pedestal was assumed to compose the soil specimen, i. e., the sand cushion, interface membrane, and the deformation plate were all assumed to be part of the soil specimen.

While the soil specimen was not elastic, as the first assumption states, the results of the computation were sufficiently accurate to make an estimate of the number of transit times which were required for a relatively uniform state of stress throughout the soil specimen. The ratios of the reflected stress to the incident stress for both the top and bottom of the test specimen were computed and showed a very close agreement with the assumed values. Finally, the third assumption was reasonable since

the modulus for the Ottawa sand cushion was approximately 10 ksi and the difference between the acoustic impedances of Ottawa sand and the test specimen was generally less than 25%.

The results of the overstress estimation indicated that the greatest overstress relative to the pressure existing in the expansion chamber occurred at an elapsed time from the start of the test of 5.8 msec. and in magnitude was 18% of average measured expansion chamber pressure. This corresponded reasonably well with the time of occurrance of the apparent excessive deformation in Test D-3.

The stress-strain characteristics of crushed limestone as determined by Tests S-3 and D-3 are presented in Figure 3.36. The elapsed time from the beginning of the dynamic test is also noted on Figure 3.36. This test data indicates that the overstress was on the order of 50% and occurred between 3 and 6 msec after the beginning of the test and indicates that at times earlier than about 9 msec, the pressure measurements do not correspond to average stress conditions in the test specimen.

Therefore, if a rise time of approximately 25 msec is employed with a specimen thickness of 14 inches in the DLG, only that data corresponding to times later than approximately 10 msec should be used. If information regarding lower stress levels is required, lower peak overpressures must be employed. Thus, the behavior over the entire stress range from a pressure slightly greater than zero to 600 psi could be obtained from a test series as presented in Table 3.2.

In order to check the assumptions made concerning the maximum accelerations to which the deformation plate and pedestal were subjected,

accelerometers were mounted on the aluminum stiffener of the deformation plate and on the bottom of one of the instrumentation plugs. The accelerometer mounted on the deformation plate was monitored for two dynamic tests and the two sets of data were, for all practical purposes, identical. The maximum accelerations to which the deformation plate was subjected occurred during the first 5 msec of the test and in magnitude amounted to 100 g's. After the first 5 msec had elapsed, the maximum accelerations were of the order of 25 g's. A typical accelerometer record is presented in Figure 3.37. The accelerometer was pressure sensitive; therefore, the base line varies with the pressure and in order to establish a base line, it was necessary to assume that equal accelerations occur in both directions.

The accelerometer mounted on one of the instrumentation plugs was monitored during one dynamic test. The measured accelerations amounted to less than the background noise of the instrumentation. Therefore, it was concluded that with rise times of the order of 25 to 30 msec's, the inertial effects on the pedestal could be neglected.

As a means to verify that the actuating rod was portraying the movement of the top surface of the soil specimen during rapid testing, a Type A-19, SR-4, wire strain gage was mounted on the deformation rod just above the slide wire pickup and approximately 15 inches below the connection to the deformation plate. This strain gage was electronically conditioned and the output recorded for three rapid tests. Analysis of the acquired data indicated that for a dynamic test with the watertight seal in place around the actuating rod, the breakout friction acting on the actuating rod resulted in an axial shortening of less than 0.002 inches. After approxi-

mately 10 msec from the beginning of a test, the axial shortening of the rod did not exceed 0.001 inches. In addition, the deformations of the rod after 10 msec were oscillatory as indicated by the slide wire gage traces and could be averaged out in the interpretation of the data. Strain gage records for one test are presented in Figure 3.38. The breakout force for static tests with the watertight seal for the actuating rod in place was measured to be less than 0.1 lb, Section 3.2.1; this force resulted in an axial shortening of the actuating rod of less than 0.0001 inches. The axial shortening of the actuating rod without the watertight seal in place was negligible.

3.3.4.3 Investigation into the Effect of Seating Error

When testing granular materials with relatively large particle sizes such as the crushed limestone tested in Test S-3, point crushing against the top plate of the pedestal and against the deformation plate represented a possible source of error. Also, with fine-grained soils, seating error was a potential source of inaccuracy because of the difficulty in establishing intimate contact between the deformation plate and the top of the specimen. To investigate seating error, a test series including two dynamic and two static tests was performed on crushed limestone. Tests S-3 and D-3 were conducted with no attempts made to eliminate seating error other than leveling the top of the soil specimen carefully before placement of the deformation plate, and Tests S-4 and D-4 were conducted employing High Expansion Hydrocal, manufactured by the United States Gypsum Co., on both the top plate of the pedestal and the bottom side of the deformation plate in an attempt to establish intimate contact

while eliminating crushing of particles against bare metal surfaces.

Prior to the placement of the first lift of the test specimen in the soil container, the top plate of the pedestal was covered with a thin coat of motor oil and then a layer of Hydrocal, which varied in thickness between 1/16 and 1/8 inch. Before the Hydrocal hardened, the first lift of the specimen was placed in the container and compacted. After the Hydrocal set up, the remainder of the specimen was placed. Following measurement of the height of the specimen, a layer of Hydrocal, which varied in thickness from 1/16 to 1/8 inch, was applied to the bottom side of the deformation plate, and the deformation plate placed on the top of the soil specimen. Immediately following placement of the deformation plate on the test specimen, a weight of approximately 180 lb was placed on the deformation plate. This preloading of the test specimen amounted to only approximately 0.1 psi and was inconsequential with respect to the stress-strain characteristics of the material but was sufficient to cause the granular material to completely seat against the deformation plate while being seated in a matrix of Hydrocal as shown in Figure 3.39.

The stress-strain curves for Tests S-3 and S-4 and Tests D-3 and D-4 are presented in Figures 3.29 and 3.30, respectively. The effect of the Hydrocal in reducing seating error is obvious. Upon removal of the specimens from the container subsequent to testing, the Hydrocal was examined. The areas of contact between the granular particles and the Hydrocal were well preserved and demonstrated that the thin layers of Hydrocal were sufficient to eliminate crushing of point contacts by the

deformation plate and the top plate of the pedestal. Some deformation of the Hydrocal occurred and introduced an error; however, this deformation was slight since the maximum thickness of Hydrocal was between 1/16 and 1/8 inch. The one-dimensional stress-strain characteristics of Hydrocal are presented in Figure 3.40. Also, the granular material was in direct contact with the top plate of the pedestal and the bottom side of the deformation plate; the Hydrocal merely served to eliminate high point-contact stresses.

3.3.4.4 Analysis of Pressure Distribution over Top of Specimen

The overpressure was applied to the top of a dynamic test specimen by means of gas which was stored in the charging chamber of the DLG. Upon firing of the DLG, the main valves of the load cells opened and the gas flowed through two sets of grids and onto the surface of the loading diaphragm, as described in Appendix B.

Because the operation of the load cells was an electronically initiated mechanical operation, there was variation in the time required for the operation. A time delay of approximately 32 msec occurred between the time when the load solenoid was actuated and when the main valve opened, as indicated by a magnetic pickup. The time required for each load-cell operation had a variance from its average time of operation of ±0.75 msec. As a consequence of the individual load-cell time variance, the time for all load cells to operate when set for coincident firing varied and could exceed 1.50 msec. Prendergast (1968) reported a maximum time delay between the initial and final load-cell operation of 0.39 and 1.89 msec with an average time of 1.12 msec for his test series utilising the DLG.

In order to investigate the effect of the noncoincident operation of the load cells on the surface pressure profile, Prendergast installed soil stress gages at the surface of a test specimen. The soil stress gages were used primarily to measure the time delay between the initial arrival of pressure below a load cell and the subsequent arrivals of peak pressure below the other load cells, and the initial arrival of peak pressure below a load cell and the subsequent arrivals of peak pressure below the other load cells. Examination of this data indicates that the time delays between initial and subsequent arrival times of initial and peak surface pressures can be correlated with the time delays between the load-cell firings. The time delays between initial and subsequent pressure arrivals are related to the time delays between the load-cell firings in a complex manner because of the pressure gradients and consequent gas flow patterns over the surface of the specimen.

An estimation of the pressure variation over the surface of the test specimen with time during the test was made by Prendergast by superimposing the surface pressure profiles obtained from the soil stress gages which were located on the surface of the test specimen. The surface pressure profiles for two stress gages with relatively large time delays between load-cell firings are presented in Figure 3.41. The maximum pressure variations are less than 50 psi which is less than 20% of the peak surface pressures. Further, these pressure variations should diminish for tests with slower rise times such as are employed in the testing program covered by this report rather than the low rise times (t ≈ 3 msec) employed by Prendergast. With respect to the objectives of the investigation of the

characteristics of granular material in one-dimensional compression as covered by this study, the pressure distribution over the surface of the test specimen may be considered uniform since only the latter half, with respect to time, of the stress-strain data is of interest, as was discussed in Section 3.3.4.2.

As was described in Section 2.3.1, the axial pressure on a dynamic test specimen was measured by four Kistler quartz pressure transducers, models 601A and 606A, mounted in the seal ring. The uniformity of pressure along the seal ring was analyzed by superimposing the pressure-time traces from Test D-1, C-2, as presented in Figure 3.42. The individual pressure-time traces for Test D-1, C-2, are presented in Figures 3.43 through 3.46. The interpreted traces are superimposed and presented in Figure 3.47. By examination of that portion of Figure 3.47 which is of interest, i.e., approximately the latter half of the pressure-time plot, it can be seen that the maximum variation between any two pressure traces is approximately 10 psi and that the maximum variation from the average pressure is ±5 psi, this variation being relatively constant for the portion of the test of interest.

TABLE 3.1 PROOF-TESTING PROGRAM

Test	Cycle	Material	Initial Dry Density (pcf)	Moisture Content (%)	Stress Rate psi/ms	Rise Time msec	Static Preload psi	Maximum Stress Level psi	Comments
S-1	C-1	Ottawa Sand	107.1	air dry	20	--	0	986	
	C-2		--	--	20	--	0	993	
	C-5		--	--	20	--	0	993	
S-2	C-1	Ottawa Sand	110.3	air dry	20	--	0	590	
	C-2		--	--	20	--	0	70	Loading diaphragm ruptured
	C-3		--	--	20	--	0	1000	
	C-4		--	--	20	--	0	1000	
	C-5		--	--	20	--	0	1000	
	C-6		--	--	20	--	0	950	
S-3	C-1	Crushed Limestone	107.8	air dry	variable	--	0	600	No Hydrocal used
	C-2			--	--	--	0	900	
	C-3			--	--	--	0	1000	
	C-4			--	--	--	0	1000	
	C-5			--	--	--	0	1000	
S-4	C-1	Crushed Limestone	103.8	air dry	variable	--	0	800	Hydrocal used
D-1	C-1	Ottawa Sand	110.8	air dry	--	18	50	108	
	C-2		--	--	--	24	50	258	
D-2	C-1	Crushed Limestone	107.5	air dry	--	27	0	584	Loading diaphragm ruptured
D-3	C-1	Crushed Limestone	107.3	air dry	--	26	0	620	No Hydrocal used
D-4	C-1	Crushed Limestone	107.3	air dry	--	29	0	609	Hydrocal used

TABLE 3.2 TEST PROGRAM FOR DETERMINING DYNAMIC STRESS-STRAIN BEHAVIOR OF TEST SPECIMEN FROM 25 TO 600 PSI

Test	Cycle	Static Preload (psf)	Rise Time (msec)	Dynamic Stress Increment (psi)	Valid Stress Range
A	C-1	γh	25	50	25-50
	C-2	γh	25	100	50-100
	C-3	γh	25	200	100-200
	C-3	γh	25	400	200-400
	C-4	γh	25	600	300-600

γ = unit weight of soil overlying sample in situ
h = depth to top of sample in situ

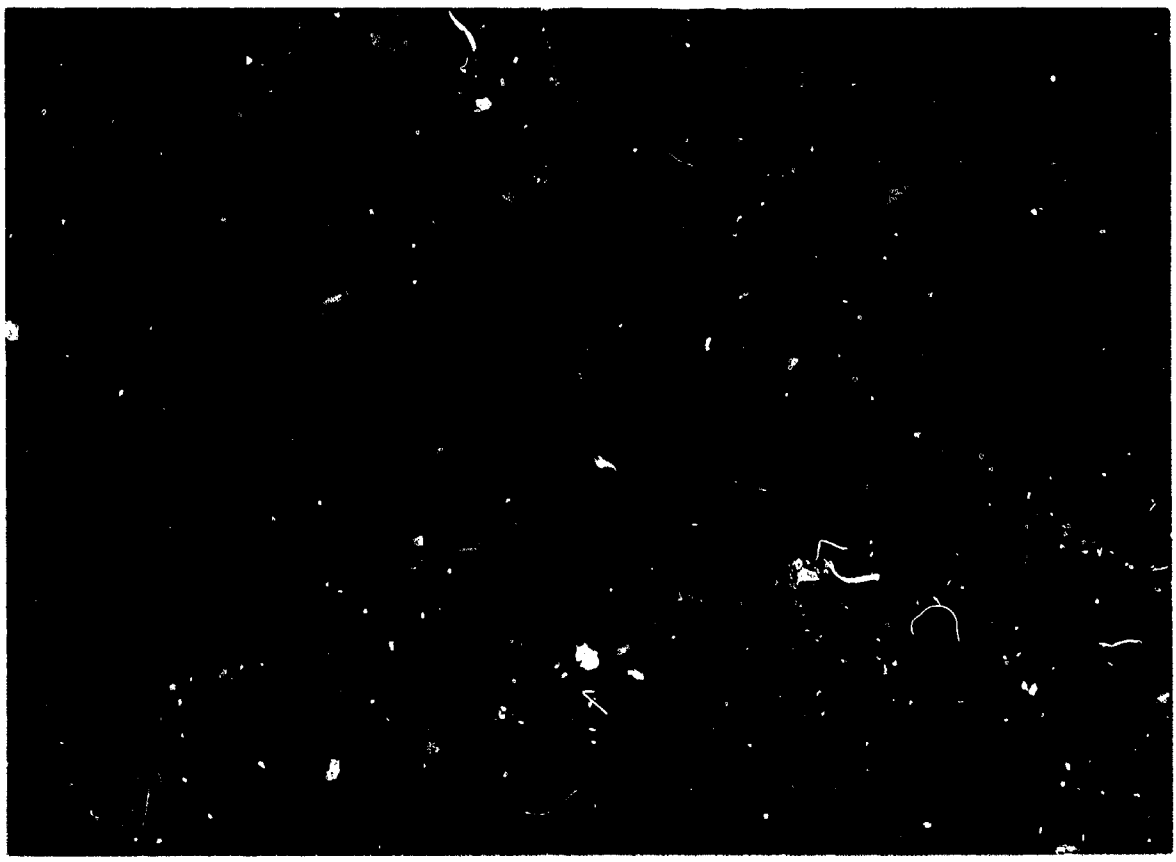

FIGURE 3.1 PHOTO OF STATIC PROOF-TEST STAND FOR SLIDE WIRE GAGE

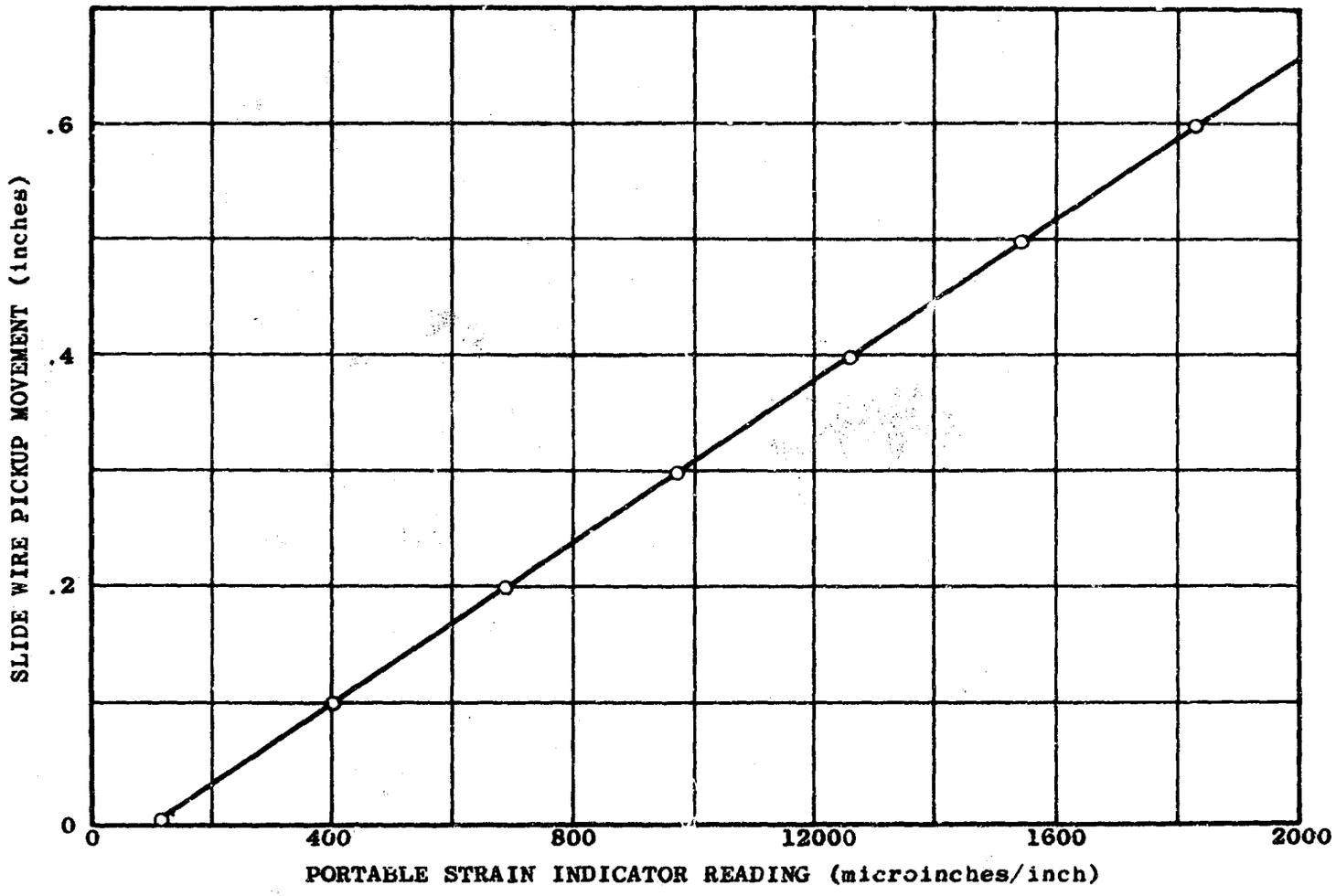

FIGURE 3.2 STATIC PROOF-TEST RESULTS

FIGURE 3.3 PHOTO OF STATIC PROOF-TEST STAND FOR SLIDE WIRE GAGE

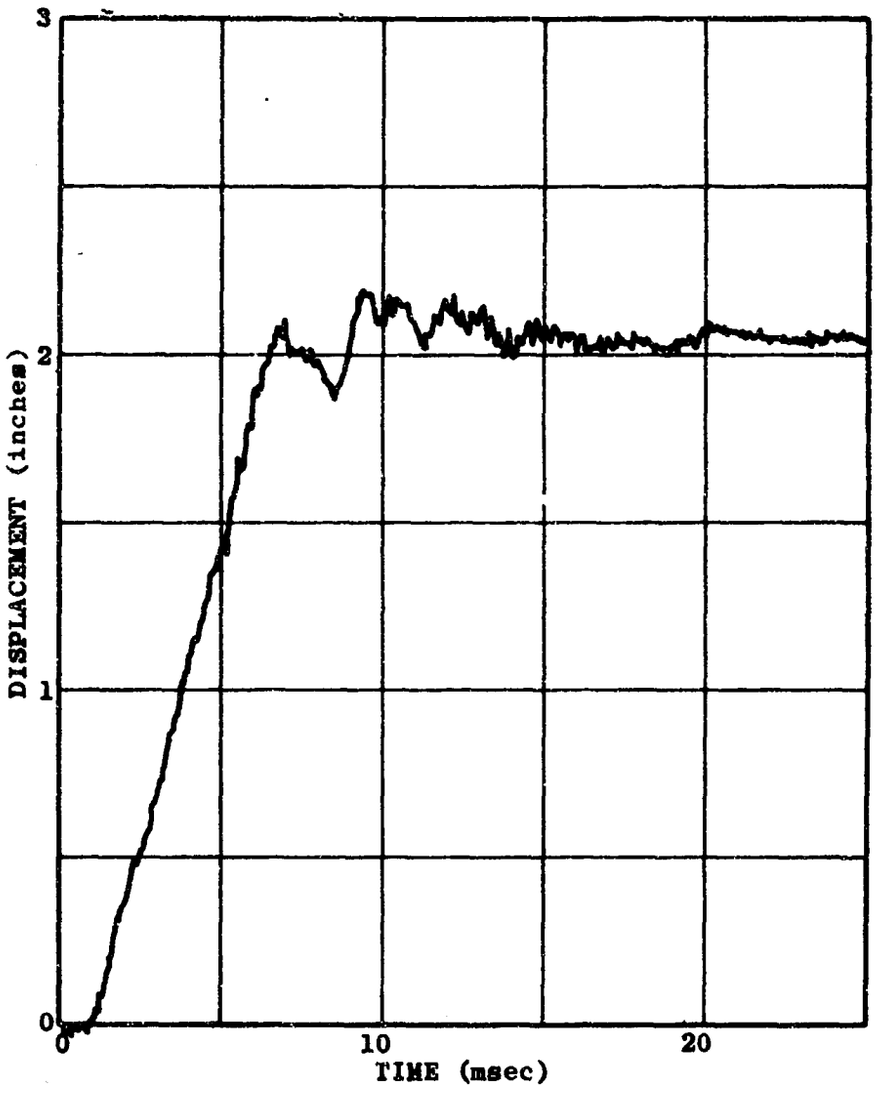

FIGURE 3.4 DISPLACEMENT-TIME CURVE FOR A DYNAMIC PROOF-TEST OF SLIDE WIRE GAGE

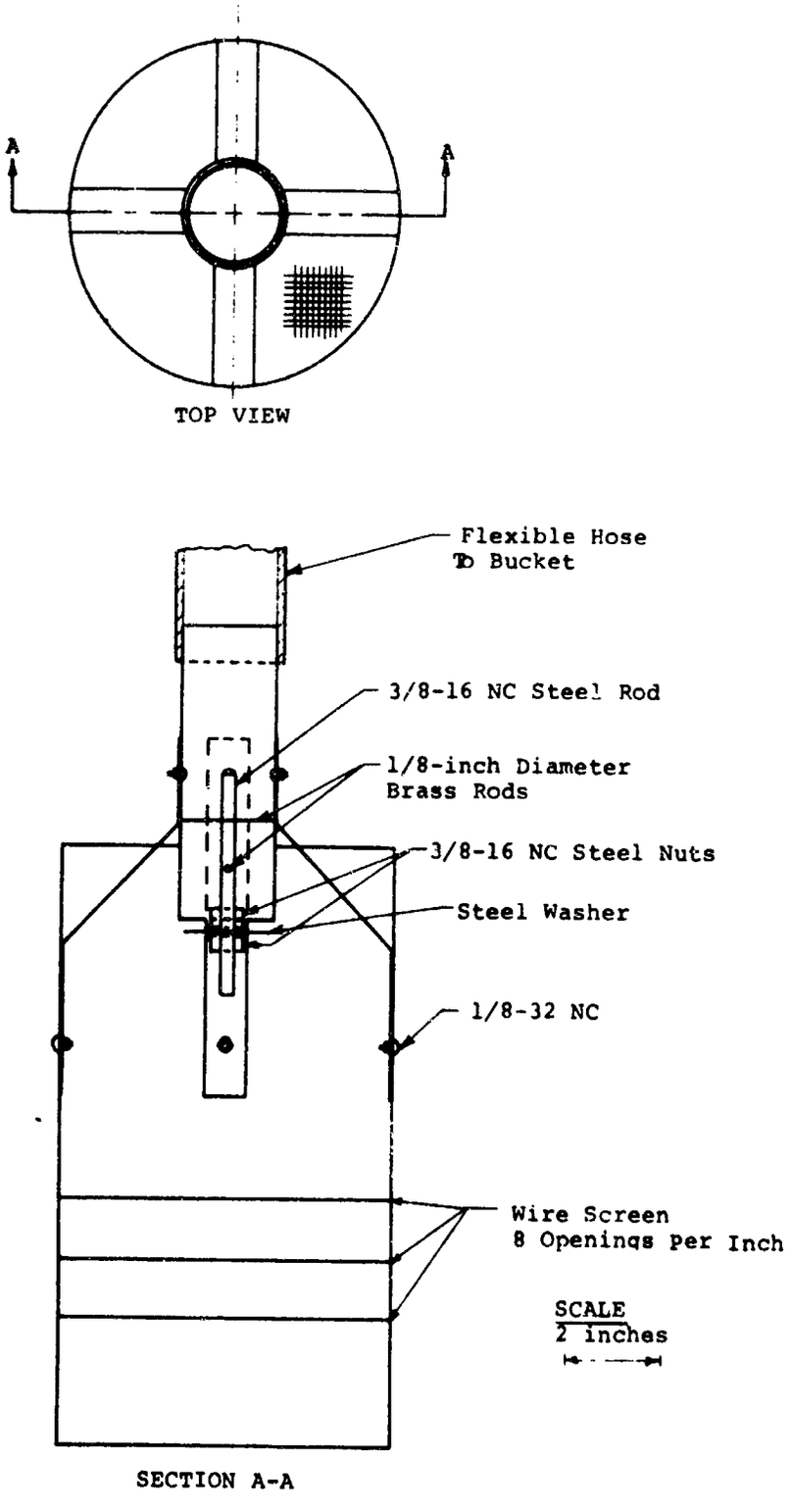

FIGURE 3.5 DETAILED DRAWING OF RAINER

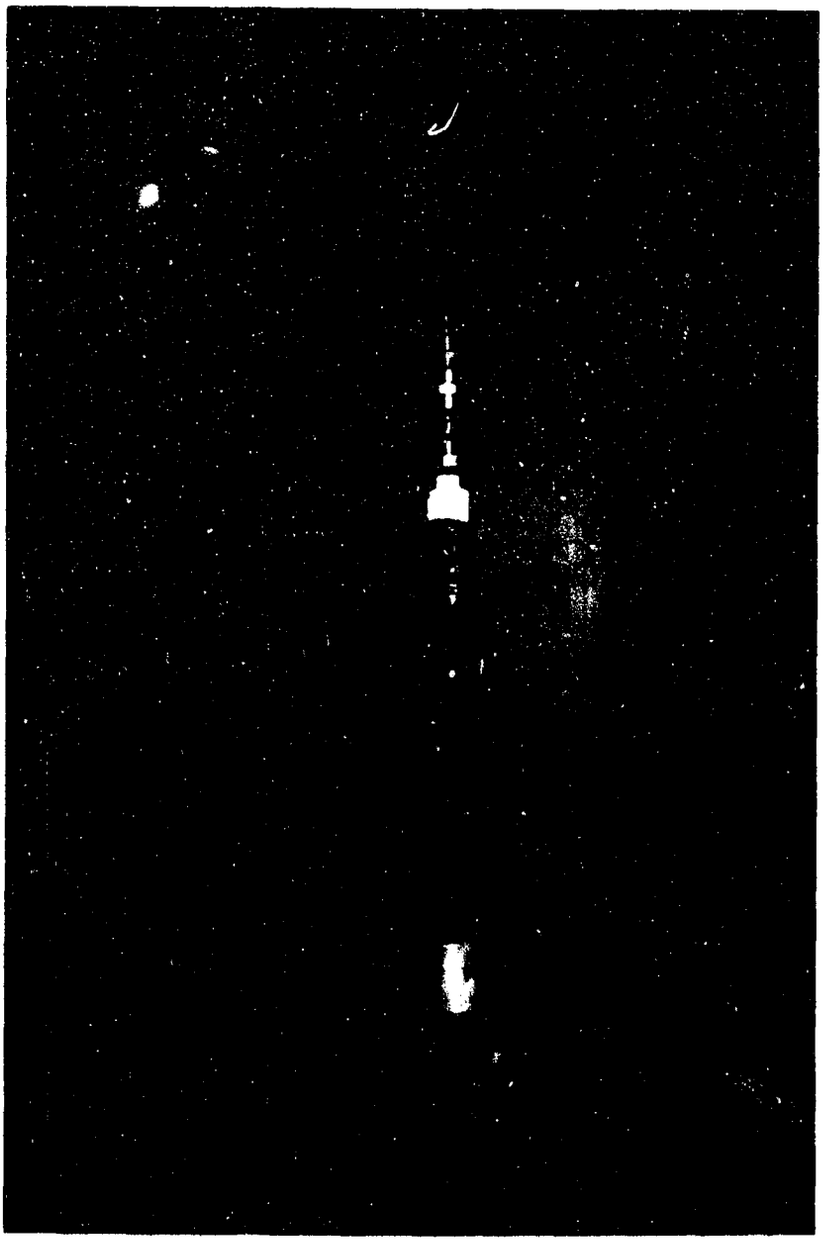

FIGURE 3.6 PHOTO OF SOIL TAMPER WITH FOOT IN PLACE

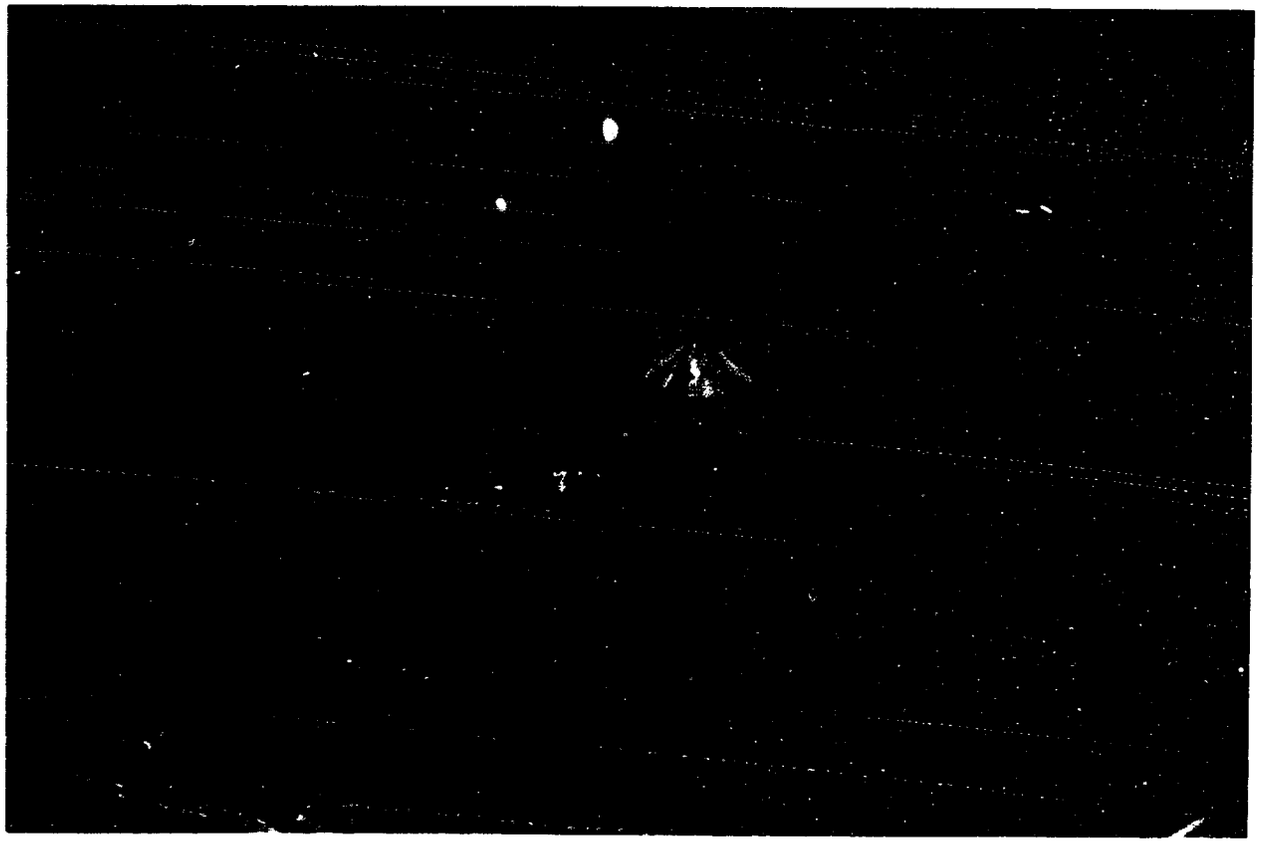

FIGURE 3.7 PHOTO OF SOIL CONTAINER WITH SPECIMEN IN PLACE

Axial Pressure (psi)	Check Gage (μin./in.)	Slide Wire #1 Reading (μin./in.)	Slide Wire #1 Increment (μin./in.)	Deformation (inches)	Strain (%)
0	31787	30198	0	0	0
1		30106	92	.02556	.213
2		30045	153	.04250	.354
3	31787	30000	198	.05500	.458
4		29945	253	.07028	.586
5	31787	29915	283	.07861	.655
10		29785	413	.11472	.956
20	31787	29640	558	.15450	1.287
35		29495	703	.19528	1.627
50		29393	805	.22361	1.863
75		29263	935	.25972	2.164
100	31787	29075	1123	.31194	2.599
150		28716	1482	.41167	3.431
200		28275	1923	.53417	4.451
300	31787	27560	2638	.73278	6.106
400		26803	3395	.94306	7.859
500		26175	4023	1.11750	9.312
600	31787	25535	4663	1.29528	10.794
500		25399	4799	1.33306	11.109
400		25409	4789	1.33028	11.086
300	31787	25420	4778	1.32722	11.060
200		25437	4761	1.32250	11.021
100		25474	4724	1.31222	10.935
75	31787	25500	4698	1.30500	10.875
50		25570	4628	1.28556	10.713
25		25785	4413	1.22583	10.215
10		25848	4350	1.20883	10.069
0	31787	26190	4068	1.13000	9.417

FIGURE 3.8 TYPICAL STATIC TEST COMPUTATIONS

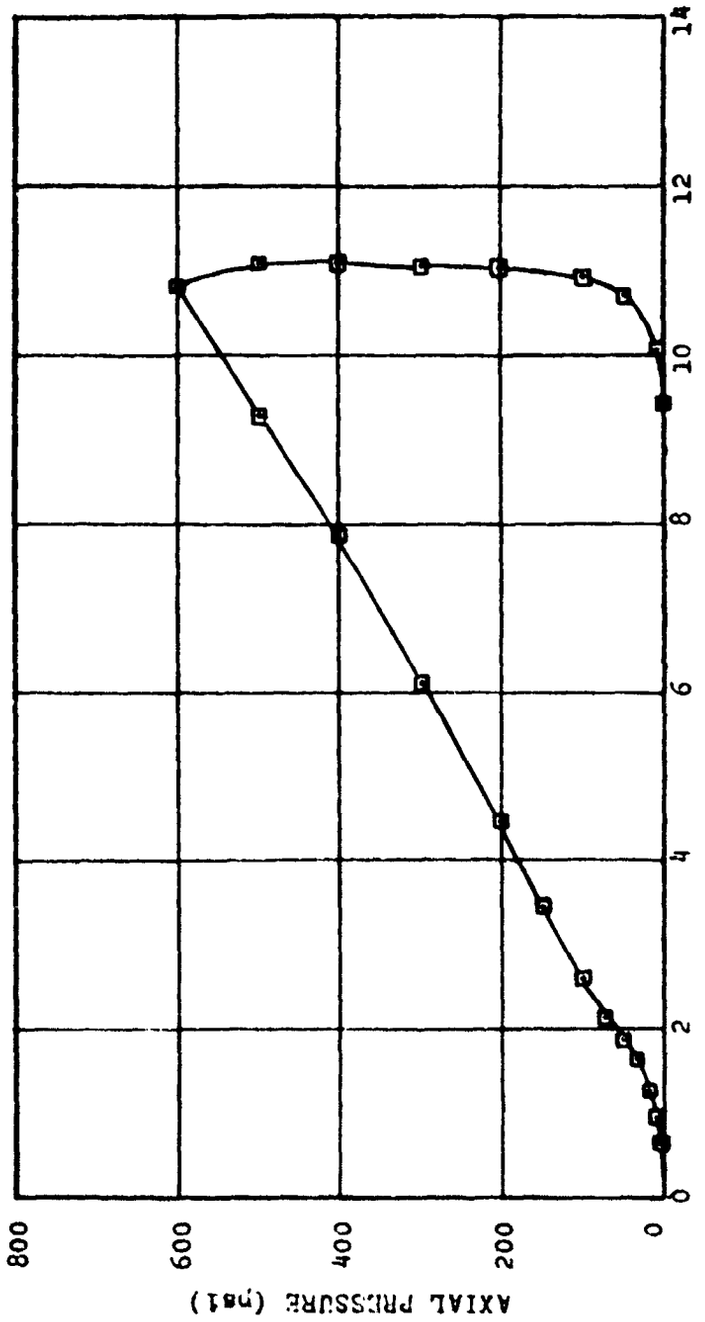

FIGURE 3.9 TYPICAL STATIC STRESS-STRAIN PLOT

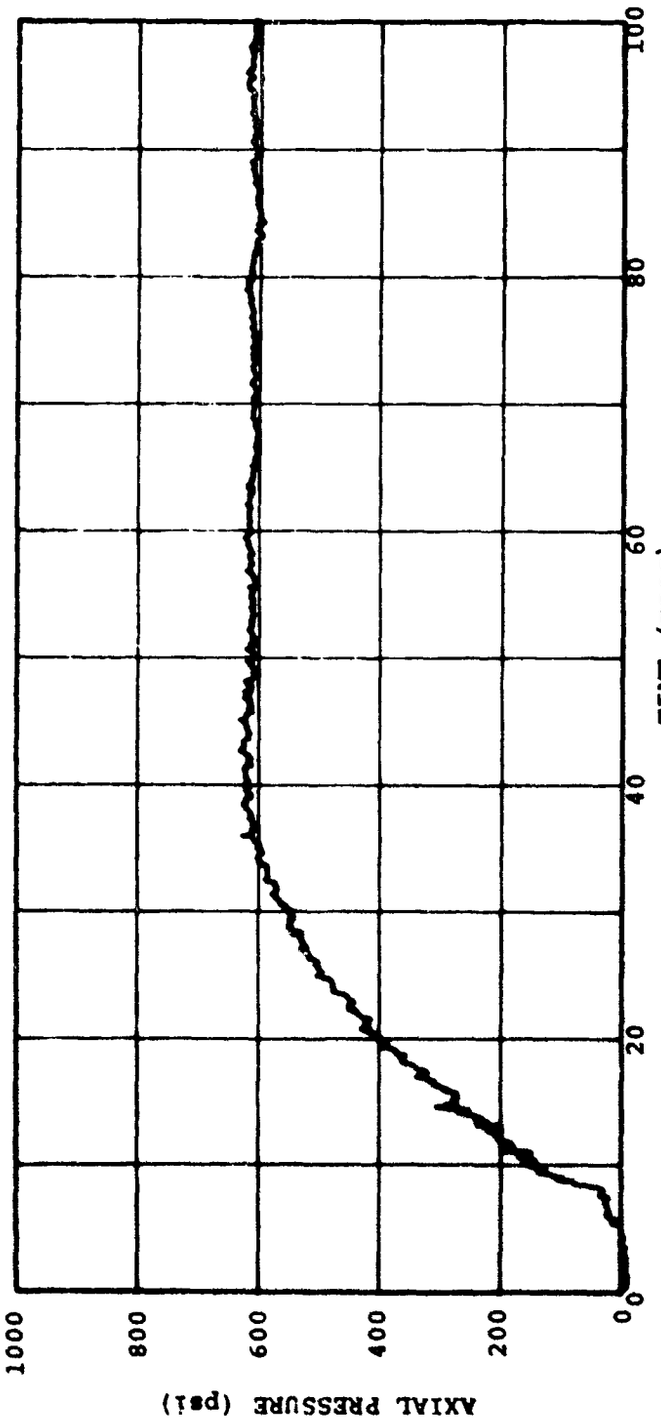

FIGURE 3.10 PRESSURE-TIME CURVE FOR TEST D-5, TRANSDUCER No. 1982

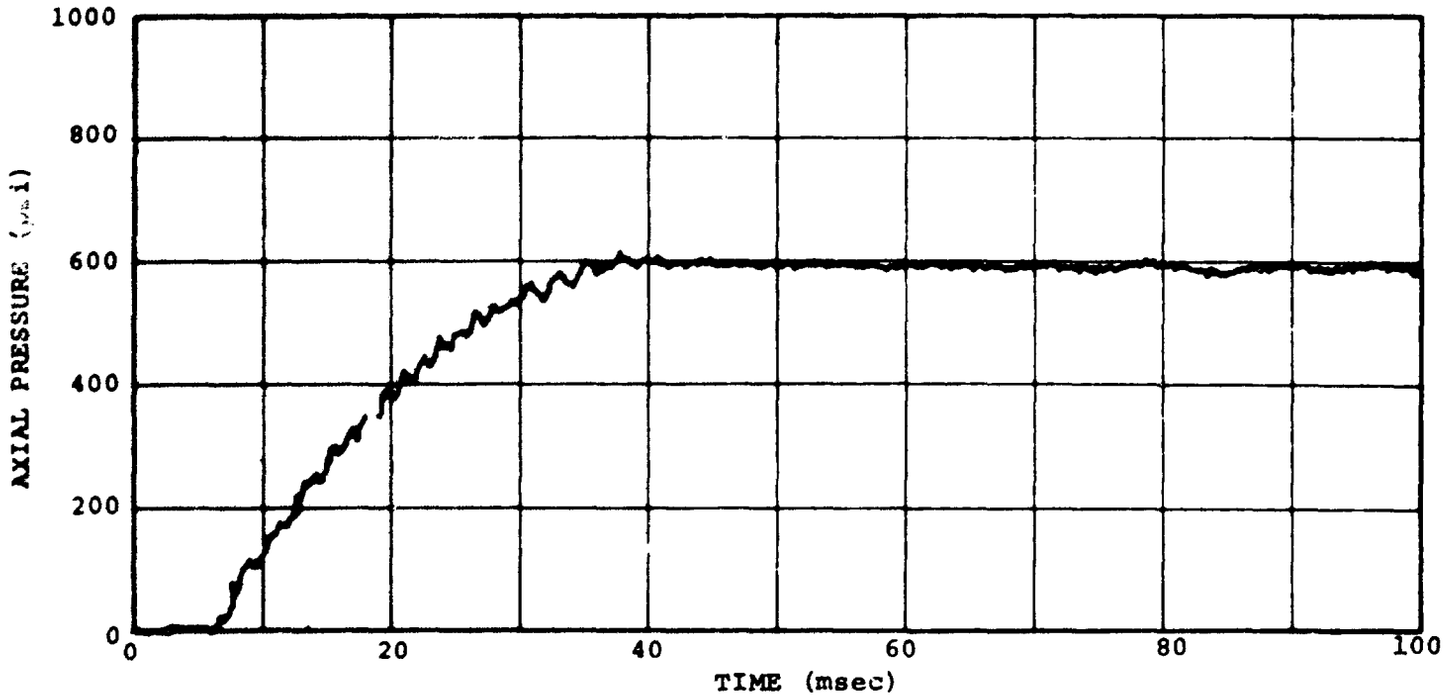

FIGURE 3.11 PRESSURE-TIME CURVE FOR TEST D-5, TRANSDUCER No. 16059

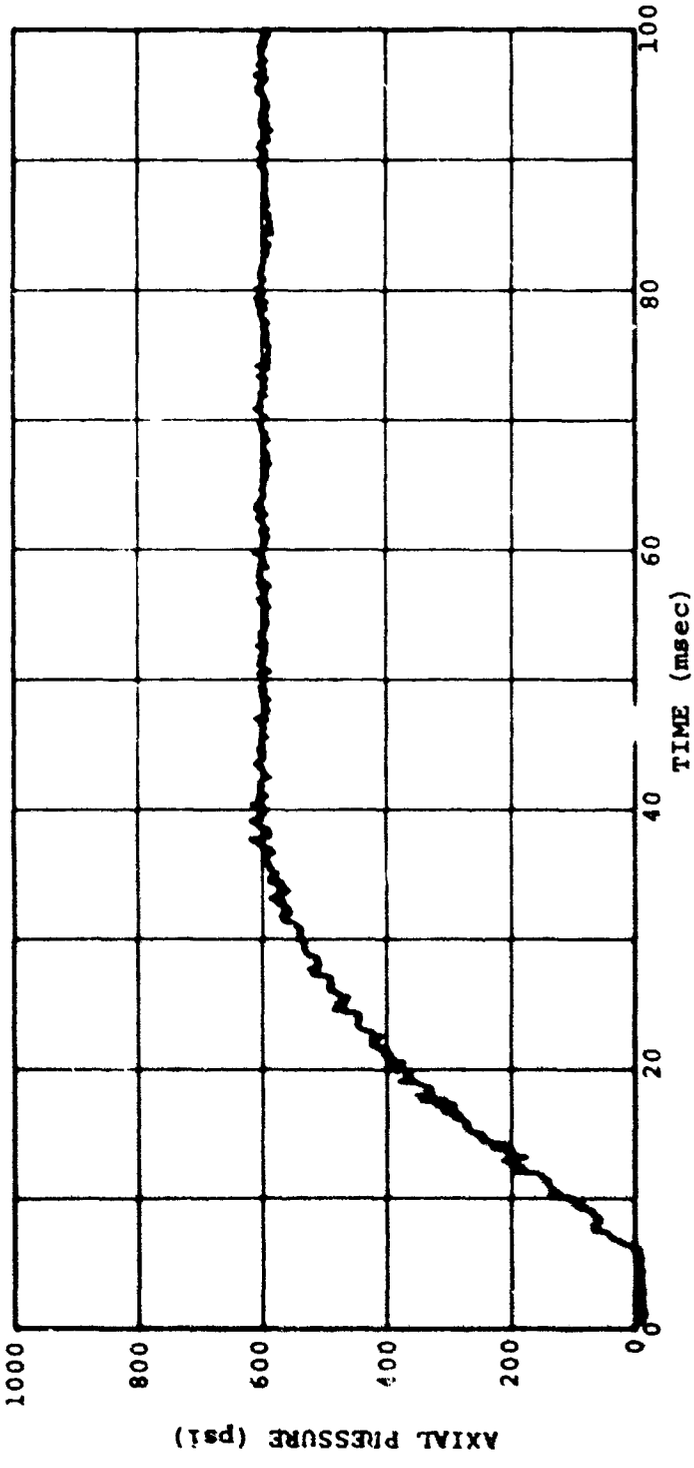

FIGURE 3.12 PRESSURE-TIME CURVE FOR TEST D-5, TRANSDUCER No.16379

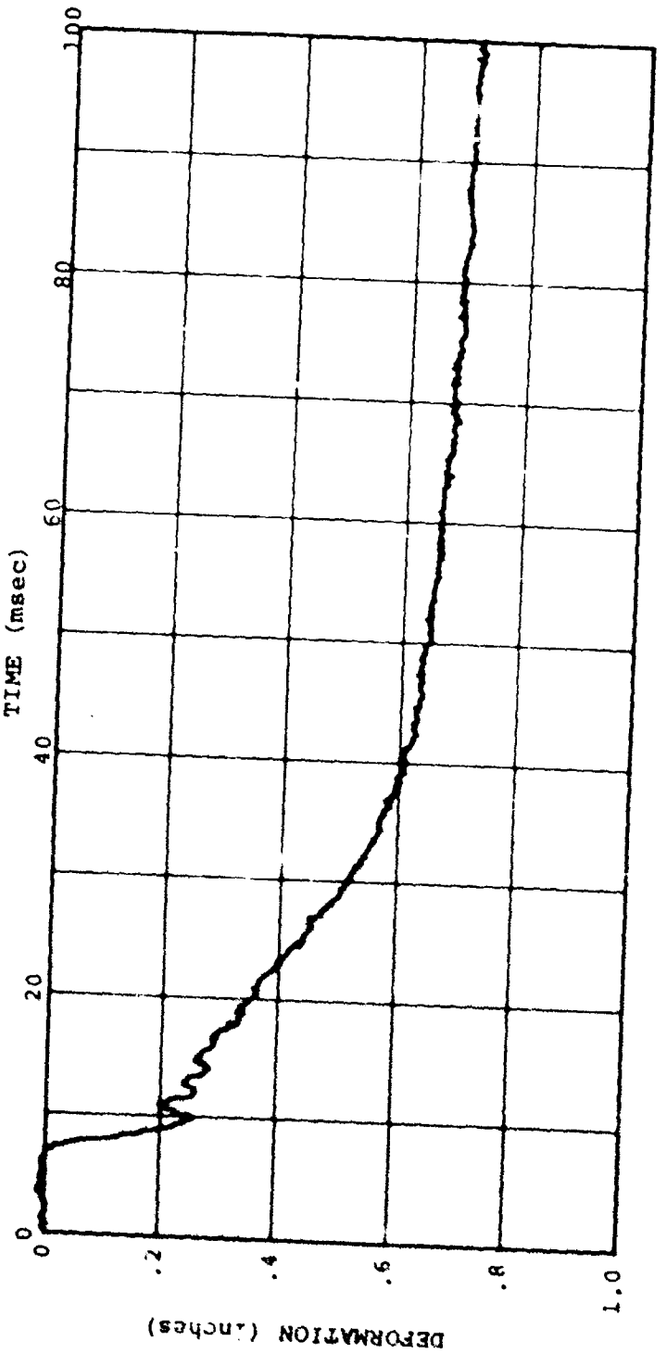

FIGURE 3.13 DEFORMATION-TIME CURVE FOR TEST D-5

Time	Deformation		Strain	Pressure				
	SW I	SW II		1132	1982	16059	16379	avg.
(msec)	(inches)		(%)	(psi)	(psi)	(psi)	(psi)	(psi)
0		0	0	0	0	0	0	0
2		.17	2.109		50	70	55	58.3
4		.225	2.791		125	140	110	125
6		.255	3.162		190	205	170	188.3
8		.280	3.473		240	260	230	243.3
10		.310	3.845		295	305	280	293.3
12		.340	4.217		245	350	335	343.3
14		.370	4.589		385	395	375	385
16		.400	4.962		425	[illegible]	420	425
18		.440	5.458		465	[illegible]	455	461.7
20		.470	5.830		495	[illegible]	490	493.3
22		.505	6.264		520	[illegible]	515	520
24		.530	6.574		540	[illegible]	540	541.7
26		.555	6.884		560	[illegible]	560	560
28		.570	7.070		575	[illegible]	575	576.7
30		.590	7.318		590	590	590	590
32		.605	7.504		600	600	600	600
34		.615	7.628		600	600	600	600
36		.625	7.752		600	600	600	600
final		.705	[illegible]5		600	600	600	600

Data in agreement with SW II, therefore, not reduced

Kistler #1132 malfunctioned ------

FIGURE 3.14 REDUCTION OF DATA FOR TEST D-5

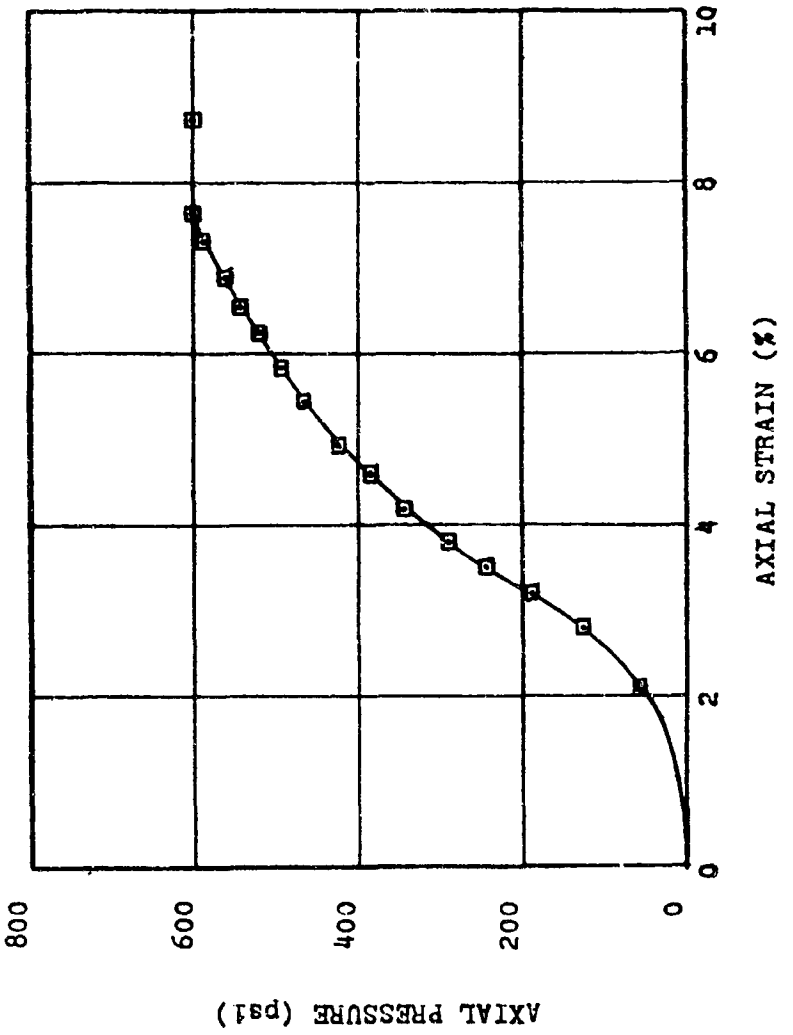

FIGURE 3.15 STRESS-STRAIN CURVE FOR TEST D-5

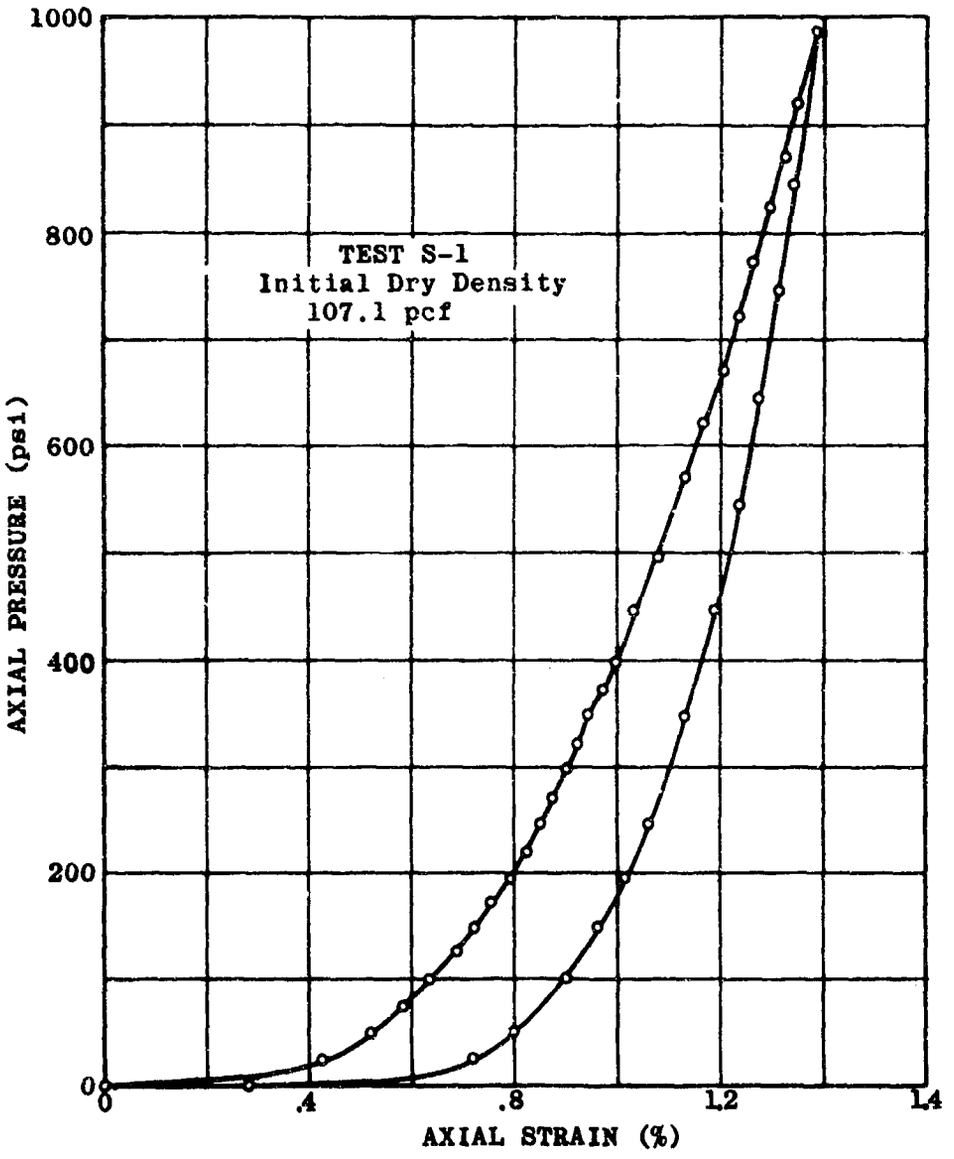

FIGURE 3.16 STRESS-STRAIN RELATIONSHIP FOR 20-30 OTTAWA SAND IN ONE-DIMENSIONAL COMPRESSION, TEST S-1

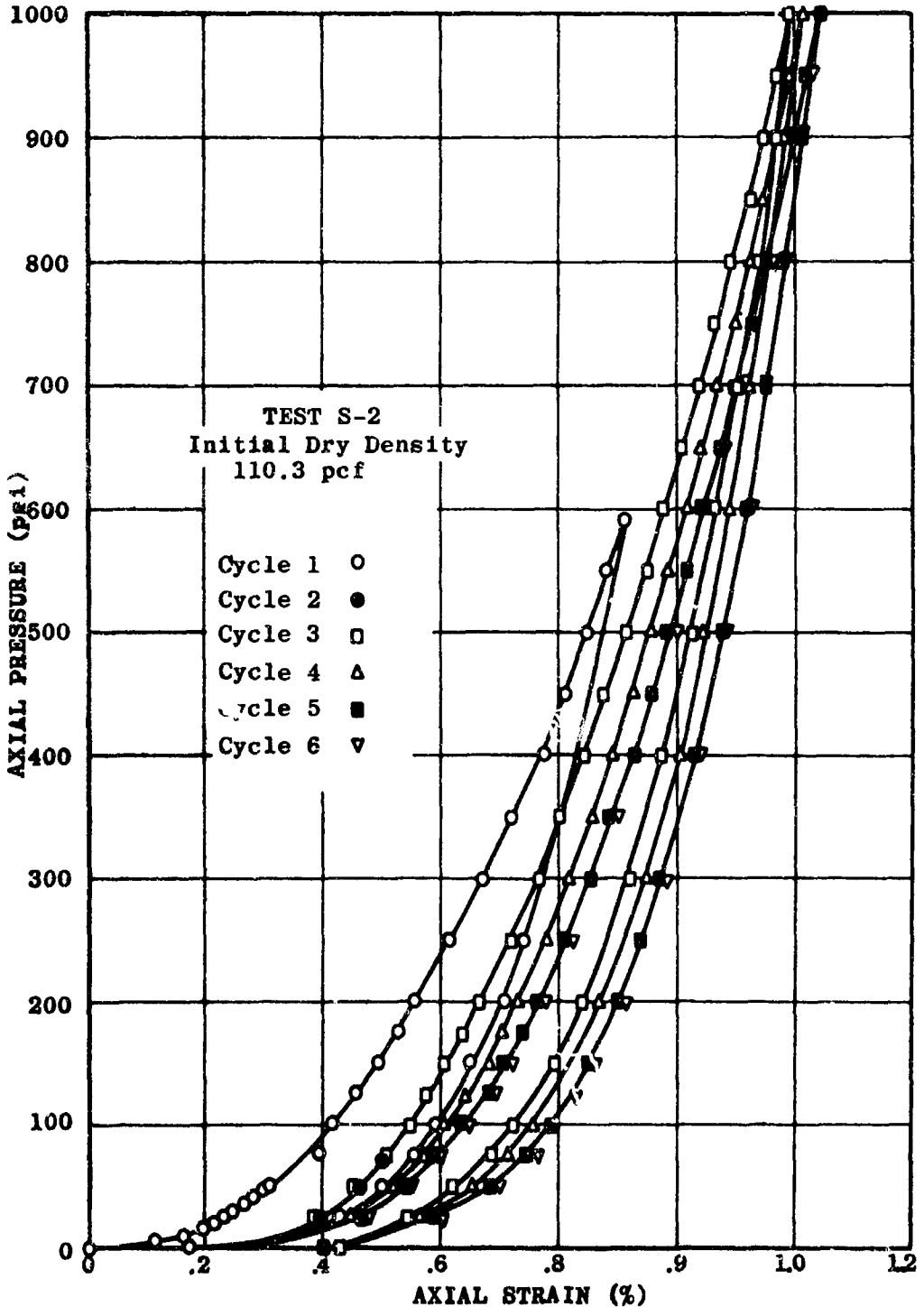

FIGURE 3.17 STRESS-STRAIN RELATIONSHIP FOR 20-30 OTTAWA SAND IN ONE-DIMENSIONAL COMPRESSION, TEST S-2

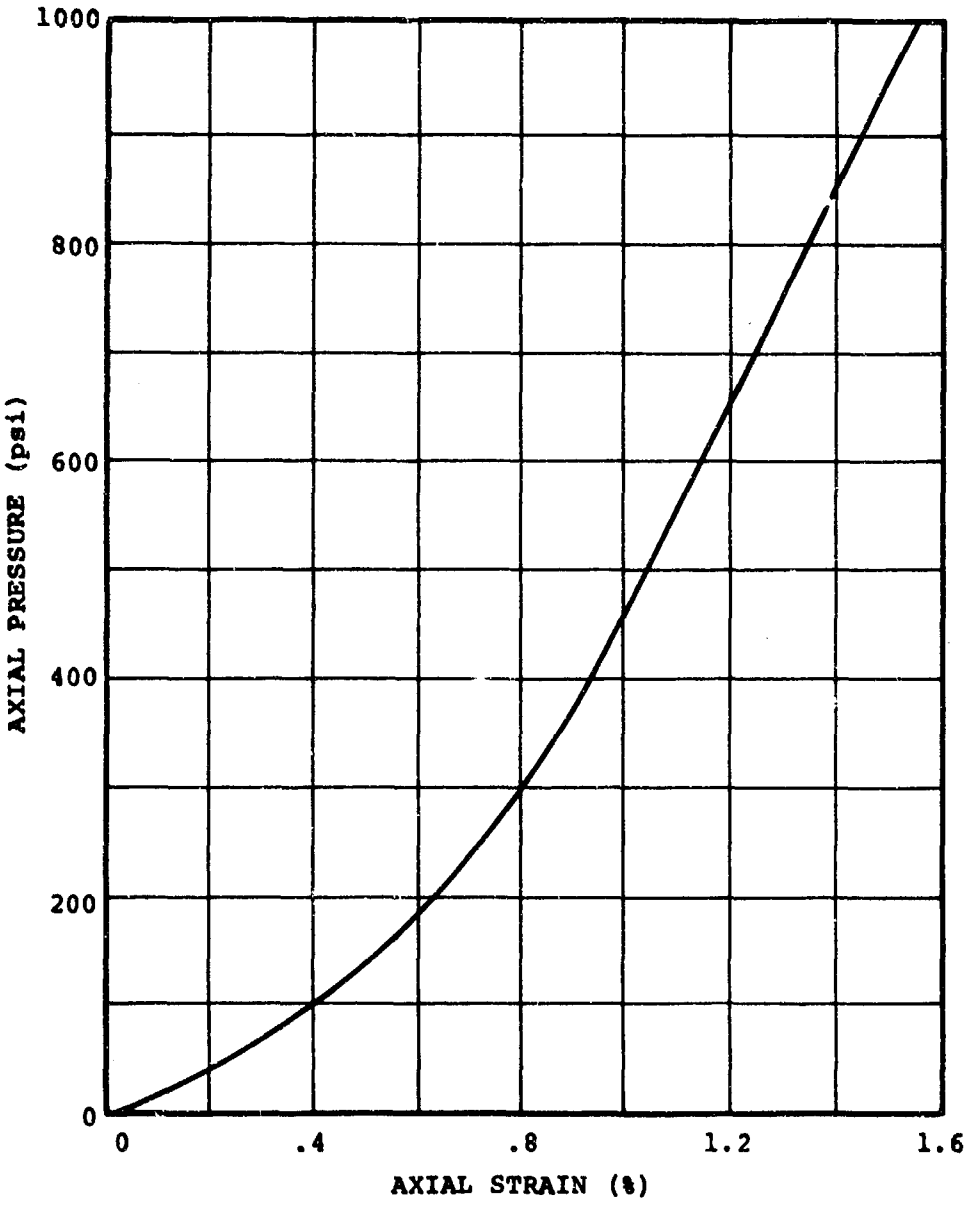

FIGURE 3.18 STRESS-STRAIN RELATIONSHIP FOR 20-30 OTTAWA SAND IN ONE-DIMENSIONAL COMPRESSION AS DETERMINED BY WHITMAN

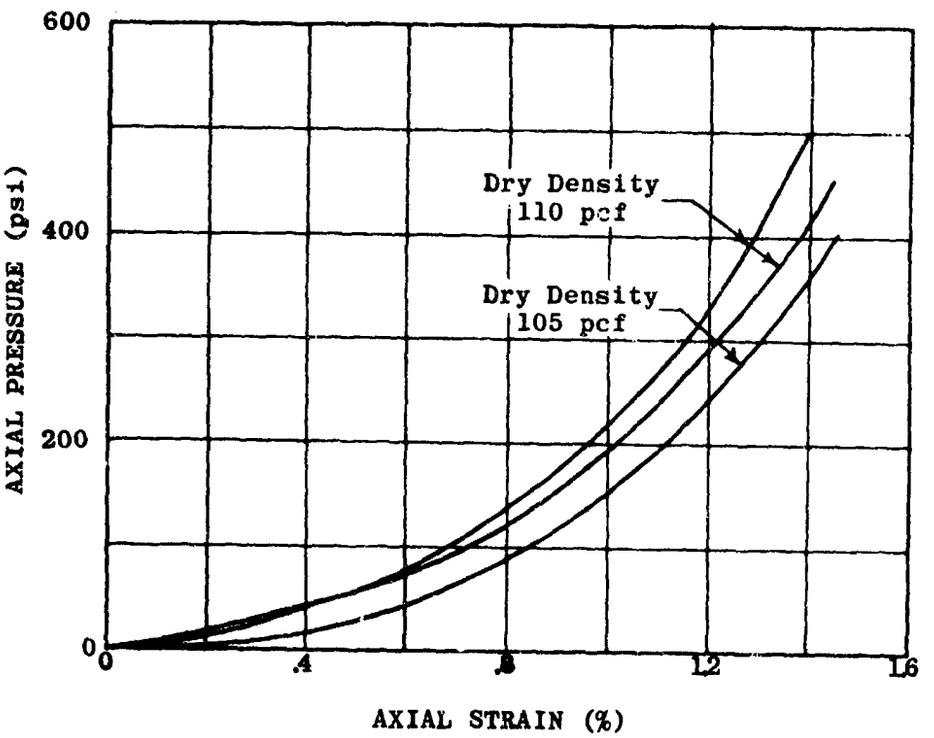

FIGURE 3.19 STRESS-STRAIN RELATIONSHIP FOR 20-30 OTTAWA SAND IN ONE-DIMENSIONAL COMPRESSION AS DETERMINED BY DURBIN

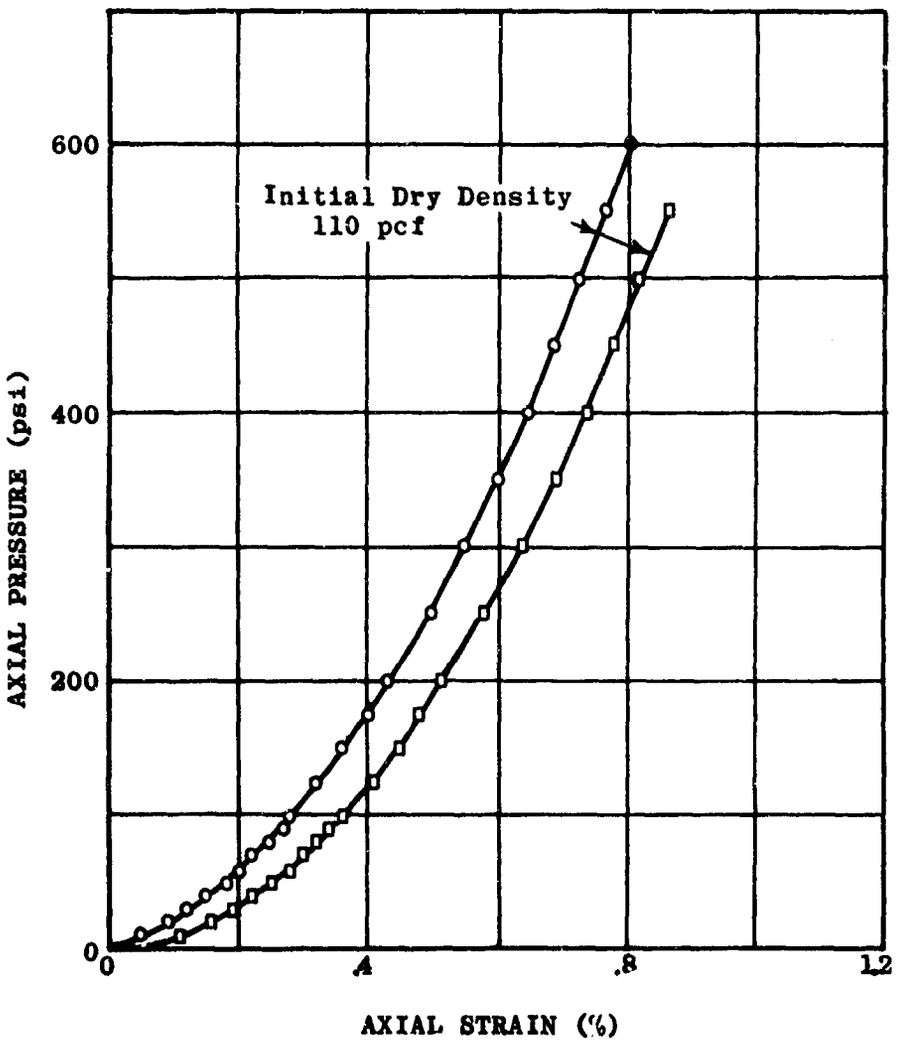

FIGURE 3.20 STRESS-STRAIN RELATIONSHIP FOR 20-30 OTTAWA SAND IN ONE-DIMENSIONAL COMPRESSION AS DETERMINED BY ZACCOR

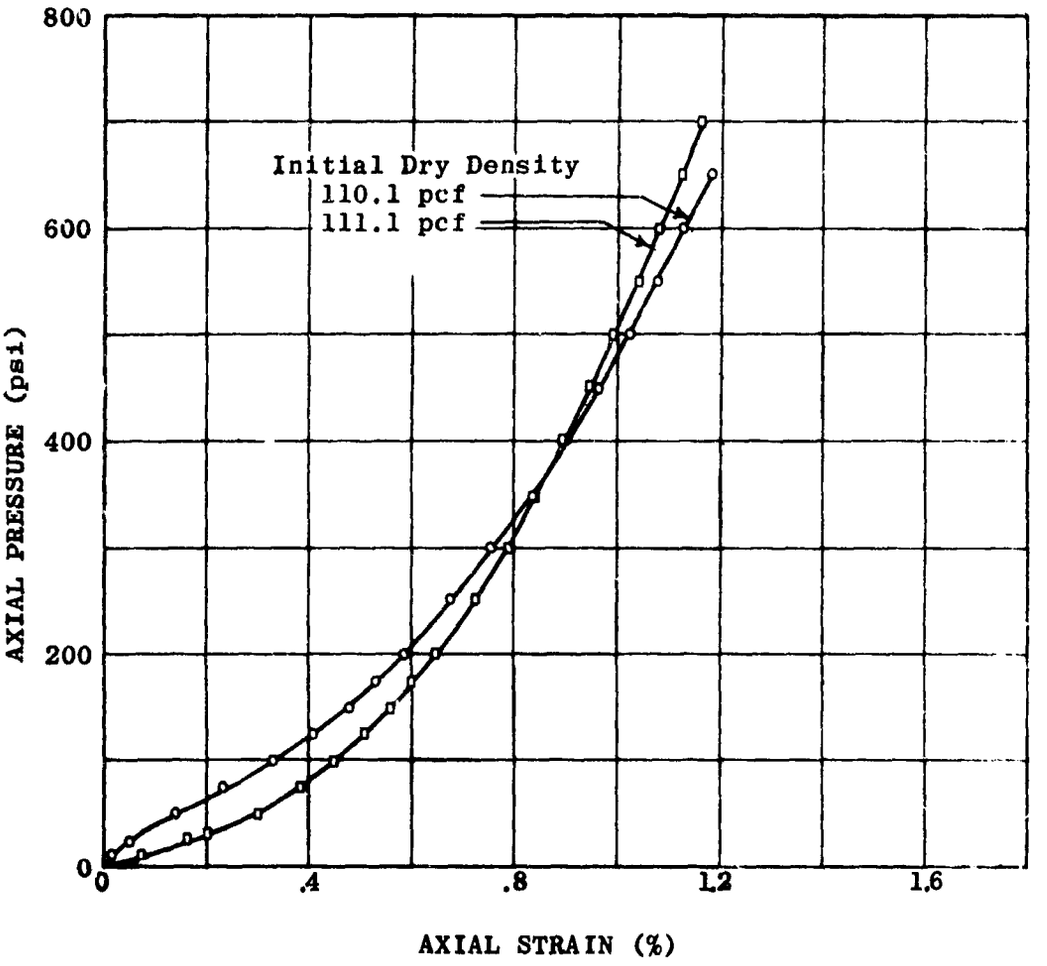

FIGURE 3.21 STRESS-STRAIN RELATIONSHIP FOR 20-30 OTTAWA SAND IN ONE-DIMENSIONAL COMPRESSION AS DETERMINED BY PRENDERGAST AND EMERSON USING HENDRON'S DEVICE

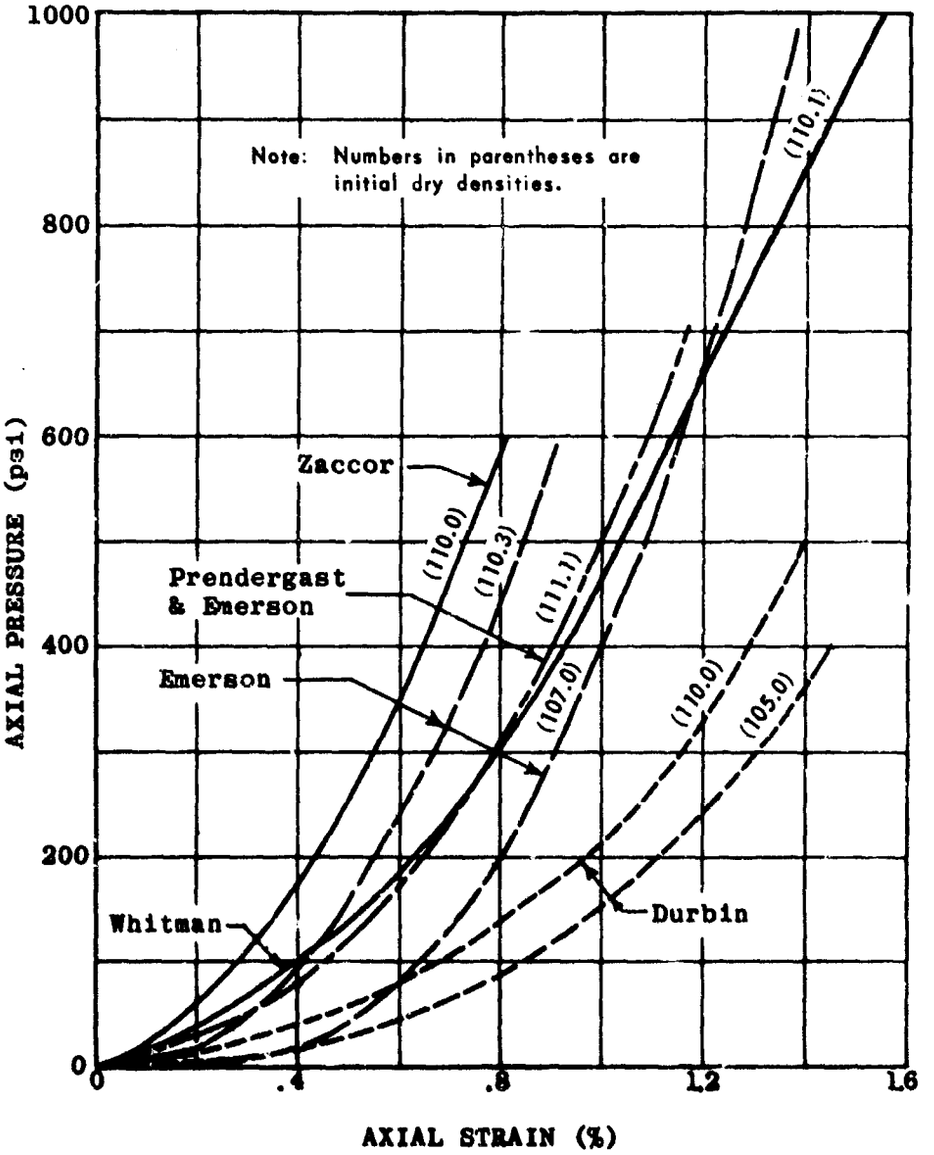

FIGURE 3.22 COMPARISON OF STRESS-STRAIN RELATIONSHIPS FOR 20-30 OTTAWA SAND IN ONE-DIMENSIONAL COMPRESSION AS DETERMINED BY DIFFERENT DEVICES

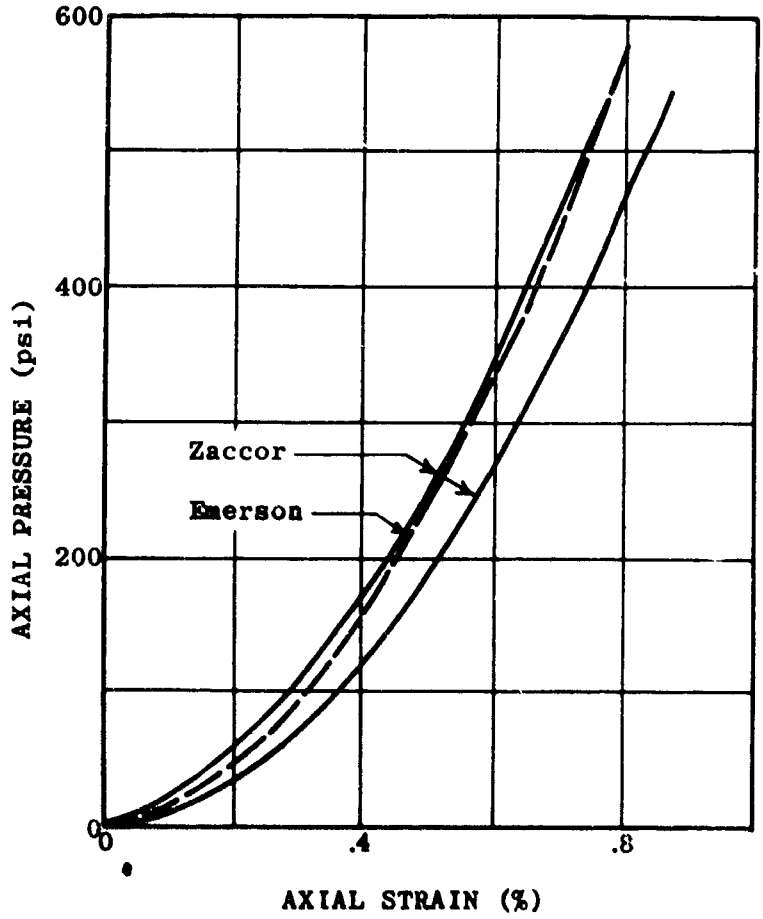

FIGURE 3.23 COMPARISON OF STRESS-STRAIN RELATIONSHIPS FOR 20-30 OTTAWA SAND IN ONE-DIMENSIONAL COMPRESSION AS DETERMINED BY ZACCOR AND EMERSON

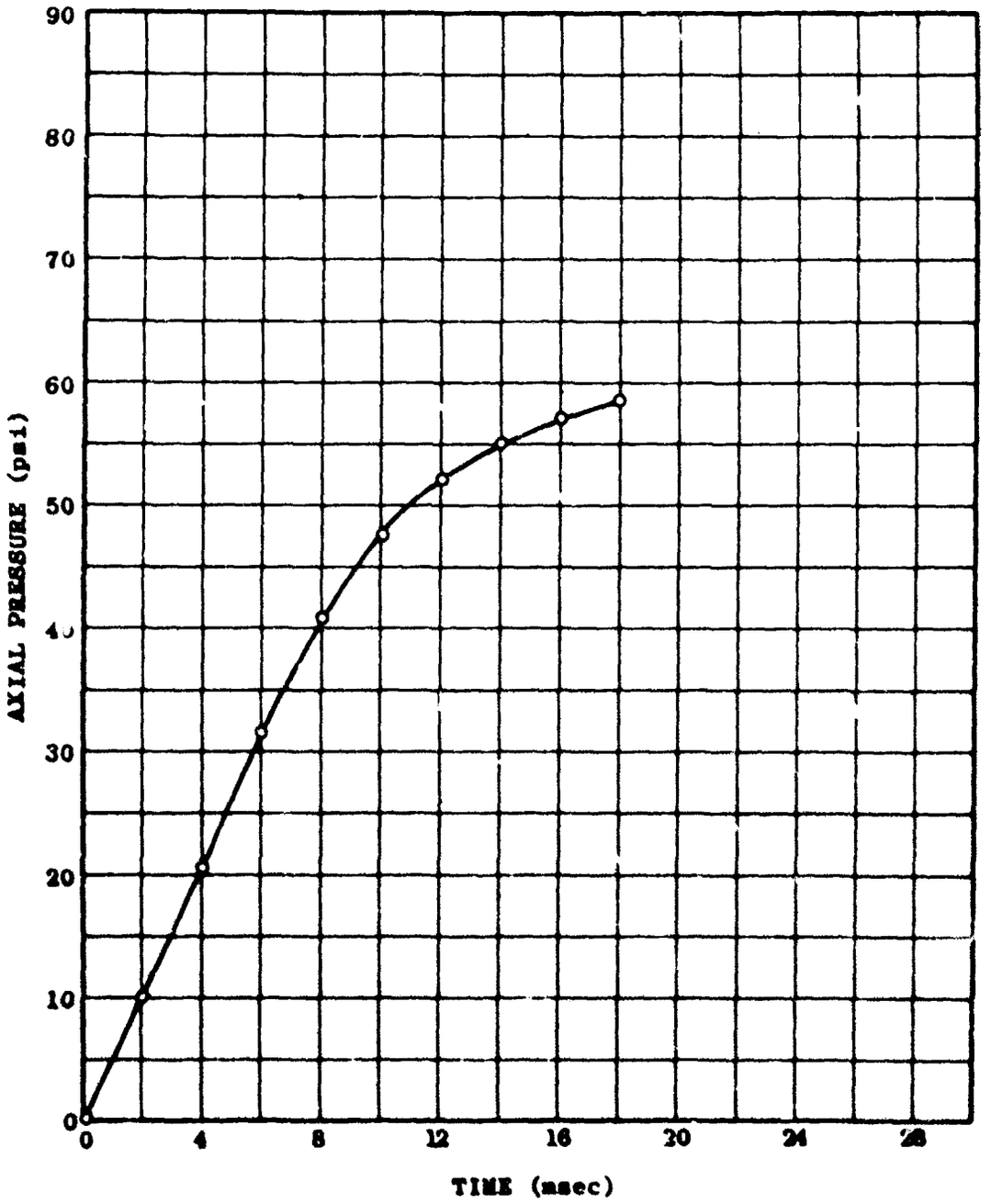

FIGURE 3.24 PRESSURE-TIME CURVE FOR TEST D-1, C-1

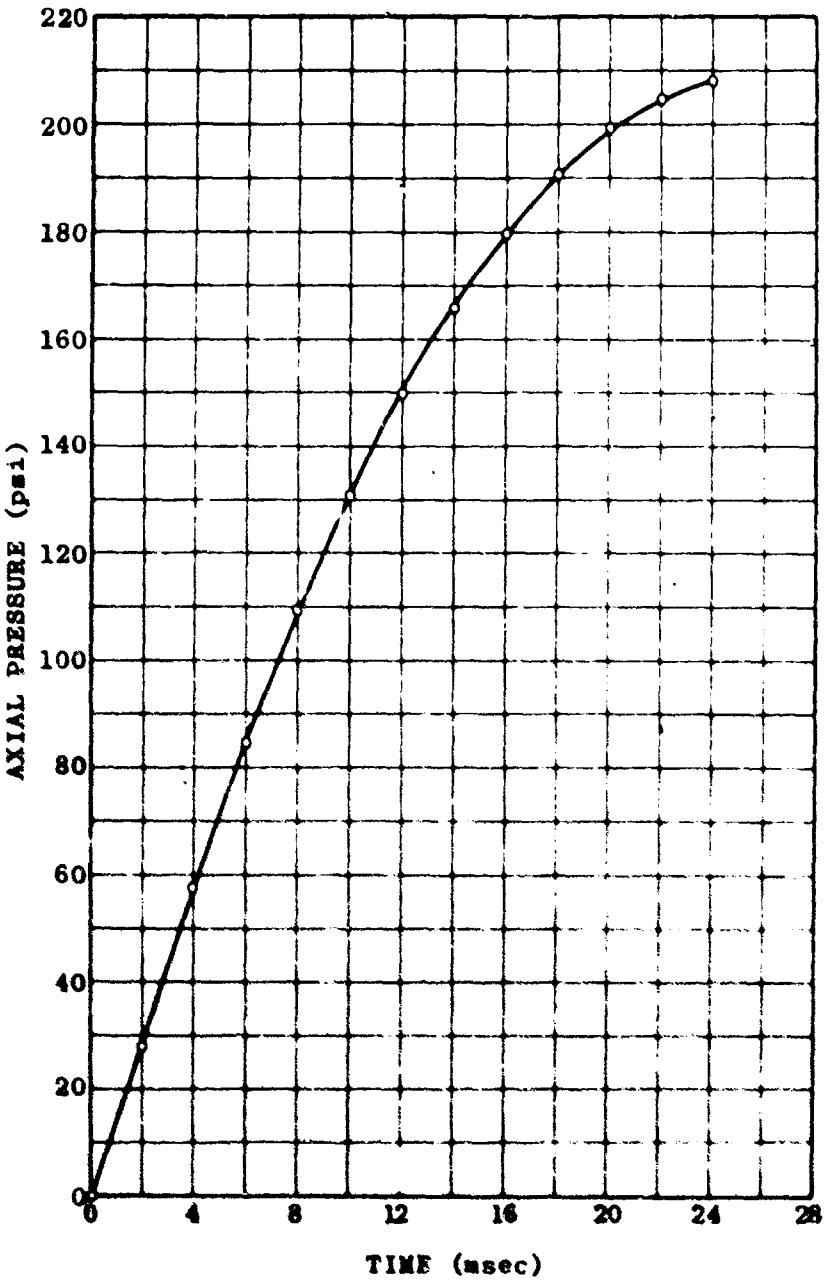

FIGURE 3.25 PRESSURE-TIME CURVE FOR TEST D-A,C-2

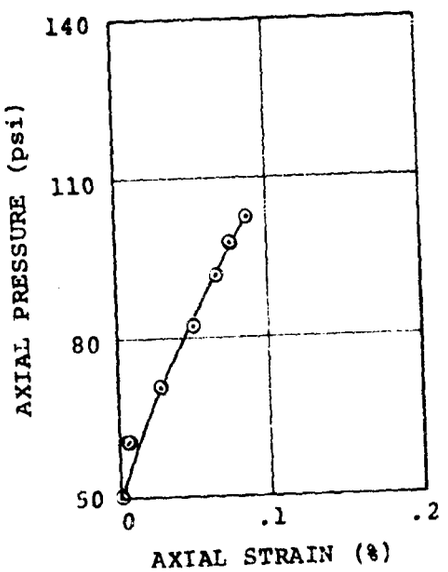

FIGURE 3.26 STRESS-STRAIN CURVE FOR TEST D-1, C-1

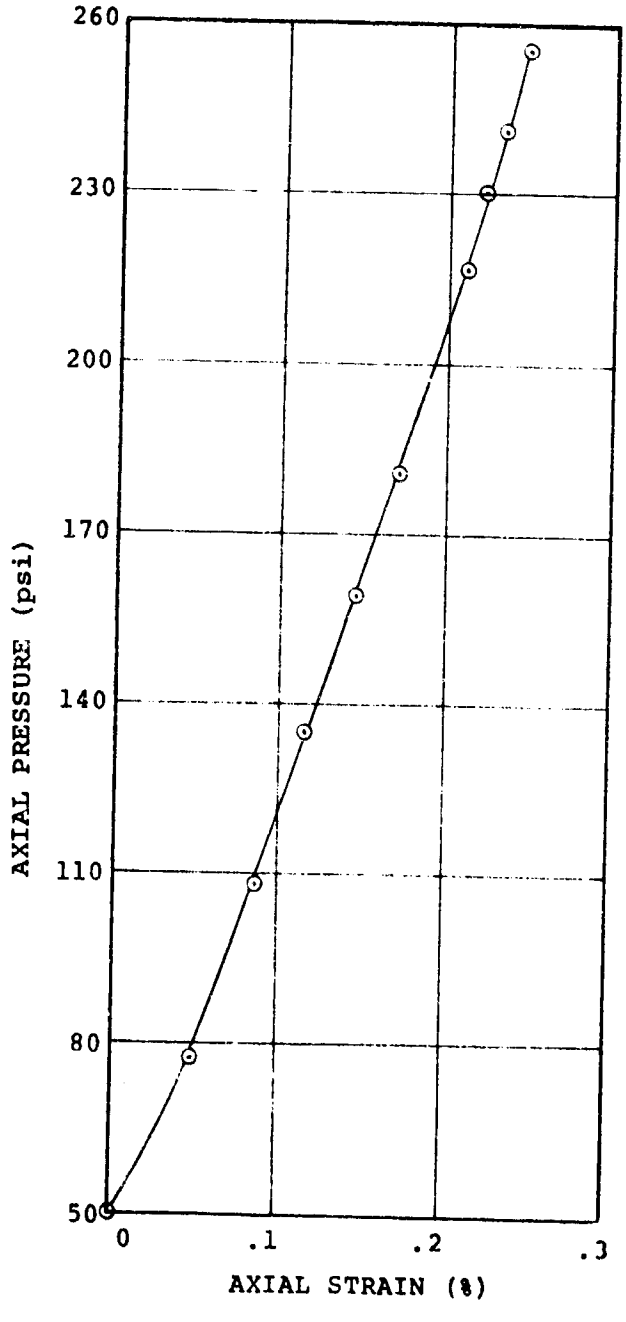

FIGURE 3.27 STRESS-STRAIN CURVE FOR TEST D-1, C-2

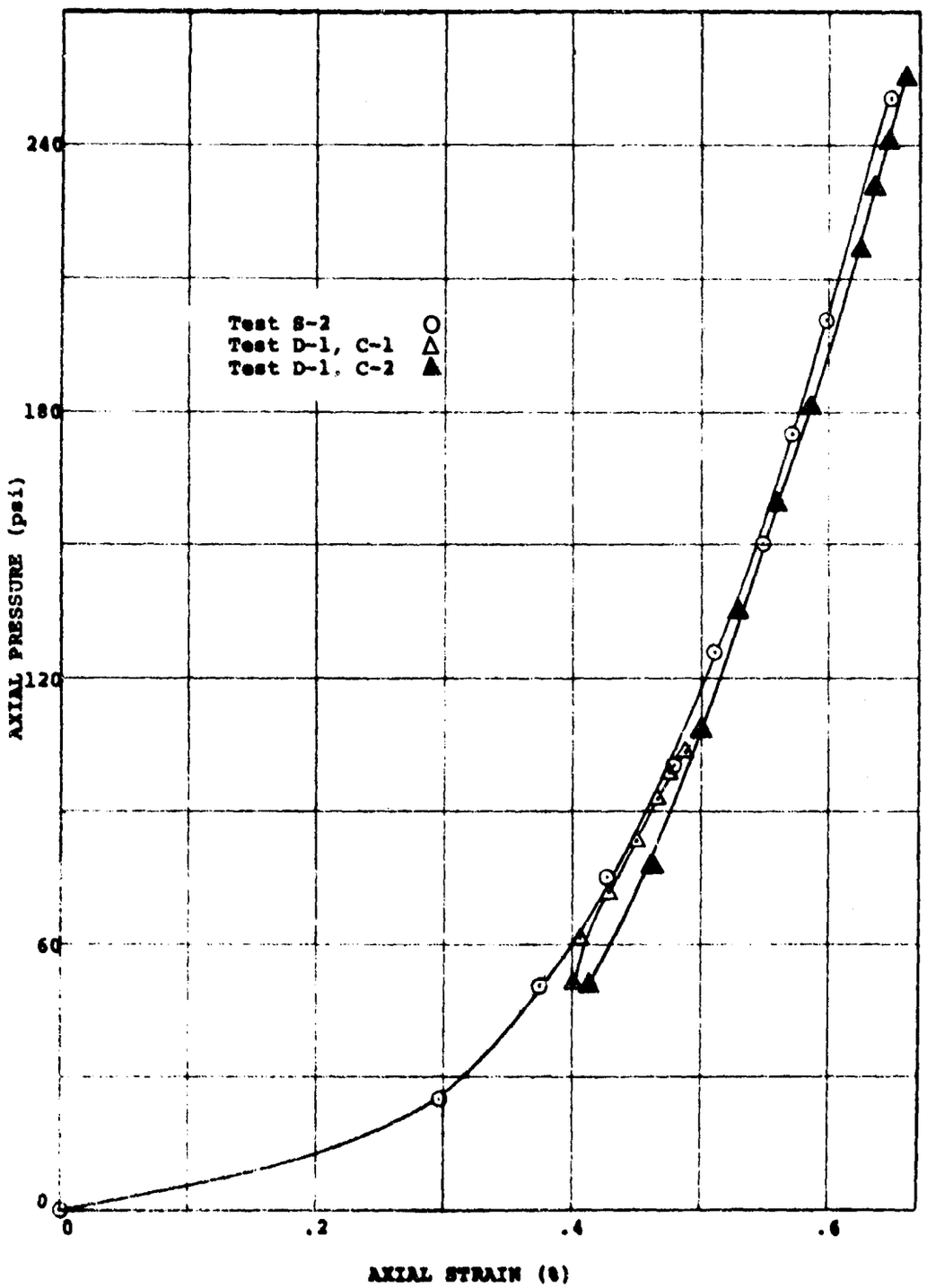

FIGURE 3.28 COMPARISON OF DYNAMIC AND STATIC STRESS-STRAIN CURVES FOR OTTAWA SAND

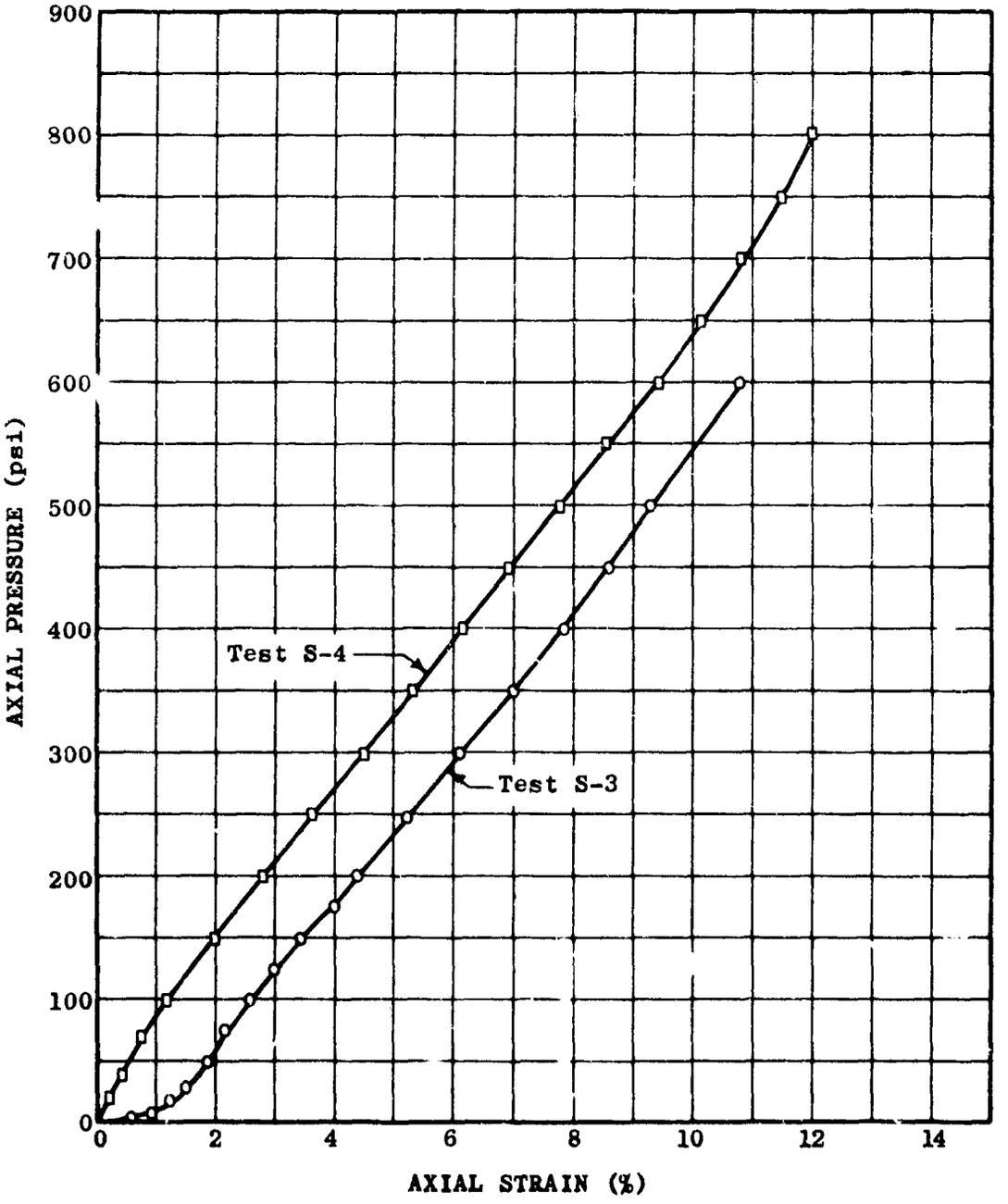

FIGURE 3.29 **COMPARISON OF STATIC STRESS-STRAIN CURVES FOR CRUSHED LIMESTONE DEMONSTRATING EFFECT OF SEATING ERROR**

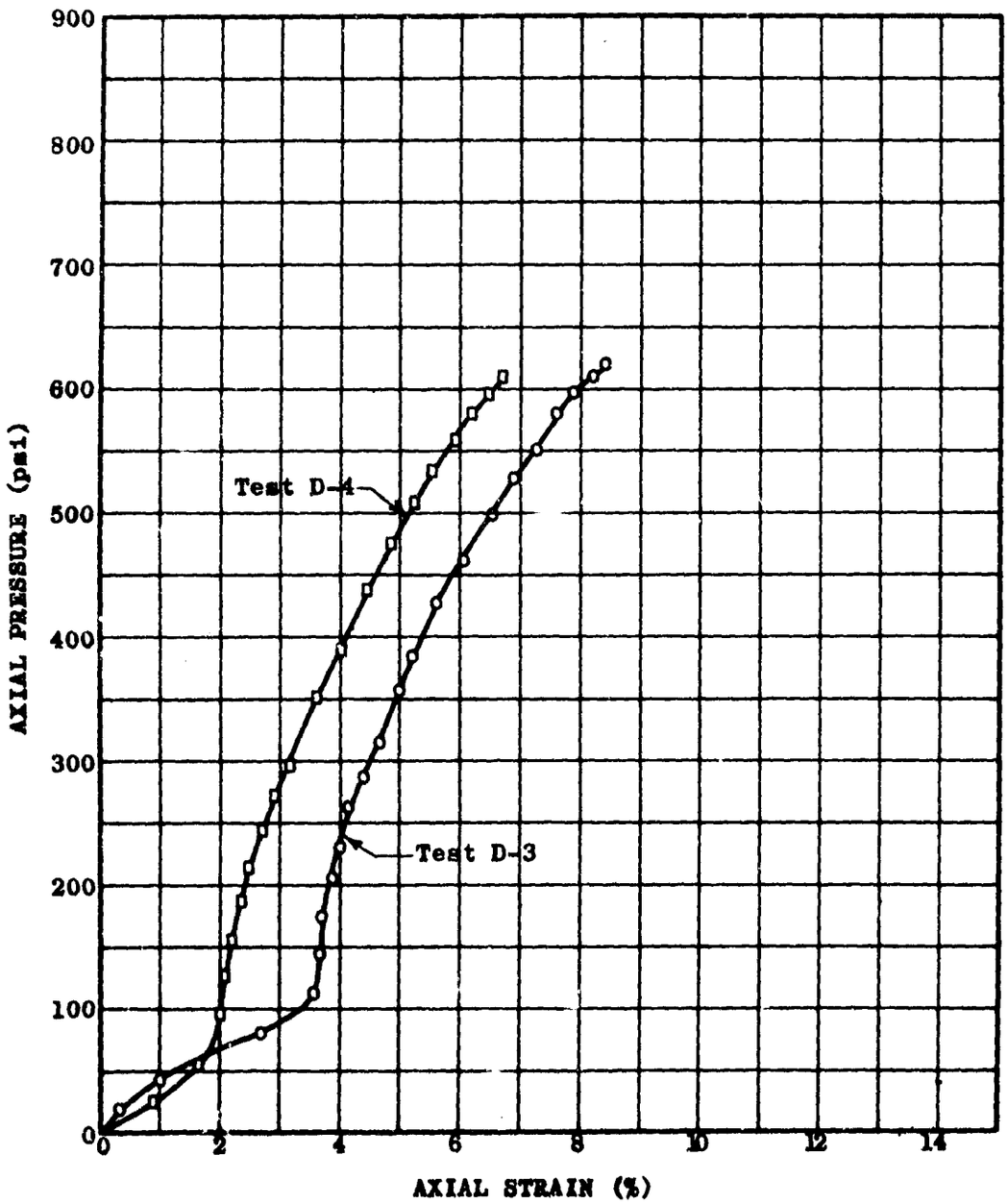

FIGURE 3.30 COMPARISON OF DYNAMIC STRESS-STRAIN CURVES FOR CRUSHED LIMESTONE DEMONSTRATING EFFECT OF SEATING ERROR

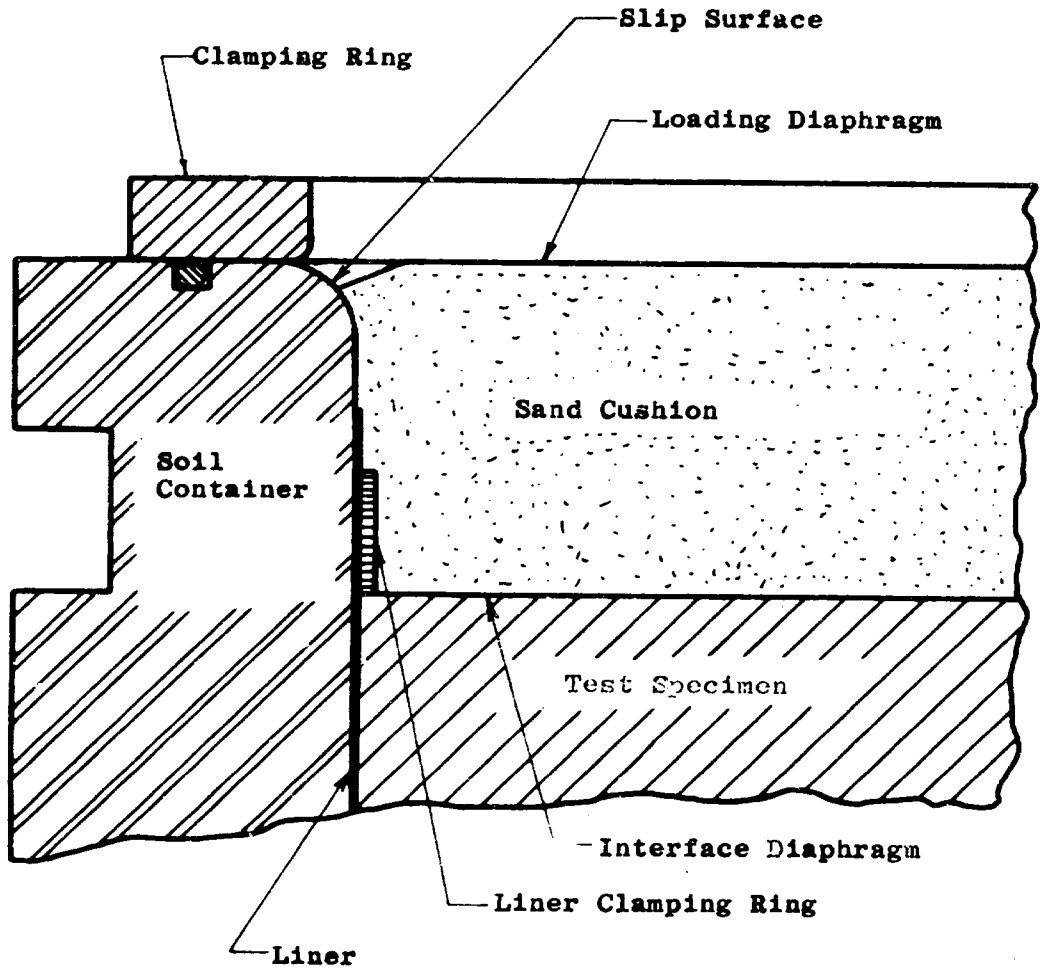

FIGURE 3.31 CROSS SECTION OF THE JUNCTION OF THE DIAPHRAGM, SAND CUSHION, AND SOIL CONTAINER

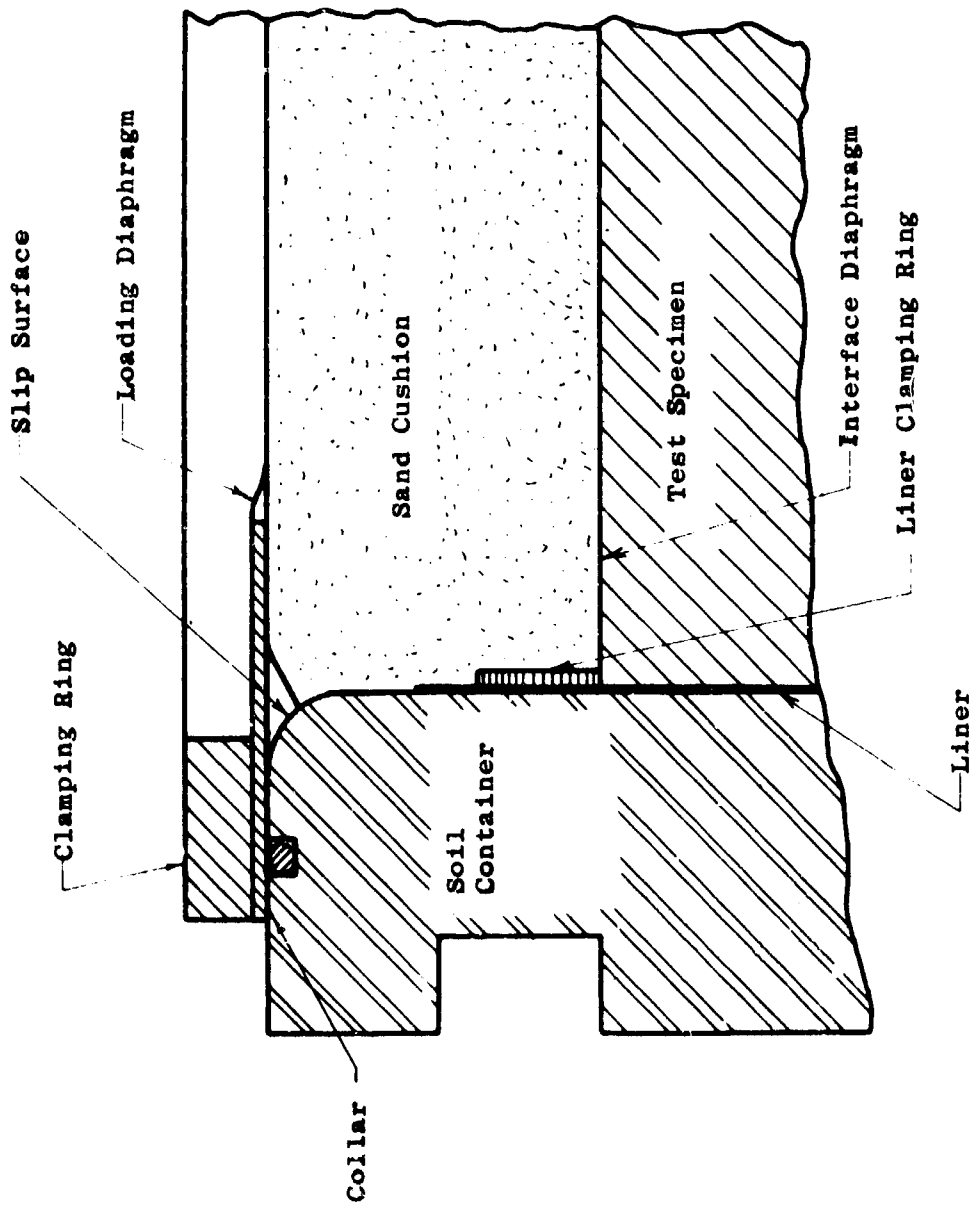

FIGURE 3.32 CROSS SECTION OF THE JUNCTION OF THE DIAPHRAGM, SAND CUSHION, AND SOIL CONTAINER WITH COLLAR

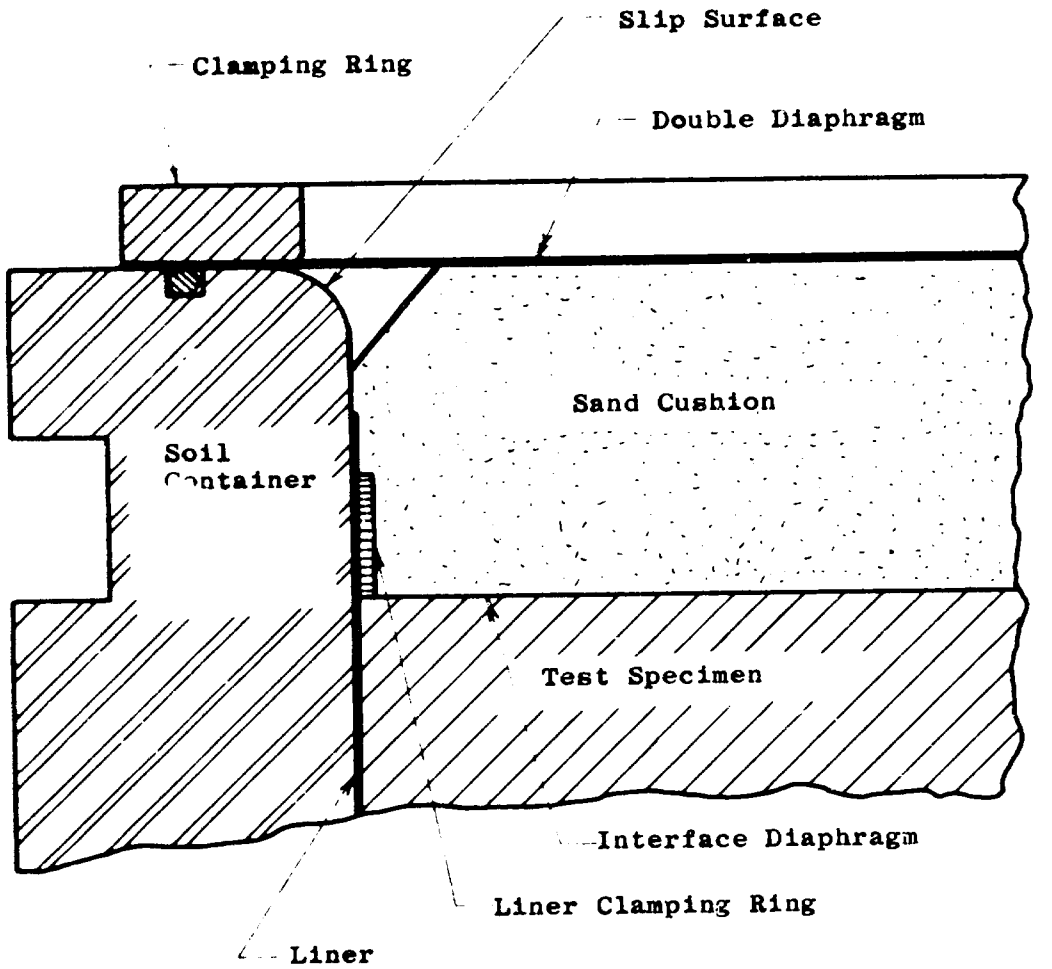

FIGURE 3.33 CROSS SECTION OF THE JUNCTION OF THE DIAPHRAGM, SAND CUSHION, AND SOIL CONTAINER WITH DOUBLE DIAPHRAGM AND INCREASED SLIP AREA

Basic relations

$$t > 25\ L/c \text{ and } c = \sqrt{M_c/\rho}$$

where

t = pressure rise time

L = test specimen height

M = constrained modulus of test specimen

ρ = mass density of test specimen

c = propagation velocity of stress wave

then

$$c = \sqrt{M_c/\rho} = \sqrt{\frac{10{,}000\ \text{lb/in.}^2}{105\ \text{lb/ft} \div 32.2\ \text{ft/sec}^2}} \doteq 8000\ \text{in./sec}$$

$$t > 25\ L/c = 25 \times 14\ \text{in.} \div 8000\ \text{in./sec}$$

$$= 44\ \text{msec}$$

FIGURE 3.34 COMPUTATION OF WHITMAN'S RECOMMENDED RISE TIME

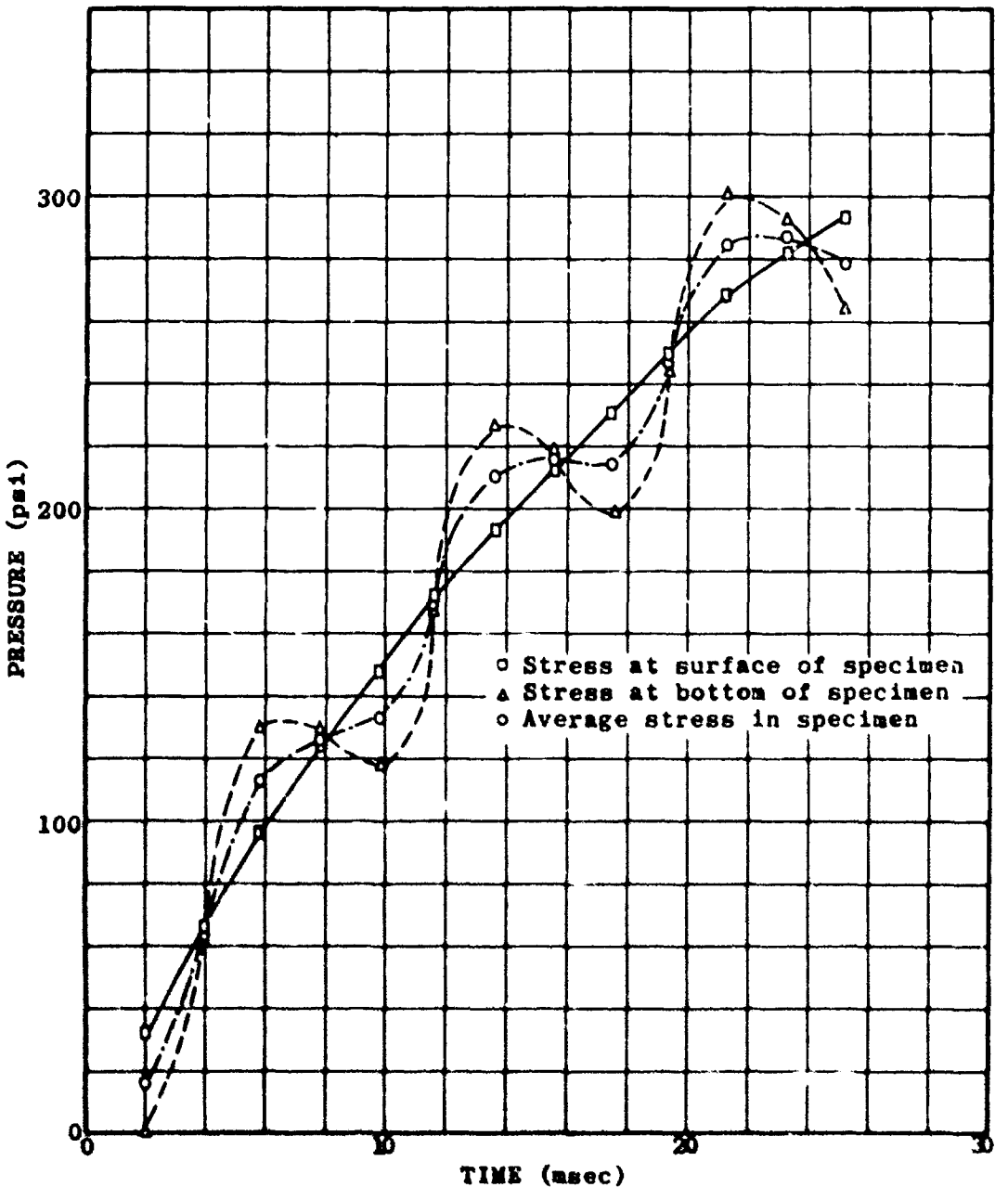

FIGURE 3.35 COMPUTED STRESS VARIATION THROUGH SOIL SPECIMEN WITH TIME

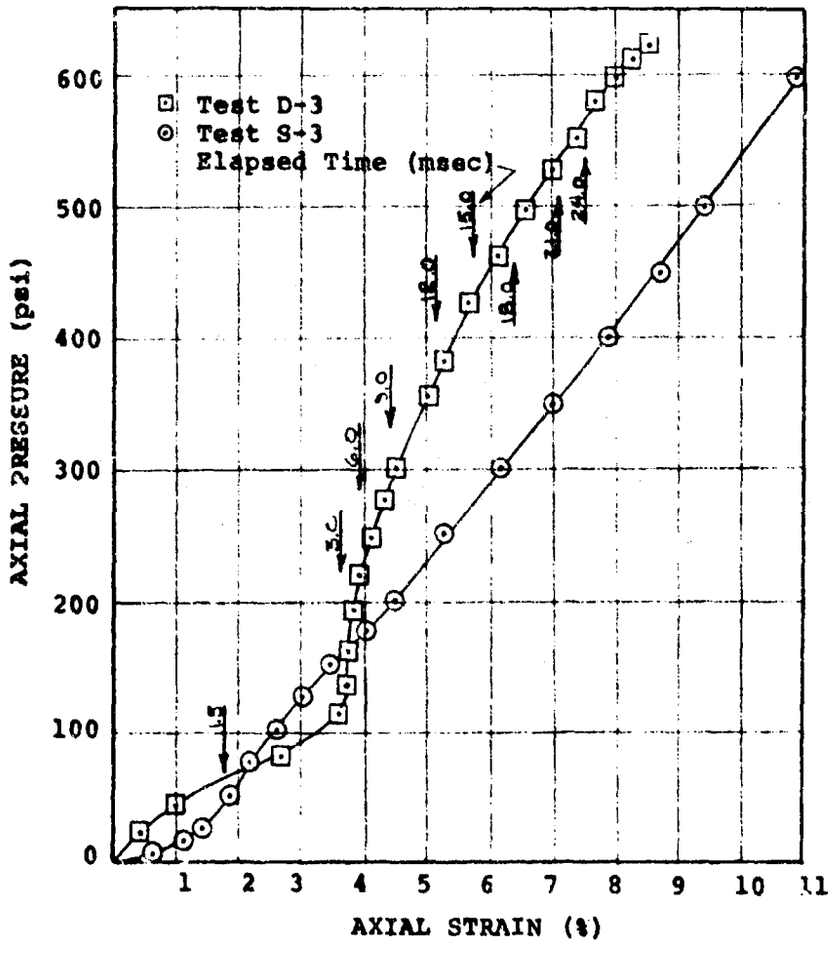

FIGURE 3.36 **STRESS-STRAIN CURVES FOR CRUSHED LIMESTONE AS DETERMINED BY TESTS D-3 AND S-3**

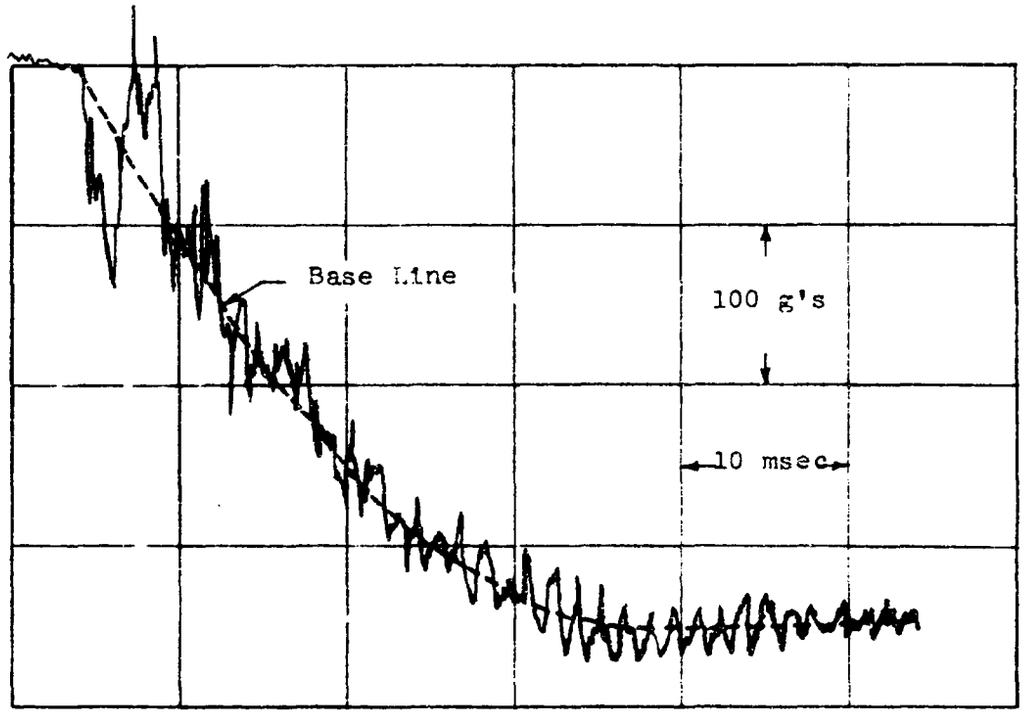

FIGURE 3.37 TYPICAL ACCELEROMETER RECORD FOR DEFORMATION PLATE

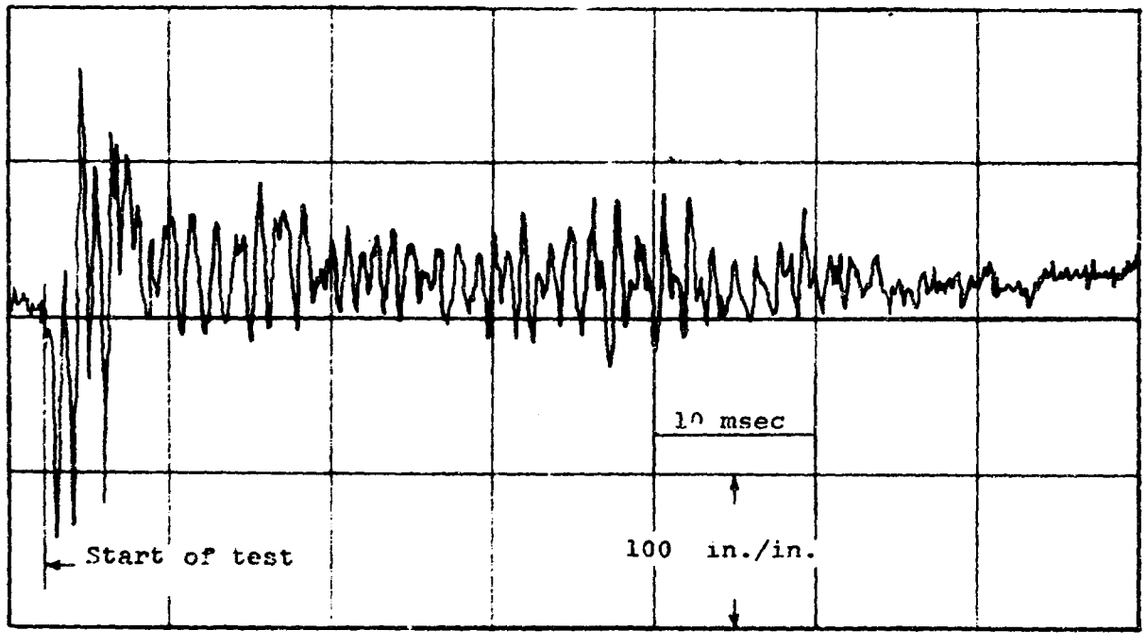

FIGURE 3.38 ACTUATING ROD STRAIN GAGE RECORDS FOR TEST D-7

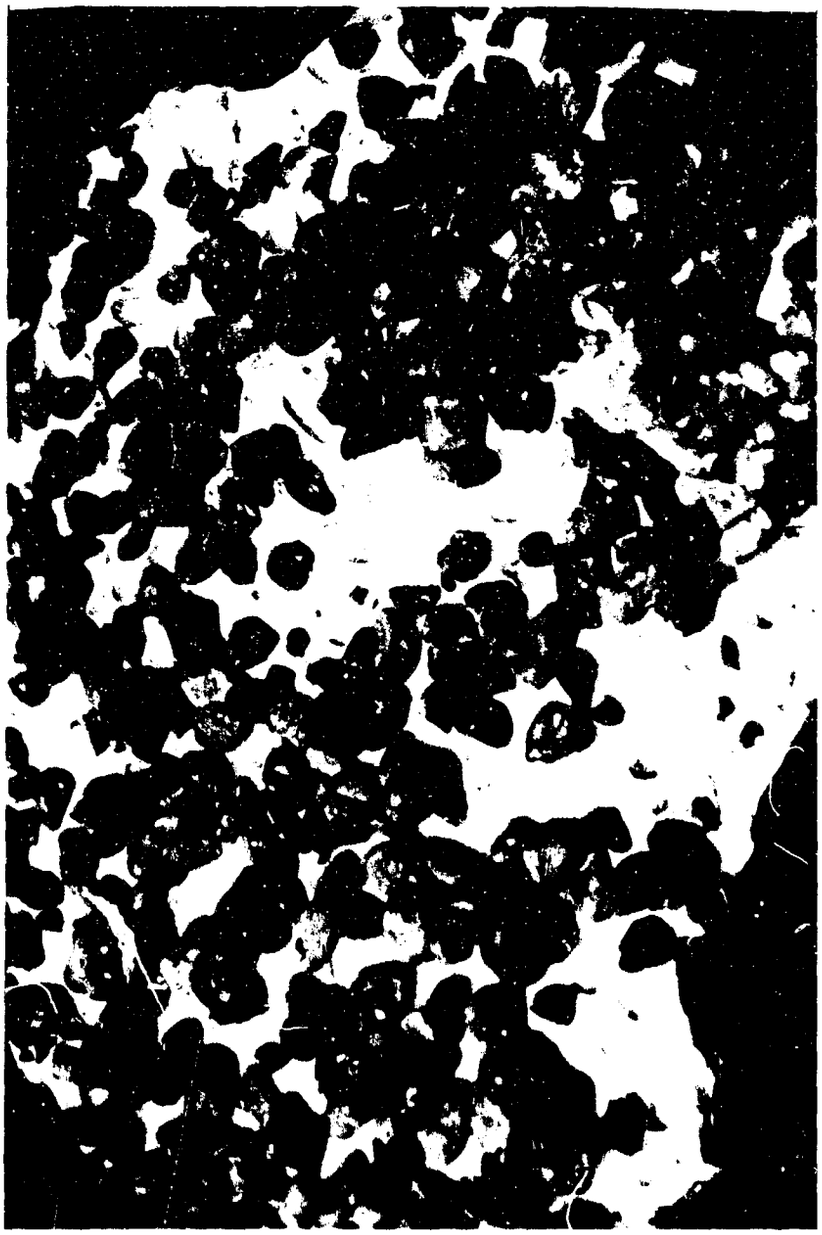

FIGURE 3.39 PHOTO OF LARGE GRANULAR PARTICLES SEATED IN HYDROCAL

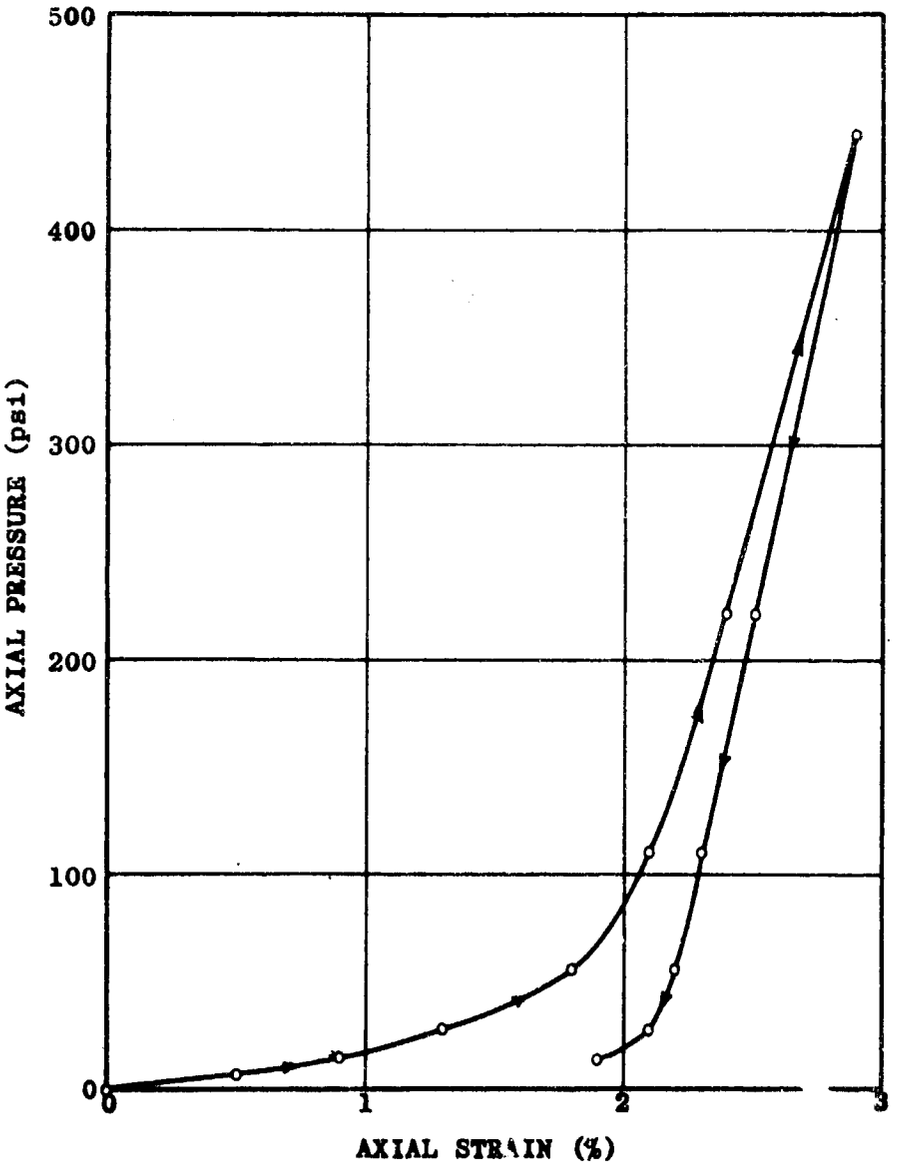

FIGURE 3.40 STRESS-STRAIN CURVE FOR HYDROCAL IN ONE-DIMENSIONAL COMPRESSION

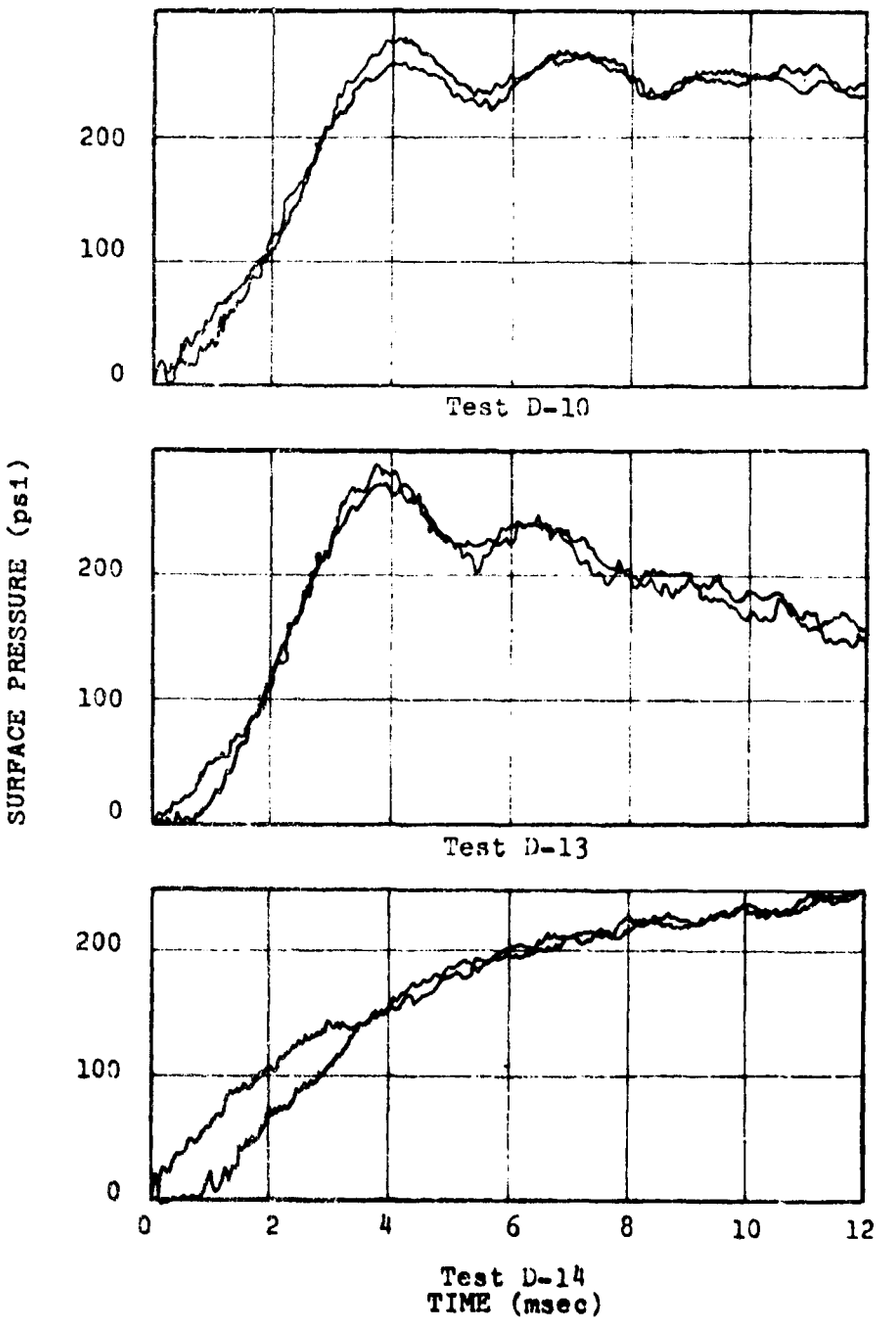

FIGURE 3.41 SURFACE PRESSURE PROFILES (after Prendergast)

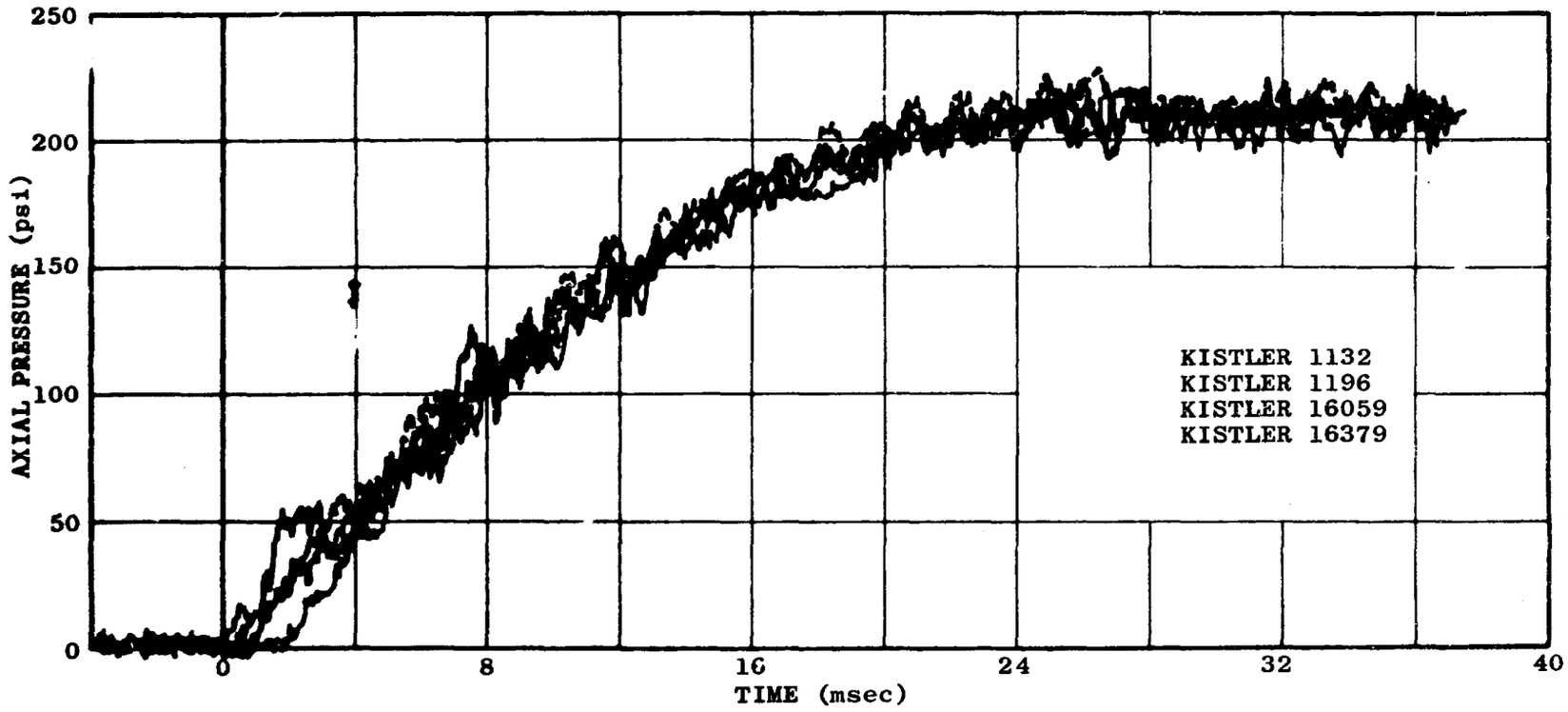

FIGURE 3.42 SUPERIMPOSED PRESSURE-TIME TRACES FOR TEST D-1, C-2

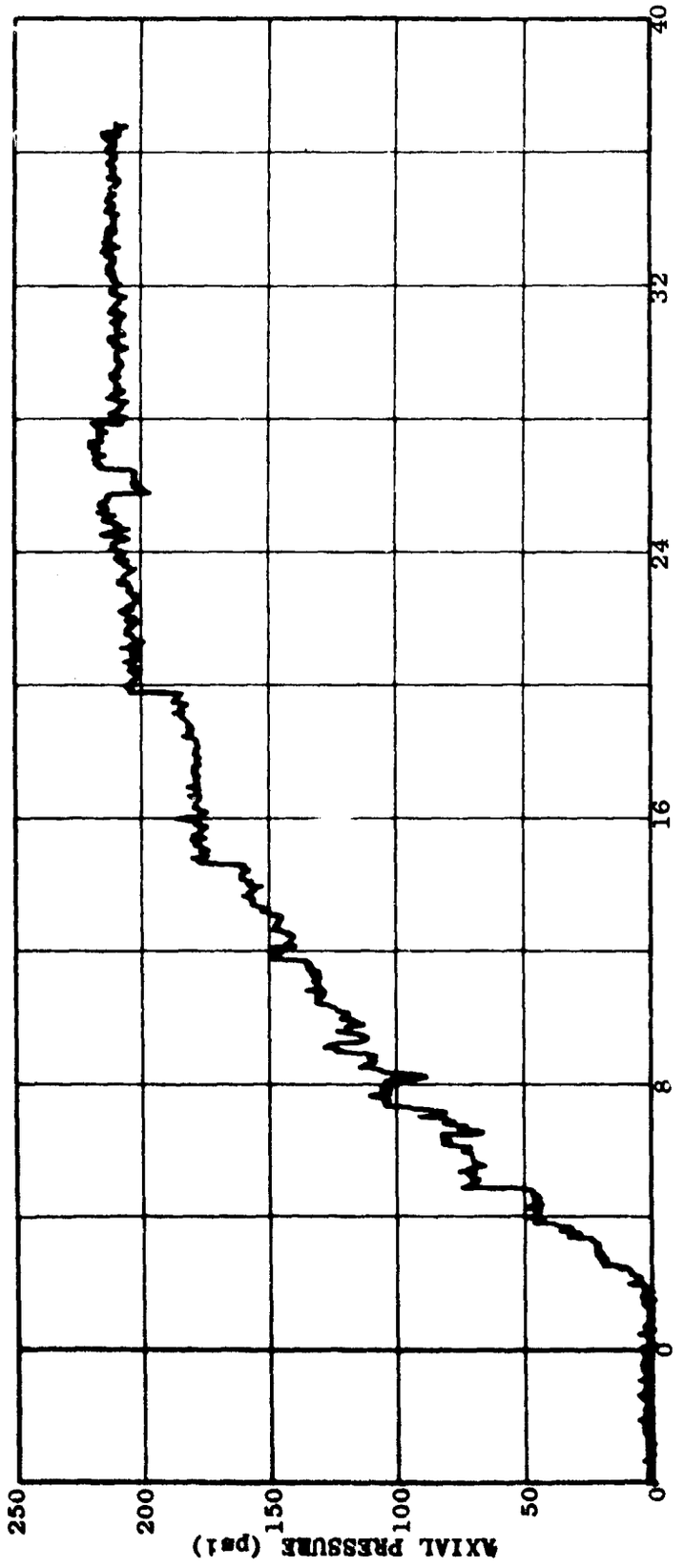

FIGURE 3.43 PRESSURE-TIME TRACE FOR TEST D-1, C-2, AS PORTRAYED BY KISTLER No. 1132

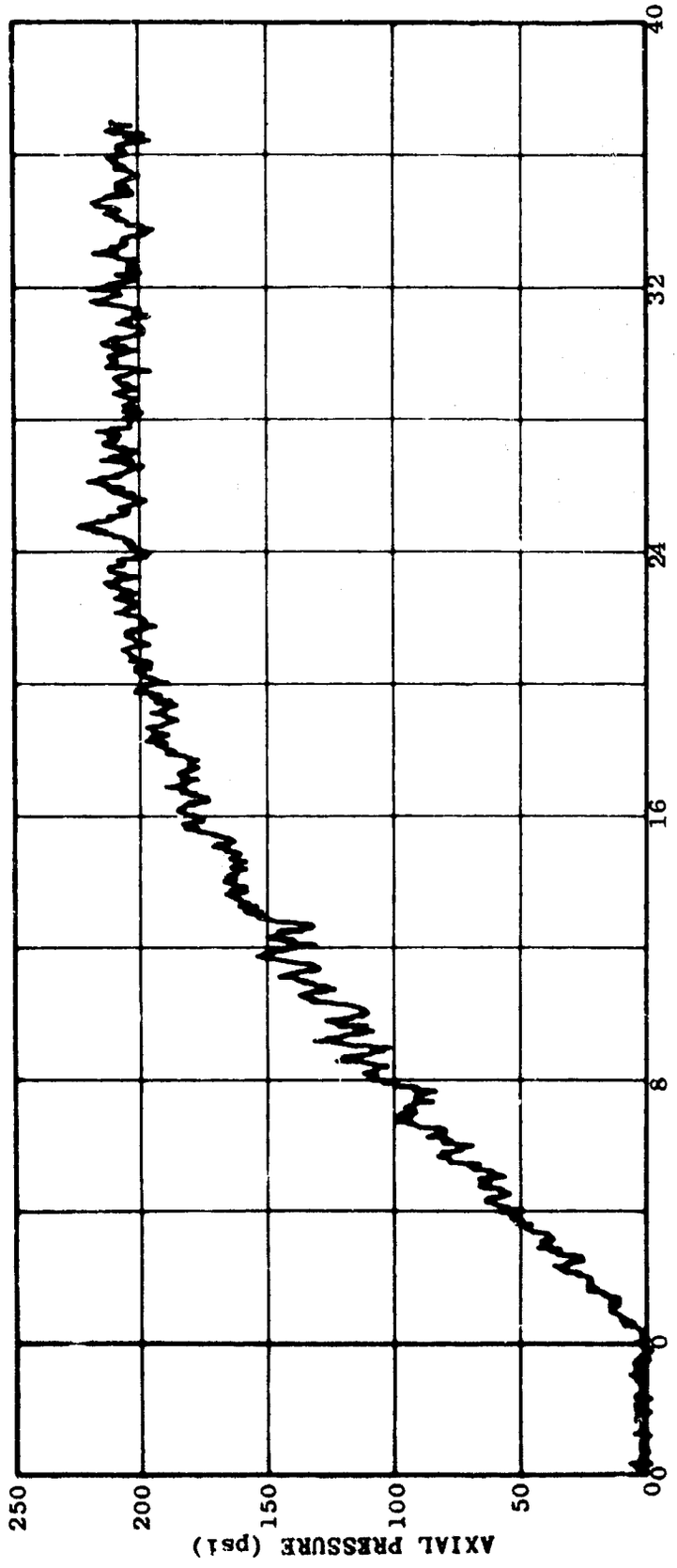

FIGURE 3.44 PRESSURE-TIME TRACE FOR TEST D-1, C-2, AS PORTRAYED BY KISTLER No. 1196

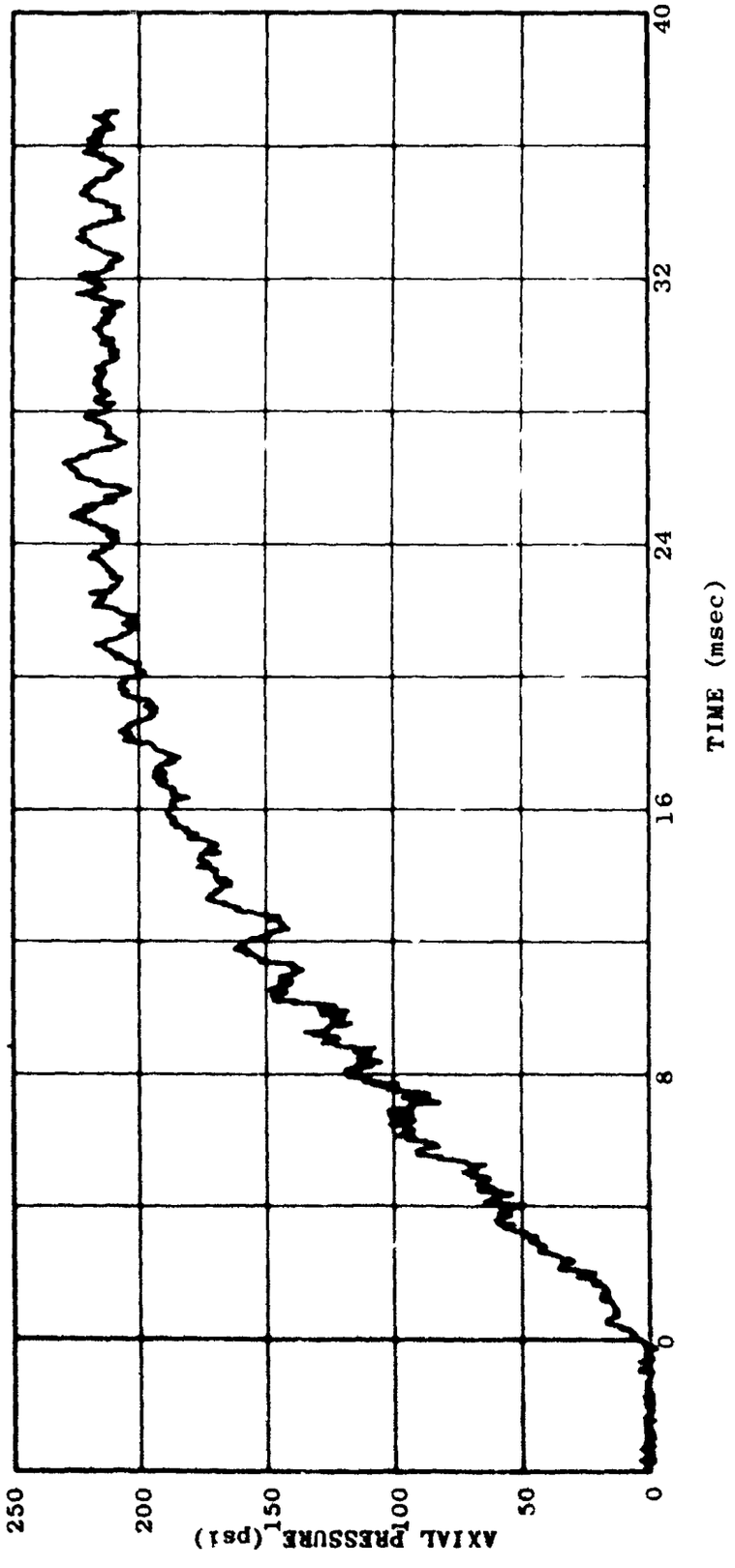

FIGURE 3.45 PRESSURE-TIME TRACE FOR TEST D-1, C-2, AS PORTRAYED BY KISTLER No. 16059

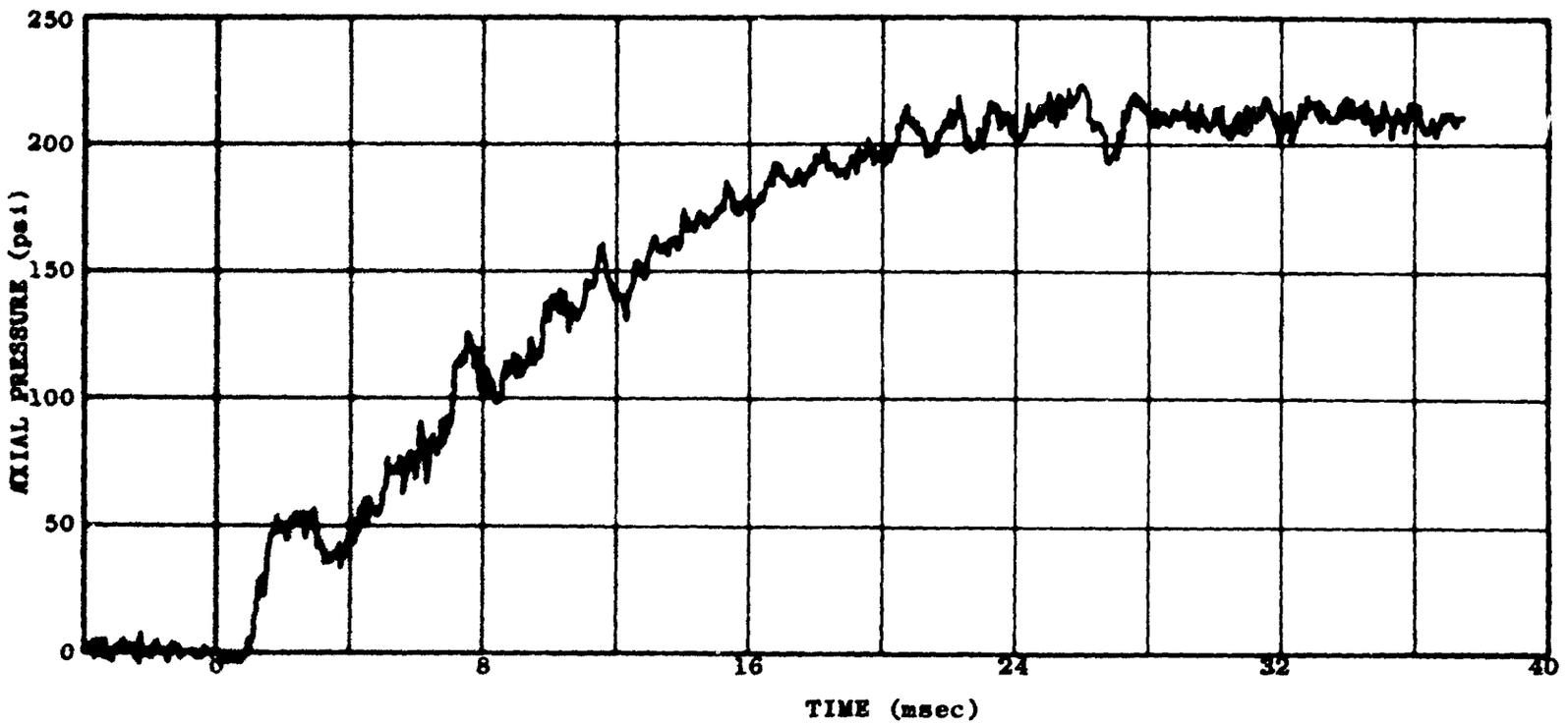

FIGURE 3.46 PRESSURE-TIME TRACE FOR TEST D-1, C-2, AS PORTRAYED BY KISTLER No. 16379

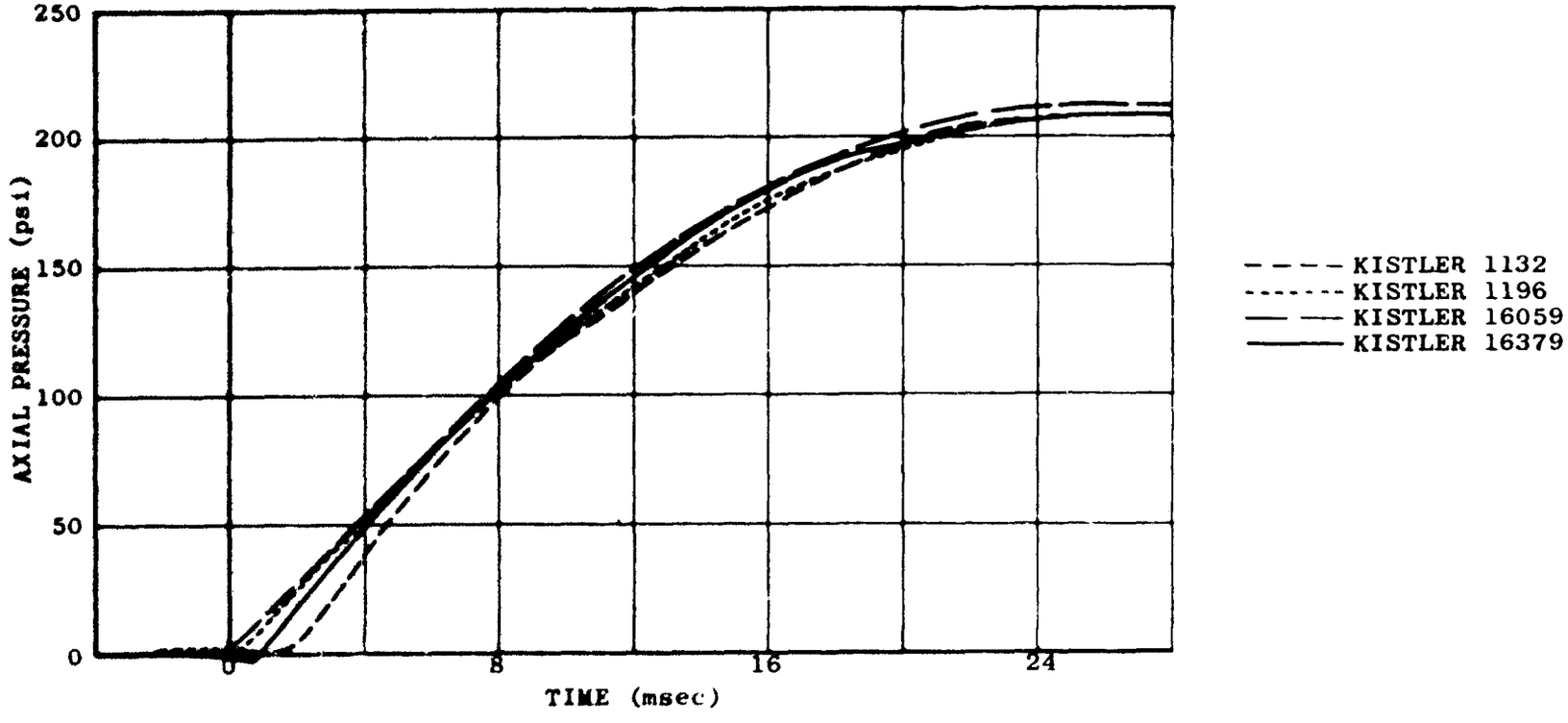

FIGURE 3.47 SUPERIMPOSED INTERPRETED PRESSURE-TIME TRACES FOR TEST D-1, C-2

CHAPTER 4

VARIATION OF PARAMETER STUDY

4.1 INTRODUCTION AND SUMMARY

Subsequent to the completion of the dynamic testing program on the samples from the missile sites as reported in Appendix A, a variation of parameter study was conducted utilizing large granular materials which were readily available locally. The study was designed to demonstrate the effects of parameters such as particle shape and gradation on the behavior of granular materials in one-dimensional compression. The effects of saturation and rate of loading were also investigated.

4.2 TESTING PROGRAM

The variation of parameter testing program was comprised of static and dynamic tests on three types of granular materials: Ottawa sand, crushed limestone, and river gravel. The Ottawa sand was employed primarily to serve as a standard of reference for the tests conducted on the river gravel and the crushed limestone. A crushed limestone and two river gravels were employed as the basic materials for the test program because of the contrast in the particle shapes; the crushed limestone was highly angular while the river gravels were subrounded to rounded. These materials were readily available locally and have been used extensively throughout the midwest in construction applications.

The testing program consisted of 21 tests, 16 static, and 5 dynamic. The program was designed to demonstrate the effect on the one-

dimensional compression behavior of granular materials of the following: 1) the elimination of point crushing at the top and bottom of a test specimen caused by the specimen being in direct contact with a flat rigid surface; 2) the variation of particle shape from angular to rounded; 3) the variation in the mineralogical composition of the specimen and, consequently, variation in the intact compressive strength of the individual particles; 4) the variation of the particle size of the specimens; 5) the variation of the gradation of the specimens; 6) the addition of moisture before loading and after loading; and 7) the rate of loading of the specimens.

4.2.1 Description of Samples

4.2.1.1 Ottawa Sand

The sample of sand employed was 20-30 Ottawa sand which was mined from a quarry of St. Peter sandstone located near Ottawa, Illinois. The specific gravity of the sand was 2.65 and the maximum and minimum dry densities were 114.5 and 95.2 pcf as reported by Prendergast (1968). The individual grains of the Ottawa sand were highly spherical. The results of a mechanical grain-size analysis on the sample are presented in Figure 4.1.

4.2.1.2 Crushed Limestone

The sample of crushed limestone employed was purchased from Alpha Material and Fuel Company, Champaign, Illinois. The limestone had been mined and processed at the Fairmount quarry of Material Service Company, Fairmount, Illinois. The crushed limestone was a dolomitic limestone from the Bond formation. The sample as purchased was rather well graded as demonstrated by the results of a mechanical grain-size analysis presented

in Figure 4.2 and is referred to as well graded in this study. The particle shape was angular as shown by the photograph of the individual particles presented in Figure 4.3. The average unconfined compressive strength of an intact specimen of the rock was 7900 psi. The hardness as measured by a Schmidt hammer was 45.

The unconfined compressive strength of an intact specimen of the rock was determined by running strength tests on cores taken from block samples. Several intact samples of the limestone were obtained from the Fairmount quarry and from these, 2-inch diameter cores were drilled using a diamond bit. A test specimen 4 inches high was then cut from the core and the ends lapped to a smooth finish. The specimens were then tested in unconfined compression. Prior to the testing of the specimens in unconfined compression, the rebound hardness of the specimen was measured using a Schmidt hammer. The hardness value was determined by taking the average of the higher half of the readings obtained on a given specimen with 12 readings taken per specimen.

4.2.1.3 River Gravels

Two different types of river gravel were employed in the testing program, a well-graded gravel from North Dakota and a well-graded gravel from the Wabash River in Indiana.

The sample of Wabash River gravel was purchased from the Covington Quarry of Interstate Sand & Gravel, Covington, Indiana. The gravel was subrounded to rounded and was composed of a random mixture of igneous and sedimentary rocks. A photograph of the individual particles is presented in Figure 4.4. The sample was rather well graded as shown by the mechanical grain-size analysis presented in Figure 4.5 and is referred

to as well graded in this study. The sample of river gravel from North Dakota was obtained from a construction site in southeast North Dakota. The gravel was subrounded to rounded and was composed primarily of igneous rocks. A photograph showing the individual particles is presented in Figure 4.6. The material was also fairly well graded as shown by the results of the mechanical analysis presented in Figure 4.7.

4.2.2 Testing Program

The testing program as completed is presented in Tables 4.1 and 4.2. Specimen placement was not varied from the procedure described in Section 3.3.2 with the exception that Hydrocal was employed on the top plate of the pedestal and the bottom of the deformation plate to eliminate seating error for all tests in this program except D-1, D-2, and D-3.

During specimen placement, the materials were placed in uncompacted lifts which varied from 3-1/2 to 4-1/2 inches in thickness. The compaction effort was varied by the force applied to the tamper by the operator. Light compaction was achieved by the operator applying no downward force to the tamper. Heavy compactive effort was achieved by the operator applying as much force as possible to the tamper, approximately 60 lb, and medium compaction was achieved by application of a medium force to the tamper, approximately 25 lbs.

The investigation into the effects of seating error was accomplished by four tests: two static tests, S-3 and S-4, and two dynamic tests, D-3 and D-4. Tests S-3 and S-4 were conducted on crushed limestone with no measures taken to reduce seating error for Test S-3 and Hydrocal used to reduce seating error for Test S-4. Tests D-3 and D-4 were also conducted on crushed limestone with no measures taken to reduce seating error for Test D-3 and Hydrocal used for Test D-4.

The effect of variation of particle shape was investigated by two tests: S-13 and S-16. Test S-13 was conducted on a well-graded sample of Wabash River gravel, the particle shape being subrounded to rounded. Test S-16 was conducted on a well-graded sample of crushed limestone which had an angular particle shape. The difference in particle composition is a factor which affects the test results and tends to mask the effects of particle-shape variation; however, this shortcoming could not be avoided.

The effect of variation of particle composition was investigated by three tests: Tests S-2, S-5, and S-13. Test S-2 was conducted on a specimen of 20-30 Ottawa sand; Test S-5 was conducted on a well-graded specimen of river gravel from North Dakota; and Test S-13 was conducted on a well-graded specimen of Wabash River gravel. The test specimens for Tests S-5 and S-13 were similar in grain size and shape while the test specimen for Test S-2 was composed of much smaller grains and the specimen was uniformly graded. The test results from Test S-2 were utilized primarily to demonstrate the behavior of a particulate specimen when particle crushing was for all practical purposes eliminated.

The effect of variation in particle size was investigated by a series of four tests on Wabash River gravel: Tests S-6, S-8, S-12, and S-15. The samples for the four tests were taken from a well-graded sample of Wabash River gravel and broken on screens such that the D_{10} sizes for the four samples were 0.19, 0.29, 0.59, and 0.95 inches for Tests S-8, S-12, S-6, and S-15, respectively. The uniformity coefficients for the four samples were 1.47, 1.48, 1.41, and 1.28, respectively.

The effect of variation in gradation of different samples was investigated by a series of four tests on Wabash River gravel: Tests S-6, S-8, S-12 and S-13. Tests S-6, S-8, and S-12 were conducted as a part of the investigation into the effect of variation of particle size and S-13 was a well-graded sample of gravel made up by mixing definite proportions of material from the samples broken for the test specimens for Tests S-6, S-8, and S-12.

The effect of saturation on the behavior of granular materials was investigated by the results of Tests S-8, S-9, S-10, S-13, S-14, S-15, S-16, S-17, S-18, and S-19. These tests were primarily conducted to investigate the effects of variation of other parameters; however, the time of saturation and, in two instances, the placement water content were varied to provide additional data for this study.

The last parameter to be investigated was the effect of the rate of loading. Changes in the rate of loading are a variation in the test conditions rather than some property of the sample tested; however, the properties of the given specimen such as density, intact compressive strength, particle shape and permeability are probably responsible for the effects resulting from variation in the rate of loading. The materials employed in this investigation were Ottawa sand and crushed limestone. The rate of loading was varied from static to dynamic with pressure rise times as fast as 600 psi in 25 msec.

4.3 TEST RESULTS

4.3.1 Effect of Seating Error

The investigation into the effect of seating error caused by point crushing on the top surface of the specimen at the deformation plate-

specimen interface and at the pedestal-specimen interface has been reported in Section 3.3.4.3.

4.3.2 Effect of Variation of Particle Shape and Particle Composition

Particle shape is one of the more important factors in the behavior of particulate materials in one-dimensional compression. At a given stress level, the more angular material will suffer greater deformation than the more rounded material, other parameters being equivalent, because of greater stress concentration and lower strength at points of contact.

The effect of variation of particle shape was investigated by two static tests: Tests S-13 and S-16. Test 13 was conducted on a well-graded sample of Wabash River gravel with a D_{10} size of 0.22 inches, a D_{60} size of 0.47 inches, and an initial dry density of 117.7 pcf. The specimen was placed and loaded in an air-dry condition. Test S-16 was conducted on a well-graded sample of crushed limestone with a D_{10} size of 0.20 inches, a D_{60} size of 0.50 inches, and an initial dry density of 102.4 pcf. The specimen was placed and loaded in an air-dry condition. Medium compactive effort was employed for the placement of both specimens. The descriptions of the samples and mechanical grain-size analyses are presented in Figure 4-8.

The effect of the variation of the particle shape is shown by the stress-strain curves for the two tests as presented in Figure 4-9. The specimen of crushed limestone varied nearly linearly from being 1.5 times more compressible than the Wabash River gravel at an axial pressure of 50 psi to 2.7 times more compressible at an axial pressure of

300 psi. Above 300 psi to the maximum axial stress of the test, 500 psi, the compressibility factor remained constant at approximately 2.7. The difference in the behavior is believed to have resulted primarily from the difference in the particle shapes and the resultant high stress concentrations resulting between the particles of crushed limestone because of the high angularity. However, the difference in the strengths of intact specimens of the rock composing the two materials must also be considered. If the angular particles were composed of the materials making up the Wabash River gravel rather than the softer limestone, the stress-strain behavior would undoubtedly be stiffer than that measured in Test S-16.

In an effort to establish relative values for the strengths of intact specimens of the two samples, an intact specimen of the limestone was tested in unconfined compression and the average intact strength of the Wabash River gravel was estimated from data published by Miller (1965). The unconfined compressive strength of the crushed limestone was measured to be 7900 psi and the Schmidt rebound hardness was measured to be 45. The Wabash River gravel was primarily composed of a mixture of igneous and sedimentary rocks; therefore, no single intact strength could be assigned to the material comprising the sample. Since the river gravel suffered considerable abrasion in being transported and consequently rounded, all particles were assumed to be fairly sound. Thus, the lowest intact strength probably corresponds to that of sound sandstone, 10,000 psi, while the highest strength probably corresponds to that of sound granite, 20,000 psi, and an average intact strength in unconfined compression for the sample of 15,000 psi is probably reasonable.

If a sample consisting of particles of sufficient strength to resist particle crushing is tested in one-dimensional compression, then the resulting stress-strain curve is concave upward or "locking". Such behavior indicates a higher degree of interlocking of particles, more contact area, and a greater number of particle-to-particle contacts with increased stress. A specimen of 20-30 Ottawa sand was tested and the resulting "locking" behavior is demonstrated in the stress-strain curve presented in Figure 4.10. Examination of the stress-strain curves for Tests S-13 and S-16 indicates no locking behavior which indicated that both specimens suffered considerable particle crushing.

Some of the difference in stress-strain behavior indicated by Tests S-13 and S-16 must be attributed to the difference in the strengths of intact specimens of the rock, 15,000 psi for the gravel and 8000 psi for the limestone; however, even if the strains suffered by the crushed limestone are assumed to correspond to a stress level of one-half that measured, the Wabash River gravel would still be the stiffer material. Therefore, it is concluded that the more angular particles caused the specimen of crushed limestone to suffer greater deformation for any given stress level because of greater stress concentrations and lower strengths at points of contact.

The difference in the stress-strain behavior caused by variation in the composition of the individual particles was demonstrated by comparison of the test results from Tests S-2 (Figure 4.10) and Tests S-5 and S-13 (Figure 4.11). The stress-strain behavior of the North Dakota river gravel was "locking" relative to that of the Wabash River gravel,

but the strains for any given stress level did not vary by more than 25% and in general did not differ by more than 10%. The tangent modulus of the North Dakota river gravel was the lower until an axial stress of approximately 175 psi was reached and was the higher at greater stress levels. It should be noted that the origins for the curves presented in Figure 4.11 were taken as the strains corresponding to a stress level of 10 psi to eliminate possible seating error.

The specimen for Test S-2 was Ottawa sand, which is a highly spherical quartz sand. The density, grain size, and gradation do not correlate with the specimens for Tests S-5 and S-13; however, Test S-2 illustrates the locking behavior which granular materials exhibit in one-dimensional compression if particle crushing does not dominate the behavior. The test specimens for Tests S-5 and S-13 were composed of a North Dakota river gravel and Wabash River gravel. Both specimens were composed of subrounded to rounded particles as shown in Figures 4.6 and 4.4, respectively. Gradation curves for both samples are presented in Figure 4.12. The only significant difference in the two samples was the composition. The sample of North Dakota river gravel was nearly devoid of softer rocks while the Wabash River gravel had a relatively large percentage of softer rocks. Thus it is concluded that the higher the intact strength of the material composing the individual particles, the stiffer the one-dimensional stress-strain behavior.

4.3.3 Effect of Variation of Particle Size

The effect of variation of particle size was demonstrated by a series of tests on a sample of Wabash River gravel. The gravel was separated into four samples containing essentially single particle sizes by screening.

Grain-size distribution curves for the four samples are presented in Figure 4.13. The particle shape, composition, and source of the gravel were discussed in Section 4.2.1.3. Specimens of the four samples were placed air-dry with approximately the same compactive effort, loaded to 500 psi statically, saturated and allowed to creep, and then unloaded. The results of the tests are presented in Figure 4.14. The effect of saturation is discussed in Section 4.3.5.

The general behavior of a uniformly graded (monogranular) particulate material in one-dimensional compression has been discussed by numerous authors; however, for clarity, a brief review is in order. At low stress levels, i.e., stress levels which do not exceed the crushing strength of the individual particles, deformation of an uncemented particulate material in one-dimensional compression results primarily from the rearrangement of particles as the most stable possible configuration of particles is achieved. As the stress level is increased, the tangent modulus, in general, increases until the crushing strength of the individual particles is exceeded, at which time the stress-strain curve becomes concave to the strain axis. the stress level is further increased, the stress-strain curve becomes concave to the stress axis until the crushing strength of the minerals constituting the particles is reached, at which time the stress-strain curve once again becomes concave to the strain axis. Further stress application causes the stress-strain curve to become concave to the stress axis. With large granular materials such as those tested in this study, additional reversals in the concavity of the stress-strain curve may occur as the individual particles are broken down to

smaller and smaller sizes. However, as the axial pressure in a static test with the DLG is limited to 1600 psi and in this study to 1000 psi, such high-pressure behavior was not demonstrated.

The particle crushing stress levels observed durir testing are denoted on the stress-strain curves for the different test specimens in Figure 4.14. These particle crushing stress levels were 275, 225, 175 and 165 psi for the very coarse, coarse, medium, and fine specimens, respectively. These crushing stress levels were inferred from the general shape of the stress-strain curves, i.e., the reversal of the concavity of the curves. The reason for the fine particles crushing first and the very coarse particles crushing last was not determined; however, it is speculated that the size of the particle of a river gravel is related to the intact compressive strength of the material composing the particle. Assuming that all particles in a given river gravel were broken from the parent rock at approximately the same time and that all the particles have been exposed to approximately the same conditions, then it is reasonable to conclude that the larger the particle, the greater the compressive strength of the material composing the particle. Consequently, the larger the particle size of the particles in a monogranular test specimen, the higher the particle crushing strength and the stiffer the behavior in one-dimensional compression.

The behavior of the four test specimens at low stress levels is presented in Figure 4.15. The specimens composed of the larger particles suffered greater strains at very low axial pressures, less than 20 psi. The interface membrane developed leaks during some of the tests on mono-

granular specimens with large particle sizes and required removal of the specimen container. Examination of the specimens removed indicated that for pressures less than approximately 100 psi, very little particle crushing occurred. Therefore, it was concluded that the greater strains suffered by the monogranular specimens composed of the larger particles resulted from particle relocation rather than particle crushing. Another indication of particle breakage was the audible cracking and popping of the individual particles, which was quite pronounced when the particle crushing strength of the particles was attained. This phenomenon of the greater particle relocation and associated strain for the specimens composed of the larger particles could be associated with the relative density of the specimens; however, the means and the time required to investigate the relative densities of the different specimens was beyond the scope of this investigation.

The effect of particle relocation at low stresses can be eliminated by translating the stress-strain curves to the origin at a common stress level. In Figure 4.16, the stress-strain curves for the four specimens were translated to the origin at a stress level of 40 psi. This translation revealed an orderly trend in the behavior pattern. The very coarse gravel was the stiffest specimen and the fine gravel was the least stiff. The medium gravel was slightly stiffer than the coarse gravel to a stress level of approximately 110 psi at which point the coarse gravel became the stiffer. This general behavior is indicated by translation at any stress level above 40 psi and below the lowest crushing stress level of 165 psi.

There appear to be four primary effects of particle size variation on the one-dimensional compression behavior of monogranular specimens.

These effects are: 1) the specimens composed of the larger particles suffered greater particle relocation at low stress levels; 2) the crushing strength of the particles increased as the particle size increased; 3) the stiffness of the specimens below a stress level of approximately 200 psi varied directly with the size of the particles composing the specimens if the effect of particle relocation below a stress level of 20 psi was eliminated; and 4) above a stress level of approximately 300 psi, there appeared to be no practical difference in the stress-strain behavior of the four different sizes of Wabash River gravel tested.

4.3.4 Effect of Variation of Gradation

The effect of variation of gradation from uniformly graded to well graded was investigated by comparison of the tests on monogranular samples, Tests S-6, S-8 and S-12, with a test on a well-graded specimen composed of particles taken from the monogranular samples, Test S-13. The results of these four tests are presented in Figure 4.17 and the gradation curves are presented in Figure 4.18.

The stress-strain behavior for the well-graded specimen does not appear to have a well-defined level of particle crushing as was noted for the poorly graded specimens. Also, the stress-strain behavior for the well-graded specimen seems to be intermediate to the two extremes demonstrated by the very coarse and fine monogranular specimens.

4.3.5 Effect of Saturation Prior to and Subsequent to Load Application

In an effort to determine the effect of moisture on the one-dimensional stress-strain behavior of large granular materials, tests were conducted on samples of Wabash River gravel and crushed limestone in

which the specimens were saturated both subsequent to and prior to loading. The testing program is outlined in Table 4.1. Grain-size distribution curves for the samples of crushed limestone and Wabash River gravel are presented in Figures 4.8 and 4.13. The specimens which were saturated prior to loading were placed in an air-dry state to produce the same initial dry density and then saturated. Subsequent to saturation, the specimens were allowed to stand at least 8 hours prior to applying the first load increment. During loading, the free water surface was maintained within 1/2 inch of the cushion-specimen interface; therefore, the excess pore water head was never greater than 1/2 inch. The specimens which were saturated subsequent to loading were subjected to a constant vertical stress (500 psi) until all measurable creep had occurred and then unloaded.

The results of tests performed to investigate the effect of saturation prior to loading are presented in Figure 4.19. The specimens for Tests S-11 and S-18 were placed air-dry, saturated, and loaded. The specimen for Test S-10 was placed at a moisture content of 4%, loaded to 500 psi, saturated, and then unloaded.

The most obvious effect of the saturation prior to loading was the reduction of the stress level at which particle crushing was evident for the different sized samples. The crushing levels are denoted on Figure 4.19 and were 215, 170 and 150 psi for the very coarse, coarse, and fine specimens, respectively. It should be noted that, as with the specimens which were loaded air-dry, the crushing strength of the saturated particles increased as the particle size increased.

The results for the tests on crushed limestone are presented in Figure 4.20. The specimen for Test S-16 was placed air-dry, statically

loaded to 500 psi, and then saturated; the specimen for Test S-17 was placed air-dry, saturated, and then loaded statically to 500 psi; and the specimen for Test S-19 was placed at a moisture content of 3%, loaded at different rates to 500 psi, and then saturated. The loading rate for Test S-19 was varied to provide test results for the rate of loading study reported on in Section 4.3.6. All tests were conducted under drained conditions.

Comparison of the measured behavior for Tests S-17 and S-19 shows a trend toward greater compressibility for the specimen saturated prior to loading. The specimen which was placed and loaded air-dry experienced a 27% increase in total deformation when saturated at a stress level of 500 psi. This final deformation was approximately 21% greater than that experienced by the specimens saturated before loading.

Test results on a sample of well-graded Wabash River gravel demonstrating the effect of specimen saturation prior to and subsequent to loading are presented in Figure 4.21. The stress-strain curves for the two samples were for practical purposes identical to a stress level of approximately 350 psi. Above this level, the saturated specimen was less stiff. At a stress level of 500 psi, the total deformation of the saturated specimen was approximately 10% greater than that of the unsaturated. When the specimen which was loaded to 500 psi air-dry was saturated, the additional deformation which occurred amounted to an increase of approximately 25%. This final deformation was approximately 15% greater than that of the specimen which was loaded in a saturated condition to 500 psi.

Test results for a uniformly graded specimen of medium Wabash River gravel are presented in Figure 4.22. The additional deformation which this

specimen suffered upon saturation at a stress level of 500 psi amounted to an increase of 42%. A test was not conducted on a specimen of this material which had been saturated prior to loading.

The results of three tests performed on a uniformly graded sample of fine Wabash River gravel are presented in Figure 4.23. The specimen for Test S-8 was placed and loaded air-dry to a level of 500 psi and then saturated. The sample for Test S-4 was placed air-dry, saturated, and loaded (in a drained state) to 500 psi. The sample for Test S-10 was soaked for 24 hours, placed at a residual water content of 4%, loaded to 500 psi, and then saturated. The stress-strain curves for Tests S-8 and S-9 are nearly identical. Based on the results of the aforementioned tests on well-graded Wabash River gravel (S-13 and S-14) and the test on medium uniformly graded Wabash River gravel (S-12), the test results for Test S-9 should have been similar to those for Test S-10. Therefore, Test S-9 was ignored and Tests S-8 and S-10 were assumed to be valid. When the specimen which was loaded to 500 psi air-dry (S-8) was saturated, the additional deformation which occurred amounted to an increase of approximately 45%. This final deformation was approximately 20% greater than that of the specimen which was loaded in a moist condition to 500 psi (S-10). The specimen for Test S-10 was saturated at a stress level of 500 psi and no additional deformation resulted.

Test results for a coarse, uniformly graded sample of Wabash River gravel are presented in Figure 4.24. The specimen for Test S-6 was placed and loaded air-dry; this specimen was never saturated. The specimen for Test S-11 was placed air-dry, saturated and loaded (in a drained condition). The specimen which was loaded in a saturated condition (S-11) suffered a total deformation which was approximately 65% greater than that suffered by the specimen placed and loaded air-dry (S-6) at a stress level of 500 psi.

Test results for a very coarse uniformly graded sample of Wabash River gravel are presented in Figure 4.25. The specimen for Test S-15 was placed and loaded air-dry and then saturated. The specimen for Test S-18 was placed air-dry, saturated, and then loaded. When the specimen which was placed and loaded air-dry (S-15) was saturated, an additional deformation of approximately 30% occurred. The specimen which was loaded in a saturated condition (S-18) suffered a total deformation which was approximately 25% greater than the deformation suffered by the specimen loaded air-dry after saturation at a stress level of 500 psi.

Thus, the well-graded samples of Wabash River gravel and crushed limestone and the sample of fine uniformly graded Wabash River gravel all experienced less total deformation when saturated prior to loading rather than subsequent to loading. However, the coarse and very coarse samples of Wabash River gravel experienced more total deformation when saturated prior to loading than when saturated subsequent to loading.

4.3.6 Effect of Rate of Loading

4.3.6.1 Introduction

Three samples were employed in this test series. These materials were 20-30 Ottawa sand, well-graded crushed limestone, and a coarse to fine sandy silt with some coarse to fine gravel. The Ottawa sand is described in Section 4.2.1.1 and the results of a mechanical grain-size analysis for the sample are presented in Figure 4.1. The crushed limestone is described in Section 4.2.1.2, and the results of a mechanical grain-size analysis are presented in Figure 4.2. The sample of sandy silt was taken from missile Site-3 and is described in Appendix A. The results of a mechanical grain-size analysis are presented in Figure A.13.

4.3.6.2 Ottawa Sand

The effect of rate of loading on a sample of 20-30 Ottawa sand was demonstrated by a static test with cyclic loading and a dynamic test with two cycles and two different overpressures. These tests were discussed in Section 3.3.4.2, and the resulting stress-strain behavior is presented in Figure 3.29. The test specimen was cycled statically to pressures higher than the dynamic overpressures; therefore, no particle rearrangement or crushing should have taken place during the dynamic tests. The only possible difference in the stress-strain behavior for the static and dynamic tests would have to arise from pore pressure developed during the dynamic tests or from inherent strain rate effects in the "effective" stress-strain relationship. Neither of the effects apparently manifested themselves in the dynamic tests performed as evidenced by the close agreement between the measured static and dynamic stress-strain behavior.

4.3.6.3 Crushed Limestone

The test series designed to demonstrate the effect of rate of loading on crushed limestone included: Test S-16, which was placed and statically loaded air-dry; Test S-17, which was placed air-dry, saturated, and then statically loaded; Test S-4, which was placed and loaded air-dry with a loading rate of 50 psi per minute; Test S-19, which was placed at a water content of 3% and subjected to several loading rates; and Test D-4, which was placed and loaded air-dry with a pressure-rise time of 500 psi in 33 msec. The test results are presented in Figure 4.26. The initial dry densities were nearly equal; therefore, the differences in the measured stress-strain behavior must have been the result of differences in water content and/or differences in rate of loading.

The test specimens for Tests S-4 and S-16 were both placed and loaded air-dry. Test S-16 was a static test while a loading rate of 50 psi per minute was used for Test S-4. The measured stress-strain behavior was nearly identical to a stress level of approximately 250 psi. Above 250 psi the statically loaded specimen (S-16) deflected approximately 10% more than the specimen loaded at the rate of 50 psi per minute (S-4).

The specimen for Test S-19 was loaded as rapidly as possible, using the static loading system to approximately 45 psi. The pressure was brought up to 50 psi and held at that level until the creep amounted to less than 0.001 inches/hour. The pressure was then increased as quickly as possible to a level of 250 psi with deformation readings taken during the pressure increase. Because of the change in pressure gradient during the pressure rise to 250 psi, the rate of loading varied from approximately 200 psi/minute at a level of 50 psi to 60 psi/minute at 250 psi. This variation in loading rate resulted from the changes in pressure gradient between the gas source and the expansion chamber as the pressure in the expansion chamber was increased. Above a pressure level of 250 psi, the specimen was tested statically, i.e., the successive increments of load were not applied until the creep amounted to less than 0.001 inches/hour.

The specimen for Test S-17 was placed air-dry, saturated, and loaded statically, and the specimen for Test S-19 was placed wet and subjected to several loading rates. The initial dry densities were 102.1 and 104.7 pcf for test specimens S-17 and S-19, respectively. Therefore, with the exception of loading-rate effects, the specimens should have exhibited the same stress-strain behavior. The test specimen loaded rapidly (S-19) was approximately 35% stiffer than the test specimens loaded statically over the axial stress

range from zero to 150 psi. As the axial stress was increased and the loading rate was decreased the behavior of the test specimen loaded rapidly (S-19) approached that of the test specimen loaded statically. At an axial stress of 250 psi, the load on test specimen was held constant until the creep amounted to less than 0.001 inches/hour, the criterion for static loading. The final deformation was 10% less than that for Test S-17 at a stress level of 250 psi. Above a stress level of 250 psi, test specimen S-19 was subjected to static loading. The resulting stress-strain curve merged with that for Test S-17 at an axial stress level of approximately 400 psi. The stress-strain behavior for the specimen subjected to various loading rates (S-19) for the stress range from zero to 100 psi is presented in Figure 4.27. When the rate of loading was reduced, at an axial stress of 45 psi, the strains increased and creep occurred when the axial pressure was held constant at 50 psi. When the loading was resumed with a rate of loading of approximately 200 psi/minute, the stress-strain curve resumed the trend exhibited prior to holding the static load at 50 psi. A broken line in Figure 4.27 indicates what the probable behavior would have been had the loading not been interrupted.

The specimen for Test D-4 was placed and loaded air-dry and had an initial dry density of 107.3 pcf. The measured stress-strain behavior for test specimen D-4 should be compared to that for specimen S-16. The results of the dynamic test, Test D-4, are valid only for a stress level greater than approximately 250 psi because of overstress during early times as discussed in Section 3.3.4.2. Above a stress level of 250 psi, the deformations for test specimens D-4 were measured to be approximately 40% stiffer than for the static specimen, S-16.

4.3.6.4 Sandy Silt

The coarse to fine sandy silt with some gravel was subjected to a series of three dynamic overpressures to demonstrate the method which could be employed to measure the stress-strain behavior over a stress-range in excess of the stress range valid for one dynamic test because of nonuniformity of stresses throughout the test specimen. The stress range of interest was from 20 to 300 psi. In accordance with the criterion established in Section 3.3.4.2, the measurement of the stress-strain behavior over the stress range from 20 to 300 psi required three separate test cycles. The overpressures for these cycles are presented in Figure 4.28. The measured stress-strain behavior is presented in Figure 4.29. Those portions of the stress-strain curves which are valid are connected by a smooth curve.

4.4 CREEP TIMES

The samples tested in this study were subject to creep deformations particularly when tested with a water content other than air-dry. Sowers, et al. (1965) determined that approximately 90% of the creep resulting from saturation occurred within 500 to 1000 minutes from the time the load was applied or the time the specimen was saturated. For the purpose of this study, test specimens were allowed to creep under constant load until the rate of creep was less than 0.001 inches per hour. The total time to conduct a given static test varied from one day to several days.

TEST	MATERIAL	INITIAL DRY DENSITY (pcf)	WATER CONTENT (%)	SATURATED BEFORE LOADING	SATURATED AFTER LOADING	GRADATION	D_{10} (in.)	D_{60} (in.)	UNIFORMITY
S-1	Ottawa sand	107.1	0			poor	.02	.03	1.50
S-2		110.3	0			poor	.02	.03	1.50
S-16	crushed limestone	102.4	0		X	well	.20	.50	2.50
S-17		102.1	0	X		well	.20	.50	2.50
S-19		104.7	3		X	well	.20	.50	2.50
S-8	Wabash River gravel	102.6	0		X	poor	.19	.28	1.47
S-9		105.6	0	X		poor	.19	.28	1.47
S-10		108.6	4		X	poor	.19	.28	1.47
S-12		106.5	0		X	poor	.29	.43	1.48
S-6		106.8	0			poor	.59	.83	1.41
S-11		105.9	0	X		poor	.59	.83	1.41
S-15		110.9	0		X	poor	.95	1.22	1.28
S-18		109.1	0	X		poor	.95	1.22	1.28
S-13		117.7	0		X	well	.22	.47	2.14
S-14		113.3	0	X		well	.22	.47	2.14
S-5	N. Dakota river gravel	122.9	0			well	.35	.95	2.71

TABLE 4.1 SUMMARY OF STATIC TESTS CONDUCTED FOR VARIATION OF PARAMETER STUDY

TEST	MATERIAL	INITIAL DRY DENSITY (pcf)	WATER CONTENT (%)	SATURATED BEFORE LOADING	SATURATED AFTER LOADING	GRADATION	D_{10} (in.)	D_{60} (in.)	UNIFORMITY
D-1	Ottawa sand	110.8	0			poor	.02	.03	1.50
D-2	crushed limestone	----------loading diaphragm ruptured and test data lost----------							
D-3		107.3	0			well	.20	.50	2.50
D-4		107.3	0			well	.20	.50	2.50
D-5		131.2	2.5			well	.20	.50	2.50

TABLE 4.2 SUMMARY OF DYNAMIC TESTS CONDUCTED FOR VARIATION OF PARAMETER STUDY

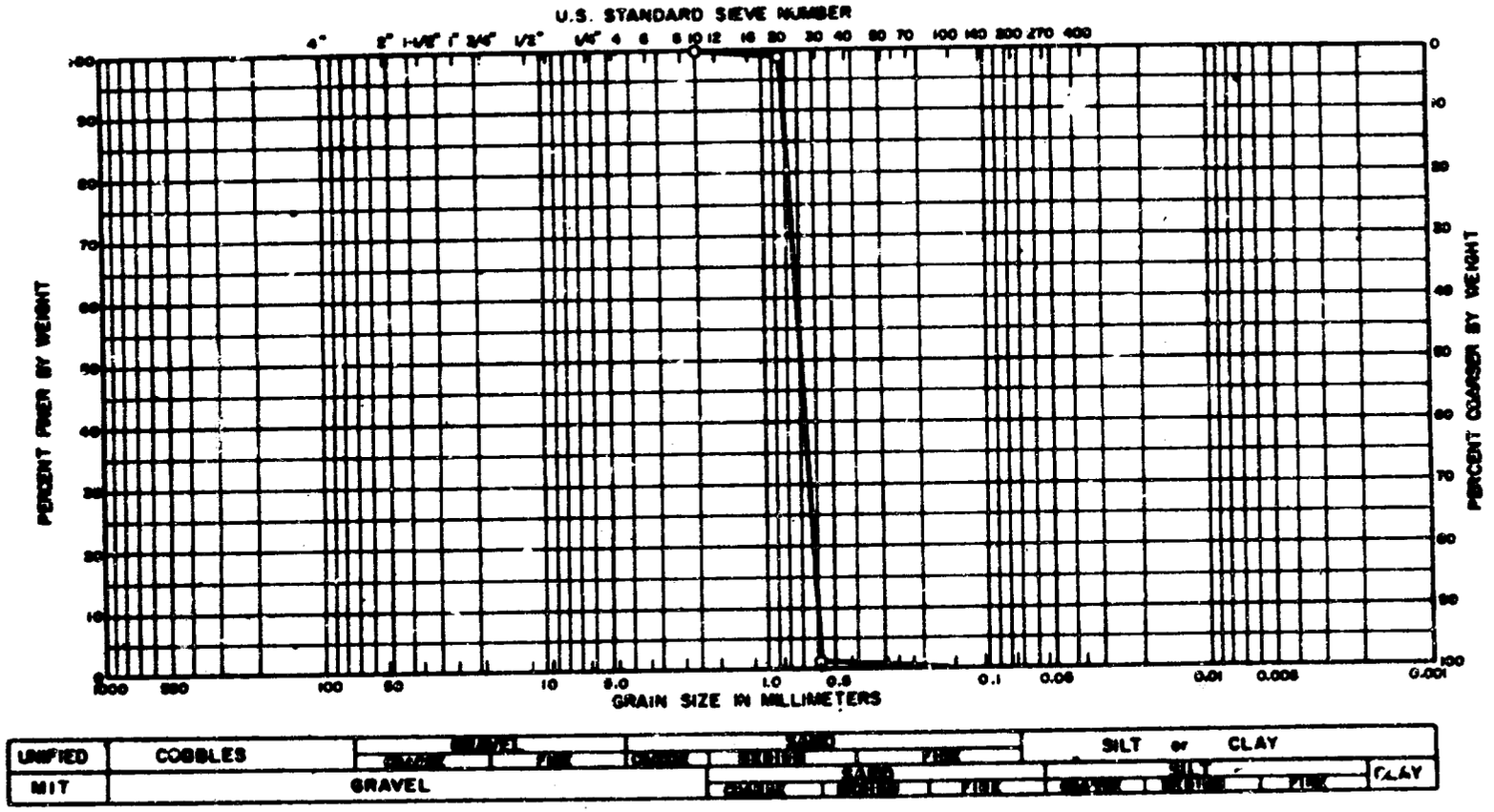

FIGURE 4.1 GRADATION CURVE FOR 20-30 OTTAWA SAND

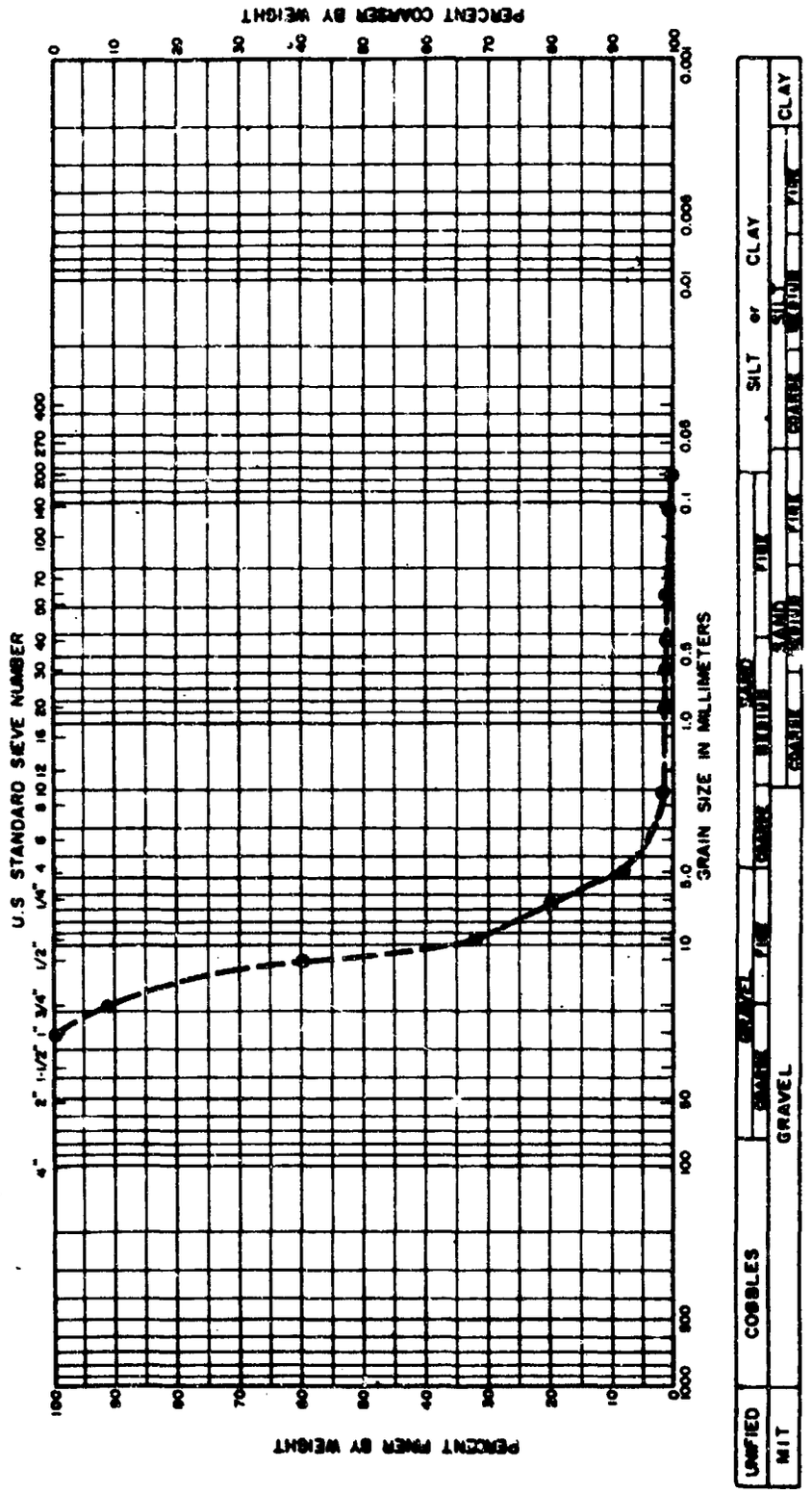

FIGURE 4.2 GRADATION CURVE FOR CRUSHED LIMESTONE

FIGURE 4.3 PARTICLES OF CRUSHED LIMESTONE

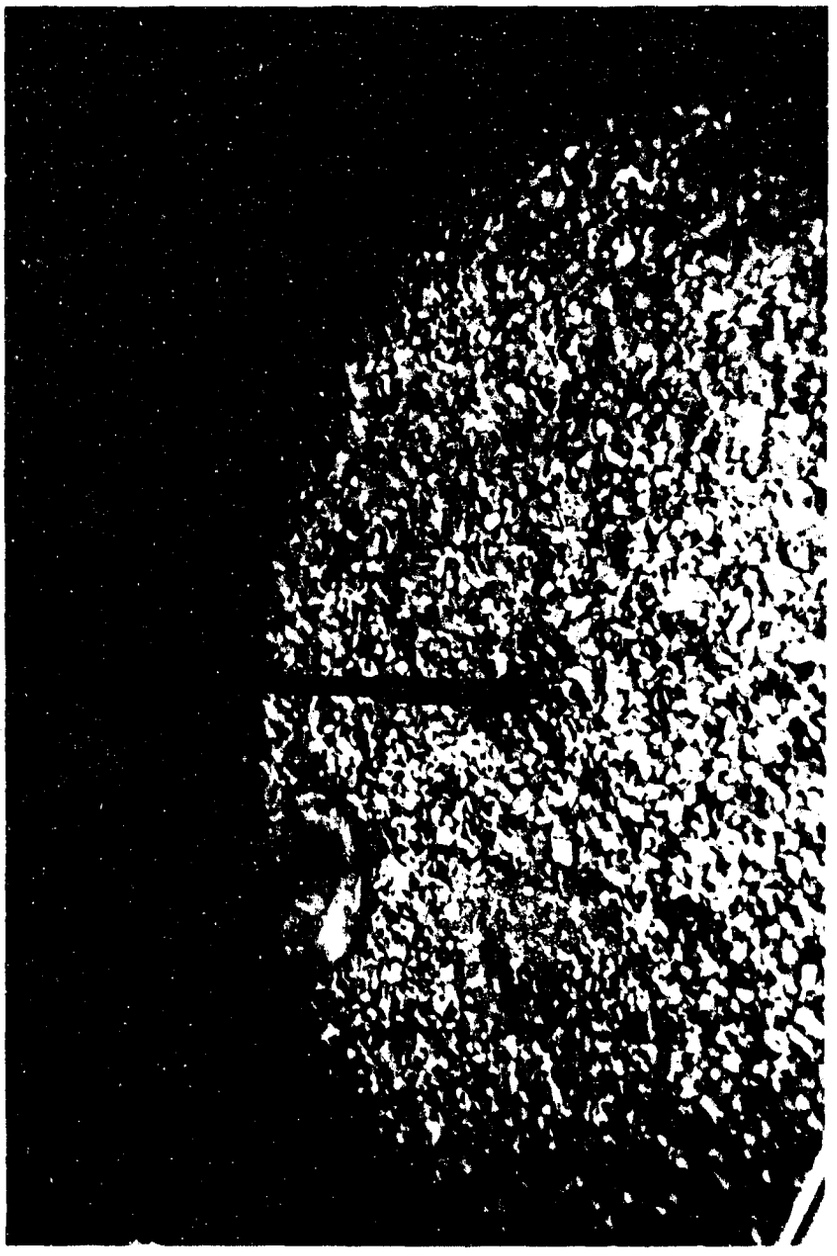

FIGURE 4.4 PARTICLES OF WABASH RIVER GRAVEL

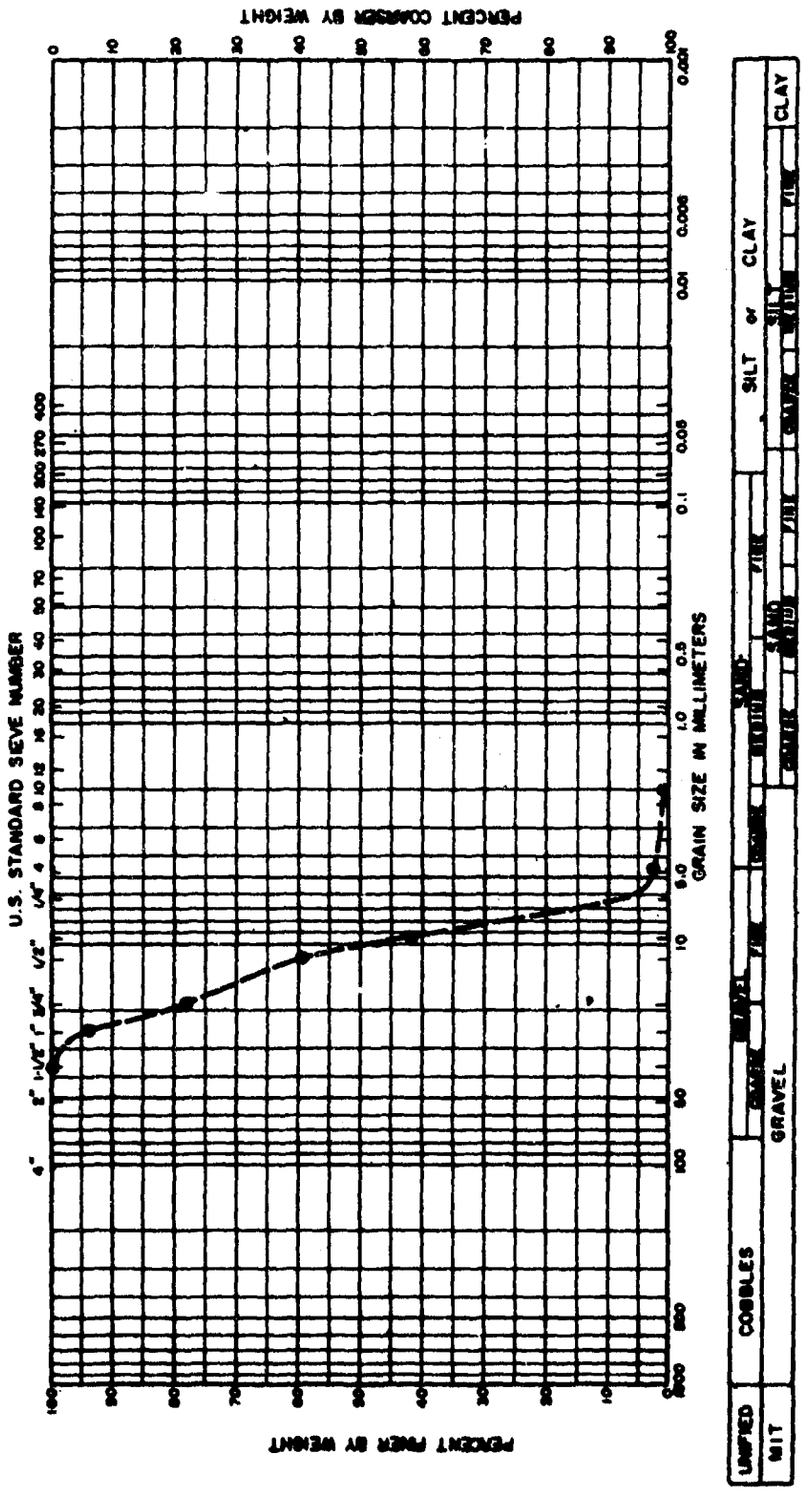

FIGURE 4.5 GRADATION CURVE FOR WABASH RIVER GRAVEL

FIGURE 4.6 PARTICLES OF NORTH DAKOTA RIVER GRAVEL

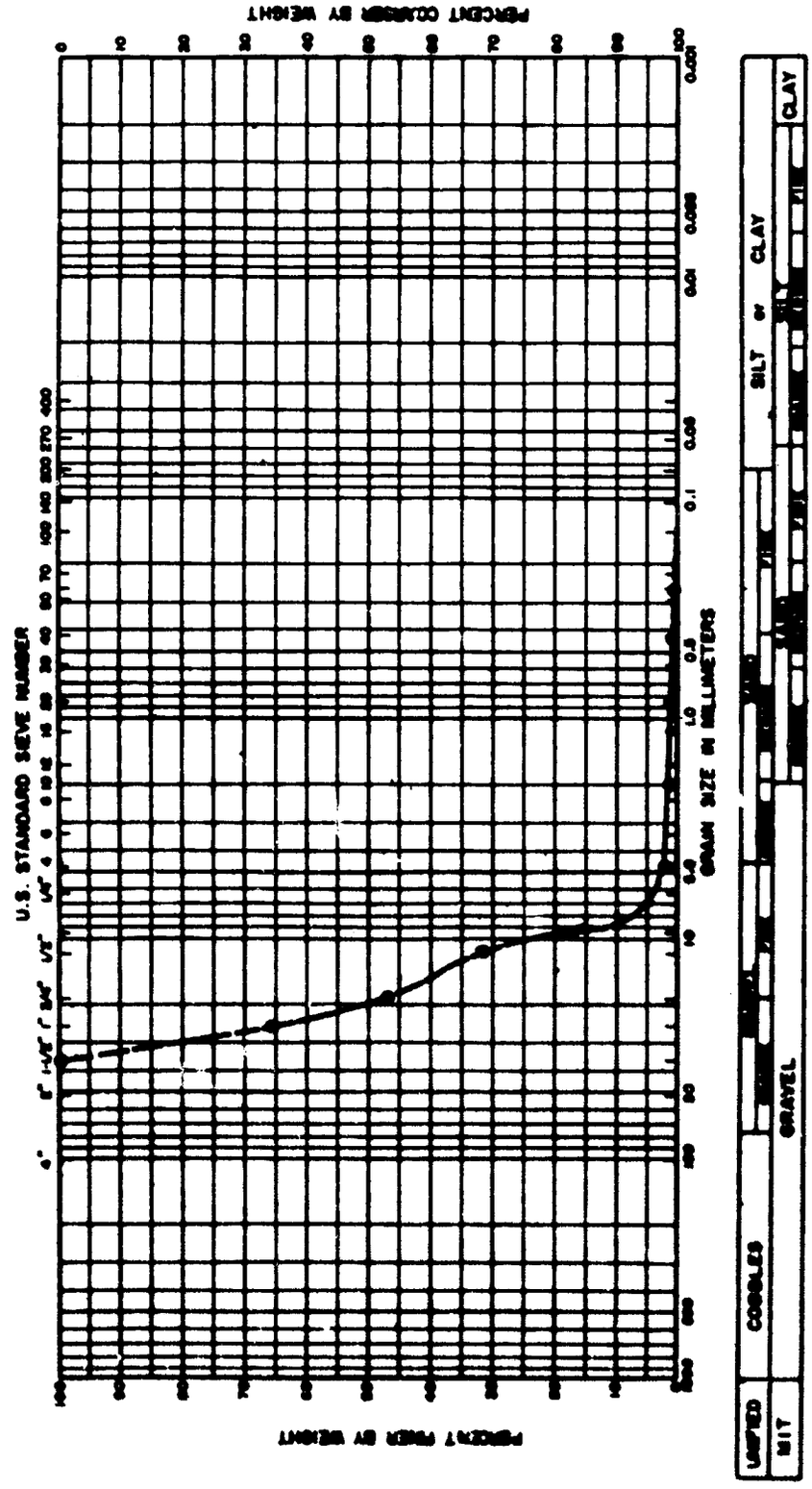

FIGURE 4.7 GRADATION CURVE FOR NORTH DAKOTA RIVER GRAVEL

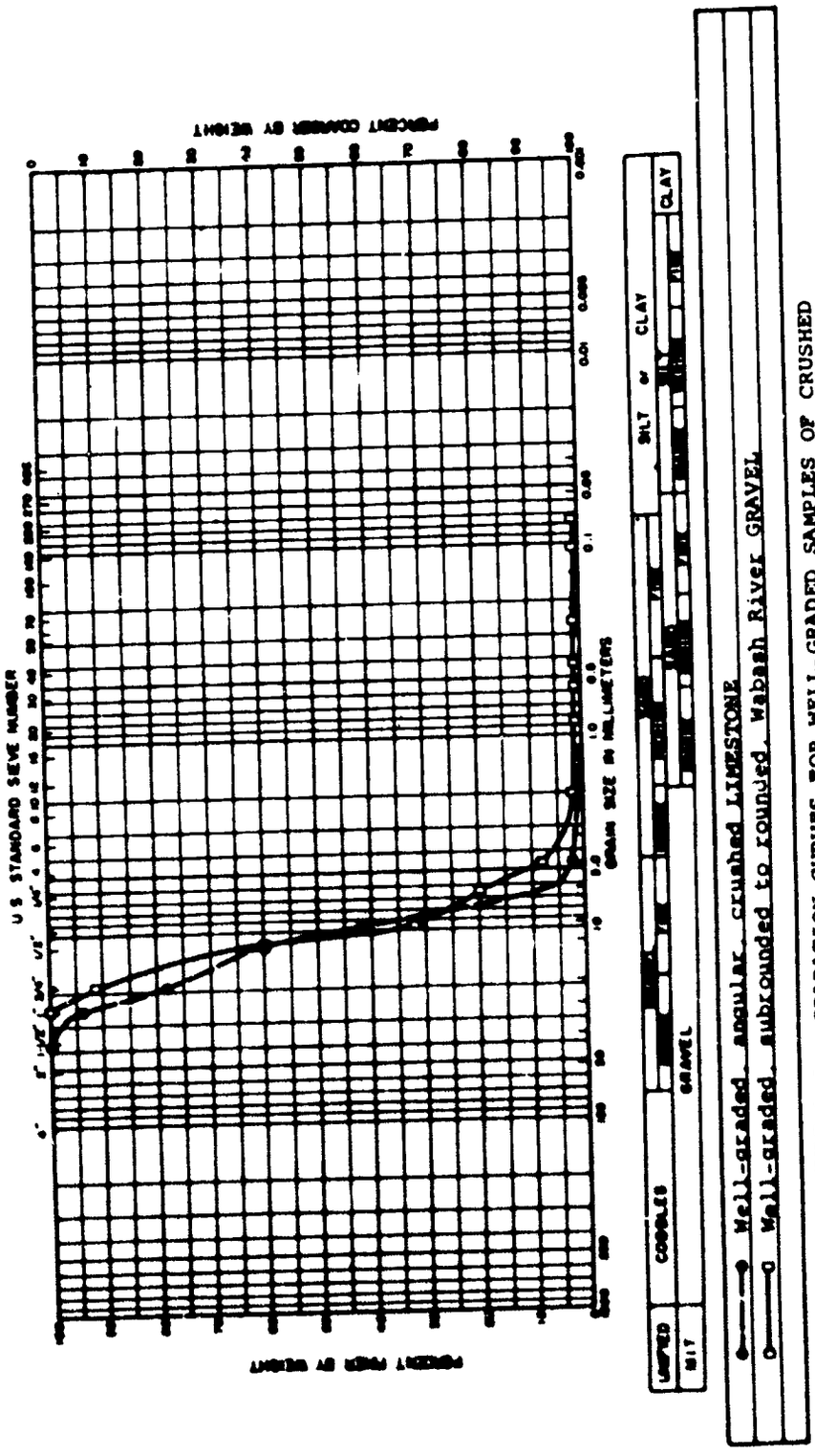

FIGURE 4.8 GRADATION CURVES FOR WELL-GRADED SAMPLES OF CRUSHED LIMESTONE AND WABASH RIVER GRAVEL

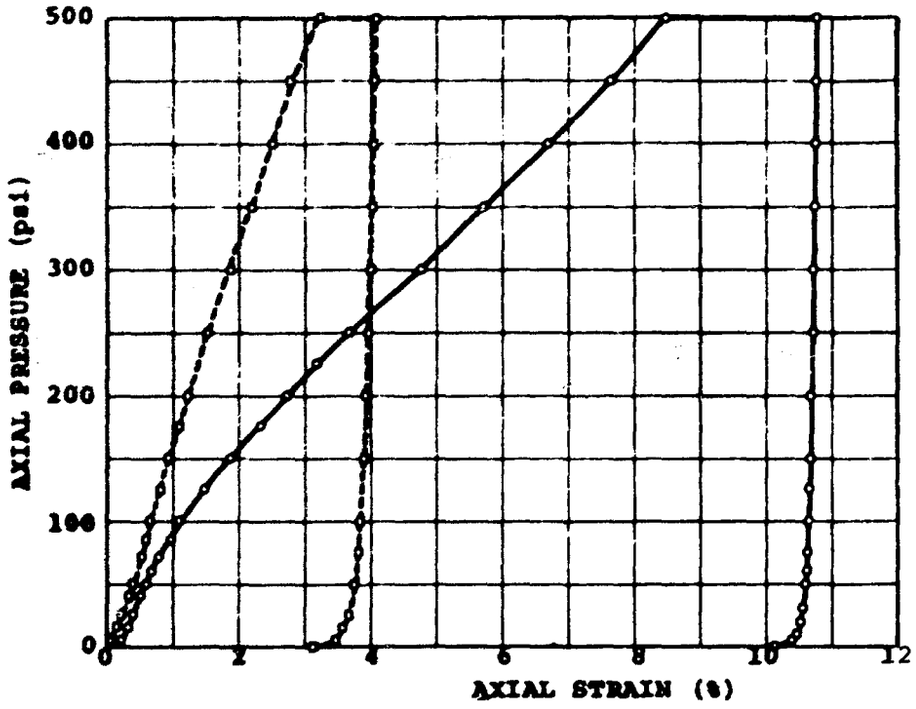

TEST S-16 ○
Crushed Limestone
well-graded
initial dry density 102.4 pcf
placed and loaded air-dry,
saturated, then unloaded

TEST S-13 □
Wabash River Gravel
well-graded
initial dry density 117.7 pcf
placed and loaded air-dry,
saturated, then unloaded

FIGURE 4.9 STRESS-STRAIN CURVES DEMONSTRATING EFFECT OF VARIATION OF PARTICLE SHAPE IN ONE-DIMENSIONAL COMPRESSION

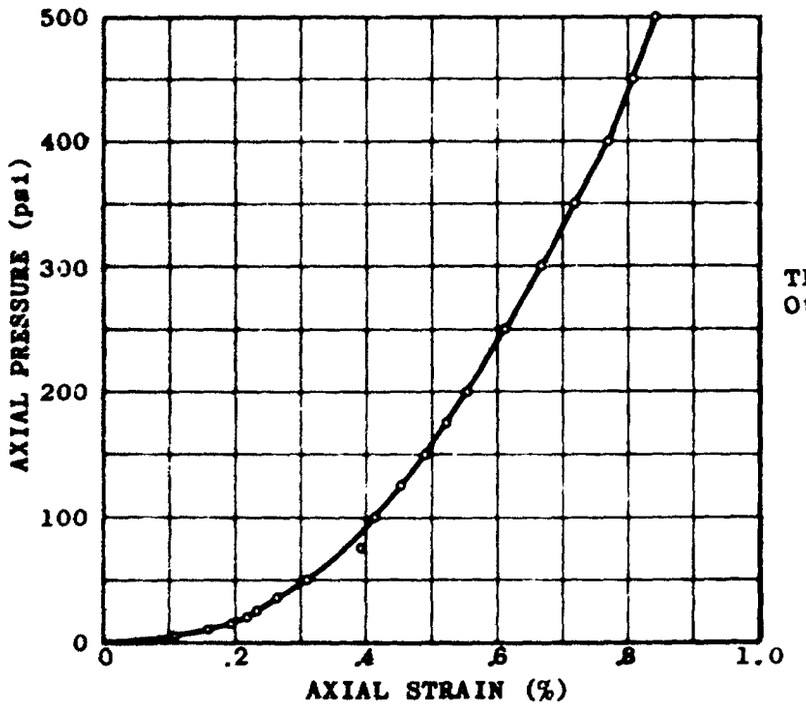

FIGURE 4.10 STRESS-STRAIN RELATIONSHIP FOR 20-30 OTTAWA SAND IN ONE-DIMENSIONAL COMPRESSION

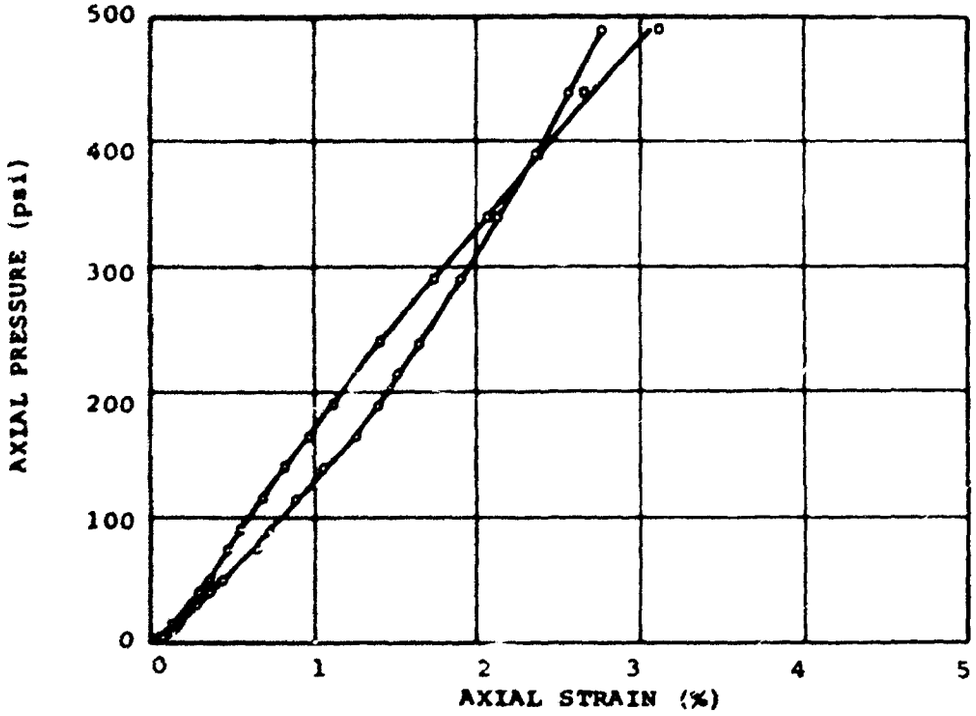

FIGURE 4.11 STRESS-STRAIN CURVES DEMONSTRATING EFFECT OF PARTICLE COMPOSITION IN ONE-DIMENSIONAL COMPRESSION

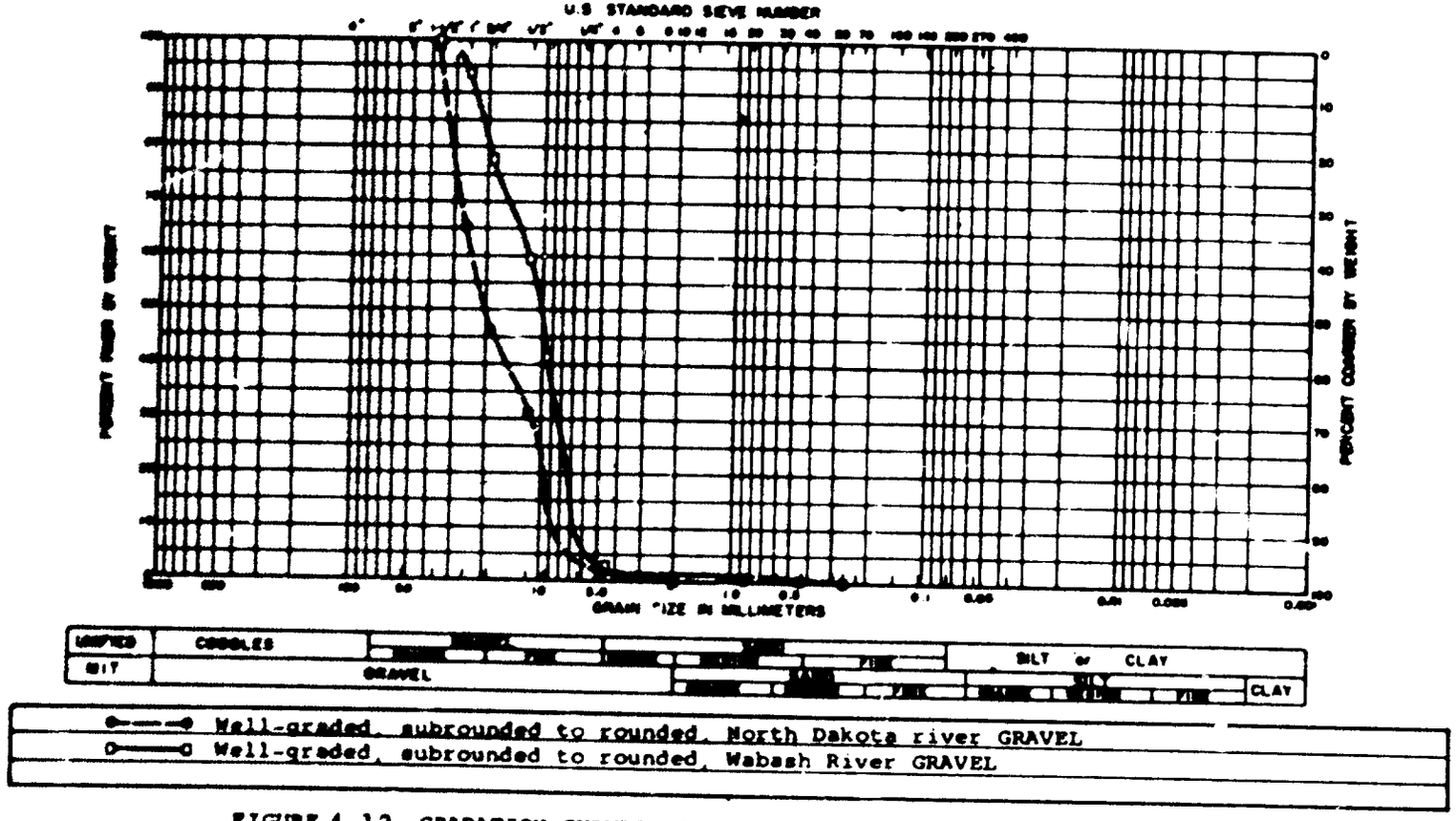

FIGURE 4.12 GRADATION CURVES FOR WELL-GRADED SAMPLES OF NORTH DAKOTA RIVER GRAVEL AND WABASH RIVER GRAVEL

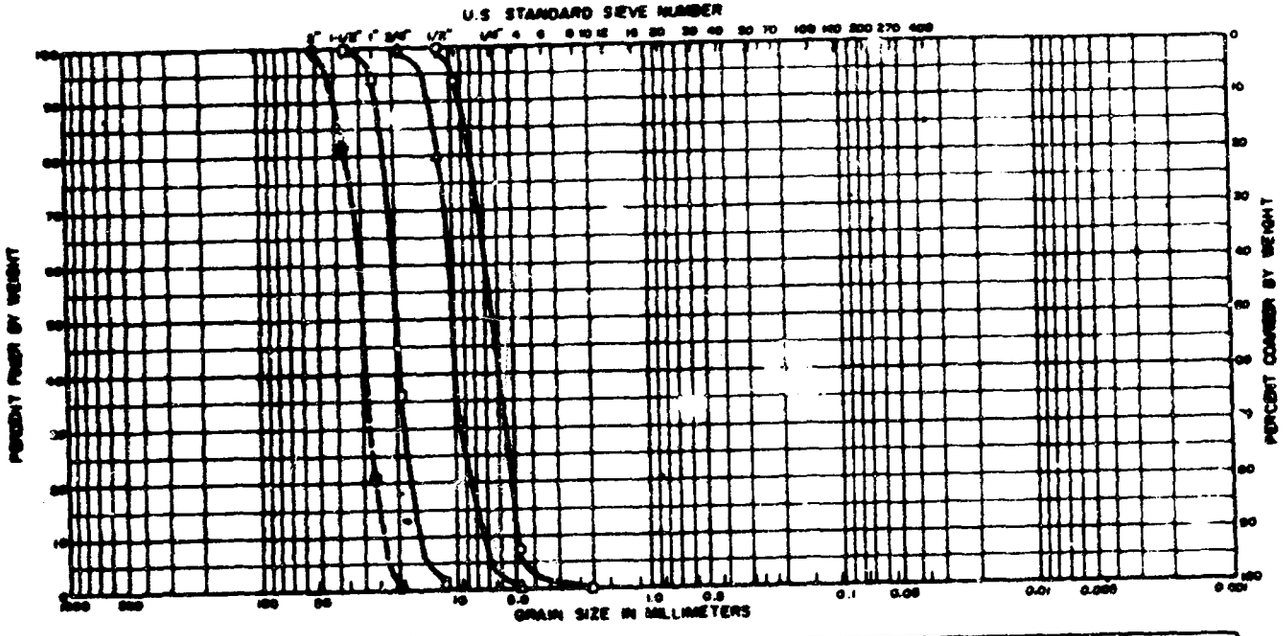

FIGURE 4.13 GRADATION CURVES FOR POORLY GRADED SAMPLES OF W[redacted]R GRAVEL

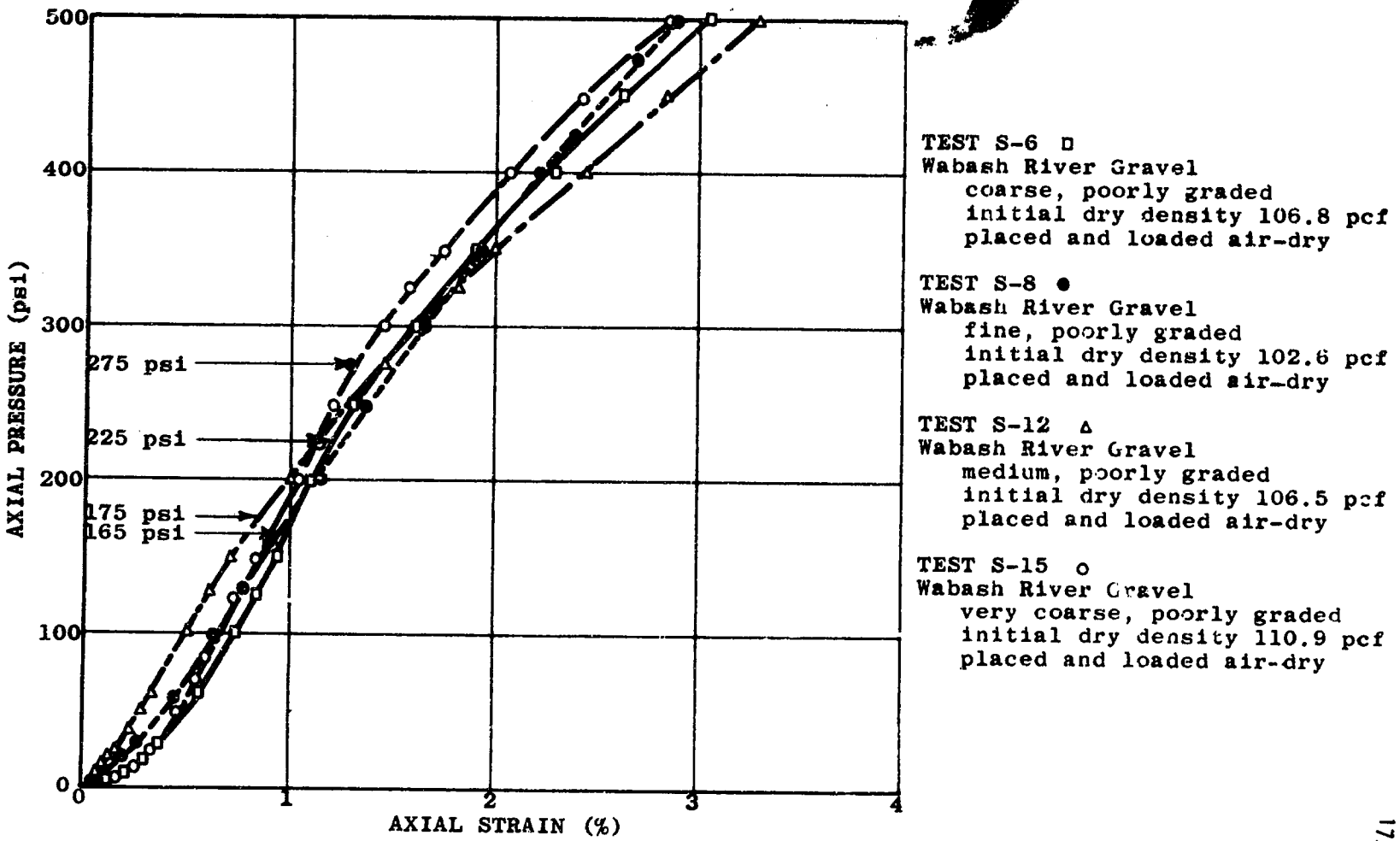

FIGURE 4.14 STRESS-STRAIN CURVES DEMONSTRATING EFFECT OF VARIATION OF PARTICLE SIZE IN ONE-DIMENSIONAL COMPRESSION

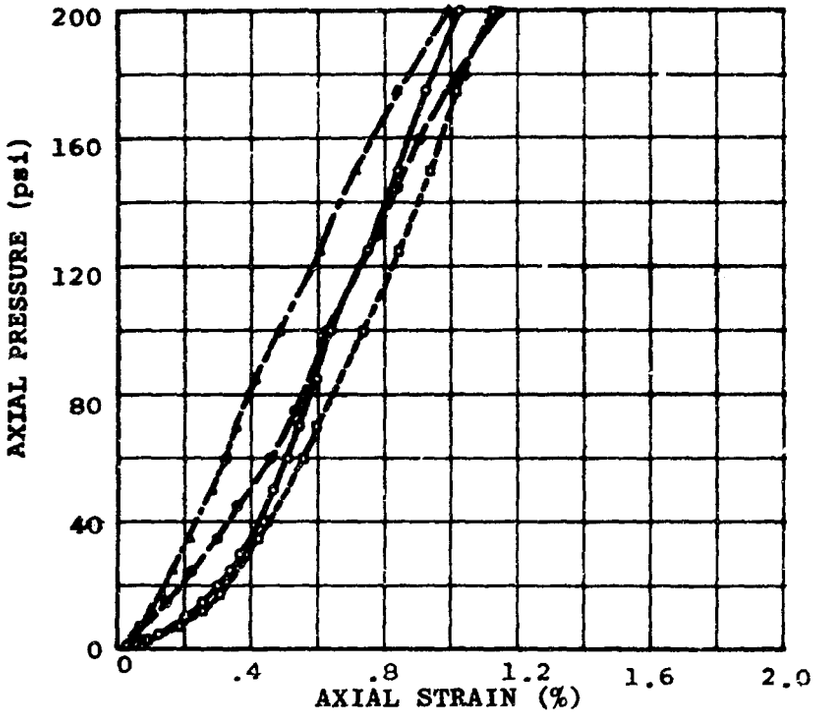

TEST S-6 □
Wabash River Gravel
coarse, poorly graded
initial dry density 106.8 pcf
placed and loaded air-dry

TEST S-8 ●
Wabash River Gravel
fine, poorly graded
initial dry density 102.6 pcf
placed and loaded air-dry

TEST S-12 △
Wabash River Gravel
medium, poorly graded
initial dry density 106.5 pcf
placed and loaded air-dry

TEST S-15 ○
Wabash River Gravel
very coarse, poorly graded
initial dry density 110.9 pcf
placed and loaded air-dry

FIGURE 4.15 STRESS-STRAIN CURVES DEMONSTRATING EFFECT OF VARIATION OF PARTICLE SIZE IN ONE-DIMENSIONAL COMPRESSION (LOW STRESS LEVEL)

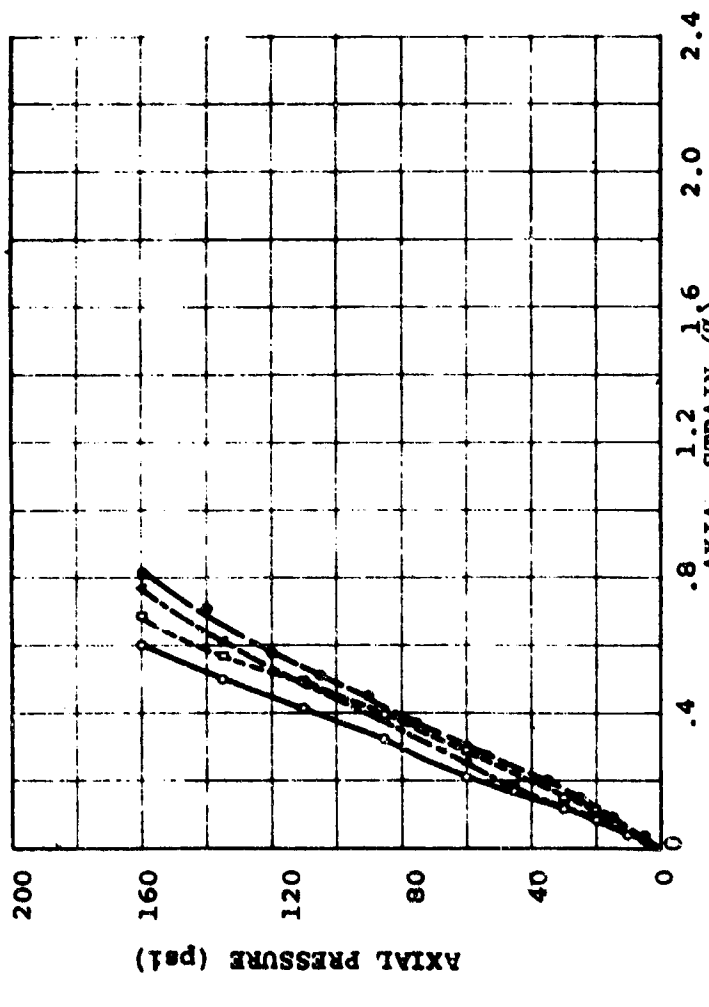

FIGURE 4.16 STRESS-STRAIN CURVES DEMONSTRATING EFFECT OF VARIATION OF PARTICLE SIZE IN ONE-DIMENSIONAL COMPRESSION (TRANSLATED ORIGIN)

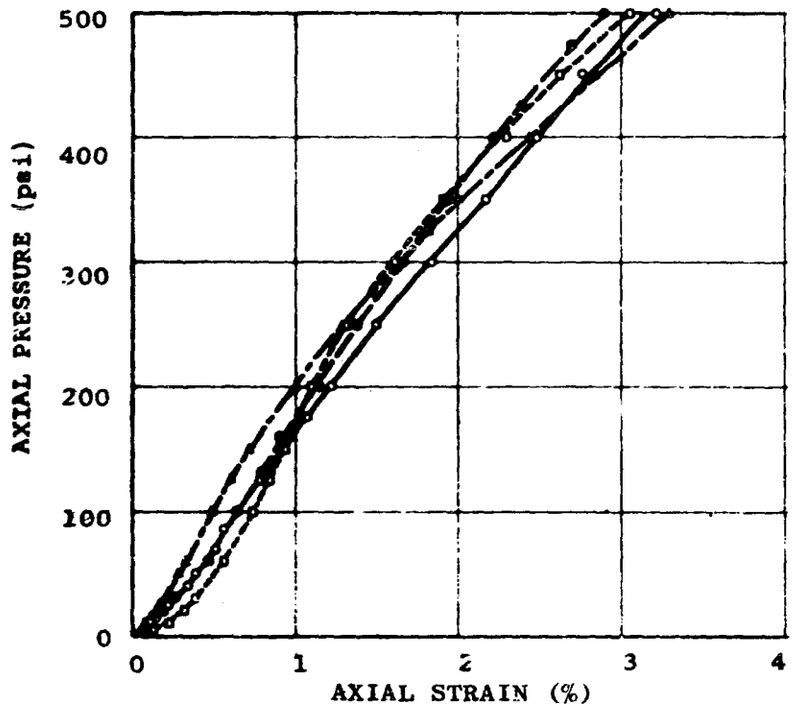

TEST S-6 □
Wabash River Gravel
coarse, poorly graded
initial dry density 106.8 pcf

TEST S-8 ●
Wabash River Gravel
fine, poorly graded
initial dry density 102.6 pcf
placed and loaded air-dry

TEST S-12 △
Wabash River Gravel
medium, poorly graded
initial dry density 106.5 pcf
placed and loaded air-dry

TEST S-13 ○
Wabash River Gravel
coarse to fine, well graded
initial dry density 117.7 pcf
placed and loaded air-dry

FIGURE 4.17 STRESS-STRAIN CURVES DEMONSTRATING EFFECT OF VARIATION OF GRADATION IN ONE-DIMENSIONAL COMPRESSION

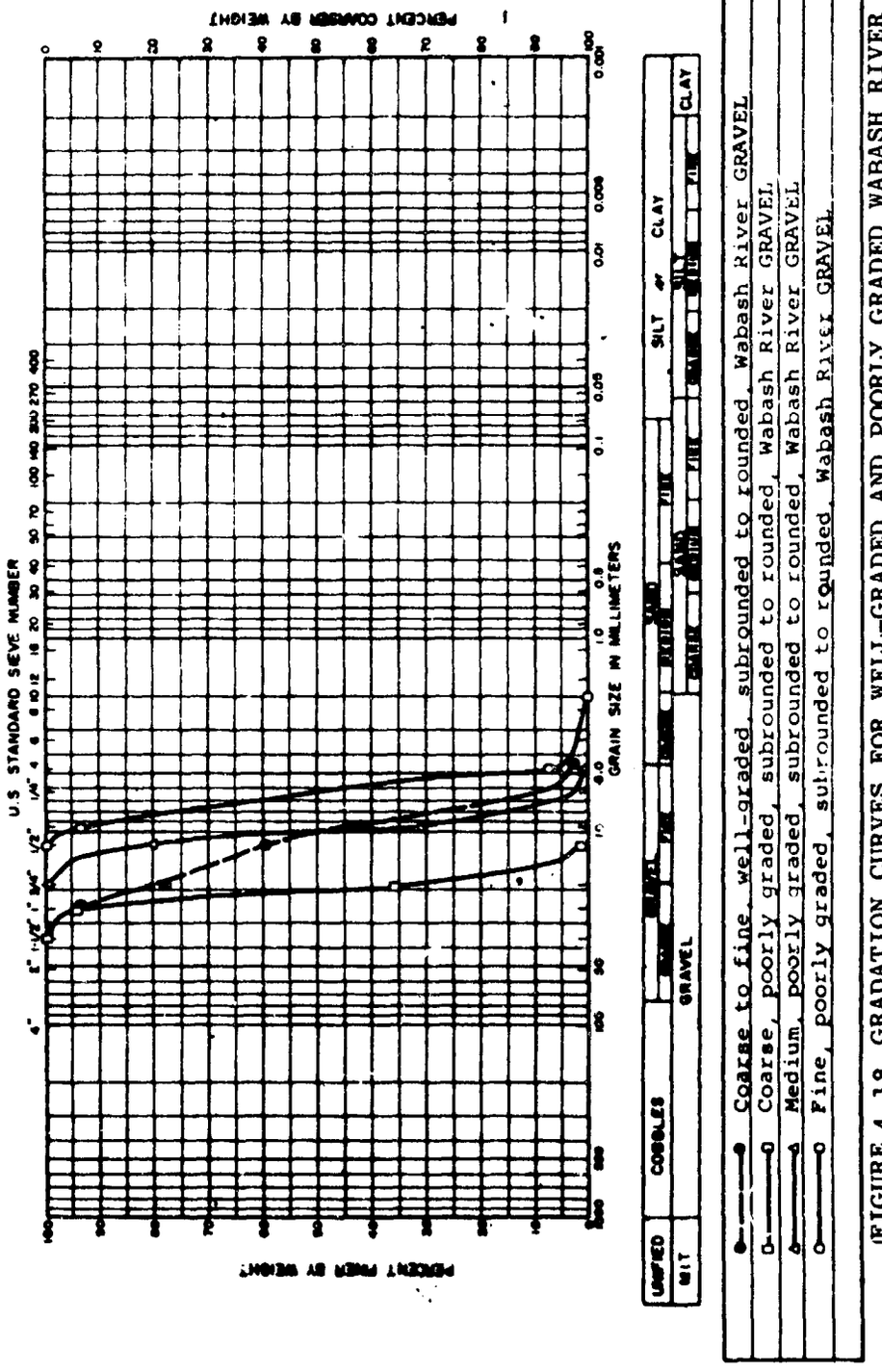

FIGURE 4.18 GRADATION CURVES FOR WELL-GRADED AND POORLY GRADED WABASH RIVER GRAVEL SAMPLES

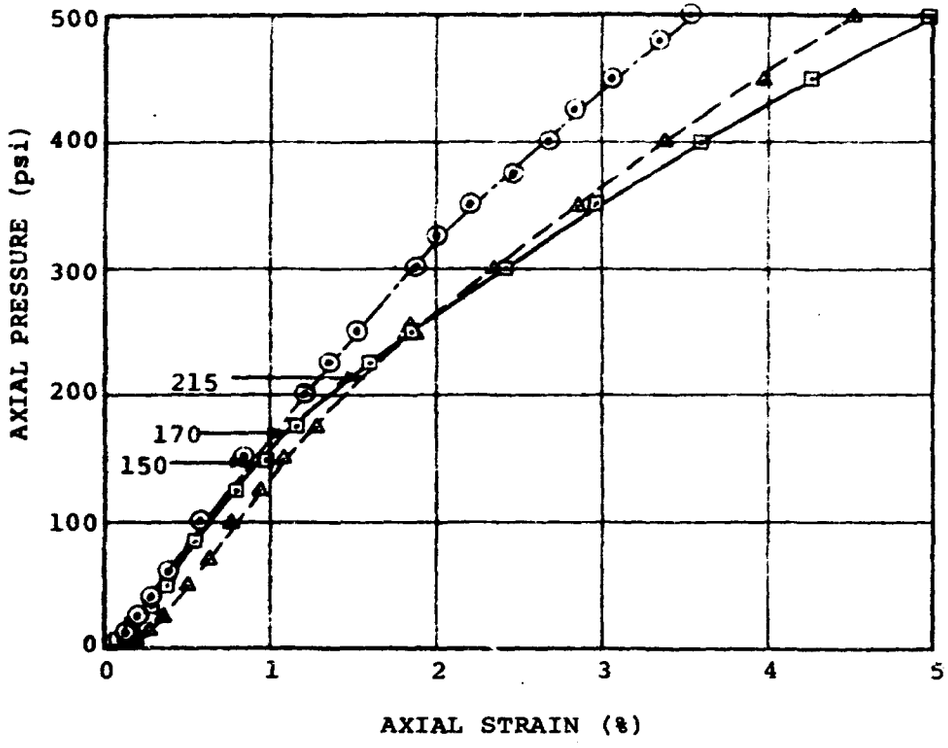

TEST S-10 ○
Wabash River Gravel
fine, poorly graded
initial dry density
108.6 pcf
placed at water content
of 4%, loaded to
500 psi, saturated,
and unloaded

TEST S-11 □
Wabash River Gravel
coarse, poorly graded
initial dry density
105.9 pcf
placed air-dry, saturated,
and then loaded

TEST S-18 △
Wabash River Gravel
very coarse, poorly graded
initial dry density
109.1 pcf
placed air-dry, saturated,
and then loaded

FIGURE 4.19 STRESS-STRAIN CURVES DEMONSTRATING EFFECT OF SATURATION ON CRUSHING STRENGTH IN WABASH RIVER GRAVEL

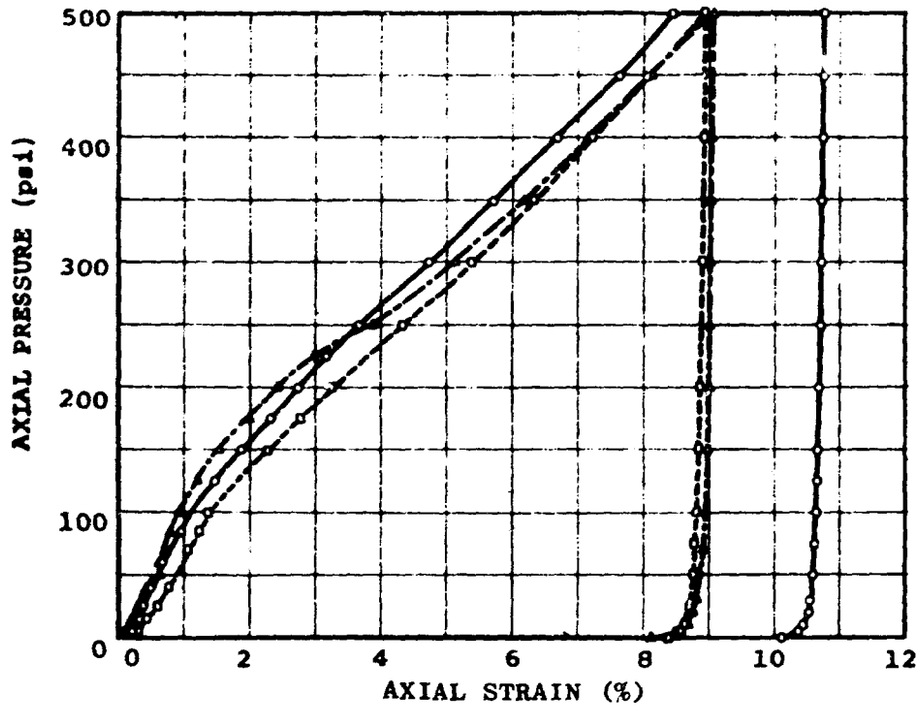

TEST S-16 ○
Crushed Limestone
coarse to fine, well graded
initial dry density 102.4 pcf
placed and statically loaded
air-dry, and then saturated

TEST S-17 □
Crushed Limestone
coarse to fine, well graded
initial dry density 102.1 pcf
placed air-dry, saturated, and
then statically loaded

TEST S-19 △
Crushed Limestone
coarse to fine, well graded
initial dry density 104.7 pcf
placed at water content of
3 %, loaded at varying
rate, and then saturated

FIGURE 4.20 STRESS-STRAIN CURVES DEMONSTRATING EFFECT OF SPECIMEN SATURATION PRIOR TO AND SUBSEQUENT TO LOADING IN ONE-DIMENSIONAL COMPRESSION FOR CRUSHED LIMESTONE

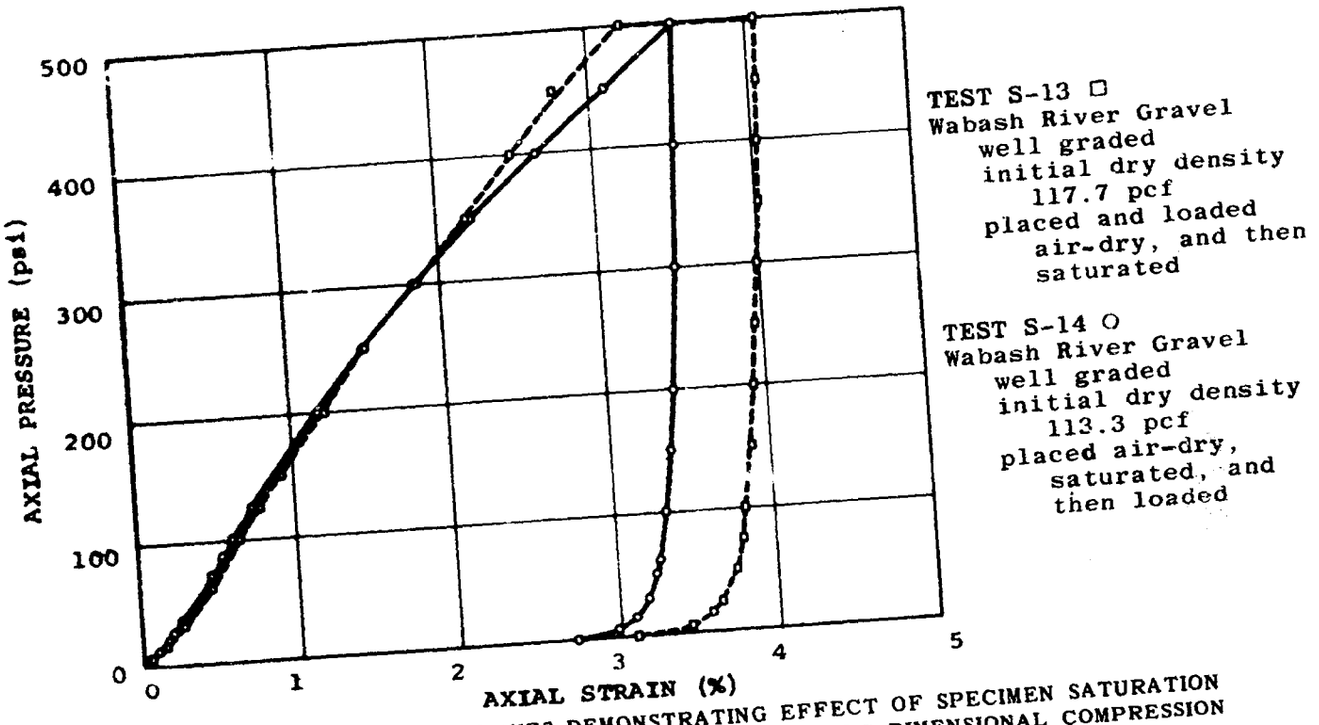

FIGU FIGURE 4.21 STRESS-STRAIN CURVES DEMONSTRATING EFFECT OF SPECIMEN SATURATION PRIOR TO AND SUBSEQUENT TO LOADING IN ONE-DIMENSIONAL COMPRESSION FOR WELL-GRADED WABASH RIVER GRAVEL

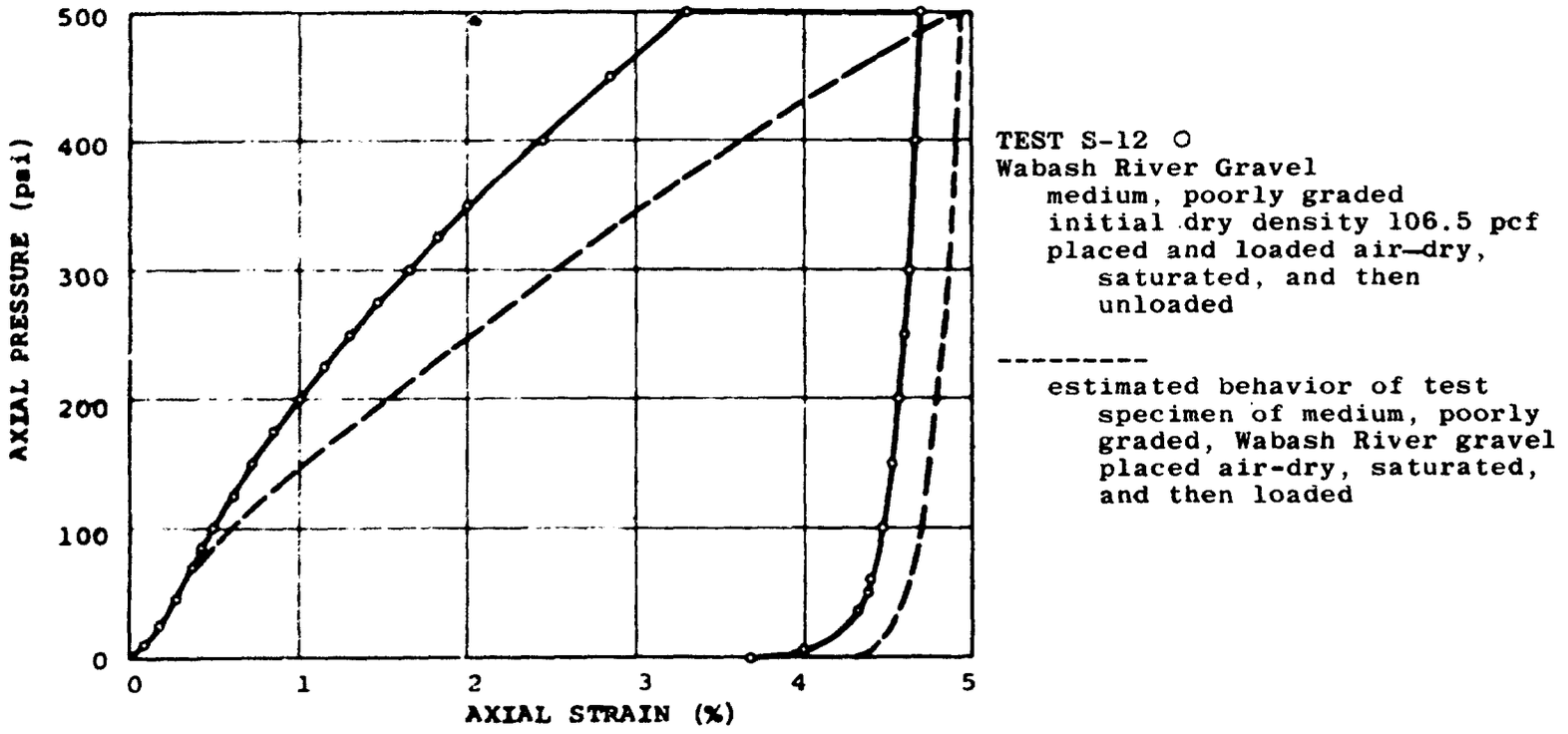

FIGURE 4.22 STRESS-STRAIN CURVES ILLUSTRATING ESTIMATED EFFECT OF SPECIMEN SATURATION PRIOR TO AND SUBSEQUENT TO LOADING IN ONE-DIMENSIONAL COMPRESSION FOR MEDIUM, POORLY GRADED WABASH RIVER GRAVEL

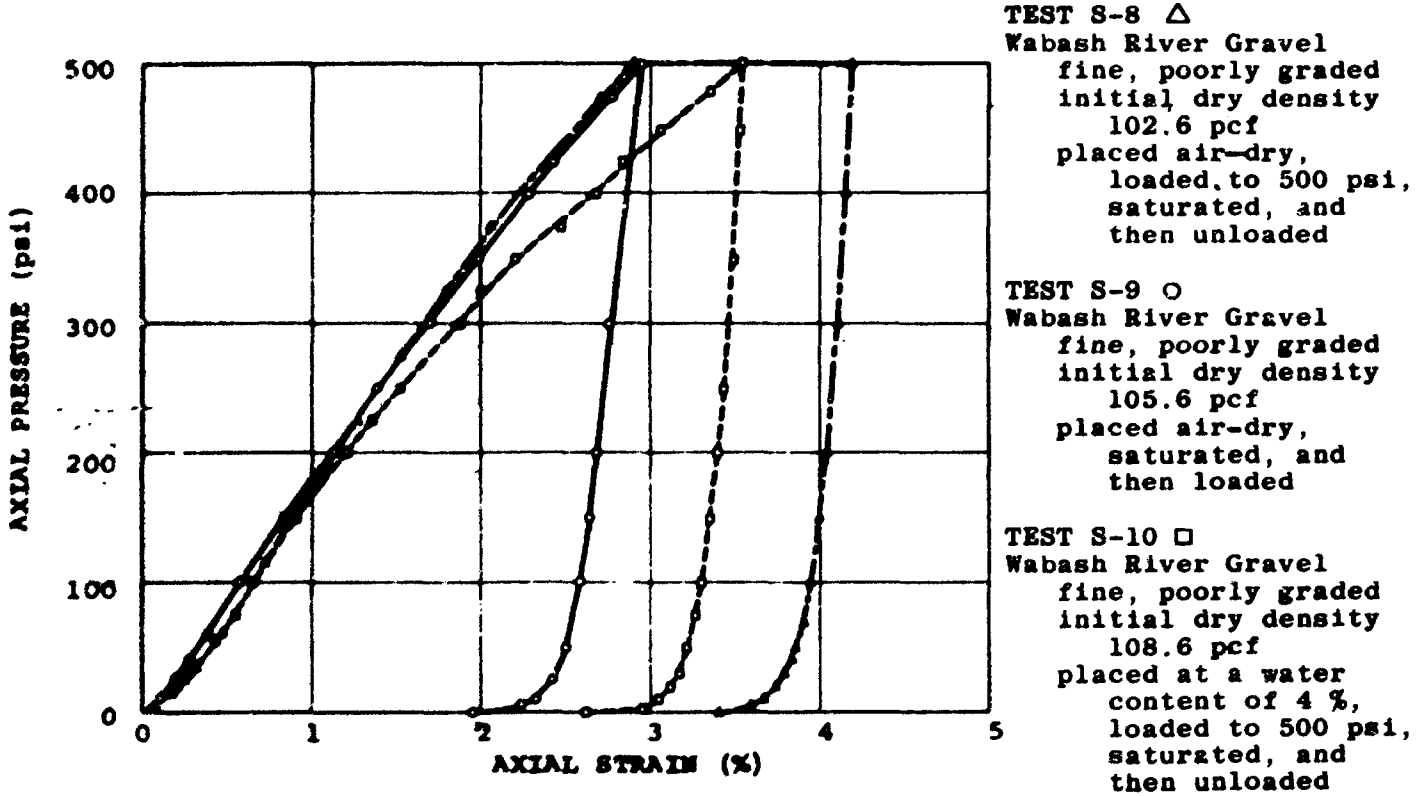

FIGURE 4.23 STRESS-STRAIN CURVES DEMONSTRATING EFFECT OF SPECIMEN SATURATION PRIOR TO AND SUBSEQUENT TO LOADING IN ONE-DIMENSIONAL COMPRESSION FOR FINE, UNIFORMLY GRADED, WABASH RIVER GRAVEL

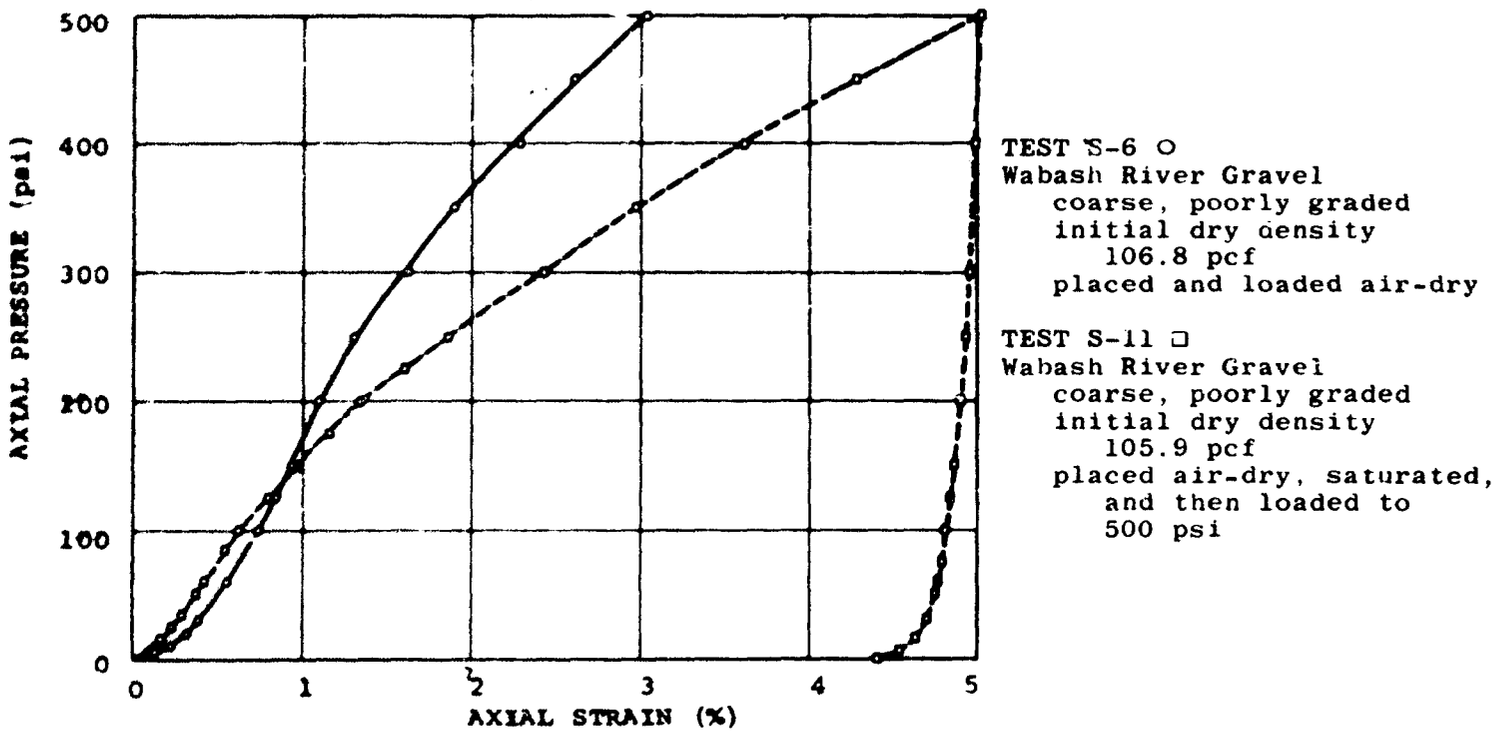

FIGURE 4.24 STRESS-STRAIN CURVES DEMONSTRATING EFFECT OF SPECIMEN SATURATION PRIOR TO AND SUBSEQUENT TO LOADING IN ONE-DIMENSIONAL COMPRESSION FOR COARSE, UNIFORMLY GRADED, WABASH RIVER GRAVEL

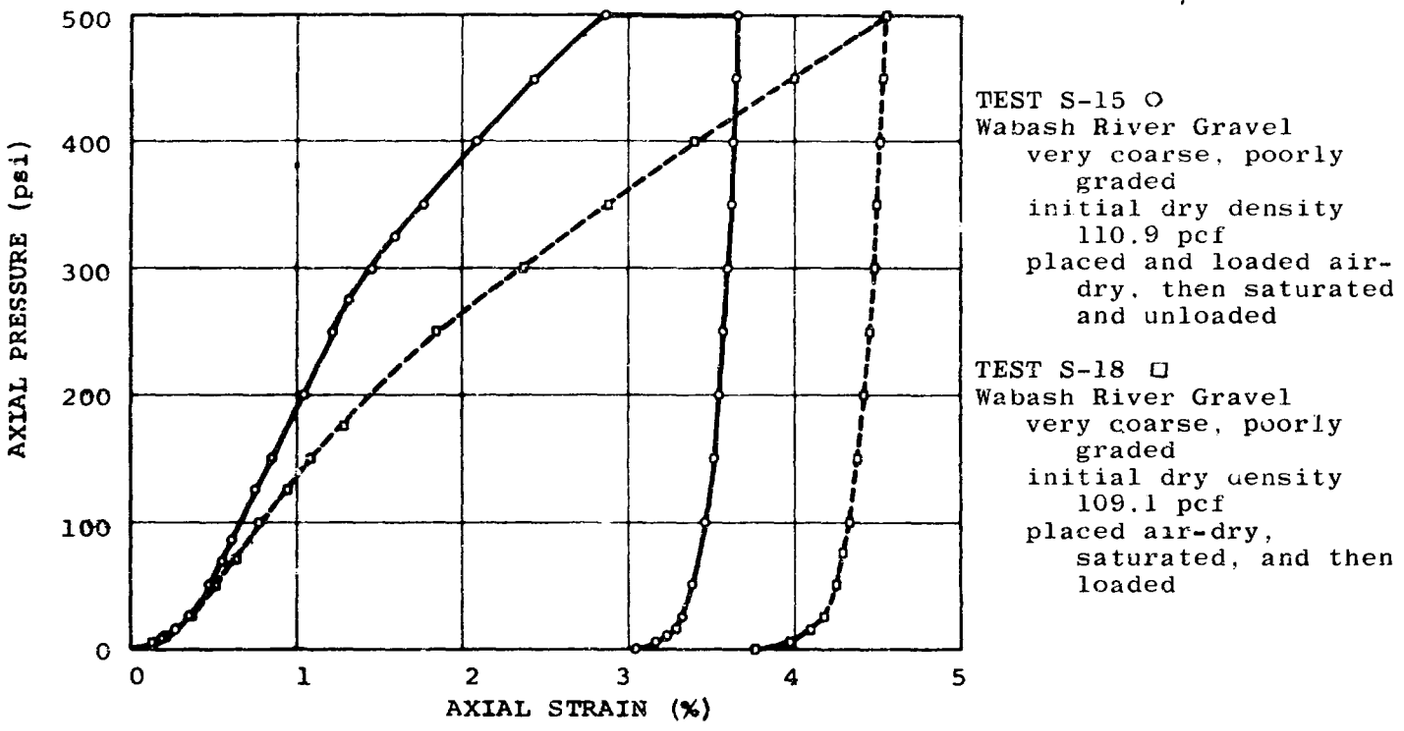

FIGURE 4.25 STRESS-STRAIN CURVES DEMONSTRATING EFFECT OF SPECIMEN SATURATION PRIOR TO AND SUBSEQUENT TO LOADING IN ONE-DIMENSIONAL COMPRESSION FOR VERY COARSE, UNIFORMLY GRADED WABASH RIVER GRAVEL

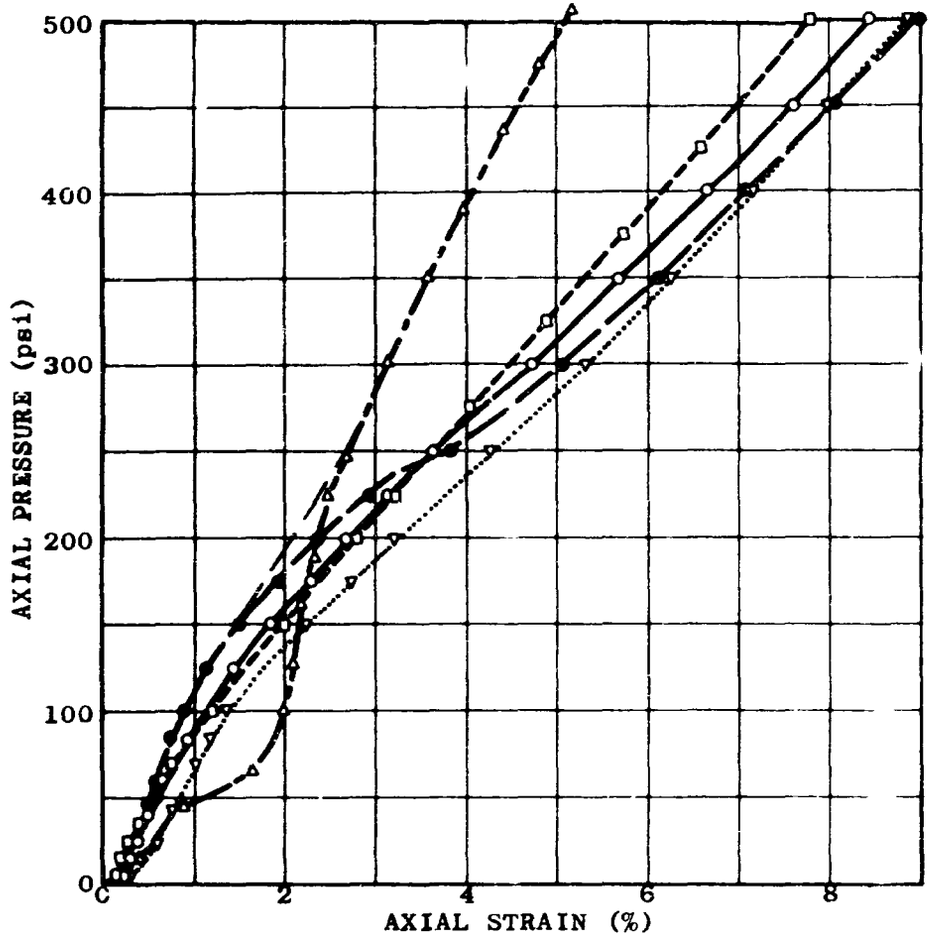

TEST S-16 ○
Crushed Limestone
well-graded
initial dry density 102.4 pcf
placed and loaded air-dry
loading rate - static

TEST S-4 □
Crushed Limestone
well-graded
initial dry density 103.8 pcf
placed and loaded air-dry
loading rate - 30 psi min

TEST D-4 △
Crushed Limestone
well-graded
initial dry density 107.5 pcf
placed and loaded air-dry
loading rate - rapid

TEST S-17 ▽
Crushed Limestone
well-graded
initial dry density 102.1 pcf
placed air-dry, saturated, and
then loaded statically

TEST S-19 ●
Crushed Limestone
well-graded
initial dry density 104.7 pcf
loading rate - variable

FIGURE 4.26 STRESS-STRAIN CURVES DEMONSTRATING EFFECT OF VARIATION OF LOADING RATE IN ONE-DIMENSIONAL COMPRESSION

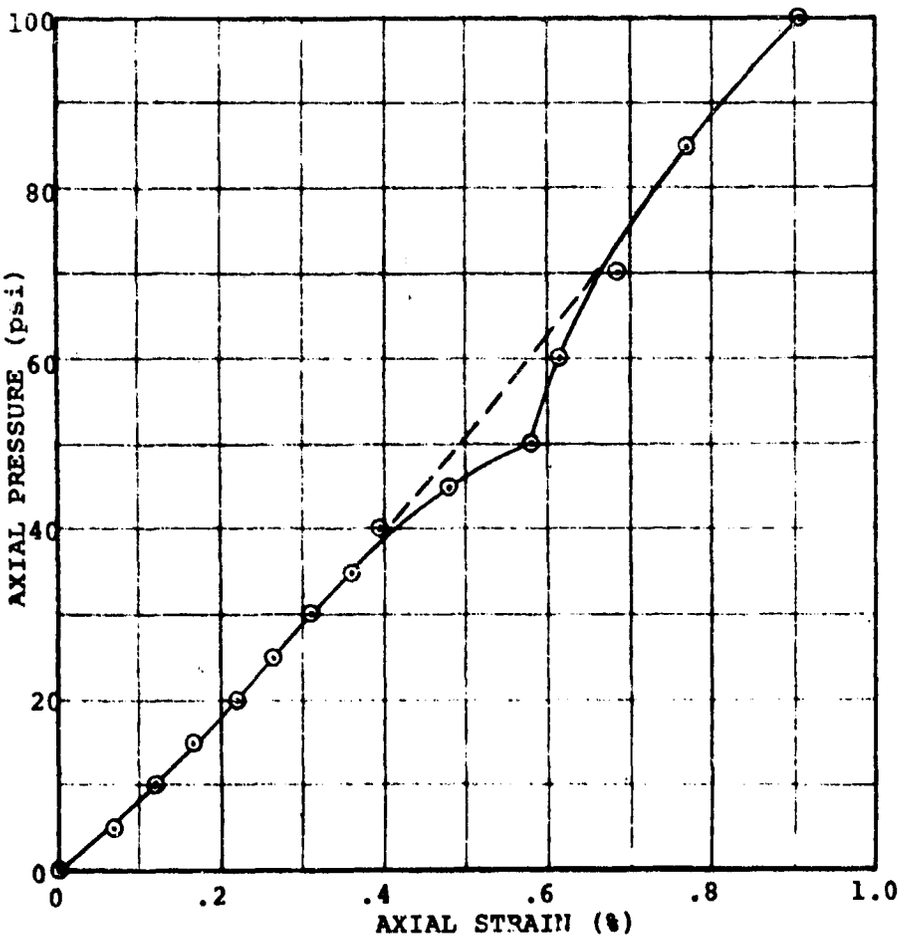

FIGURE 4.27 STRESS-STRAIN CURVE FOR TEST S-19

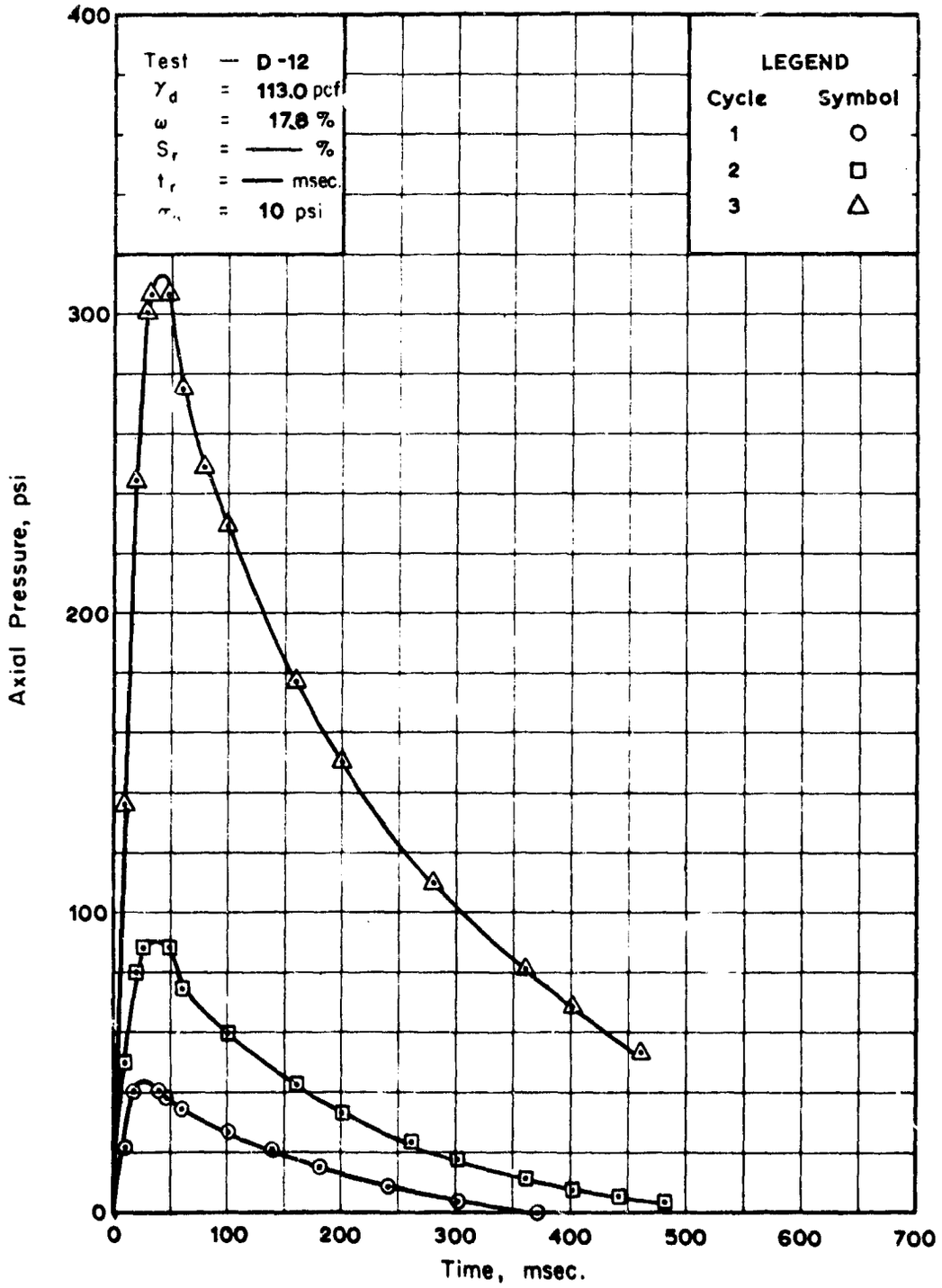

FIGURE 4.28 STRESS-TIME RELATIONSHIP MEASURED AT TOP OF SPECIMEN, TEST D-12 (SITE 3)

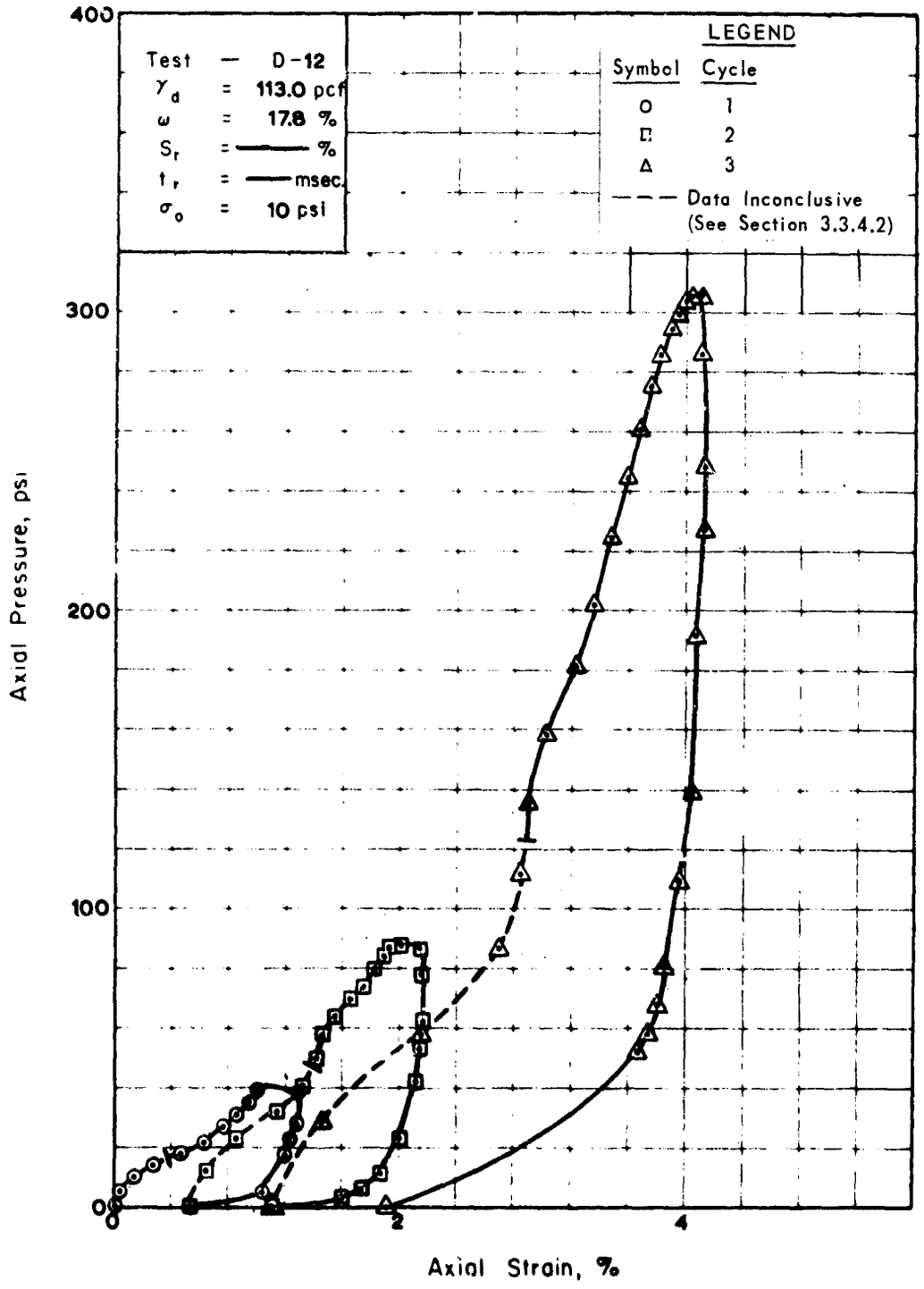

FIGURE 4.29 STRESS-STRAIN RELATIONSHIP IN ONE-DIMENSIONAL COMPRESSION, TEST D-12 (SITE 3)

CHAPTER 5

SUMMARY AND CONCLUSIONS

5.1 SUMMARY

A testing device which is capable of testing one-dimensional compression specimens 48 inches in diameter and up to 14 inches in height was developed as a part of this study. The device is capable of developing static axial pressures of 1600 psi and dynamic axial pressures of at least 800 psi with pressure rise times as fast as 3 msec with cold gas used as the loading medium. The load is applied to the test specimen by means of a flexible diaphragm, and deflections are measured by monitoring the movement of the top surface of the test specimen relative to the bottom surface with a slide wire gage which is mounted below the test specimen. The pore water pressures may be measured and the water content of the test specimen may be altered during a test if desired.

The testing device was proof-tested following construction by a series of calibration tests and a series of static and dynamic tests employing Ottawa sand as a standard.

Subsequent to the proof-testing of the testing device, an experimental study was conducted to investigate the effects of the variation of certain parameters on the one-dimensional compression characteristics of granular materials and included tests on Ottawa sand, crushed limestone, Wabash River gravel and North Dakota river gravel. The study was, in general, limited to a stress range of from 0 to 500 psi, although some

tests were carried to 1000 psi. The variation of parameter study included investigation into: 1) the effect of variation of particle shape and composition; 2) the effect of variation of particle size; 3) the effect of variation of gradation; 4) the effect of saturation prior to and subsequent to load application; and 5) the effect of rate of loading.

Soil samples were also collected from three missile sites in the United States. Specimens which simulated in situ conditions were prepared from the samples collected and subjected to both static and dynamic loading.

Representative static and dynamic stress-strain curves for the materials tested are presented in Figures 5.1 and 5.2. In Figure 5.2 only those portions of the dynamic stress-strain curves considered valid are presented; therefore, the curves do not pass through the origin. The stiffest material tested statically was Ottawa sand; Wabash River gravel and North Dakota river gravel were intermediate; and crushed limestone was the least stiff material. Typical secant moduli for a stress level of 500 psi were 62,500 psi, 15,200 psi and 5,500 psi for Ottawa sand, river gravel, and crushed limestone, respectively. The stiffest material tested dynamically was Ottawa sand. No dynamic tests were conducted on samples of river gravel. The Ottawa sand had a contrained modulus of approximately 25,000 psi at an axial stress level of 150 psi, and crushed limestone had a constrained modulus of approximately 10,000 psi at an axial stress level of 450 psi. It should be noted that dynamic tests D-6 through D-12 were conducted on soil specimens placed at densities

and water contents simulating field conditions at missile sites and small variations in water contents may change the results considerably.

5.2 CONCLUSIONS

5.2.1 Static Testing Capabilities

The comparison of the static test results with the DLG on Ottawa sand compare favorably with those published by other researchers. In particular, the results obtained using the zero lateral strain device developed by Hendron and the segmented ring boundary device developed by Zaccor show very close agreement with those obtained with the DLG. Therefore, we may conclude that with respect to static tests on specimens composed of sand-sized particles, results obtained with the DLG are at least as accurate as the best devices currently being employed.

This conclusion regarding the accuracy of the DLG may be broadened to include test results on specimens with larger particle sizes. There is, however, an upper limit to the particle size which can be tested with any degree of accuracy. This upper limit cannot be determined exactly until devices capable of testing much larger specimens have been developed. For the purpose of this study, it was assumed that with a specimen height of 12 inches and a specimen diameter of 48 inches, a maximum particle size of 3 inches could be tolerated in a well-graded specimen. Subsequent to the construction of this testing device, Fumagalli (1969) published results which indicate that perhaps the maximum particle size for a well-graded specimen should not exceed 2.5 inches and that the maximum particle size for a uniformly graded specimen should be somewhat smaller. All the samples tested met Fumagalli's limits with the exception of that

from missile site-1. The test specimens for this site were restricted to a maximum particle size of 3 inches (see Figure A.1). Therefore, it is concluded that the test results were not adversely affected by testing particle sizes too large for the test specimen dimensions.

5.2.2 Dynamic Testing Capabilities

The accuracy with which the DLG could measure the dynamic stress-strain characteristics of a granular material were determined from the proof-test results on the individual components of the DLG and dynamic proof tests on a specimen of Ottawa sand.

The slide wire gage was tested statically on a test stand and found to have a threshold of 0.0003 inches and a repeatability of better than 99% as indicated by a percentage deviation from the mean of less than 1%. The slide wire gage was also tested dynamically on the test stand and shown to experience no wiper lift. The maximum breakout friction was measured to be 0.1 lb which corresponds to a shortening of the actuating rod connecting the deformation plate and the slide wire gage of less than 0.0001 inches; the dynamic characteristics of the actuating rod-slide wire gage pickup system were shown to be negligible; and finally a strain gage was attached to the actuating rod immediately above the slide wire gage pickup, and the shortening of the rod was measured to be less than 0.002 inches during the first 10 msec of a dynamic test and after approximately 10 msec, deformations of the actuating rod did not exceed 0.001 inches. Therefore, with respect to the measurement of deformations, we may conclude that after the first 10 msec, the error in measurement should be less than 0.0015 inches.

The pressure acting on the surface of a test specimen was measured by four Kistler quartz pressure transducers, models 601A and 606A, which were mounted in the seal ring at 40 degrees to one another. These transducers were calibrated immediately prior to the application of the dynamic overpressure and, therefore, the error in pressure measurement was assumed to be the maximum deviation from the average pressure. This deviation was measured to be as great as 5 psi regardless of stress level. Therefore, it is concluded that the error in the measurement of pressure acting on the top surface of the test specimen did not exceed 5 psi. However, because of the dynamic character of the pressure applied to the top of a test specimen, the axial stress within a test specimen is not necessarily known to within 5 psi.

In order to determine the dynamic stress-strain properties of a test specimen, it was necessary to employ a fast pressure rise time and the fast pressure-rise time produced nonuniform stress conditions throughout the test specimen during a portion of the test. The passage of the stress wave through the test specimen was computed by making several simplifying assumptions. The results of this computation indicated that the maximum overstress occurred between 3 and 6 msec after the start of a test and that this overstress could be as great as 18% of the measured expansion chamber pressure. The time of the overstress corresponded well with the observed experimental behavior; however, the magnitude of the overstress as determined experimentally was about twice that computed theoretically. It is concluded that the measured axial pressure should not be considered as representing the axial stress acting within a test specimen except for times later than 9 msec after the start of the test assuming that a

pressure-rise time of approximately 25 msec is employed and that the average stress within a test specimen may vary from the measured axial pressure by as much as 10%. Thus, the maximum dynamic stress to which a specimen is subjected must be selected so that the stress range of interest occurs between approximately 10 and 25 msec after the start of the test.

In order to verify that the DLG could measure the dynamic one-dimensional stress-strain characteristics accurately, a static and dynamic test series was conducted on a material whose one-dimensional stress-strain characteristics were nearly the same under both static and dynamic conditions. A specimen of Ottawa sand was repeatedly loaded until the shapes of the stress-strain curves did not vary from cycle to cycle with the exception of a slight increase in strain. Subsequent to the sixth cycle, the specimen was preloaded to 50 psi and loaded dynamically to approximately 100 psi, then preloaded to 50 psi again and loaded to approximately 250 psi. The dynamic and static test results showed excellent agreement.

Therefore, based on the proof testing of the individual components of the system and the results of the proof tests, it is concluded that dynamic one-dimensional stress-strain characteristics of a test specimen can be determined to within 10% of the accuracy with which the one-dimensional static stress-strain characteristics can be determined with the DLG.

5.2.3 Variation of Parameter Study

5.2.3.1 General

The conclusions drawn from the variation of parameter study are based on tests conducted on four materials, viz., 20-30 Ottawa sand, crushed limestone,

Wabash River gravel, and North Dakota river gravel. Because of the length of time required to conduct a test and reduce the data, the conclusions are based on the results of a limited number of tests.

5.2.3.2 Effect of Seating Error

The effect of seating error was demonstrated by tests on crushed limestone. Static and dynamic tests were conducted on the same sample of crushed limestone with no measures taken to prevent seating error for one static test and one dynamic test and a matrix of Hydrocal employed to eliminate seating error and point crushing against the deformation plate and the bottom of the specimen container in the other test. The total strains corresponding to a stress level of 50 psi for the static test and 250 psi for the dynamic test were larger by a strain of approximately 1.5% for the specimens which did not employ a seating medium. This difference in total strain remained approximately constant throughout the test. The strain differential for the dynamic test appeared to occur at a stress level of approximately 100 psi; however, because of nonuniformity of stress conditions, the test results are not valid below about 250 psi.

Therefore, it is concluded that for the testing of coarse-grained granular materials, a seating medium should be employed to eliminate seating error and particle crushing against the top and bottom plates of the specimen container. Further, with even fine-grained soils, a seating medium should be employed for the deformation plate to ensure intimate contact between the plate and the top of the test specimens.

5.2.3.3 Effect of Variation of Particle Shape and Composition

The effect of particle shape was investigated by static tests on samples of angular crushed limestone and subrounded to rounded Wabash

River gravel. The one-dimensional stress-strain behavior measured for the crushed limestone was much less stiff than that for the Wabash River gravel. This effect is related to particle composition as well as shape; however, it is concluded that the primary factor which controlled the behavior was the greater stress concentrations and lower strength at points of contact for the more angular particles of crushed limestone. Therefore, other specimen characteristics being equivalent, the more angular the individual particles of a given specimen, the greater deformation of the specimen at any given stress level.

The effect of particle composition was investigated by static tests on samples of Ottawa sand, North Dakota river gravel, and Wabash River gravel. The test on Ottawa sand demonstrated the "locking" behavior characteristics of a particulate material below the stress level which induces particle crushing and the tests on the river gravels provided test data for two test specimens which had similar characteristics but were composed of particles with different crushing strengths. The last results indicated that the specimen composed of the particles with the higher particle crushing level exhibited "locking" behavior relative to the other gravel. Therefore, it is concluded that for a given gradation, particle shape, and density, the higher the crushing level of the individual particles, the stiffer the behavior in one-dimensional compression.

5.2.3.4 Effect of Variation of Particle Size

The effect of variation of particle-size investigation was conducted on a sample of Wabash River gravel which was broken into four samples with essentially single particle sizes.

The test results showed the uniformly graded specimen with the larger particle sizes to suffer greater strains than the specimens

with smaller particle sizes at low stress levels, below 20 psi. Also the stress level at which particle crushing occurred was shown to be lowest for the smallest particle size and highest for the largest particle size. Between the stress levels of 20 and 300 psi, the stiffness of the specimens varied directly with the particle sizes making up the specimens and above a stress level of 300 psi, there appeared to be little difference in the stress-strain curves for the different specimens.

It was concluded that the difference in the behavior of the uniformly graded specimens reflected the different compressive strengths of the individual particles. That is, the smaller the particle in a river gravel, the lower the compressive strength of the material composing the particle. And the larger the particle, the greater the strength and the more resistant to breakage. The greater particle relocation suffered by the uniformly graded specimens with large particle sizes probably resulted from initial relative densities indicating that the larger the grain size, the greater the compactive effort required to achieve a given relative density.

5.2.3.5 Effect of Variation of Gradation

The effect of variation of gradation was investigated by comparison of the results of tests performed on fine, medium, and coarse monogranular specimens and one specimen made up by equal weights of the fine, medium, and coarse materials. The stress-strain behavior was intermediate to that of the poorly graded specimens, and there was no well-defined stress level at which particle crushing occurred. Because the differences in the stress-strain curves were so slight, it can not be ascertained whether these differences indicated a behavior trend or merely were the result of random variability between test specimens.

5.2.3.6 Effect of Saturation Prior to and Subsequent to Load Application

The effect of saturation prior to and subsequent to load application was investigated by testing two specimens of most of the samples of granular materials. One of the specimens of a given sample would be placed and loaded in the air-dry state, then saturated and unloaded. The other specimen of the same sample would be placed air-dry, saturated, and then loaded and unloaded.

Saturating the specimens prior to loading caused a decrease in the particle crushing stress level relative to that measured for the samples placed and loaded air-dry. This decrease in crushing level amounted to approximately 25% for the coarse and very coarse specimens and 10% for the fine specimen. The saturated specimens demonstrated the same relative crushing strengths as the unsaturated specimens, i.e., the fine monogranular specimen crushed at the lowest stress, the coarse specimen at an intermediate stress and the very coarse specimen at the highest stress level. It is concluded that the addition of water causes a reduction in the compressive strength of the Wabash River gravel and a decrease in the friction between the individual grains.

The difference in the behavior of well-graded and uniformly graded specimens saturated prior to and subsequent to loading differed markedly. Well-graded specimens of Wabash River gravel and crushed limestone which were saturated prior to loading suffered 5 to 10% more strain at a stress of 500 psi than the specimens placed and loaded air-dry before saturation. Upon saturation the specimens loaded air-dry experienced between 20 and 25% additional strain. Therefore, the specimens which were placed and loaded air dry and then saturated suffered a final deformation which was from 15 to 20% greater than that of the specimens placed air-dry, saturated, and then loaded. The saturated tests were loaded in a drained condition.

The monogranular specimens of Wabash River gravel which were placed and loaded air-dry suffered an additional deformation of between 25 and 45% at a stress level of 500 psi when saturated. The uniformly graded specimens which were placed air-dry, saturated, and then loaded suffered between 20 and 60% more strain than the specimens loaded air-dry before saturation. The fine specimen which was saturated subsequent to loading had a greater total deformation after saturation than did the specimen which was saturated prior to loading as did the well-graded specimens of both Wabash River gravel and crushed limestone. However, the coarse and very coarse specimens which were saturated subsequent to loading suffered less total deformation than the specimens saturated prior to loading.

It is concluded that well-graded fills constructed dry may suffer 20 to 25% additional deformation upon saturation with no increased load. This additional settlement resulting from saturation once in place can be avoided by using sufficient moisture during placement.

5.2.3.7 Effect of Rate of Loading

Dynamic tests were conducted on samples of Ottawa sand and crushed limestone as well as the missile site samples. The tests of missile site samples were conducted on specimens prepared to simulate in situ conditions and were, therefore, not subjected to repeated tests as required for a variation of parameter study. Dynamic tests on Ottawa sand have been conducted by others and the tests included in this study were primarily for proof testing of equipment. Thus, tests to investigate the effects of rate of loading were limited primarily to a sample of crushed limestone.

The test results on crushed limestone indicated that the strain rate effects are dependent on the stress rate employed. A loading rate of

50 psi/minute caused an increase in stiffness relative to a specimen loaded statically of approximately 10%; a loading rate of 200 psi/minute caused an increase in stiffness of approximately 35%; and a dynamic test caused an increase in stiffness of approximately 40%.

The increasing of the rate of loading to pressure-rise times of the order of 25 to 30 msec produced nonuniform stress conditions throughout the test specimens at early times during a test. It is concluded that the dynamic stress-strain data should not be considered valid for times less than 9 msec when pressure-rise times of from 25 to 30 msec were employed. Nearly complete stress ranges can be investigated by varying the maximum overpressure such that the pressures of interest occur between 9 and 25 msec after the start of a test. This procedure was demonstrated by Test D-12.

5.2.4 Creep Deformation

Some of the materials tested, particularly when saturated, were subject to creep. The specimens which were subject to creep were allowed to deform under constant load until the rate of creep was less than 0.001 inches/hour. It is concluded that this rate of creep criterion corresponded to at least 90% of the total deformation and was the practical limit of the total time of the test.

5.3 SUGGESTIONS FOR FURTHER RESEARCH

The variation of parameter study as reported herein was intended to define general trends in the one-dimensional compression behavior of large granular materials. The mechanisms of these trends are only speculated on. In order to establish conclusively the mechanisms involved, many more

series of tests must be conducted on samples which are selected to eliminate as nearly as possible variations of all parameters except that one parameter being investigated.

The first variable which should be investigated is the effect of the initial dry density. In order to investigate this variable, a means must be developed for determining the relative density for large granular materials. Knowledge of the influence of initial dry density is essential for evaluating the results of the variations of all other parameters.

Subsequent to establishing a means for evaluating relative densities and investigating the effect of variation of initial dry density, the effects of variations of the other parameters should be investigated in a systematic manner with the scope of the investigation limited to the extent that several tests can be performed on each sample, thereby demonstrating the repeatability of the behavior. Further to establish the mechanisms of the variations in behavior of the materials, extensive grain-size analyses should be performed on the test specimens after being subjected to different axial pressures.

Finally, new sources for materials should be sought. The samples should be fresh from the parent rock and the engineering properties of the parent rock should be determined.

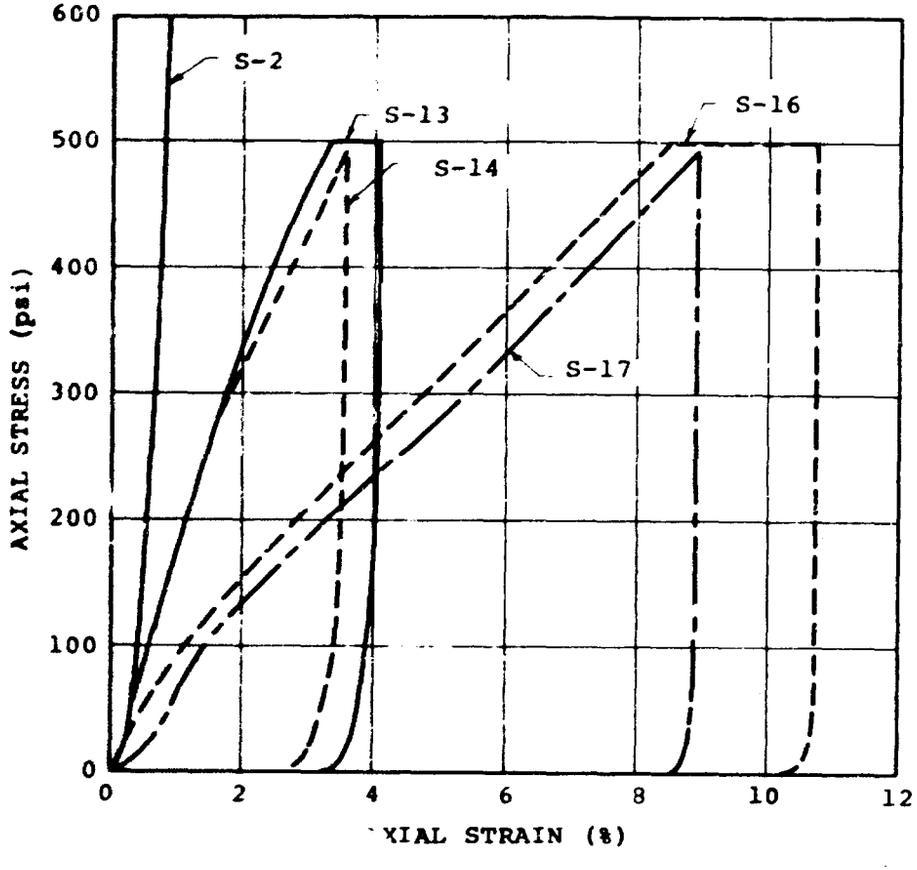

S-2 20-30 OTTAWA SAND
γ = 110.3 pcf w = 0%

S-13 COARSE TO FINE WABASH RIVER GRAVEL
γ = 117.7 pcf w = 0%
loaded air-dry, saturated, and unloaded

S-14 COARSE TO FINE WABASH RIVER GRAVEL
γ = 113.3 pcf w = 0%
saturated, loaded, and unloaded

S-16 COARSE TO FINE CRUSHED LIMESTONE GRAVEL
γ = 102.4 pcf w = 0%
loaded air-dry, saturated, and unloaded

S-17 COARSE TO FINE CRUSHED LIMESTONE GRAVEL
γ = 102.1 pcf w = 0%
saturated, loaded, and unloaded

FIGURE 5.1 SUMMARY OF STATIC TEST RESULTS

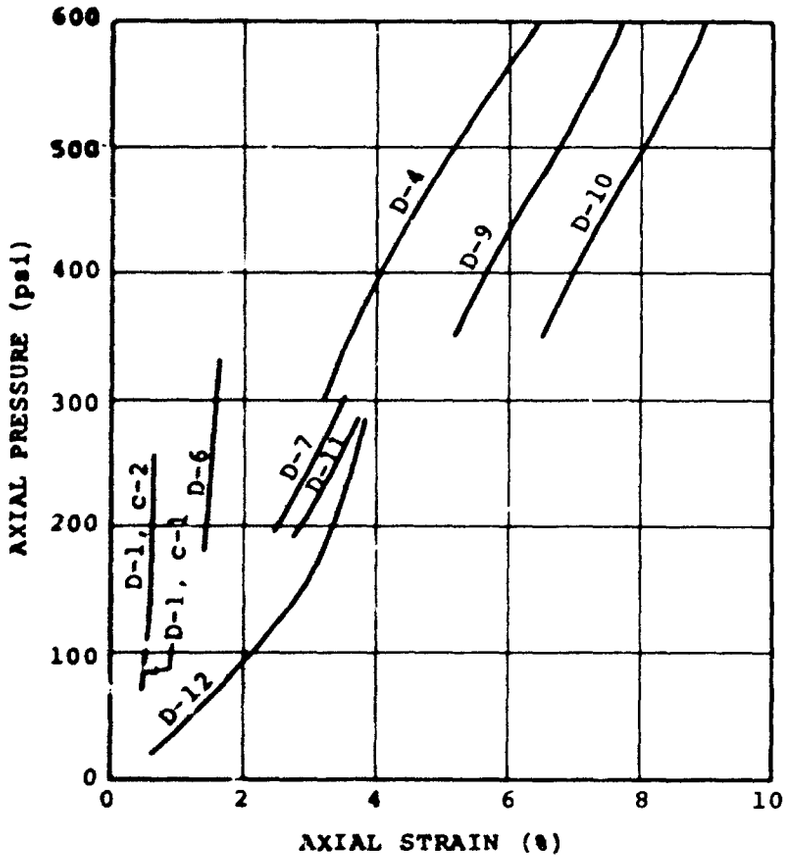

D-1 20-30 OTTAWA SAND
initial dry density 110.8 psc
water content - 0%

D-4 COARSE TO FINE CRUSHED LIMESTONE
initial dry density 107.3 pcf
water content - 0%

D-6 COARSE TO FINE SANDY SILT
initial dry density 108.2 pcf
water content - 11%

D-7 GRAVELLY COARSE TO FINE SAND
initial dry density 89.5 pcf
water content - 14%

D-9 GRAVELLY COARSE TO FINE SAND
initial dry density 108.8 pcf
water content - 9%

D-10 GRAVELLY COARSE TO FINE SAND
initial dry density 106.5 pcf
water content - 9%

D-11 GRAVELLY COARSE TO FINE SAND
initial dry density 86.4 pcf
water content - 20%

D-12 COARSE TO FINE SANDY SILT
initial dry density 113 pcf
water content - 18%

FIGURE 5.2 SUMMARY OF DYNAMIC TEST RESULTS

APPENDIX A

TESTS ON SAMPLES FROM MISSILE SITES

A.1 INTRODUCTION

The purpose of this study was to measure the dynamic constrained moduli of backfill soils from three missile sites. The sites of interest were site 1 near Cheyenne, Wyoming, site 2 near Kimball, Nebraska, and site 3 near Valley City, North Dakota.

Samples of the soils used as backfill around the buried structures at missile sites 1, 2, and 3 were obtained and returned to the Structural Dynamics Testing Laboratory at the University of Illinois. The samples were classified according to routine laboratory tests, brought to their respective field water contents, and then placed in the DLG specimen container at their approximate field densities. The specimens were preloaded with a static load equivalent to the overburden pressure acting at the particular depth below the ground surface the specimen was designed to simulate, and then loaded with a dynamic stress increment.

A.2 LABORATORY CLASSIFICATION TESTS

Routine laboratory classification tests were performed on samples from the three sites at the University of Illinois laboratories. These tests included visual classification, mechanical grain-size analyses, and determination of the specific gravities of the solids of the samples. The results of these tests are presented in Figures A.1, A.2, and A.3.

A.3 DYNAMIC TESTS

A.3.1 Testing Program

The testing program, as presented in Table A.1 was designed to determine the dynamic constrained moduli of the backfill materials around the underground structures at sites 1, 2, and 3 at two different depths beneath the ground surface. The depths simulated were determined primarily by the availability of information concerning the in situ density and water content. The static preload for a given specimen was computed using the average unit weight of the backfill and the depth the specimen was to simulate.

A.3.2 Specimen Preparation

The samples were brought to the moisture content desired and allowed to set for five days to ensure migration of the water throughout the specimen. Water content samples were taken after the fourth day and again during specimen placement. Prior to the placement of the specimen in the specimen container, compaction tests were run in a circular container approximately 13 inches in diameter in order to determine the compaction effort required to attain the desired density.

The specimen placement technique employed was identical to that described in Section 3.3.2, Specimen Placement, with Hydrocal employed on the bottom side of the deformation plate to minimize seating error and the loading diaphragm placed as described in Section 3.3.4.3, Investigation to Define Incidental Problems, to reduce the chance of rupturing the diaphragm. Hydrocal was not utilized for seating the deformation plate in test D-12 because with

the high water content, the surface of the soil specimen was quite malleable and intimate contact between the specimen and the deformation plate was easily obtained.

A.3.3 Test Results

The pressure-time plots and the stress-strain plots for the tests conducted on the missile site samples are presented in Figures A.4 to A.15, inclusive. Plots of the constrained secant modulus versus axial pressure for sites 1, 2, and 3, are presented in Figures A.16 to A.21, inclusive.

The backfill materials from site 1 were tested in tests D-7 and D-11 and both samples had constrained moduli of about 8000 psi for vertical pressures ranging from 100-300 psi. Although test D-7 had a seating load of 6 psi and D-11 had a seating load of 15 psi, this small difference in initial seating stress did not significantly affect the constrained modulus.

The results of tests D-9 and D-10 shown in Figures A.18 and A.19 indicate that the backfill material from site 2 had constrained moduli of 6000-8000 psi for pressure levels between 300 and 600 psi at the water content and densities tested. These tests also showed that the small difference in seating loads of 7 and 21 psi did not significantly affect the test results.

Specimens of site 3 backfill were tested at a low and a high degree of saturation in tests D-6 and D-12, respectively. Specimen D-6 was placed at a dry density of 108-2 pcf, degree of saturation of 50%, and a constrained modulus was measured which increased from 14,000 psi to 18,000 psi as the pressure increased from 200 to 300 psi. Specimen D-12 was placed at a dry density of 113 pcf, a degree of saturation of 92%, and a constrained modulus was measured which increased from 3500 to 7000 as the pressure increased

from 25 psi to 250 psi. These test results are somewhat of a surprise since it was expected that specimen D-12 would be stiffer than specimen D-6 due to the higher degree of saturation of specimen D-12. This result indicates that we may not yet fully understand the effects of displacement water content, compaction energy, and initial degree of saturation on the constrained modulus of soils.

SITE	1	1	2	2	3	3			
TEST	D-7	D-11	D-9	D-10	D-6	D-12	c-1	c-2	c-3
SIMULATED DEPTH (feet)	9	20	9	26	7	11			
INITIAL SPECIMEN HEIGHT (inches)	11.461	10.260	10.469	9.633	11.625	10.739			
SPECIFIC GRAVITY OF SOLIDS	2.73	2.73	2.64	2.64	2.79	2.79			
WATER CONTENT (%)	14	20	9	9	11	18			
DRY DENSITY (pcf)	89.5	86.4	108.8	106.5	108.2		113.0	113.7	114.3
DEGREE OF SATURATION (%)	33	56	49	46	50		92	93	95
RISE TIME (msec)	32	31	34	33	28		20	26	34
PRELOAD (psi)	6	15	7	21.5	6		10	10	10
DYNAMIC LOAD (psi)	310	272	605	597	348		41	88	307

TABLE A.1 DYNAMIC TESTING PROGRAM FOR SITES 1, 2, & 3 MATERIALS

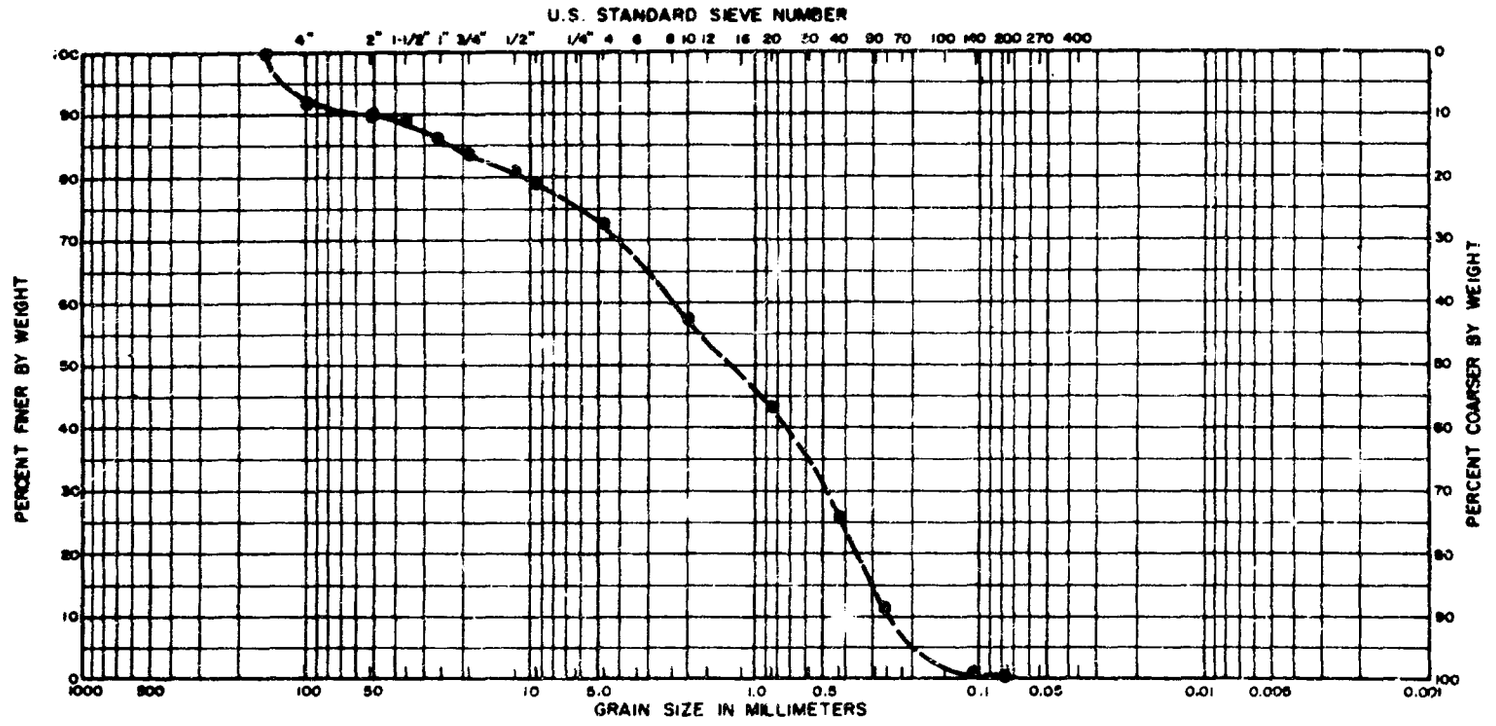

Light-brown, coarse to fine gravelly, coarse to fine SAND with cobbles
Specific gravity of solids 2.73

FIGURE A.1 GRADATION CURVE FOR SITE 1

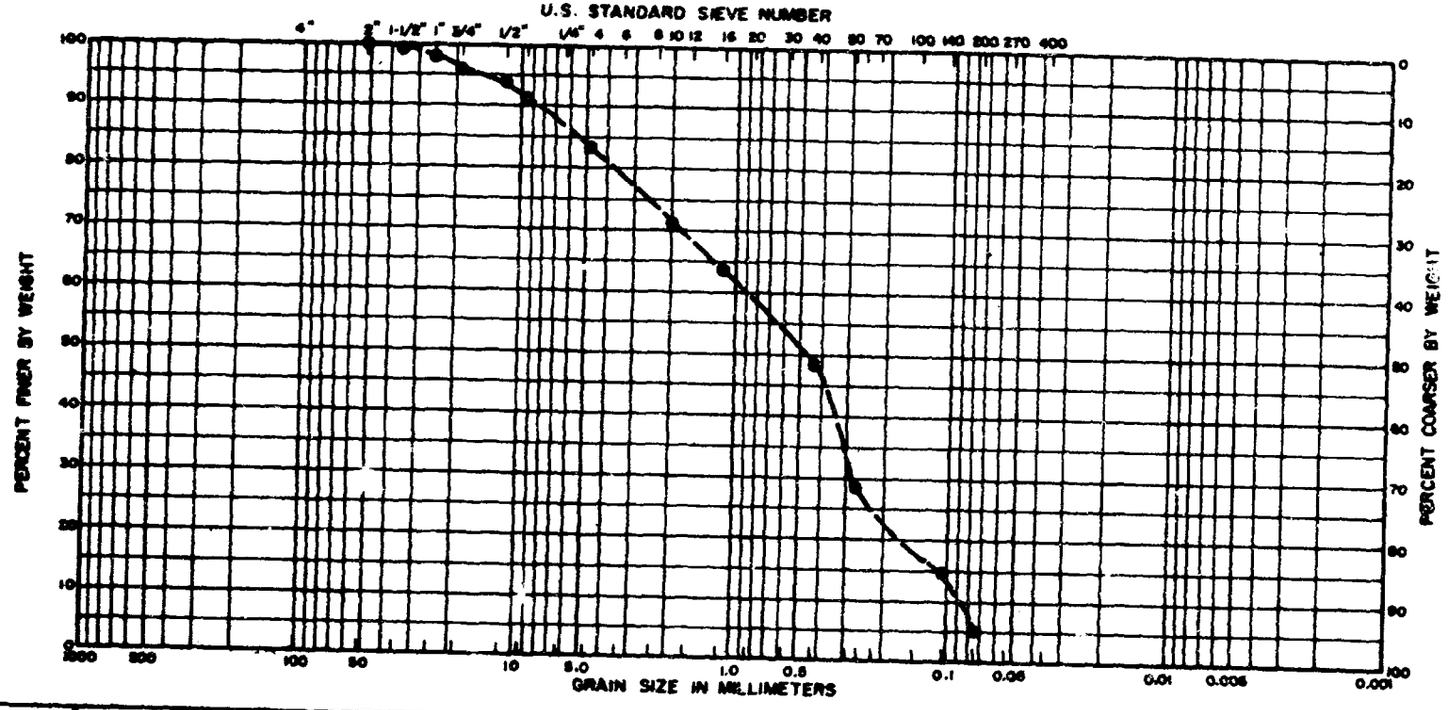

Light-brown, fine gravelly, coarse to fine SAND with some coarse gravel and silt
Specific gravity of solids 2.64

FIGURE A.2 GRADATION CURVE FOR SITE 2

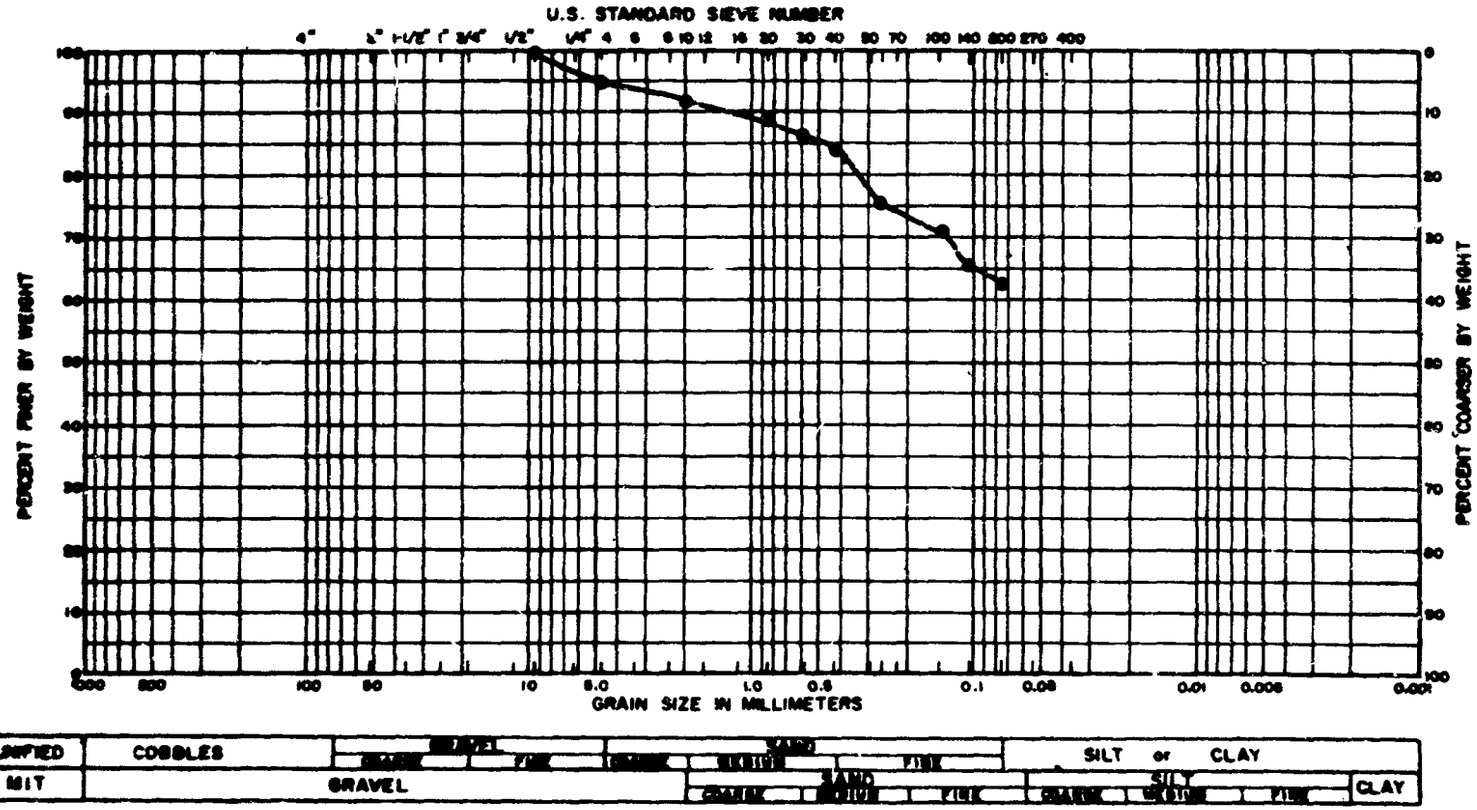

Light-brown, coarse to fine sandy SILT with some coarse to fine gravel
Specific gravity of solids 2.79

FIGURE A.3 GRADATION CURVE FOR SITE 3

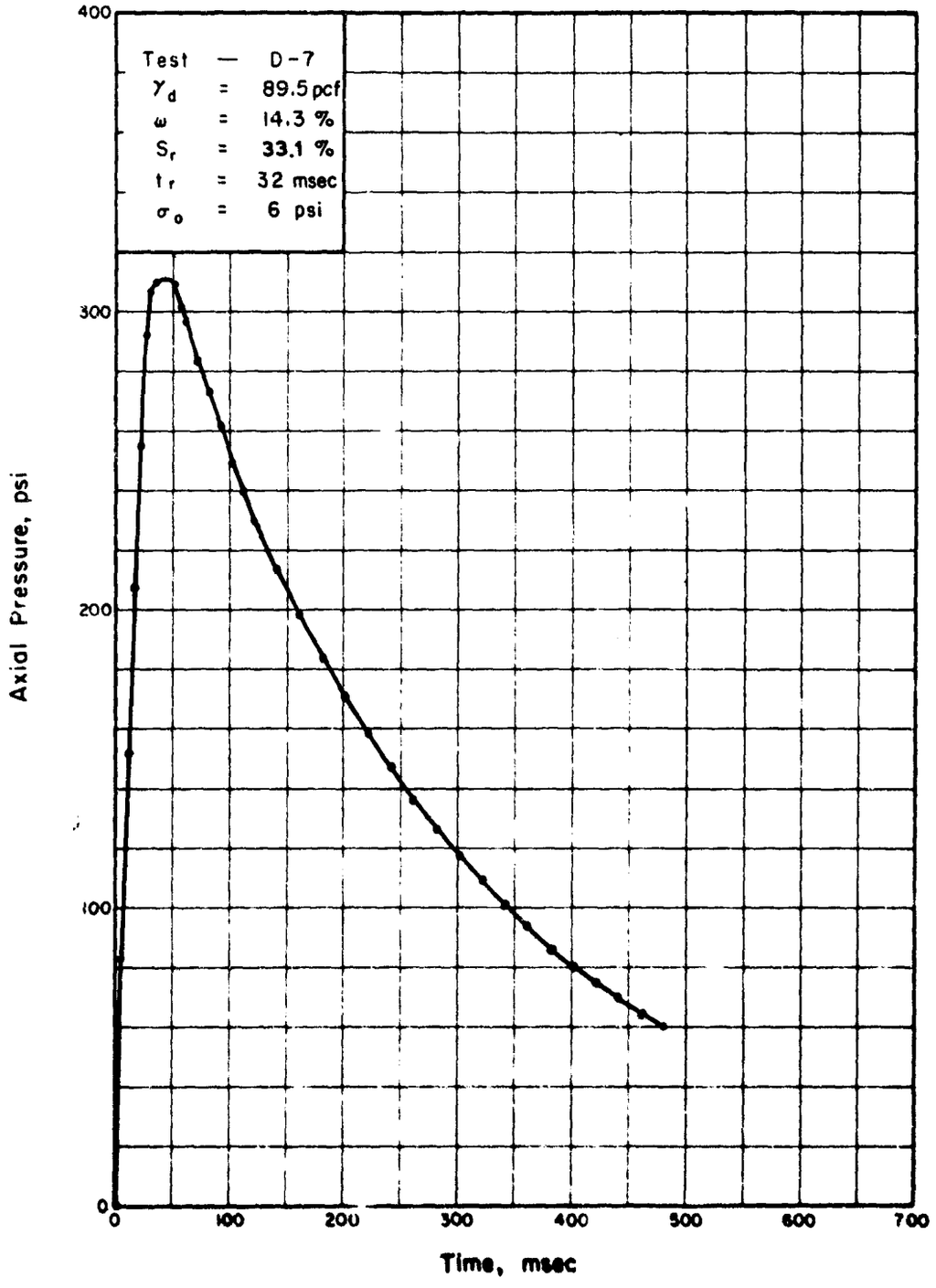

FIG. A.4 STRESS-TIME RELATIONSHIP MEASURED AT TOP OF SPECIMEN, TEST D-7 (SITE 1)

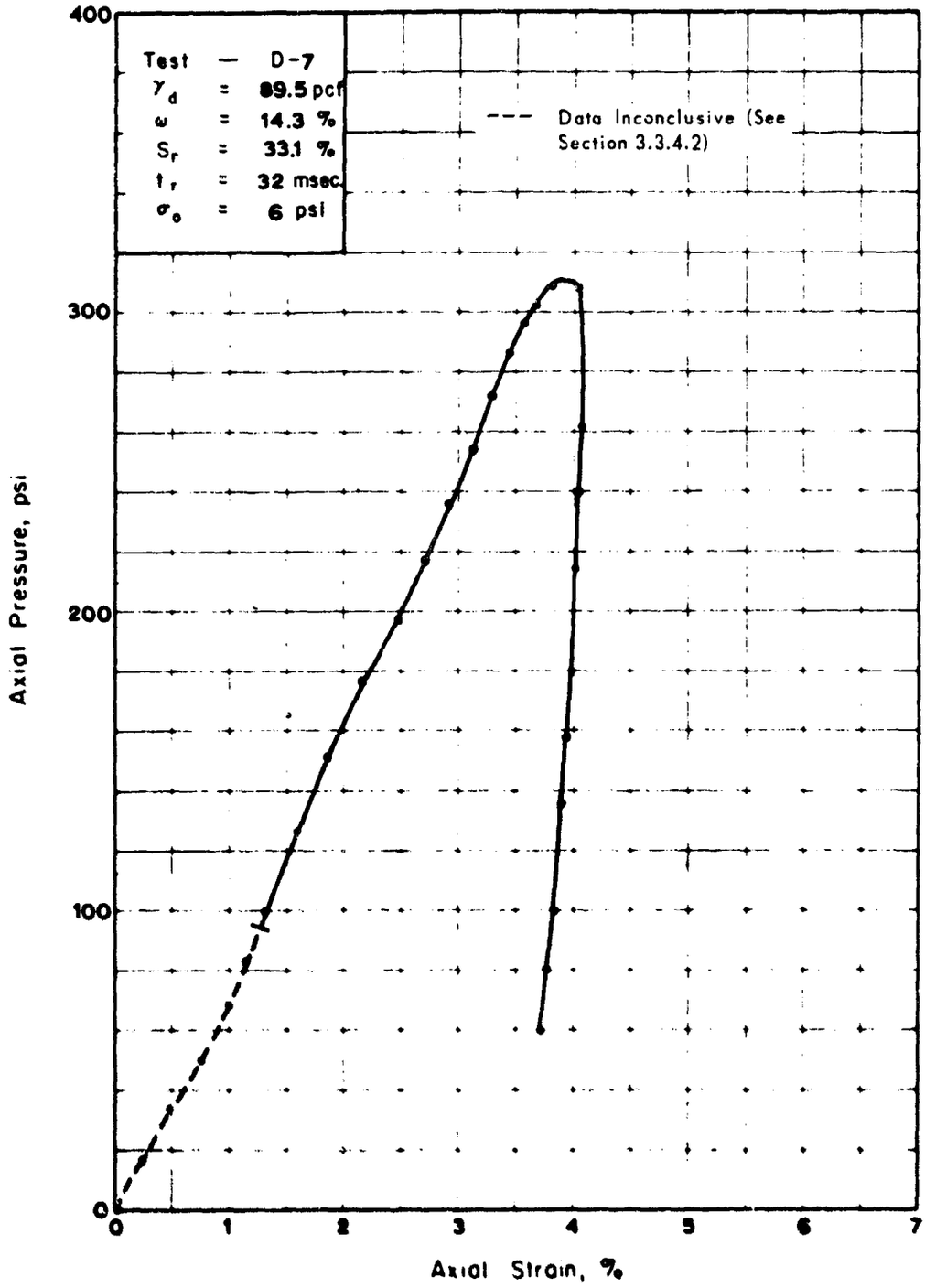

FIG. A. 5 STRESS - STRAIN RELATIONSHIP IN ONE-DIMENSIONAL COMPRESSION, TEST D-7 (SITE 1)

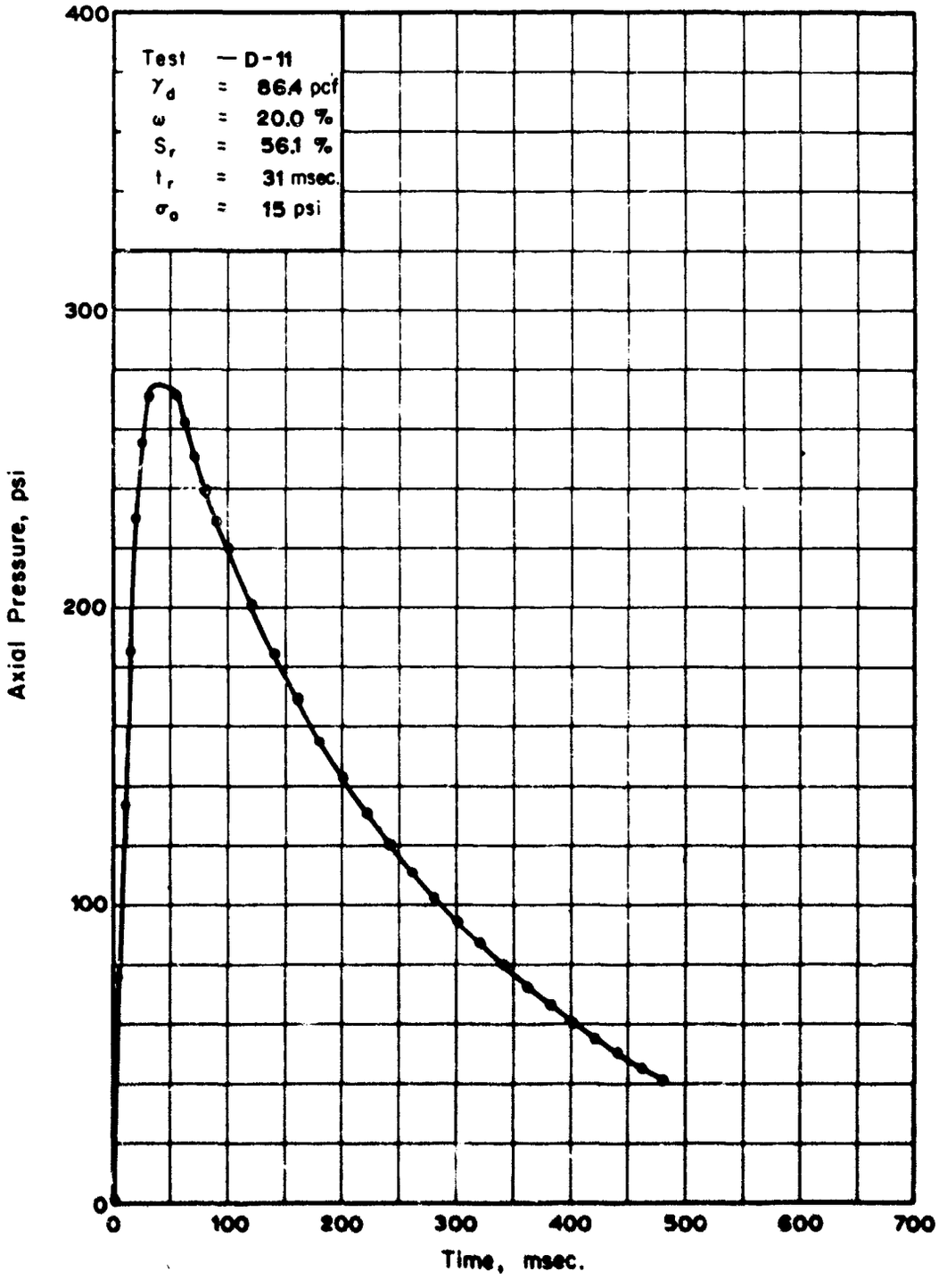

FIG. A.6 STRESS-TIME RELATIONSHIP MEASURED AT TOP OF SPECIMEN, TEST D-11 (SITE I)

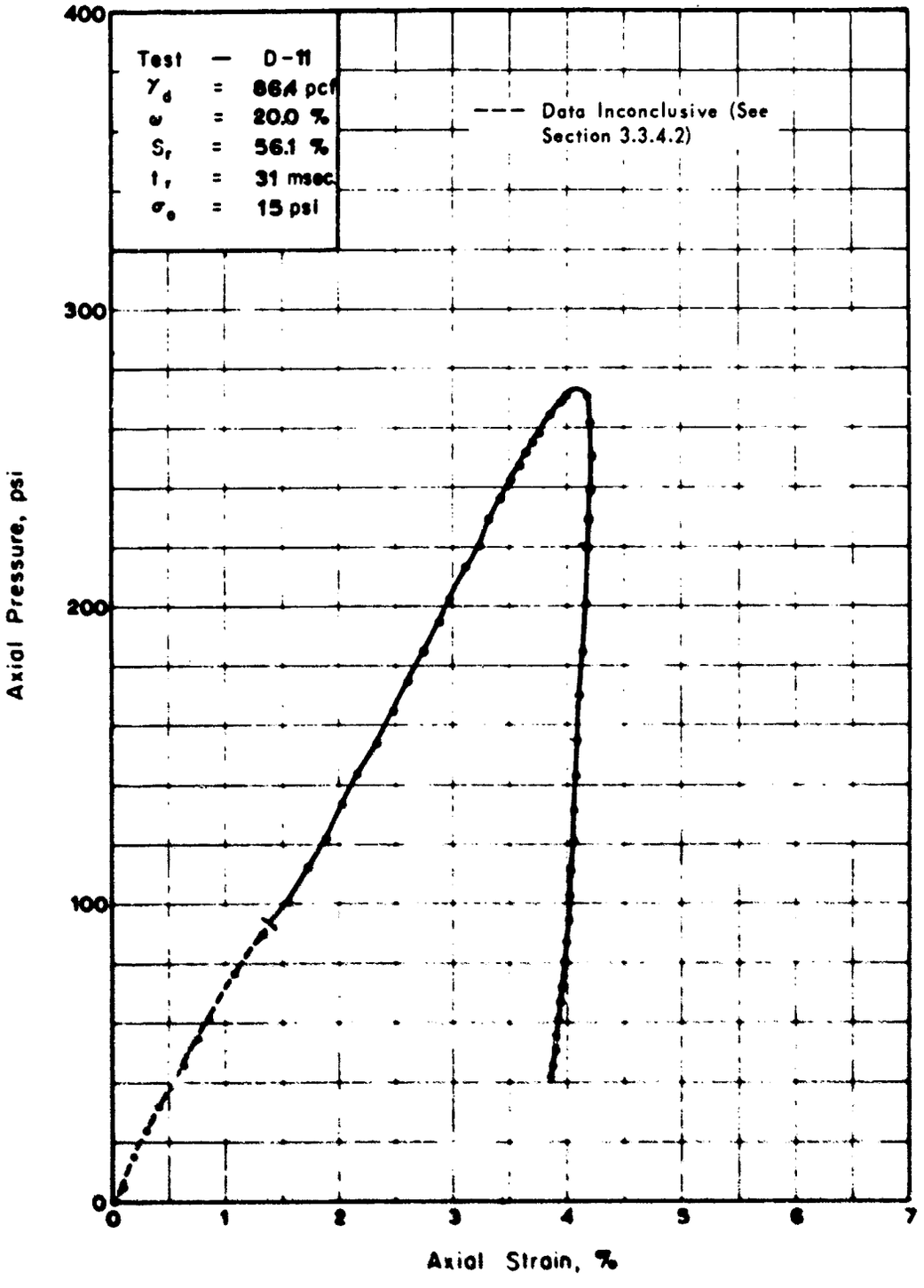

FIG. A.7 STRESS - STRAIN RELATIONSHIP IN ONE-DIMENSIONAL COMPRESSION. TEST D-11 (SITE 1)

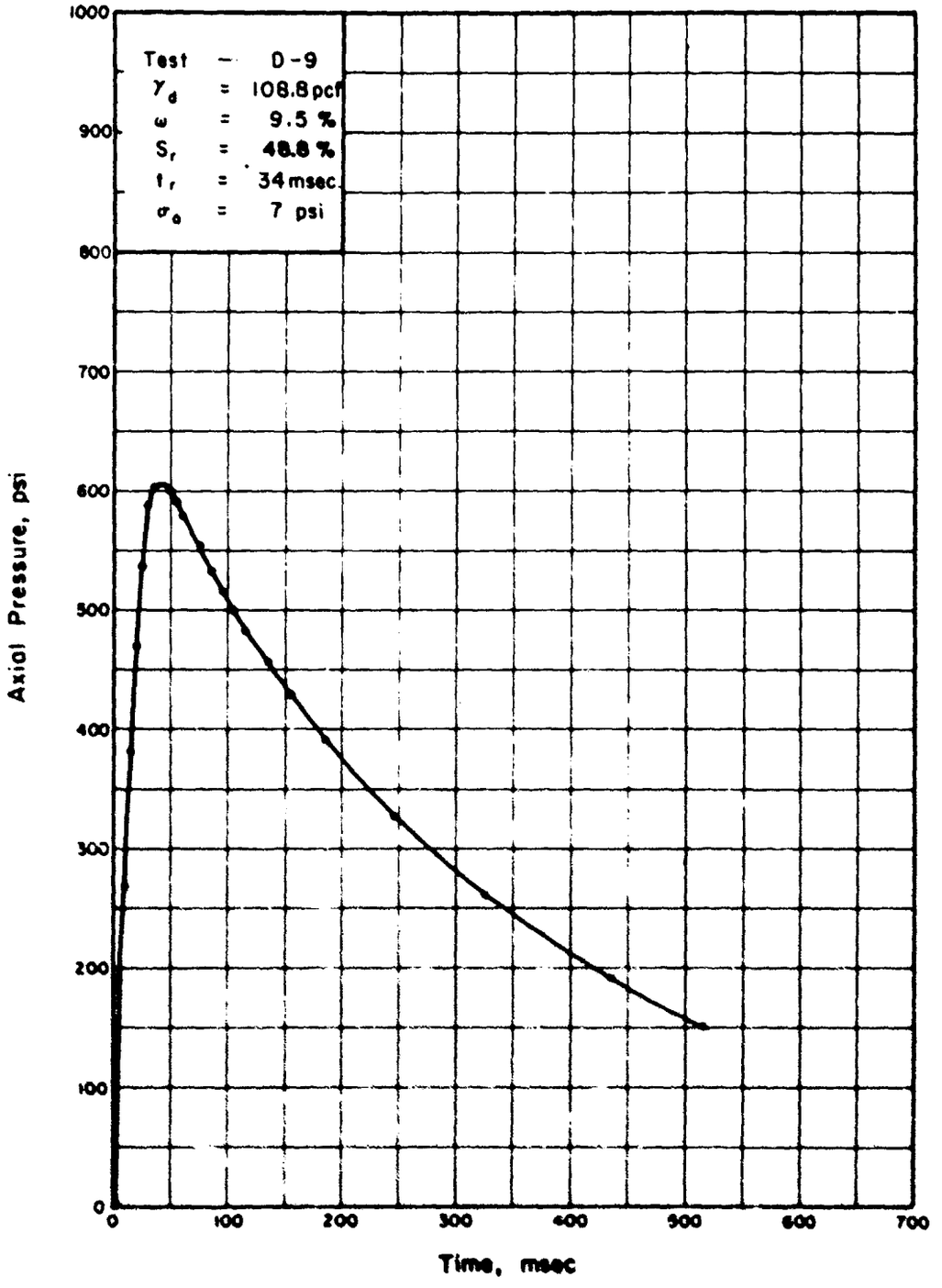

FIG. A.8 STRESS-TIME RELATIONSHIP MEASURED AT TOP OF SPECIMEN, TEST D-9 (SITE 2)

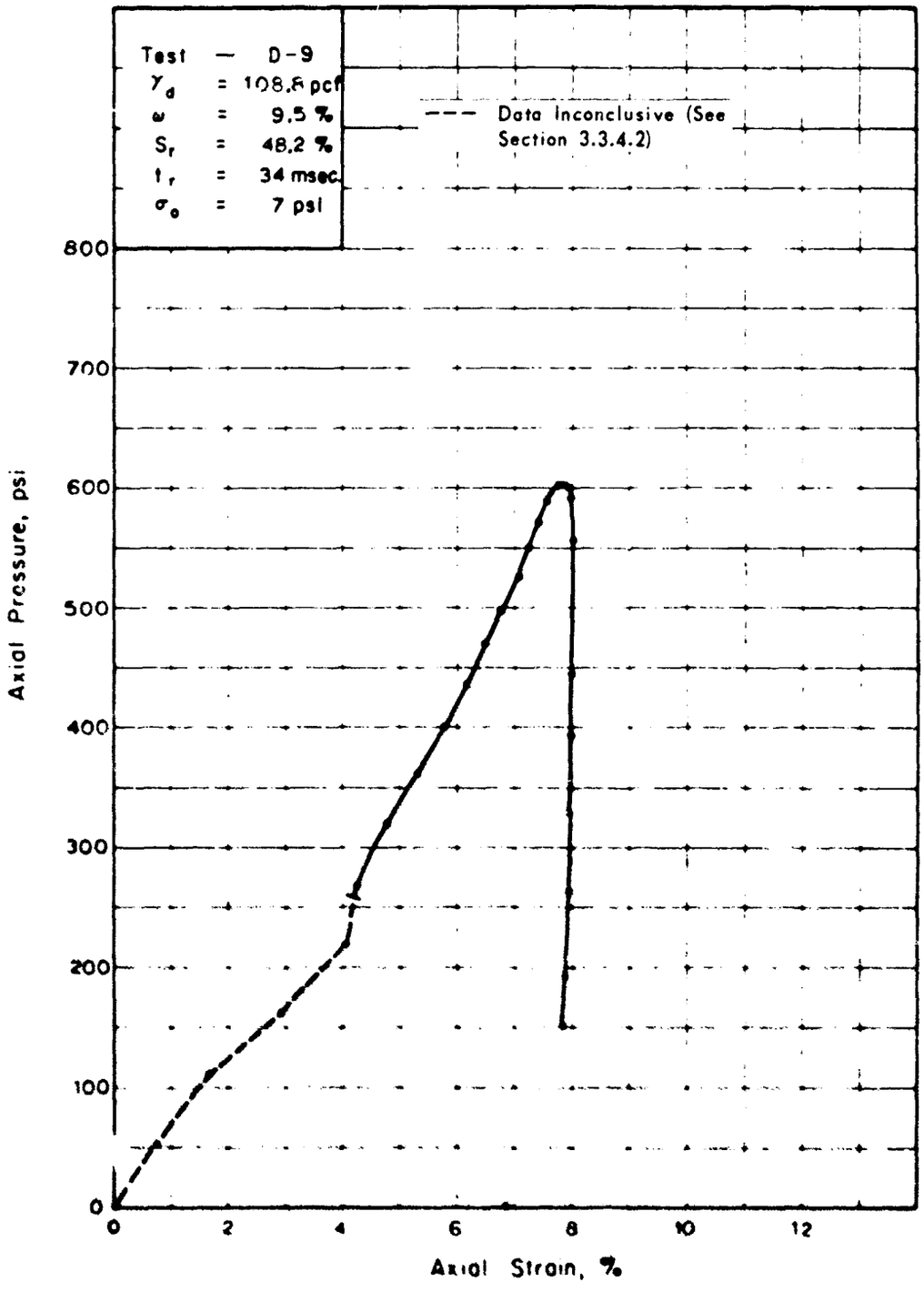

FIG. A.9 STRESS - STRAIN RELATIONSHIP IN ONE-DIMENSIONAL COMPRESSION, TEST D-9 (SITE 2)

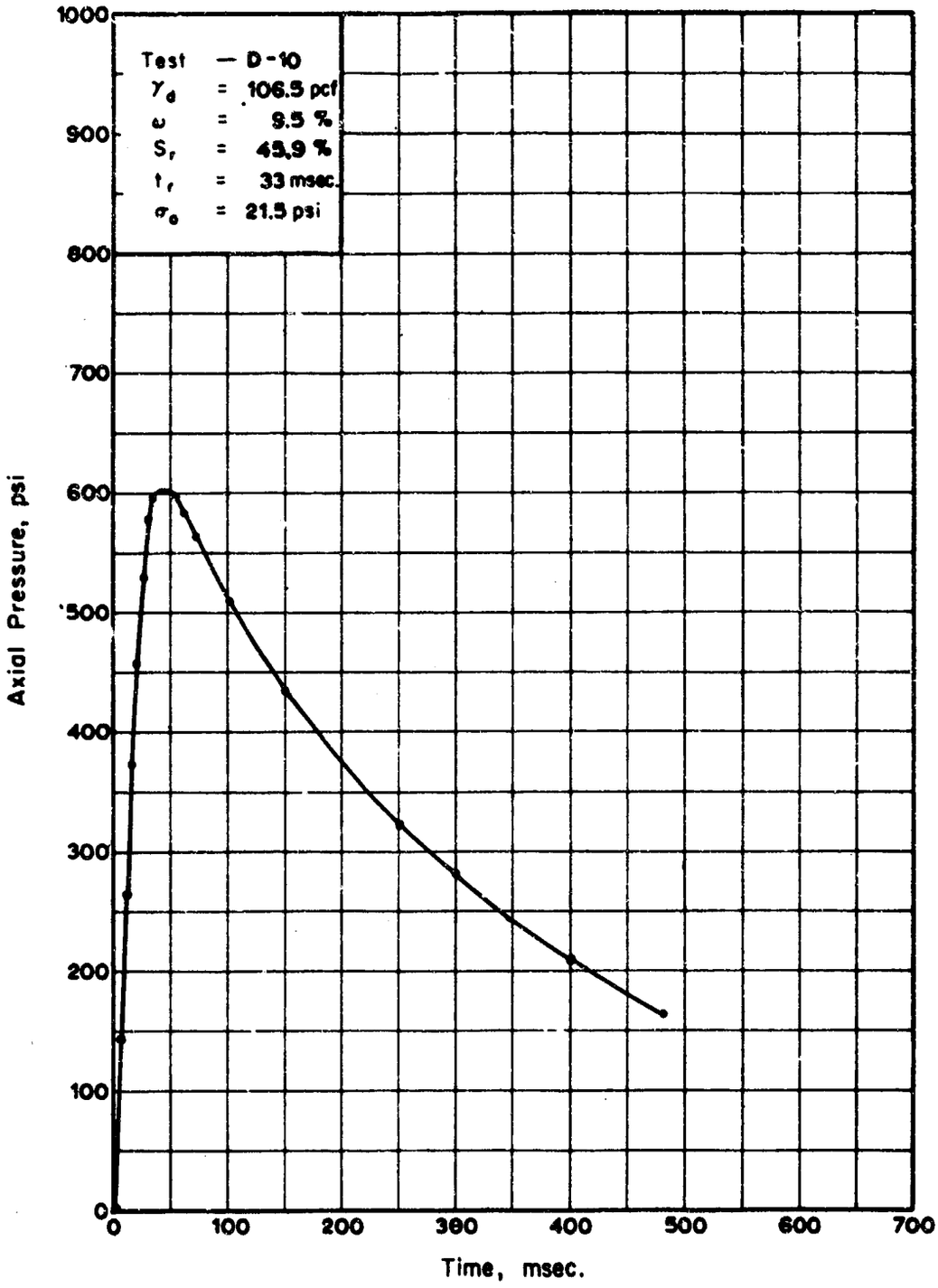

FIG. A.10 STRESS-TIME RELATIONSHIP MEASURED AT TOP OF SPECIMEN, TEST D-10 (SITE 2)

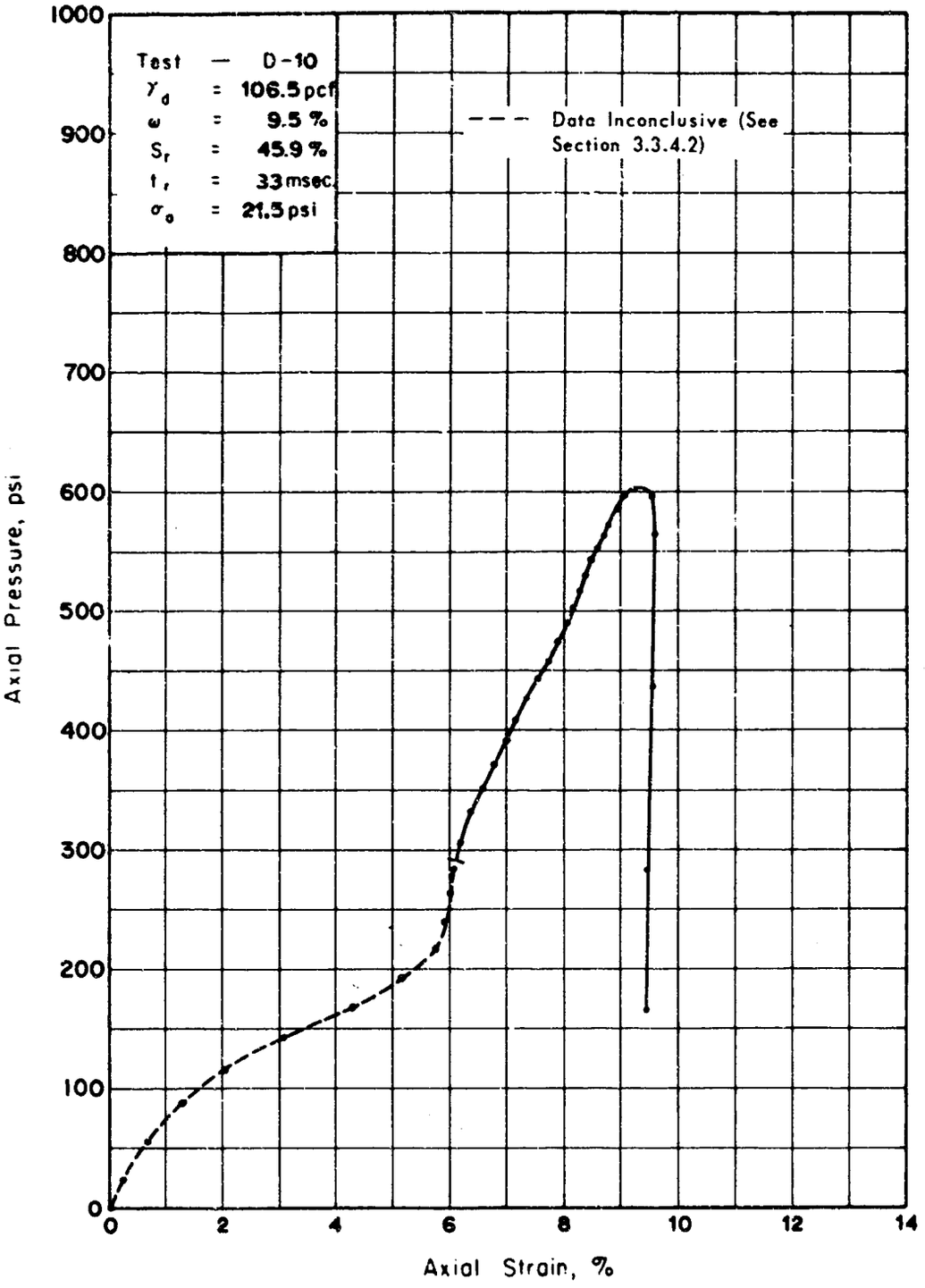

FIGURE A.11 STRESS-STRAIN RELATIONSHIP IN ONE-DIMENSIONAL COMPRESSION, TEST D-10 (SITE 2)

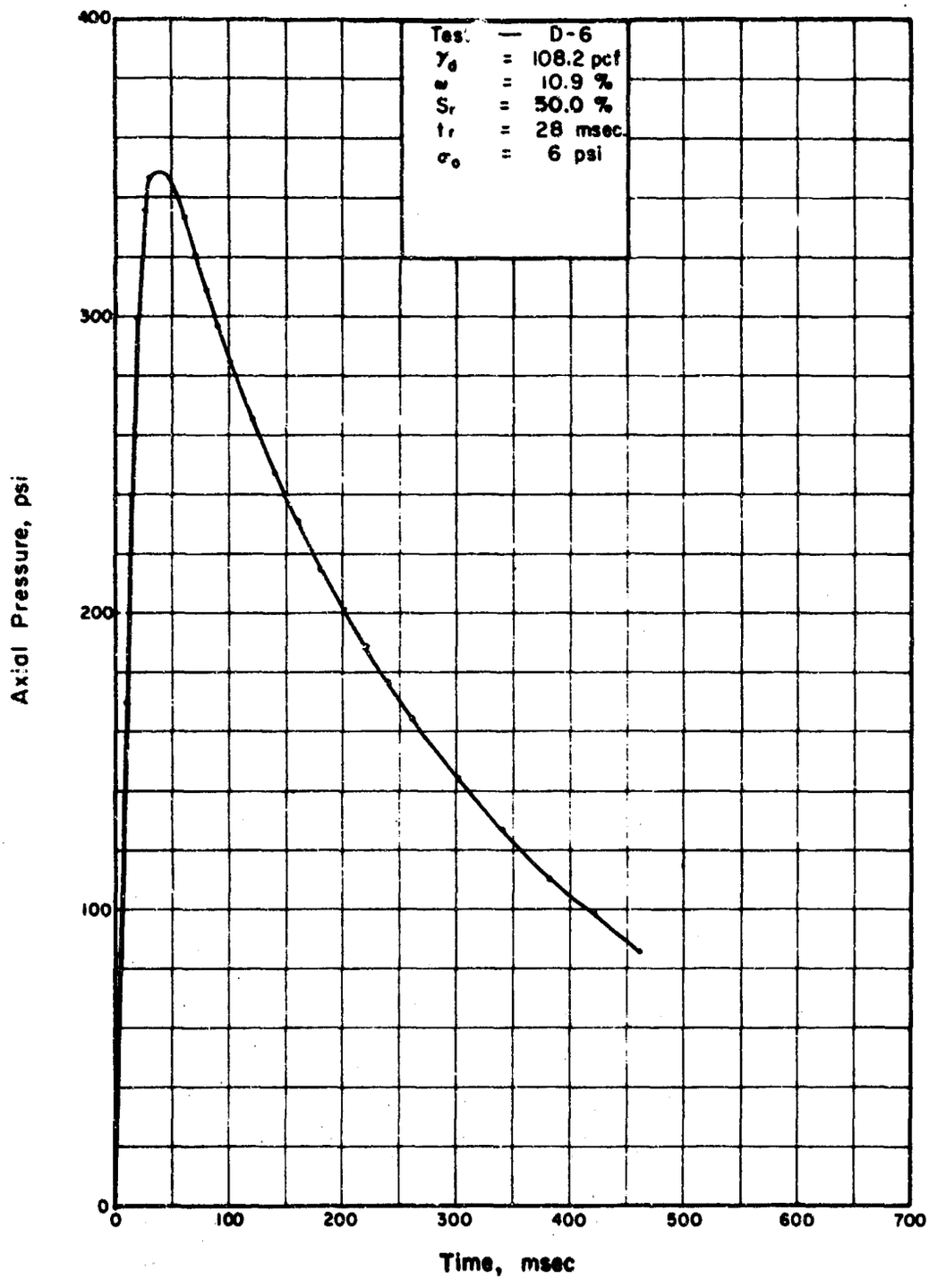

FIG. A. 12 STRESS - TIME RELATIONSHIP MEASURED AT TOP OF SPECIMEN, TEST D-6 (SITE 3)

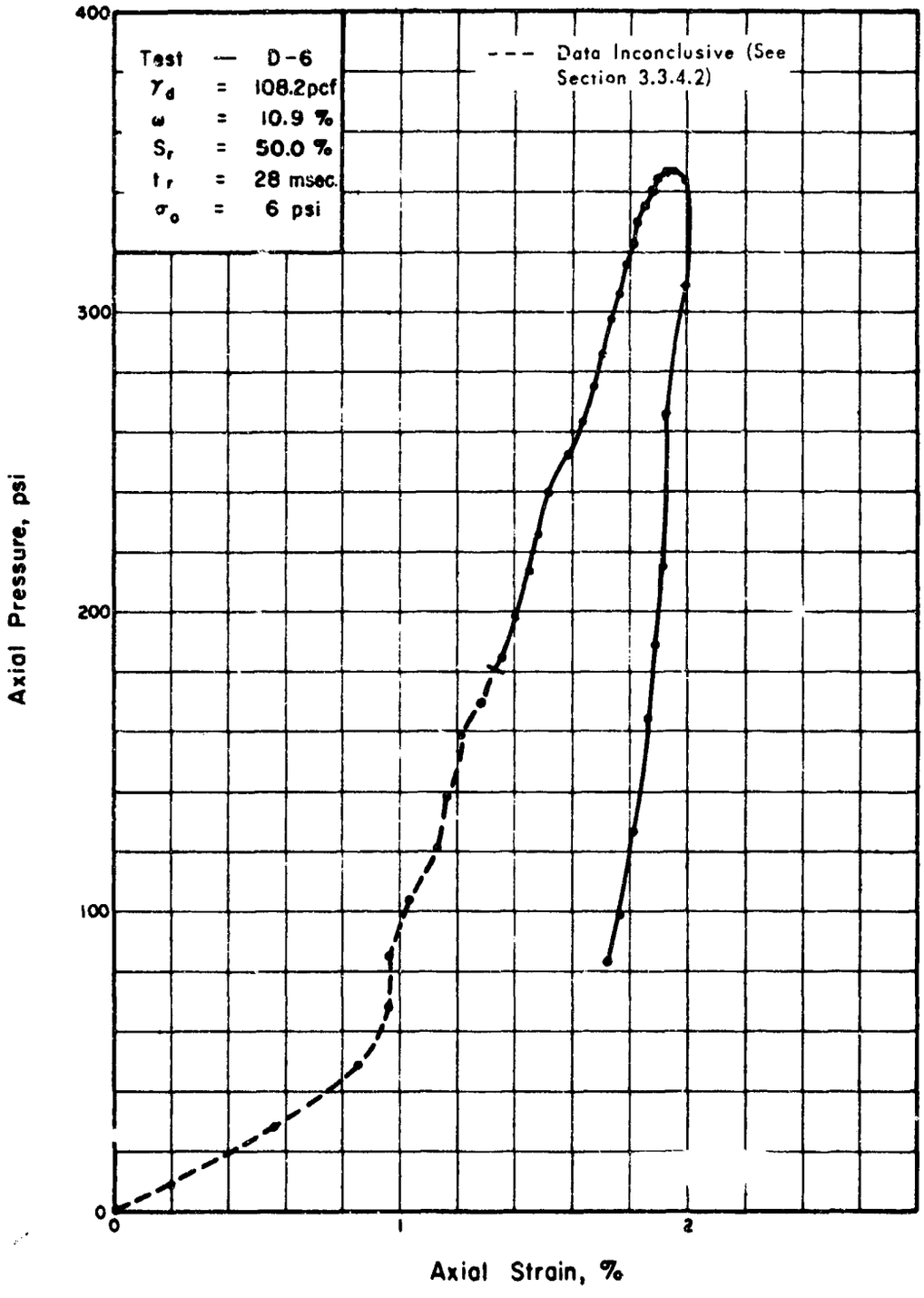

FIG. A.13 STRESS-STRAIN RELATIONSHIP IN ONE-DIMENSIONAL COMPRESSION, TEST D-6 (SITE 3)

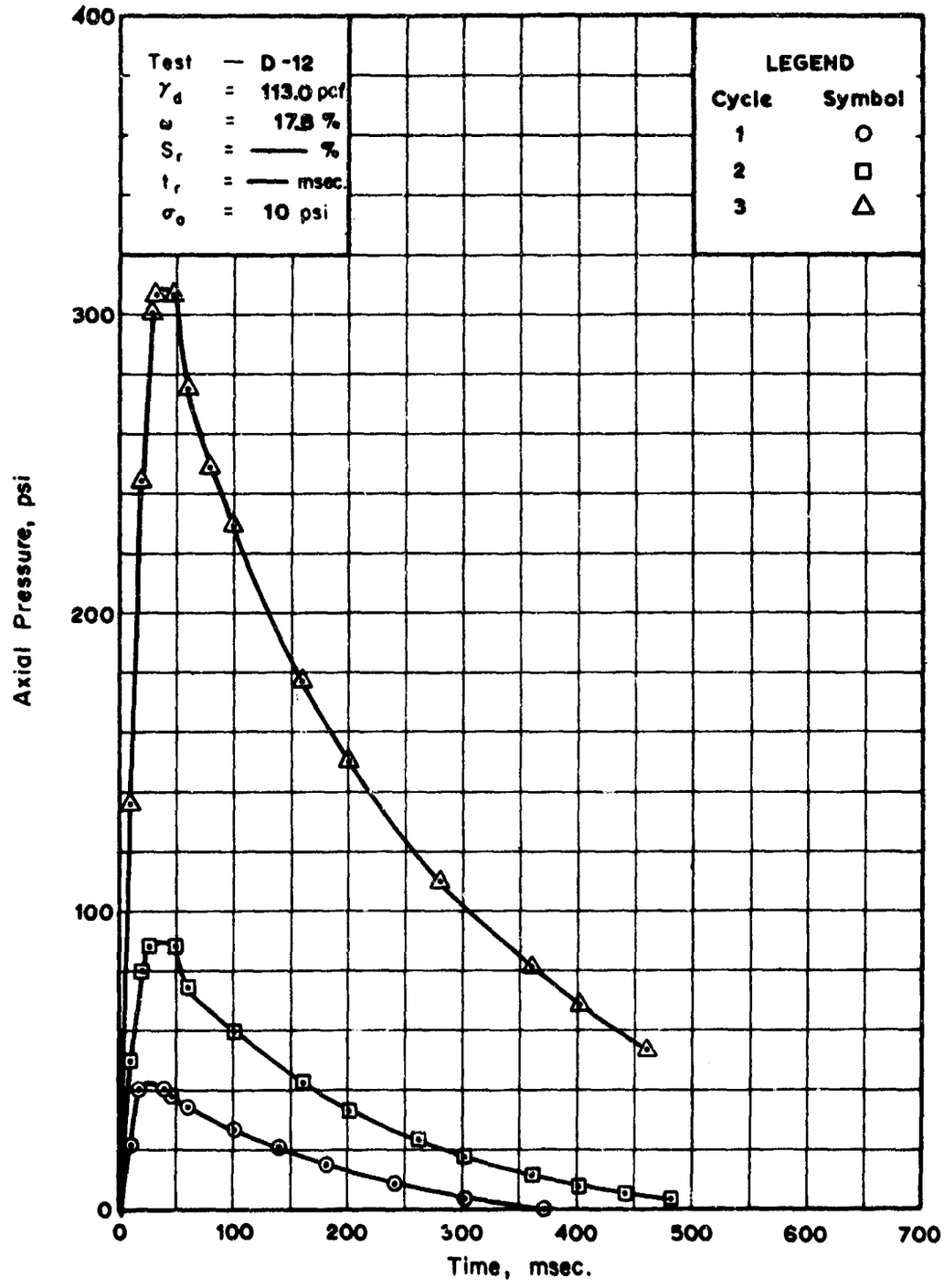

FIG. A.14 STRESS-TIME RELATIONSHIP MEASURED AT TOP OF SPECIMEN, TEST D-12 (SITE 3)

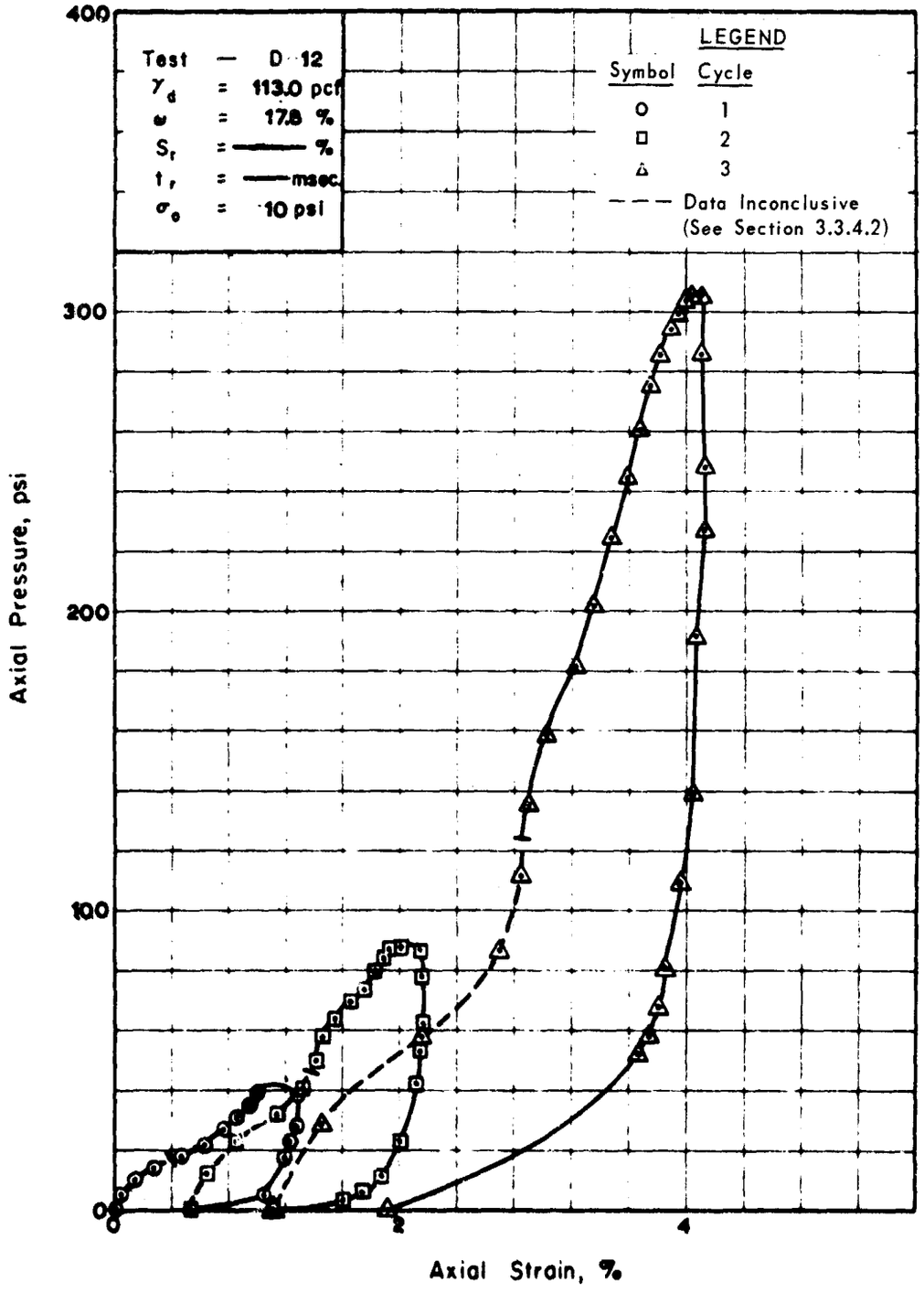

FIG. A.15 STRESS - STRAIN RELATIONSHIP IN ONE-DIMENSIONAL COMPRESSION, TEST D-12 (SITE 3)

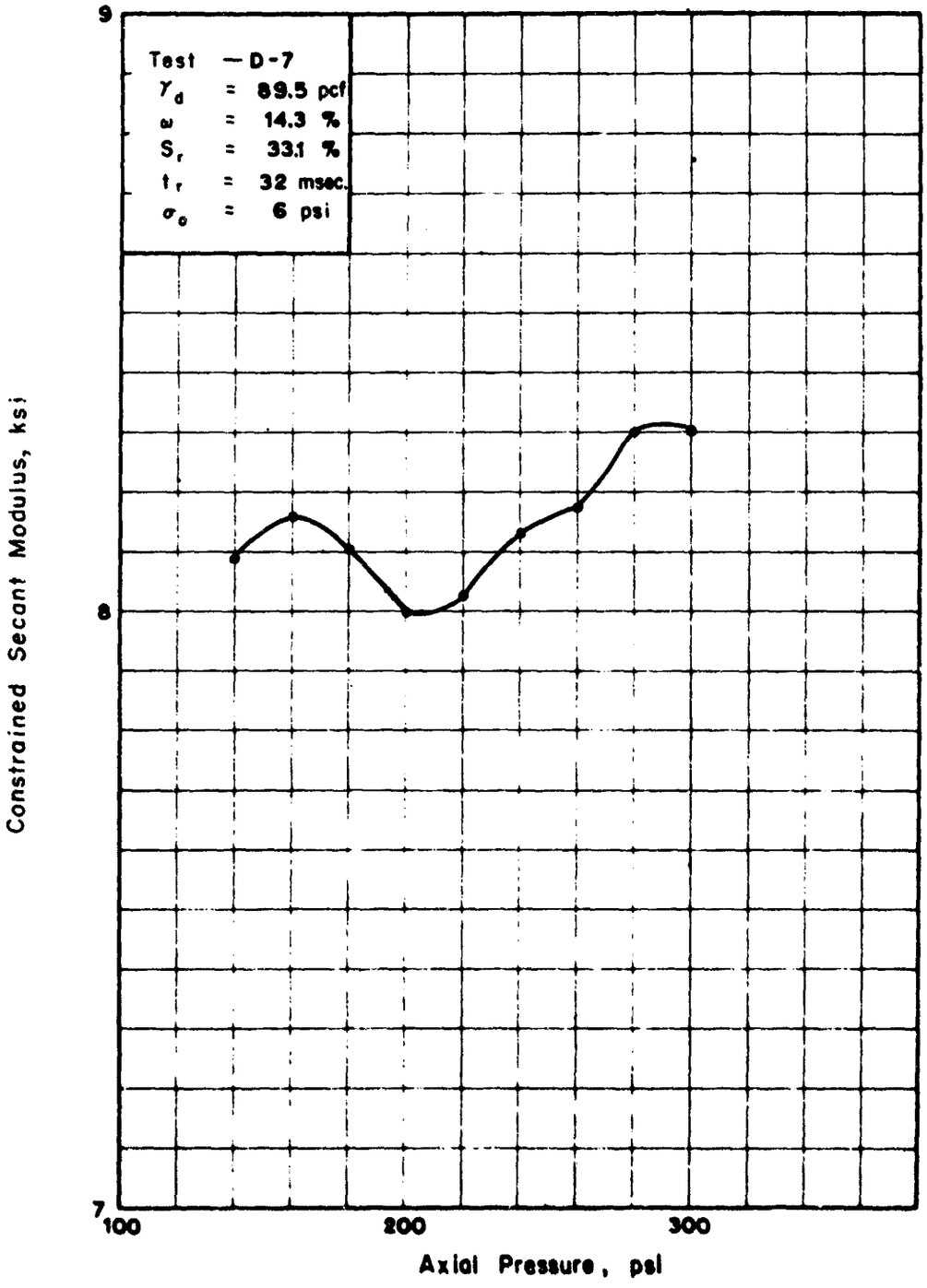

FIG. A.16 CONSTRAINED MODULUS–AXIAL STRESS RELATIONSHIP, TEST D-7 (SITE 1)

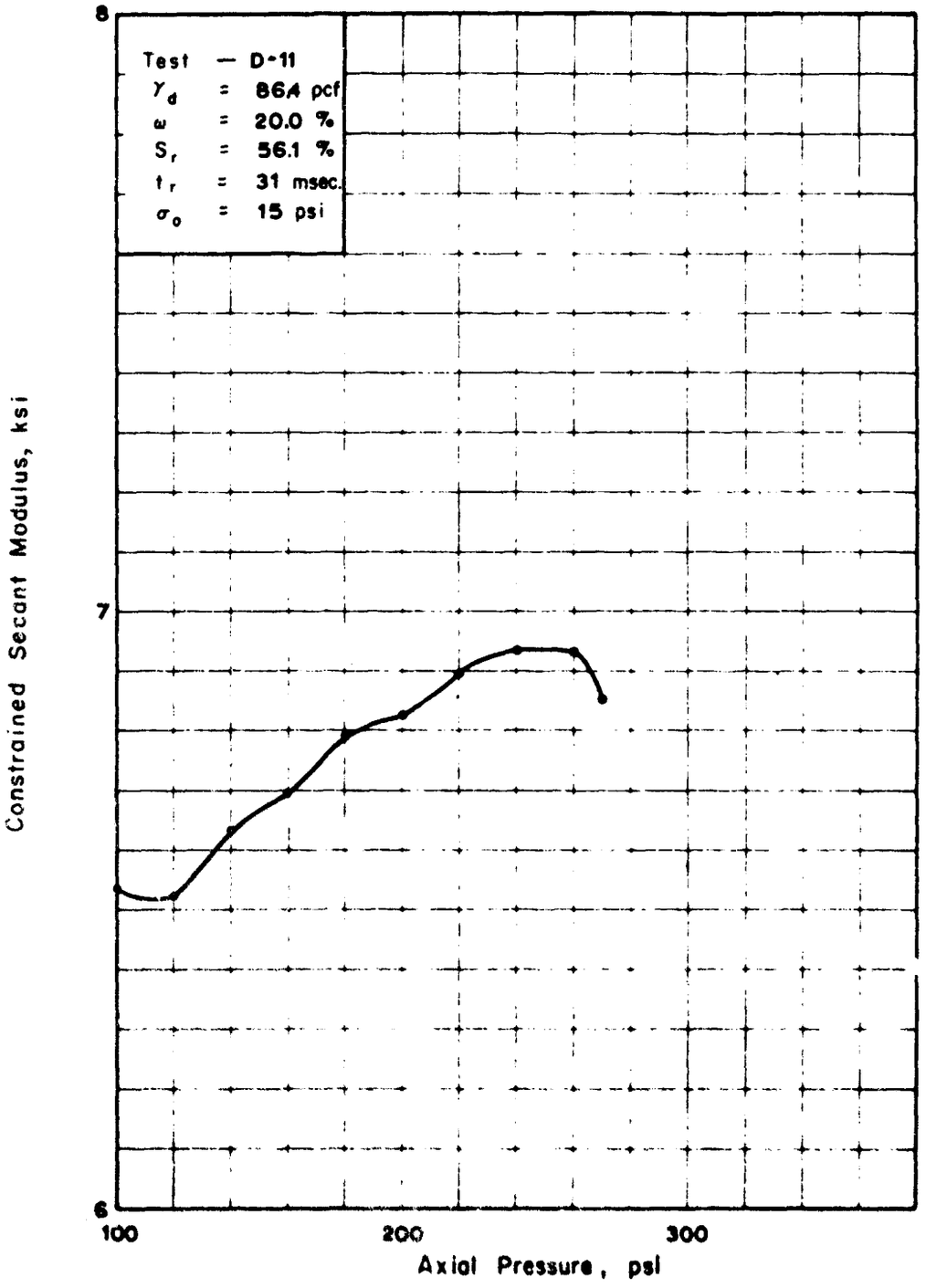

FIG. A.17 CONSTRAINED MODULUS–AXIAL STRESS RELATIONSHIP, TEST D-11 (SITE 1)

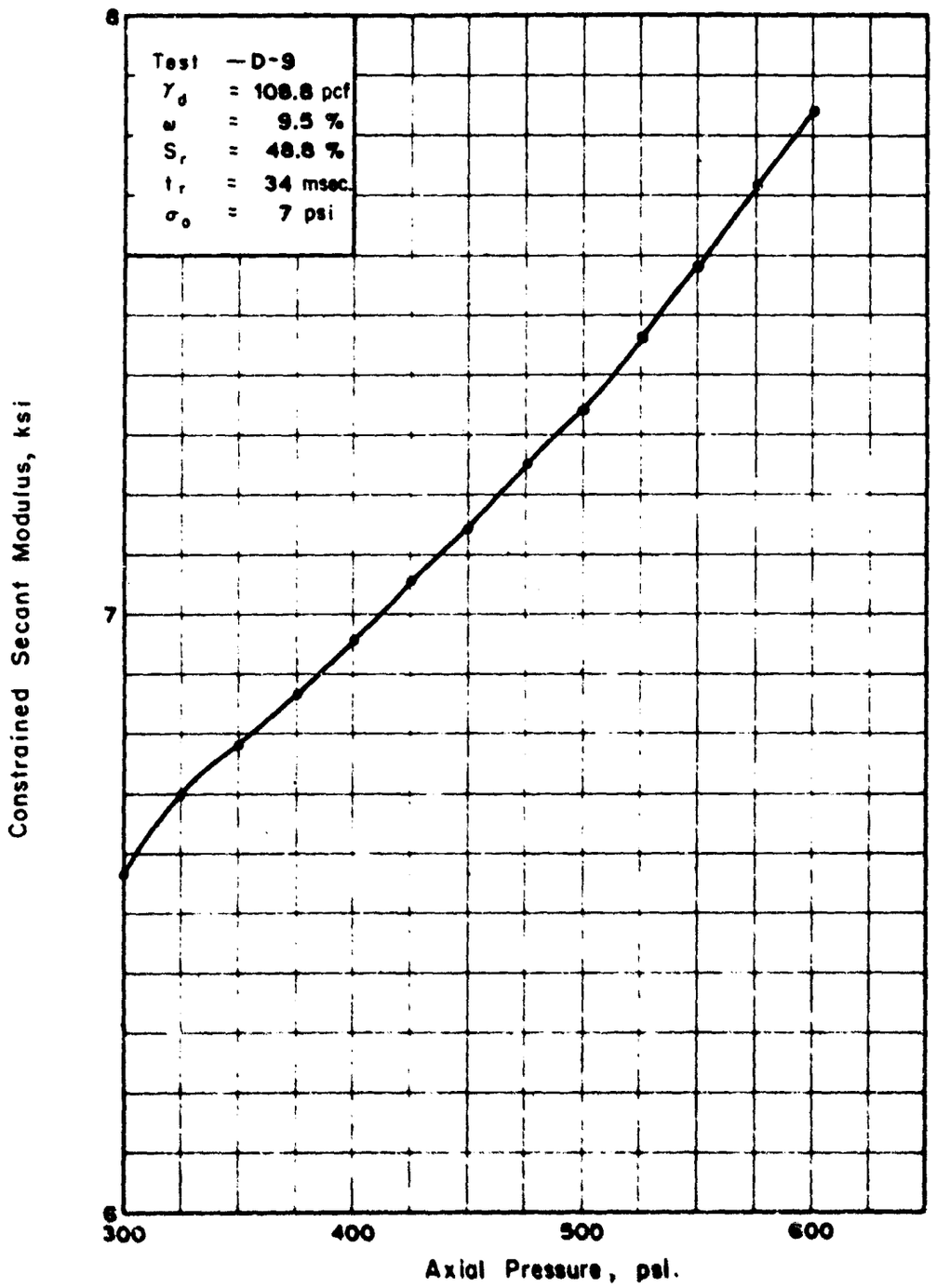

FIG. A.18 CONSTRAINED MODULUS–AXIAL STRESS RELATIONSHIP TEST D-9 (SITE 2)

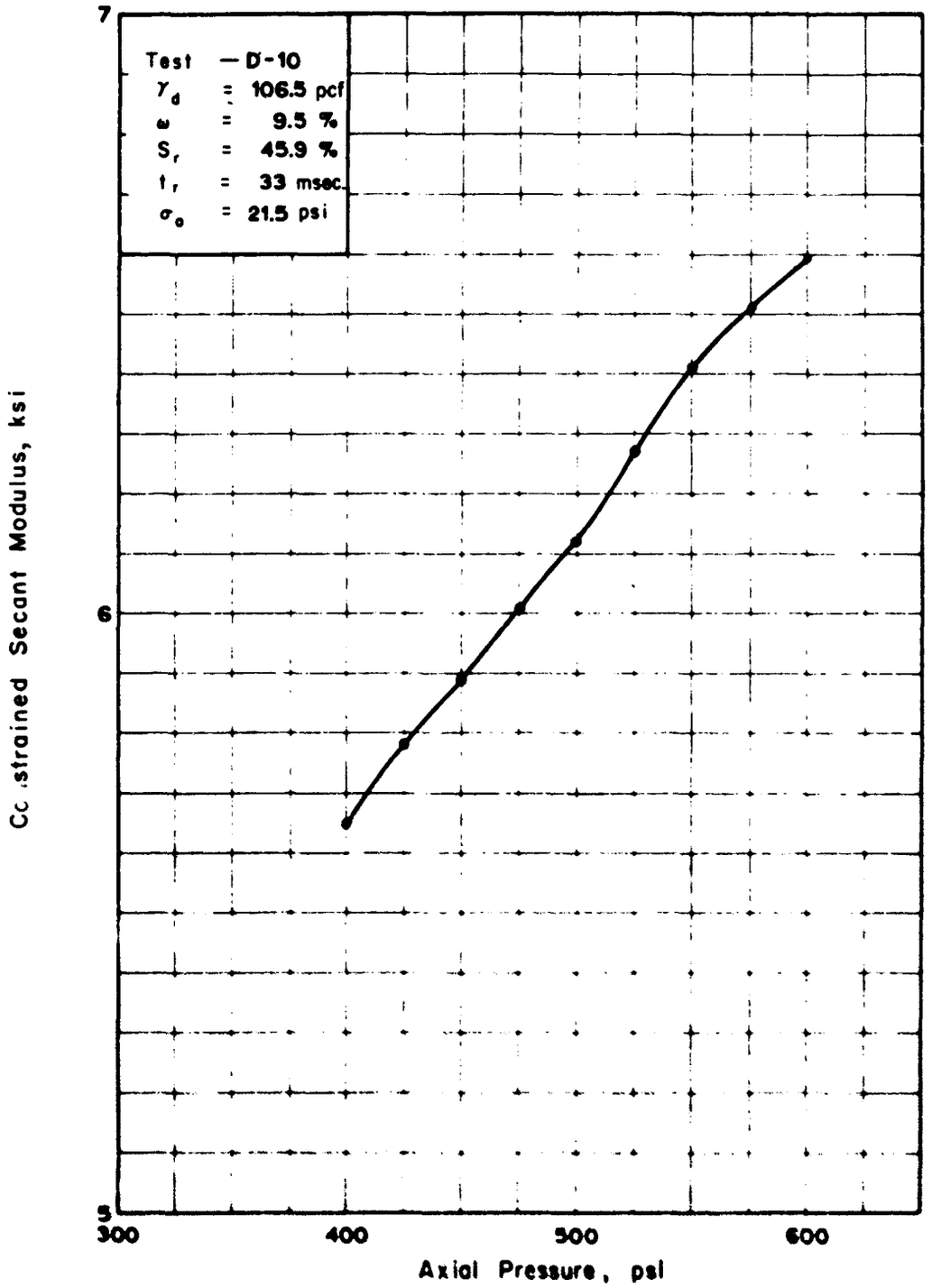

FIG. A.19 CONSTRAINED MODULUS–AXIAL STRESS RELATIONSHIP TEST D-10 (SITE 2)

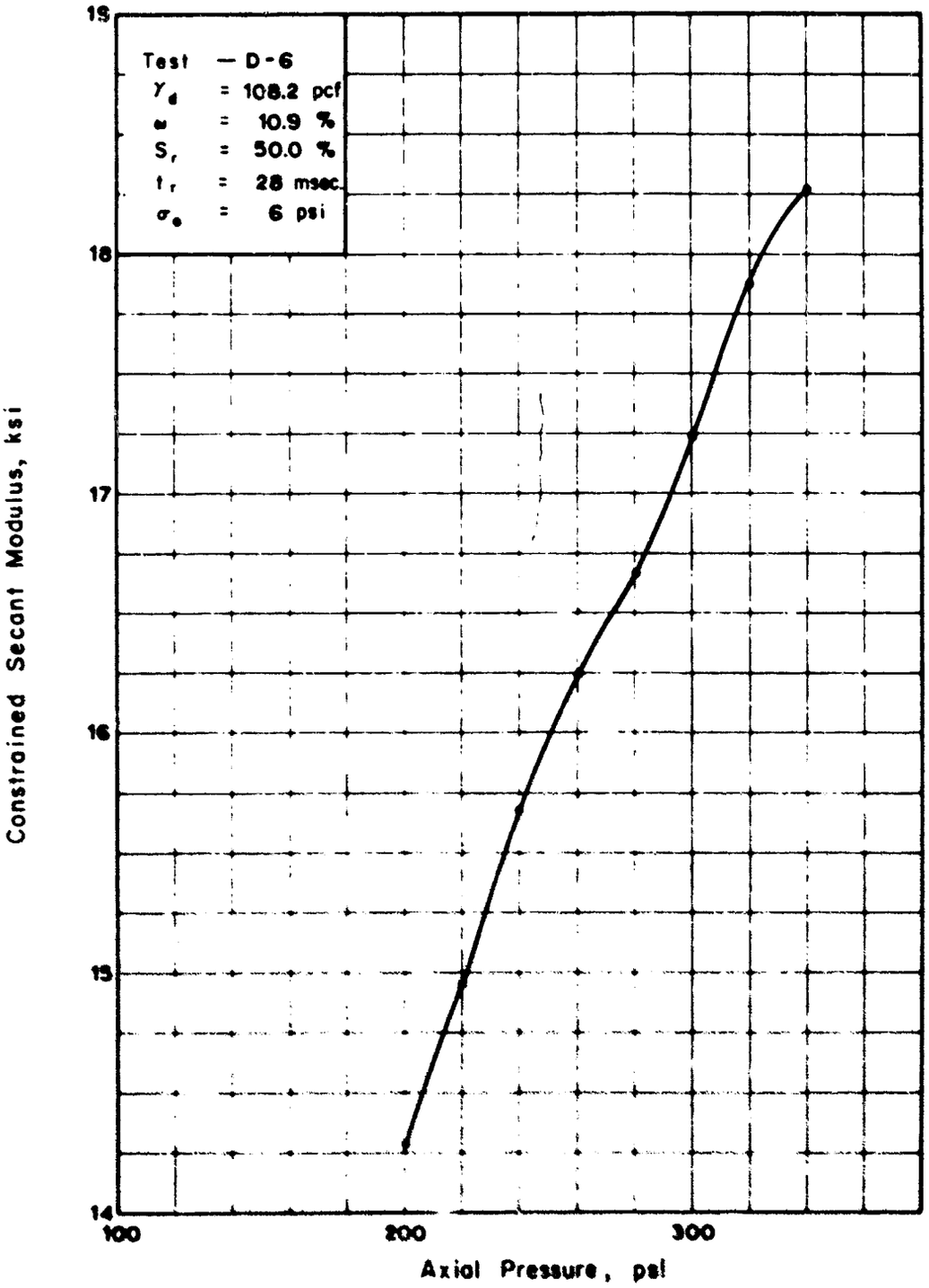

FIG. A.20 CONSTRAINED MODULUS–AXIAL STRESS RELATIONSHIP, TEST D-6 (SITE 3)

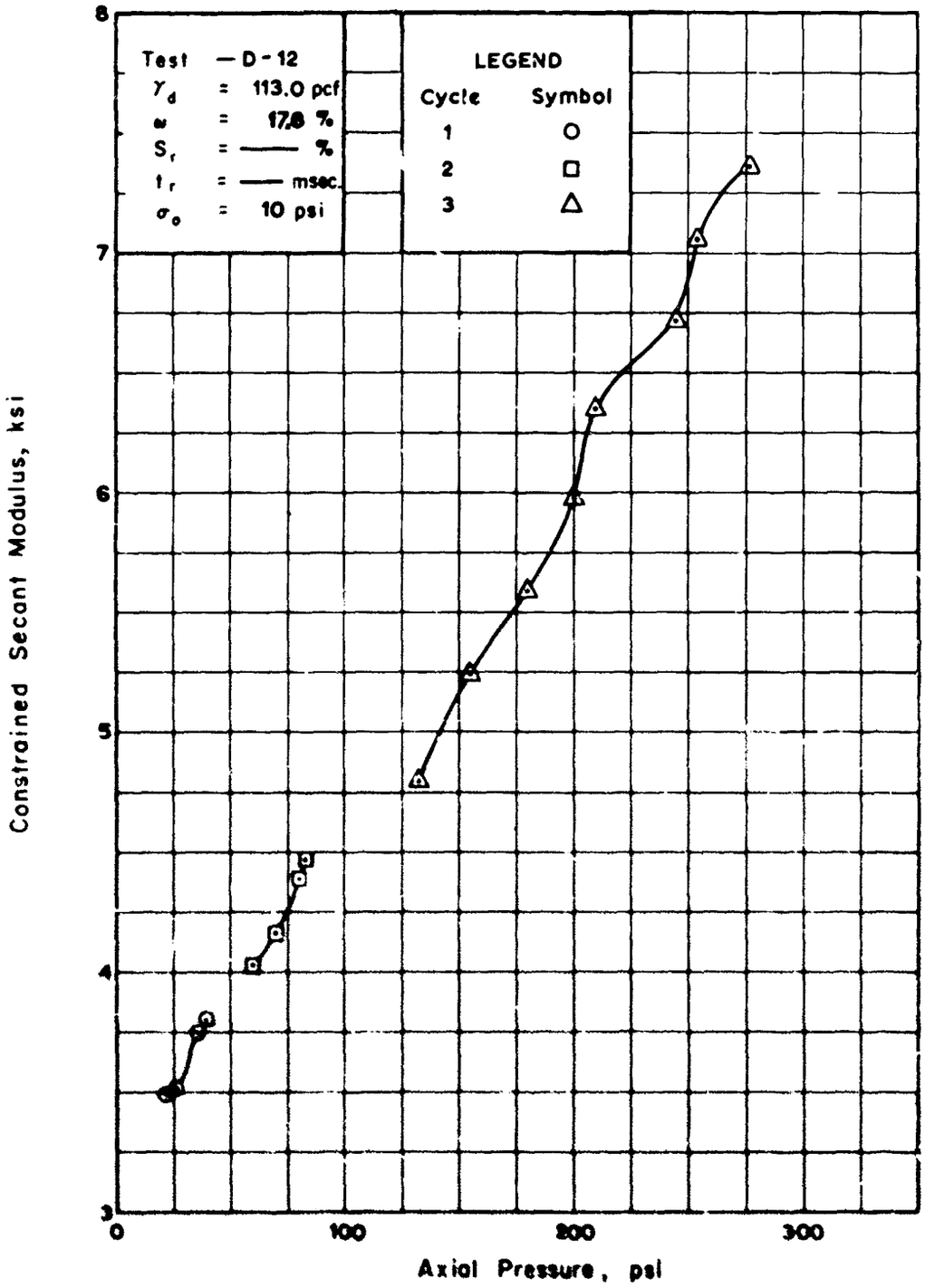

FIG. A.21 CONSTRAINED MODULUS–AXIAL STRESS RELATIONSHIP, TEST D-12 (SITE 3)

APPENDIX B

DESCRIPTION AND OPERATION OF THE DYNAMIC LOAD GENERATOR

B.1 INTRODUCTION AND SUMMARY

The Dynamic Load Generator (DLG) was developed by the Department of Civil Engineering at the University of Illinois under the joint sponsorship of the Air Force Weapons Laboratory and the Defense Atomic Support Agency. The DLG accommodates a test specimen 4 feet in diameter and 8 feet high and has the capability of producing static pressures in excess of 1000 psi or dynamic pressures up to 900 psi with controllable rise, dwell, and decay times.

An abreviated description of the DLG is presented in this report to enable the reader to better understand the utilization of the equipment in the study covered by this report. More detailed information regarding the DLG may be found in publications by Prendergast (1968), Sinnamon (1968) and Grimes (1966).

B.2 DESCRIPTION OF THE DYNAMIC LOAD GENERATOR

B.2.1 Load Cells

The load cells are mounted on the support system which is in turn affixed to the foundation as shown in Figure 2.1. The load cells house the main and decay valves and their triggering mechanisms. A schematic cross section of one of the seven load cells is presented in Figure B.1.

The main valve is composed basically of a main valve actuating piston, a main valve shaft, and a main valve piston. The main valve piston seals the ports which form an orifice for controlling the gas flow from the charging chamber to the expansion chamber with the rate of flow being controlled by the position of the adjustable main valve sleeve over the ports in the main valve cylinder. The main valve actuating piston when loaded provides the driving force to open the main valve in the individual load cells.

The main valve is maintained in the closed position by the main valve cart which is held in place by the main valve triggering mechanism. In order to open the main valve, the lead solenoid is energized thereby releasing the main valve cart which is rolled horizontally out of the path of the main valve shaft by gas pressure. The main valve shaft then is forced upward by the main valve actuating piston, and the main valve is opened.

The operation of the decay valve is quite similar to that of the main valve. The decay valve is basically composed of a decay valve piston, decay valve shaft, and a decay valve actuating piston. The decay valve piston seals the ports which form an orifice for controlling the flow of gas from the charging and expansion chambers to the decay chamber with the rate of flow being controlled by the position of the adjustable decay valve sleeves over the ports in the decay valve cylinder.

The decay valve is actuated by energizing the decay valve solenoid which actuates an exhaust valve which is in communication with the chamber above the decay valve actuating piston and allows the decay valve to open.

B.2.2 Support System and Foundation

The support system is composed of a steel forging encompased by special I-beams. The steel forging has six machined passageways on a radius of 17-1/4

inches surrounding a central passageway, the passageways serving as the charging chambers when the load cells are installed. The support system when tied to the foundation by seventy-two 1-1/4-inch diameter high-strength steel rods serves as a reaction for the gas pressure acting on the surface of a test specimen and provides mass and stiffness to reduce accelerations and vibration associated with the firing of the load cells.

The foundation for the DLG is monolithic concrete 20 feet by 22 feet in plan and 23 feet deep. The support system is tied to the foundation through two piers incorporated into the foundation and the above mentioned post-tensioned 1-1/4-inch steel rods. The rods provide sufficient force to maintain the concrete in a state of compression under the maximum upward force of approximately 1500 kips, excluding any inertial or reflection affects, arising due to the variations in the velocity of stress waves in steel, concrete, and soil. Access to the specimen container is facilitated by a recess in the foundation as shown in Figure 2.1.

B.2.3. Specimen Container

The specimen container is shown in Figures 2.1 and 2.2. The container is composed of four steel sections which are approximately 2 feet high and 2 inches thick. The individual sections are provided with O-rings such that gastight integrity can be achieved. The bottom-most ring rests on the base plate which is grooved and fitted with an O-ring. The base plate is also fitted with instrumentation plugs to provide external electrical connection to instrumentation located within the specimen container. The specimen container fully assembled provides space for a test specimen 4 feet in diameter and 8 feet in height.

To prevent the sections of the specimen container from separating during unloading of a specimen because of specimen rebound and sidewall friction, the container was put in a state of axial compression by six 1-1/8-inch-diameter post-tensioned rods which were threaded into the base plate and attached to brackets welded to the top section of the specimen container.

Mobility of the specimen container is provided by four hydraulic jacks which link the base plate and a four-wheeled cart which rides on a dual track. The cart is deleted from Figure 2.1 for clarity. A support for the base plate constructed of two steel plates on edge provides a stand for the container during specimen placement.

B.2.4 Seal Ring

The seal ring serves as the outer wall of the expansion chamber and provides airtight integrity for the connection between the support system and the specimen container. The seal ring showing the support system and specimen container is presented in Figure 2.2. The seal ring is free to slide on the top section of the specimen container when not bolted to the support system and likewise the specimen container is free to move axially within the seal ring when the ring is bolted to the support system permitting relative movement between the support system and the specimen container during loading. Movement of the seal ring container into position for bolting is accomplished by two hydraulic actuators which are mounted on the outside wall of the specimen container.

B.2.5 Grids

Two sets of perforated steel plates bolted to the support system as shown in Figure 2 2 serve to distribute the jets of high-pressure gas emitting from the load cells upon opening of the main valves. The upper grid has an unperforated central portion which is surrounded by an array of holes which vary in size and location designed to distribute the gas flow evenly while the lower grid has a uniform array of 1/4-inch-diameter holes. The lower grid was designed to smooth out any minor irregularities in the pressure distribution, thus presenting a uniform pressure distribution to the top surface of the test specimen.

B.2.6 Decay Chamber

The decay chamber was designed to serve three purposes: 1) contain the gas expelled from the charging and expansion chambers during decay operation such that the gas might be purified and reused; 2) protect the load cells from ambient contaminants; and 3) reduce the noise level associated with testing operations. The chamber consists of two sections as shown in Figure 2.1. The lower section is fitted with four access ports for tubing and electrical connections necessary for operation of the load cells. The upper section is fitted with a large access port to provide access to the load cells for adjustment and minor repair. All junctions are fitted with O-rings to provide airtight integrity.

B.3 OPERATION OF THE DYNAMIC LOAD GENERATOR

B.3.1 Loading Media

Two commercially available inert gases, nitrogen and helium, were used as media for loading test specimens and controlling operation of the DLG.

Inert gases were required to prevent an explosion which could result if a combustible gas were suddenly compressed.

Helium, being the lighter gas, is used as a loading medium when very fast rise times and/or decay times are required, while nitrogen gas is used as a loading medium at other times because of the lower cost of the gas. Facilities are available to reclaim and pressurize helium after testing. Nitrogen is used almost exclusively to control the operation of the DLG.

B.3.2 Operating Procedure

Upon completion of the preparation of a test specimen as described in Section 3.3.2, including the placement of the clamping ring and the sealing ring O-ring, the specimen container was ready to be placed on the bearing plate, as shown in Figure 2.1. The hydraulic jacks on the cart were pressurized to raise the base plate off the edge plate supports, and the specimen container was pushed in place over the bearing plate and lowered to rest on the bearing plate. The seal ring was raised hydraulically and bolted to the support system, and the necessary connections were made to the ports in the seal ring. If adjustments of the rise or decay times were required, they were adjusted inside the decay chamber. Following any such adjustments, the access port was sealed. The remainder of the loading and firing operation is dependent upon the control medium and control electronics.

As the load cell is shown in Figure B.1, the main and decay valve triggering mechanisms have been cocked and the load cell is ready to be pressurized. The chambers behind the trigger-actuating pistons are pressurized to accelerate the main valve carts when the load solenoid is energized. The chambers below the main valve actuating pistons are pressurized to accelerate the main valve pistons when the main valve carts are moved to allow the main

valve shaft to move upward. The chambers above and below the decay valve actuating pistons are pressurized such that a small net downward pressure is maintained and the decay valves are held closed until the decay valve triggering mechanisms are actuated.

The test is initiated by the energization of the load solenoids and the consequent opening of the main valves. With the main valves open, the gas in the charging chamber flows through the main cylinder ports and grids and then onto the loading diaphragm. The unloading cycle is initiated by the energization of the decay solenoids which actuate the decay valve triggering mechanisms venting the gas in the chamber above the decay valve actuating pistons. The unbalance in the pressure then is acting in the opposite direction and the decay valves open, allowing the gas in the charging and expansion chambers to flow through the ports in the decay valve cylinders to the decay chamber. Following the test the gas in the decay chamber may be reclaimed for future use or vented to the atmosphere.

B.3.3 Control Instrumentation

In order to achieve as fast a pressure-rise time as possible and maintain a relatively uniform pressure distribution over the surface of a test specimen, an electronic fourteen-channel counter was utilized to preset the time at which each of the seven solenoids was to be actuated. The time of firing of each load cell was monitored by magnetic pickup devices mounted at a common point on each load cell in conjunction with steel plates mounted on the main valve shafts. The passage of the steel plate by the magnetic pickup generated an electrical signal which was recorded on tape and served to indicate the time when a particular load cell fired. Comparison of the

times of firing for the seven load cells provided the basis for adjusting the firing presets to attain as near a simultaneous firing of the load cells as possible.

The fourteen-channel counter was also employed to preset the time at which the decay solenoids were actuated. The energizing of the decay solenoids was not as critical as the load solenoids, so no provisions were made to monitor the times at which movement of the individual decay valves occurred. The dwell of the surface pressure over the test specimen was also established by the fourteen-channel counter.

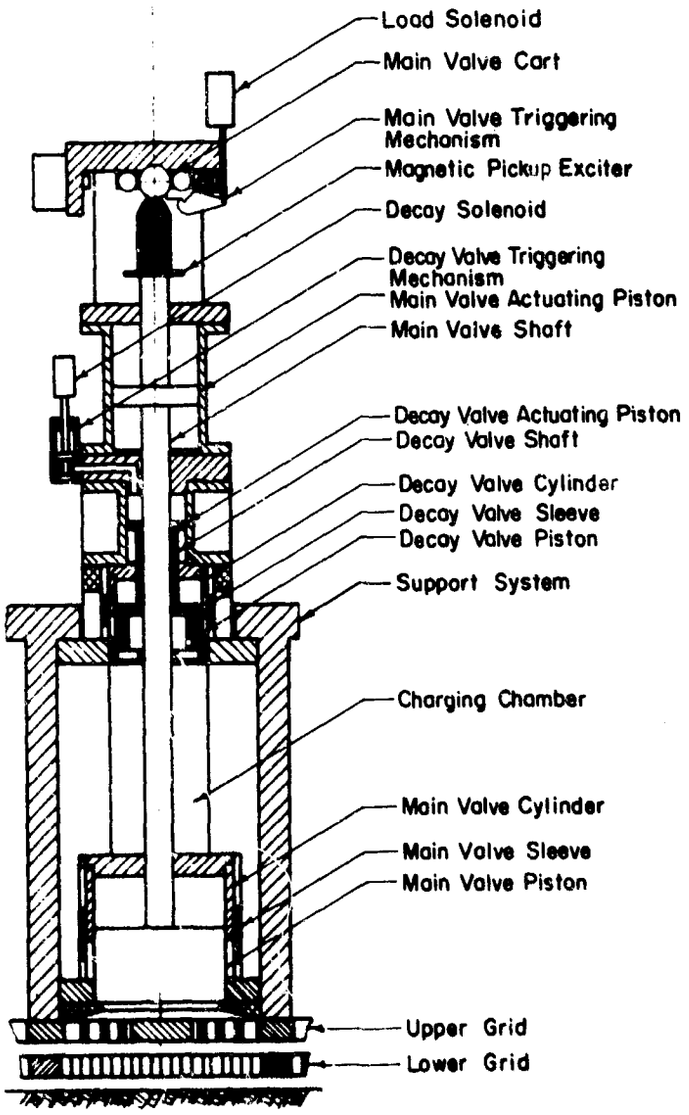

FIGURE B.1 SCHEMATIC CROSS SECTION OF LOAD CELL

LIST OF REFERENCES

Abbott, P. A., (1967), "Effects of Boundary Friction on Transmission of Static Stress Through Sand in Cylindrical Tanks," AFWL TR-64-108, Kirtland Air Force Base, Albuquerque, New Mexico.

Bauer, E. E. and Thornburn, T. H., (1962), Introductory Soil Testing, Stipes Publishing Company.

Bjerrum, L., (1962), Personal Correspondence to Professor R. B. Peck.

Borowicka, H., (1936), "Influence of Rigidity of a Circular Foundation Slab on the Distribution of Pressures Over the Contact Surface," Proceedings, First International Conference on Soil Mechanics and Foundation Engineering, Cambridge, Massachusetts.

Cerni, R. H. and Foster, L. E., (1962), Instrumentation for Engineering Measurement, John Wiley and Sons, Inc.

Durbin, W. L., (1964), "Correlation of Dynamic Constrained Moduli in Granular Media," URS 637-15, Interim Report Draft to Waterways Experiment Station, Contract No. DA-22-079-eng-373.

Feese, A., (1970), "Shear Strength Characteristics of Earth-Rock Mixtures; Survey and Evaluation of Existing Laboratory Apparatus for Large-Scale Testing of Compacted Rock and Earth-Rock Mixtures," MP S-70-7, U. S. Army Engineer Waterways Experiment Station, CE, Vicksburg, Mississippi.

Fumagalli, E., (1969), "Tests on Cohesionless Materials for Rockfill Dams," Journal of the Soil Mechanics and Foundations Division, American Society of Civil Engineers, Vol 95, No. SM1.

Grimes, M. E., (1966), Instruction Manual for Structural Dynamics Testing Laboratory Data Acquisition and Reduction System, Department of Civil Engineering, University of Illinois, Urbana, Illinois.

Hendron, A. J., Jr., (1963), The Behavior of Sand in One-Dimensional Compression, Ph. D. Thesis, Department of Civil Engineering, University of Illinois, Urbana, Illinois.

Jacobsen, L. S. and Ayre, R. S., (1958), Engineering Vibrations, McGraw-Hill Book Company, Inc.

Marsal, R. J., et al., (1965), Research on the Behavior of Granular Materials and Rockfill Samples, Comision Federal de Electricdad, Mexico.

Miller, R. P., (1965), Engineering Classification and Index Properties for Intact Rock, Ph. D. Thesis, Department of Civil Engineering, University of Illinois, Urbana, Illinois.

Paul, S. L. and Goel, S. K., (1968), "An Experimental Investigation of the Dynamic Response of Model Silo-Type Structures in Cohesive Soil, Phase II," a report submitted for publication to the Air Force Weapons Laboratory, Kirtland Air Force Base, Albuquerque, New Mexico.

Prendergast, J. D., (1968), Evaluation of the Four-Foot-Diameter, 1500-kip-Capacity Dynamic Load Generator, Ph. D. Thesis, Department of Civil Engineering, University of Illinois, Urbana, Illinois.

Rohmaller, P. L., (1968), Arching Effect for Underground Rectangular Structures Subjected to High Static Pressures, Ph. D. Thesis, Department of Civil Engineering, University of Illinois, Urbana, Illinois.

Schlinder, L., (1967), "An Improved Facility for Testing Soils in One-Dimensional Compression," draft of a report submitted to the Symposium on Wave Propagation and Dynamic Properties of Earth Materials held at Albuquerque, New Mexico.

Scott, R. F., (1963), Principles of Soil Mechanics, Addison-Wesley Publishing Company, Inc.

Sinnamon, G. K., (1968), "Development, Operation, and Characteristics of the Four-Foot-Diameter, 1500 Kip Capacity Dynamic Load Generator," a report to be submitted for publication to the Air Force Weapons Laboratory, Kirtland Air Force Base, Albuquerque, New Mexico.

Sowers, G. F., Williams, R. C., and Wallace, T. S., (1965), "Compressibility of Broken Rock and the Settlement of Rockfills," Proceedings of the Sixth International Conference on Soil Mechanics and Foundation Engineering, University of Toronto Press.

Taylor, D. L., et al., (1954), "Final Report on Laboratory Studies," Massachusetts Institute of Technology, Cambridge, Massachusetts.

Timoshenko, S., (1955), Vibration Problems in Engineering, D. Van Nostrand Company, Inc.

Timoshenko, S. and Woinowsky-Krieger, S., (1959), Theory of Plates and Shells, McGraw-Hill Book Company.

Whitman, R. V., (1963), "The Response of Soils to Dynamic Loadings; Report 17, Stress-Strain-Time Behavior of Soil in One-Dimensional Compression," Contract Report No. 3-26, U. S. Army Engineer Waterways Experiment Station, CE, Vicksburg, Mississippi, prepared and published under Contract DA-22-079-eng-224 by Soil Engineering Division, Massachusetts Institute of Technology, Cambridge, Massachusetts, Department of Civil Engineering Research Report R63-25.

Whitman, R. V., (1964), Nuclear Geophysics, DASA-1285(11), Washington 25, D. C.

Zaccor, J. V., et al., (1965), "Study of the Dynamic Stress-Strain and Wave-Propagation Characteristics of Soils," Report 4, United Research Services Incorporated, Burlingame, California.